
Università degli Studi di Napoli Federico II
Facoltà di Ingegneria



Matteo Esposito

PTED BEAM-TO-COLUMN CONNECTIONS
FOR STEEL MOMENT RESISTING FRAMES:
STRUCTURAL IDENTIFICATION
BASED ON NUMERICAL ANALYSES

*Tesi di Dottorato
XXI Ciclo*

*Il Coordinatore
Prof. Ing. Federico M. MAZZOLANI*

Dottorato di Ricerca in Ingegneria delle Costruzioni

*To my family,
slightly larger than the one in which I was born*

Acknowledgements

At the end of my PhD three years activity, I would like to thank the people who contributed to make this experience both profitable and significant, from the professional and human points of view, respectively.

I express my deep gratitude to Prof. Federico M. Mazzolani, my PhD tutor, who has passed to me his enthusiasm and passion for the research. His approach to structural problems, as well as his capacity of contributing to the advancements of knowledge in many fields of structural engineering, are an example for me. In addition, he has given to me the possibility of making many extraordinary experiences, which have formed me as both an engineer and a person.

I am sincerely grateful to Dr. Beatrice Faggiano, who has daily guided me in all my research activities, always demonstrating patience and kindness. She has always incited me to do my best and has taught me how to face up problems with strength and determination, never losing the self-confidence. The things I have learned by her go far beyond the strict field of the research.

My gratitude is addressed also to Prof. Raffaele Landolfo, who has always demonstrated to believe in me and encouraged my efforts. His helpfulness during these three years has been very important for me.

I wish to thank Prof. Gianfranco De Matteis, who has always enhanced my work, notwithstanding the small number of occasions to work together. His kindness and benevolence towards me have been very appreciated.

I express my gratitude to Dr. Gaetano Della Corte, whose concise observations have often stimulated important reflections on topics related to my research.

I wish to thank also Dr. Simeone Panico, Dr. Luigi Fiorino, Dr. Antonio Formisano, Dr. Anna Marzo, Dr. Mario D'Aniello, Dr. Enrico Barecchia, Dr. Francesco Portioli, Dr. Oreste Mammana, Dr. Gianmaria Di Lorenzo, Eng. Francesco Campitiello, Eng. Manuela Brescia, Arch. Ornella Iuorio, Eng. Lucrezia Cascini, Eng. Maria Rosaria Grippa, Eng. Giulio Martire, Eng. Daniela De Gregorio, Eng. Carmine Castaldo, and, last but not least, Mrs. Xiaoling Song. Their friendship has made me truly feel a member of a team.

I am grateful to the other members of the Department of Structural Engineering (DIST) at the University of Naples "Federico II", in particular to Prof. Bruno Calderoni, who is an example for me due to his professional and human qualities, Prof. Pietro Lenza, Prof. Antonio De Luca, Prof. Elena Mele, Dr. Aldo Giordano, for his suggestions about the ABAQUS program, Dr. Costantino Giubileo, Dr. Giuseppe Brandonisio, Dr. Emilia Cordasco, Dr. Giovanni Cuomo, Dr. Ernesto Grande, Eng. Gaetana Pacella, Eng. Roberta Santaniello, and Eng. Rosa De Lucia. They have strongly contributed to create a serene and stimulating environment for my life and work at the Department.

I wish to thank Mr. Carmine Citro for the kindness and helpfulness he has always demonstrated to me. The time spent together in talking about music, society and policy have been a very important occasion for me to grow as a person.

I am grateful to Prof. Constantin Christopoulos, at the University of Toronto (Canada), for his kind encouragement and important suggestions for my research. I am also grateful to Profs. James Ricles and Richard Sause, at the Lehigh University (USA), for the data on materials they sent to me and for the encouragement.

A very special thanks is addressed to my friend and "fellow traveller" Eng. Giuseppe Brando. His honesty in evaluating my work, his precise suggestions, his capability of understanding my thoughts, his constant helpfulness, and his deep humanity have been fundamental for me.

Beside the people I have met within the academic environment, I feel the necessity to express my gratitude to a number of other persons.

I am grateful to God, for the gifts, among the others, of patience and serenity. I always feel his hand guiding me.

I express my deepest gratitude to my father, Giuseppe, to my mother, Carmen, to my brother, Piero, and to my sister, Brunella. Their constant support and love are the basis for the person I am.

I thank all my friends, both the “old” and “new” ones, for their support and for the beautiful moments spent together. A special thanks is addressed to Francesco and Giovanni, who live with me in Naples.

I wish to thank Francesco Guccini, who has shown me the irony and poetry of ordinary things, Fabrizio De Andrè, who has taught me to look at people without judging them, and Angelo Branduardi, who has shown me the sweetness of little things.

My deepest and sincere gratitude his addressed to Mariapina, my girlfriend. Her love, friendship, kindness, carelessness, honesty, intelligence, curiosity, enthusiasm, and many other things, are the rays of sunshine in my life.

Thank you!

Naples, November 30, 2008

Matteo Esposto

Chapter 1

Introduction	1
1.1 GENERALITIES ON PTED SYSTEMS.....	1
1.2 OBJECTIVE OF THE RESEARCH AND METHODOLOGY	2
1.3 OUTLINE OF THE WORK	4

Chapter 2

Towards PTED beam-to-column connections	7
2.1 STRUCTURES IN SEISMIC AREAS	7
2.1.1 <i>Performance-Based Design fundamentals</i>	7
2.1.2 <i>Seismic resistant steel structures</i>	10
2.1.3 <i>Behaviour of steel MRFs during the 1994 Northridge earthquake</i>	13
2.2 PTED CONNECTIONS	18
2.2.1 <i>PTED connections in precast pre-stressed structures</i>	18
2.2.2 <i>Why PTED connections in steel MRFs?</i>	20
2.2.3 <i>PTED connections mechanical behaviour</i>	22
2.3 PRIOR RESEARCH ON PTED CONNECTIONS	26

2.3.1	<i>Preliminary remarks</i>	26
2.3.2	<i>PT steel strands and ED bolted steel top-and-seat angles</i>	26
2.3.3	<i>PT steel bars and ED confined steel bars</i>	30
2.3.4	<i>PT steel strands and ED friction devices</i>	32
2.3.5	<i>PT steel strands and ED reduced flange steel plates</i>	34

Chapter 3

FE analyses for the study of PTED connections	37
3.1 FINITE ELEMENT ANALYSES	37
3.1.1 <i>Why FEA for studying PTED connections?</i>	37
3.1.2 <i>Generalities on the Finite Element Method</i>	38
3.2 FEA BY THE ABAQUS COMPUTER PROGRAM	41
3.2.1 <i>Preliminary remarks</i>	41
3.2.2 <i>The ABAQUS complete environment</i>	42
3.2.3 <i>Finite Elements in ABAQUS</i>	42
3.2.4 <i>The definition of the materials</i>	44
3.2.5 <i>Non-linear problems</i>	45
3.2.6 <i>Contact</i>	46

Chapter 4

PTED connections with PT and ED bars	51
4.1 THE REFERENCE EXPERIMENTAL STUDY	51
4.2 FINITE ELEMENT MODELS	55
4.2.1 <i>The geometry of the models</i>	55
4.2.2 <i>The properties of the materials</i>	57
4.2.3 <i>The interactions between the component parts</i>	58

4.2.4	<i>The load history and the multi-step analysis</i>	59
4.2.5	<i>The mesh</i>	59
4.3	NUMERICAL VS. EXPERIMENTAL RESULTS	61
4.3.1	<i>Global response curves</i>	61
4.3.2	<i>Deformed configurations of the node</i>	62
4.4	BEHAVIOUR OF THE COMPONENT PARTS	64
4.4.1	<i>Preliminary remarks</i>	64
4.4.2	<i>Assembled node</i>	64
4.4.3	<i>Beam</i>	66
4.4.4	<i>Column</i>	68
4.4.5	<i>Contact plates</i>	70
4.4.6	<i>Reinforcing plates</i>	72
4.4.7	<i>Continuity plates</i>	73
4.4.8	<i>Stiffeners</i>	74
4.4.9	<i>Doubler plates</i>	76
4.4.10	<i>PT bars</i>	78
4.4.11	<i>ED bars</i>	79
4.5	SYNTHESIS OF RESULTS.....	80

Chapter 5

	PTED connections with PT strands and ED angles	83
5.1	THE REFERENCE EXPERIMENTAL STUDIES	83
5.1.1	<i>Preliminary remarks</i>	83
5.1.2	<i>Experimental test on bolted steel top-and-seat angles</i>	84
5.1.3	<i>Experimental test on a whole PTED connection</i>	85
5.2	PRELIMINARY NUMERICAL STUDY ON ED ANGLES.....	88
5.2.1	<i>The finite element model of ED angles</i>	88

5.2.2	<i>Numerical vs. experimental results</i>	93
5.3	FINITE ELEMENT MODELS OF THE PTED CONNECTION.....	94
5.3.1	<i>The geometry of the models</i>	94
5.3.2	<i>The properties of the materials</i>	96
5.3.3	<i>The interactions between component parts</i>	97
5.3.4	<i>The load history and the multi-step analysis</i>	97
5.3.5	<i>The mesh</i>	98
5.4	NUMERICAL VS. EXPERIMENTAL RESULTS ON THE PTED CONNECTION	100
5.4.1	<i>Global response curves</i>	100
5.4.2	<i>Deformed configurations of the node</i>	101
5.5	BEHAVIOUR OF THE COMPONENT PARTS	103
5.5.1	<i>Preliminary remarks</i>	103
5.5.2	<i>Assembled node</i>	103
5.5.3	<i>Beams</i>	105
5.5.4	<i>Column</i>	107
5.5.5	<i>Reinforcing plates</i>	108
5.5.6	<i>Shim plates</i>	110
5.5.7	<i>PT strands</i>	112
5.5.8	<i>ED angles</i>	113
5.6	SYNTHESIS OF RESULTS.....	115

Chapter 6

	Comparison with welded connections	117
6.1	INTRODUCTORY REMARKS	117
6.2	CALIBRATION OF THE WELDED CONNECTION MODEL	118
6.2.1	<i>The reference experimental study</i>	118

6.2.2	<i>Focused aspects for the calibration</i>	121
6.2.3	<i>The “calibration” finite element model</i>	122
6.2.4	<i>Numerical vs. experimental results</i>	125
6.3	PT AND ED BARS VS. WELDED CONNECTION	126
6.3.1	<i>General</i>	126
6.3.2	<i>The finite element model of the welded connection</i>	126
6.3.3	<i>Comparison between PTED and welded connection global responses</i>	130
6.3.4	<i>Behaviour of the component parts</i>	132
6.4	PT STRANDS AND ED ANGLES VS. WELDED CONNECTION	140
6.4.1	<i>General</i>	140
6.4.2	<i>The finite element model of the welded connection</i>	140
6.4.3	<i>Comparison between PTED and welded connection global responses</i>	143
6.4.4	<i>Behaviour of the component parts</i>	146
6.5	SYNTHESIS OF RESULTS.....	153

Chapter 7

	Comparative analysis of PTED connections	157
7.1	THE STUDY PTED CONNECTIONS	157
7.1.1	<i>General</i>	157
7.1.2	<i>Design of the connection with PT and ED bars</i>	159
7.2	THE NUMERICAL MODELS.....	161
7.2.1	<i>The geometry of the models</i>	161
7.2.2	<i>The properties of the materials</i>	162
7.2.3	<i>The interactions between the component parts</i>	162
7.2.4	<i>The load history</i>	164
7.2.5	<i>The mesh</i>	164
7.3	COMPARATIVE EVALUATION.....	166

7.3.1	<i>Global response curves</i>	166
7.3.2	<i>Deformation and stress states of the connections</i>	168
7.4	SYNTHESIS OF RESULTS	174

Chapter 8

Monotonic response	177	
8.1	INTRODUCTORY REMARKS	177
8.2	THE NUMERICAL MODEL	178
8.3	THE RESPONSE CURVES	181
8.4	DEFORMATION AND STRESS STATES	184
8.5	SYNTHESIS OF RESULTS	186

Chapter 9

Behaviour under vertical and horizontal loads	189	
9.1	INTRODUCTORY REMARKS	189
9.2	THE NUMERICAL MODEL	189
9.3	THE SYSTEM RESPONSE	193
9.4	SYNTHESIS OF RESULTS	195

Conclusive remarks and further developments	197
--	------------

References	209
-------------------------	------------

Chapter 1

Introduction

1.1 GENERALITIES ON PTED SYSTEMS

Post-Tensioned Energy Dissipating (PTED) beam-to-column connections are structural systems proposed in recent years as a suitable alternative to welded connections for steel moment resisting frames (MRFs) in seismic areas (Ricles et al., 2001, 2002b, 2006; Christopoulos et al., 2002a, b; Christopoulos and Filiatrault, 2002, 2003; Garlock et al., 2005; Rojas et al., 2006; Wolski et al., 2006; Chou et al., 2006; Tsai et al., 2007). They are conceived for preventing the formation of brittle fractures in the nodal areas of steel MRFs, which can cause strong reduction of the frame ductility features, as occurred in many cases during the 1994 Northridge (California, USA) earthquake. Moreover, they are in principle able to provide the structure with self-centring capability and energy dissipation capacity. In fact, the cyclic behaviour of PTED systems is flag-shaped, namely it is characterized by non-linearity, energy dissipation capacity and re-centring properties.

The non-linear behaviour is essentially due to the particular kinematics of PTED systems, consisting in the opening of a rotational gap at the beam-to-column interface, which is closed in service conditions and opens under severe seismic actions. The dissipation of the input energy is provided by ad-hoc sub-systems, usually called ED systems. During a severe earthquake, they dissipate energy through cycles of inelastic deformations or by friction mechanisms, and in this way the main structural elements, namely the beams

and the columns, are prevented from damage, which is confined to the ED elements. The re-centring capability is provided by the ad-hoc PT systems, made by high resistant steel elements, which are post-tensioned in elastic range. During a severe earthquake, due to the gap opening at the beam-to-column interface, their length increases. Consequently, the elastic returning action in the PT elements continuously tends to re-establish their initial length, so bringing the structure towards the pre-earthquake configuration.

The result of the above peculiarities is that a steel frame equipped with appropriately designed PTED connections can undergo severe earthquakes with negligible or absent cumulative damage in the main structural elements and, above all, without residual displacements after the seismic event. The latter aspect is worth of notice, the residual deformations representing an important aspect for the evaluation of the seismic performance of a structure (Pampanin et al., 2002). In fact, it is clear that large residual deformations, which are usually expected in the case of MRFs with welded rigid nodes, can impair the structural response to subsequent earthquakes, can result in partial or total collapse, and can increase the cost of repair or replacement of non-structural elements, due to the altered rest position.

Well designed PTED connections can give raise to a steel frame matching the necessary requisites of stiffness, strength, ductility and dissipation capacity. The attractive additional peculiarity of sustaining negligible residual deformations increases the appeal of such systems, which can guarantee advantages from both the structural and economic points of view.

On the basis of the above considerations, PTED connections appear as a very interesting solution for earthquake resisting steel moment frames, their “sustainable” nature making them a promising alternative to more traditional beam-to-column node typologies.

1.2 OBJECTIVE OF THE RESEARCH AND METHODOLOGY

Up to today, several technological solutions have been proposed for the practical implementation of the PTED concept in steel moment resisting frames, the differences among them essentially consisting in the way the PT and ED systems are realized. The relative novelty of PTED beam-to-column

connections for steel moment resisting frames requires deep investigations on their cyclic behaviour. Consequently, the validation process of PTED connections is ongoing in several parts of the world, and it is based on both experimental and numerical campaigns. The studies are focused on both the local behaviour of the connections and the global performances of frames incorporating them.

The research presented in this work is framed in the numerical studies aimed at the development of PTED connections. The main objectives of the research may be summarized as follows.

The first scope, which can be considered a preliminary step of the research, is the set up of reliable numerical models of PTED connections, directly calibrated against the available experimental results. The main aim is creating an investigation tool useful for achieving information complementary to the experimental ones.

Once the set up numerical models prove to be trustworthy, the first objective is investigating in detail the cyclic behaviour of some connections already tested experimentally, with the scope of acquiring behavioural information difficult to catch or measure during the experimental tests.

The second objective is represented by the comparison of the cyclic behaviour of PTED beam-to-column connections with that of the corresponding welded rigid nodes, which are considered as reference cases.

Another aim of the research is the comparative analysis between the performances of PTED connections characterized by different PT and ED arrangements, with the scope of pointing out the advantages and disadvantages of the diverse technological solutions, so to provide information useful for the system optimization.

The research is also focused on the behaviour of the considered PTED connections beyond the displacement levels considered during the experimental analyses, in order to catch their possible crisis modes, and on their performances under both vertical and horizontal loads.

The numerical analyses developed in this research are carried out by means of the ABAQUS advanced multi-purpose computer program (2004), which is based on the Finite Element Method. The actual geometrical and mechanical features of any structural system can be reproduced in detail by means of such software, so that the behaviour of any component parts can be investigated

and understood. In addition, such software allows to catch the peculiarities of the complex behaviour of PTED connections, which are characterized by the combined presence of different sources of non-linearity, such as material plasticity, large displacements and contact interactions. Consequently, the numerical results can be very reliable and so the numerical models can be used as a virtual laboratory.

1.3 OUTLINE OF THE WORK

This work is organized into nine chapters. After brief introductory remarks on the PTED concept, on the main objectives of the research and on the followed study methodology, reported in Chapter 1, the features of PTED systems are described in Chapter 2. Since the PTED beam-to-column connections are proposed as an alternative to welded rigid ones, preliminary considerations on traditional steel moment resisting frames are provided, focusing on their peculiarities in terms of stiffness, strength, ductility and dissipation capacity. A review of the unexpected fracture problems occurred in the nodal areas of welded rigid connections during the 1994 Northridge (California, USA) earthquake is outlined. Afterwards, the features of PTED beam-to-column connections are illustrated, focusing on their mechanical behaviour and on the related practical advantages. The final part of the chapter is devoted to an overview on the prior research on PTED beam-to-column connections for steel moment frames, in which the technological solutions proposed and studied up to today are presented and described.

Chapter 3 deals with the use of numerical analyses, based on the Finite Element Method, for the investigation of the cyclic behaviour of PTED connections. General information on the Finite Element Method is provided. In addition, in the second part of the chapter, the main characteristics of the ABAQUS advanced computer program are described, focusing in particular on the features and capabilities used for the set up of the refined models of PTED connections.

In Chapter 4 the attention is focused on the PTED beam-to-column connection system proposed and studied by Christopoulos et al. (2002a). After a brief description of the test assemblage and results, the corresponding

refined numerical models, whose calibration is carried out against the experimental results, are described in detail. The obtained numerical results are used for the investigation of the cyclic behaviour of the tested and reproduced system.

The structure of Chapter 5 is similar to that of Chapter 4, it being aimed at the numerical reproduction of the experimental test carried out by Ricles et al. (2002b). Also in this case, the models are calibrated against the available experimental evidence and the investigation of the connection behaviour is carried out.

Chapter 6 is devoted to the comparison of PTED connections with welded rigid ones. At this aim, the models presented in the previous chapters are used. In addition, ad-hoc numerical models of the corresponding welded nodes, characterized by the same beam and column assemblages, are developed, in order to carry out the behavioural comparison.

Chapter 7 deals with the comparative evaluation of the performances of PTED connections with different PT and ED system arrangements.

In Chapter 8 the ultimate behaviour of the PTED connection presented in Chapter 4 is addressed, focusing on the possible collapse modes.

Chapter 9 describes the preliminary analyses carried out on a steel frame sub-assembly, equipped with PTED connections, under the combination of vertical and horizontal loads.

At last, the main conclusions of the work, together with possible further developments for future research, are illustrated.

Chapter 2

Towards PTED beam-to-column connections

2.1 STRUCTURES IN SEISMIC AREAS

2.1.1 *Performance-Based Design fundamentals*

The modern approach for the structural design in seismic regions is the Performance-Based Design (PBD). According to the PBD philosophy, the structures must be able to guarantee adequate performances with relation to the different expected earthquake intensities. The seismic performance of a structure is usually associated to the damage undergone by non-structural and/or structural elements, which, in turn, is generally evaluated on the basis of the maximum displacements reached during the earthquake. The need of considering the residual displacements for the performance evaluation is also felt (Pampanin et al., 2002). In short, the key role in the performance evaluation of structures in seismic areas is played by displacements.

Different performance levels can be considered, as reported, for instance, in SEAOC Vision 2000 (1995), where the Fully Operational, Operational, Life Safe and Near Collapse performance levels are defined and correlated to displacement parameters. In the above document, the performance levels are defined as follows. At the Fully Operational level no damage occurs, and the consequences on the building user community are negligible. At the

Operational level, moderate damage to non-structural elements and contents, and light damage to structural elements occurs; in addition, the damage does not compromise the safety for the occupancy of the building. At the Life Safe level, moderate damage to structural and non-structural elements occurs; in addition, the structure's lateral stiffness and ability to resist additional lateral loads is reduced, but some safety margins against collapse remain. At the Near Collapse level, the lateral and vertical load resistance of the building is substantially compromised, so that aftershocks could result in partial or total collapse of the structure.

The above concepts may be summarized by saying that structures designed according to the Performance-Based approach should be able to withstand, on one side, frequent low-intensity earthquakes with absent or negligible damage to the structural and non-structural elements, and, on the other side, rare high-intensity earthquakes without reaching the collapse.

These aims could be achieved, at least in principle, by realizing structures which behave in the elastic field also in the case of a major earthquake. Such requisite can lead to structures characterized by very large structural members, which are strongly oversized with respect to their normal service life conditions. Considering the low probability of occurrence of the maximum expected earthquake, it is clear that, from an economical point of view, it is not convenient to design structures behaving in the elastic field also in the case of a major earthquake. In addition, a structure designed for reaching the elastic limit under the maximum expected earthquake could collapse in case of stronger seismic events, which are possible due to the random nature of earthquakes.

Based on the above considerations, the modern trend is designing structures which, in case of frequent low-intensity earthquakes, are stiff enough to limit the deformations and displacements so to prevent the damage in structural and non-structural elements. Moreover, they have to be able to withstand a severe earthquake without collapses. The latter condition can be achieved also at the price of undergoing severe damage in the structural elements, provided that their load carrying capacity is not reduced in case of large inelastic excursions: in few words, through a ductile structural behaviour.

It is consequently clear that, besides the obvious strength requirements, seismic resistant structures must be endowed with both stiffness and ductility features. In addition, another fundamental requirement is the capacity of dissipating the input energy received during the earthquake.

With particular regard to the ductility, it can be observed that it is strictly related to the capacity of dissipating the input energy. In fact, since a ductile structure is able to reach large inelastic displacements, under a seismic excitation it is characterized by a cyclic hysteretic behaviour.

Ductility may be referred to different scales, namely material, cross-section, structural member and structure. The ductility of the material is its capacity to undergo inelastic deformations without substantial stress reduction. The flexural ductility of the cross-section is usually defined as the capability of undergoing large curvature demands in the inelastic field without substantial reduction of the bending moment. The ductility of the structural member is generally referred to as the capability of the member of undergoing displacements or rotations in the inelastic field without substantial reduction of the force or bending moment. At last, the ductility of the structure is its capability of undergoing large displacements in the inelastic field without reduction of forces.

The above different levels of ductility are undoubtedly interrelated, but the relationship is not immediate, in the sense that, for example, a structure made of a ductile material is not necessarily ductile at global level, and so on. As a general rule, different damage or collapse modes, which can be either ductile or brittle, may occur in a given structure. In order to obtain a ductile collapse mechanism, the structure must be designed and constructed so that the ductile mechanisms are attained before the occurrence of brittle ones. At this aim, the ductile elements, which are the ones devoted to the dissipation of the input energy, must be designed so to be the first ones to reach the plastic field and, thanks to a stable hysteretic cyclic behaviour, to dissipate the input energy. The non-dissipative structural elements, on the other hand, must be designed to remain in the elastic field during the earthquake excitation, when the dissipative ones reach their own resistance. Consequently, a different approach is needed for the design of the dissipative and non-dissipative structural elements. The former ones must be designed for the actual demand deriving from the structural calculations. The latter ones, on the contrary, must

be designed for the demand corresponding to the achievement of the whole resistance of the dissipative elements, taking into account also the over-strength phenomena. This approach is usually called Capacity Design, due to the fact that the non-dissipative elements are designed for the capacity of the dissipative ones. Definitely, the achievement of a global ductile behaviour strongly depends on the conception of the whole structure and on the care in the realization of the constructional details.

The main advantages of ductile structures may be summarized as follows (Petrini et al., 2004): (1) brittle collapses, which can lead to sudden and catastrophic consequences, are prevented; (2) the input seismic energy is reduced cycle by cycle, due to the dissipative features of the structure; (3) the total cost of the structure is lower than that in the case of linear elastic design; (4) the increase of the periods of vibration, due to the inelastic deformations in some parts of the structure, causes a reduction of the structural response.

2.1.2 *Seismic resistant steel structures*

In the case of steel structures, the capability to bear horizontal actions may be achieved in several ways, which correspond to diverse combinations of the initial stiffness, strength and ductility characteristics. Consequently, different types of earthquake resistant steel structures may be conceived, which depend on the selected load carrying mechanism. The most spread types of earthquake resistant steel structures are the Moment Resisting Frames (MRFs), the Centrically Braced Frames (CBFs) and the Eccentrically Braced Frames (EBFs), whose main features are summarized in the following.

Moment Resisting Frames (Fig. 2.1a) are made of straight members rigidly connected each other at their ends. This guarantees evident architectural advantages, since the meshes of the frame are not occupied by structural elements, leading to extreme functional flexibility. The capability of resisting to the horizontal actions is essentially based on the flexural regime occurring in the beams and the columns. In general, the initial lateral stiffness of steel MRFs is quite poor, and so this kind of structures may have excessive deformability problems, with consequent potential damage to non-structural elements in case of low-intensity earthquakes. On the other side, with regard to the energy dissipation capacity, steel MRFs are in principle able to exhibit very good performances under severe earthquakes. Ductile collapse behaviour

in MRFs is achieved if the energy dissipation takes place through cycles of plastic deformations in bending at the ends of the structural members. These areas are interested by the so called plastic hinges, and the most convenient collapse distribution in a steel MRF foresees plastic hinges at the beam ends and at the column bases (Fig. 2.1b). This leads to a global mechanism, which maximises the amount of dissipated energy and, in addition, causes a local ductility demand lower than that corresponding to other collapse mechanisms, such as those with plastic hinges at the ends of the columns. In the perspective of the capacity design, it is clear that the beams are the dissipative elements, whereas the connections and the columns are the non-dissipative ones, and must be designed accordingly. In particular, the conception and realization of the beam-to-column nodes is rather delicate, since they must be over-resistant with respect to the connected beams and must, at least in principle, prevent any relative rotation between the connected members.

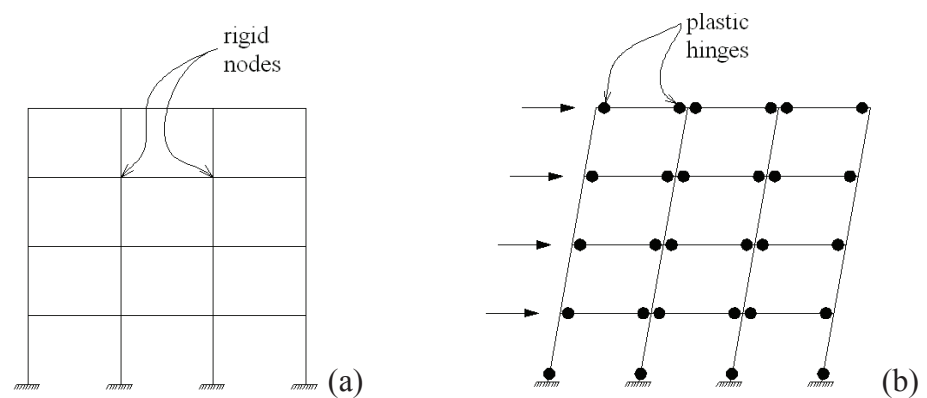


Figure 2.1. Moment Resisting Frames: (a) general scheme; (b) global collapse mechanism

Concentrically Braced Frames (Fig. 2.2a) are made of structural members which, from a theoretical point of view, may be connected each other by means of simple flexural hinges. The resistance to horizontal forces is achieved by means of ad-hoc braces, which essentially work in tension or compression. From an architectural point of view, the meshes of the frame which are occupied by the braces can not be used for openings, with

consequent functional flexibility reduction. The initial lateral stiffness of CBFs is generally high, due to the axial stiffness of the braces. On the other hand, the capacity of dissipating the input seismic energy is quite poor, it being based on the plasticization of braces in tension. The effectiveness of this dissipation mechanism is reduced cycle by cycle, due to the degradation caused by the repeated buckling undergone when braces are subjected to compression (Fig. 2.2b). From the capacity design point of view, the dissipative elements are the braces, whereas the connections, the beams and the columns must be over-resistant, behaving in the elastic field up to the failure of the braces.

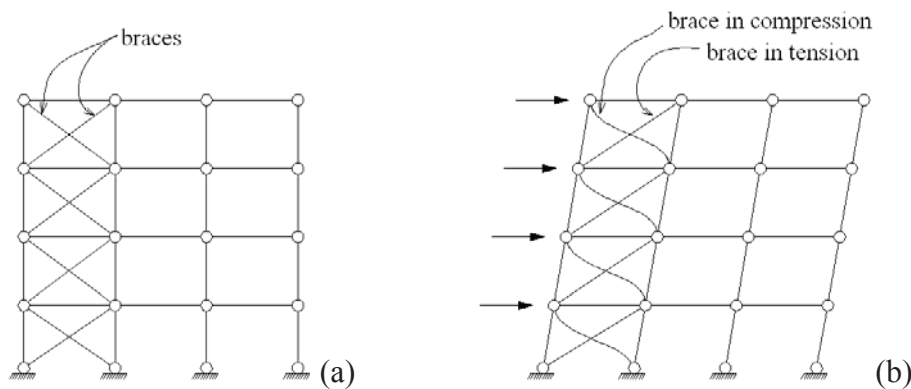


Figure 2.2. Concentrically Braced Frames: (a) general scheme; (b) collapse mechanism

Eccentrically Braced Frames (Fig. 2.3a) are a sort of “compromise” between Moment Resisting Frames and Concentrically Braced Frames. They are conceived for combining the advantages of MRFs, in terms of ductility and energy dissipation capacity, with those of CBFs, in terms of lateral stiffness. Also in terms of architectural flexibility, the EBF solution shows intermediate peculiarities. The basic idea is to endow Moment Resisting Frames with appropriate braces, which reduce the lateral deformability of the frame. At the same time, since at least one end of the braces is connected to the beams, a part of these, usually called “link”, is devoted to the dissipation of the input energy, by yielding in shear and/or bending moment (Fig. 2.3b).

In this way, the stiffness and ductility properties can be in principle adequately calibrated, so leading towards optimal structural solutions. The performances of the structure are strongly dependent on the behaviour of the links, which require particular care in phase of design.

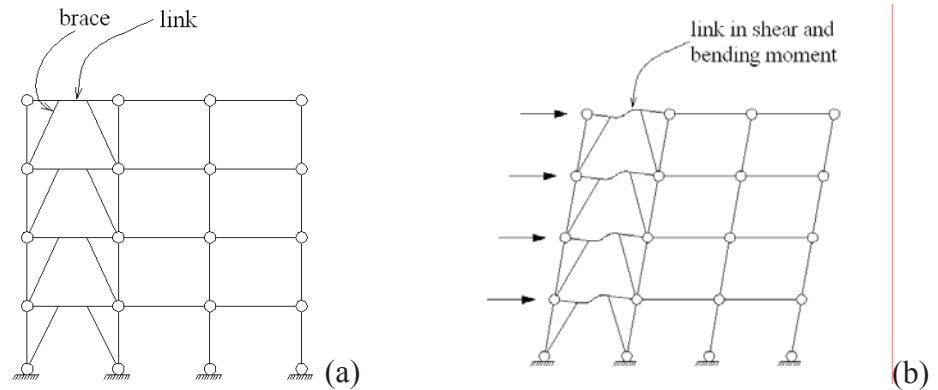


Figure 2.3. Eccentrically Braced Frames: (a) general scheme; (b) collapse mechanism

The connections dealt with in this work are conceived for steel Moment Resisting Frames, due to their unexpected non-ductile behaviour shown during the 1994 Northridge (California, USA) earthquake. Consequently, in the following the attention is focused on steel MRFs, with particular care to the aspects related to the nodal constructional details, to their performances in the above mentioned earthquake, and to the research developed subsequently.

2.1.3 Behaviour of steel MRFs during the 1994 Northridge earthquake

During the second half of 20th Century, a large diffusion of steel moment resisting frames took place, since they were regarded as the most ductile earthquake resistant systems. It was agreed that steel MRFs were practically invulnerable to earthquake-induced structural damage, which was expected to consist, at the maximum, in ductile yielding of members and connections, the earthquake-induced collapse being considered impossible (FEMA, 2000). Unfortunately, during the 1994 Northridge (California, USA) earthquake, this

belief proved to be faulty. In fact, although the above mentioned earthquake caused damages also in other types of steel structures, affecting for example base plates and diagonal braces, the most common damage pattern consisted in unexpected brittle fractures in the beam-to-column connections of steel MRFs (Youssef et al., 1995).

A wide variety of buildings was affected by this type of damage. Their height ranged from 1 to 27 storeys and they could be new constructions as well as 30 years old ones. Moreover, the damaged buildings were spread over a large geographical area, including sites which experienced only moderate levels of ground shaking (Youssef et al., 1995).

Broadly speaking, it can be observed that the MRFs damaged by the Northridge earthquake essentially met the code intent, since the undergone structural damage was quite limited and no collapses occurred. The real problem was that the structures did not behave as it was expected, showing an extremely low ductility due to the occurrence of brittle fractures. In addition, the damage in the connections caused significant economic losses, which, in some cases, concerned structures subjected to ground shakings less severe than the design one (FEMA, 2000).

In the typical pre-Northridge beam-to-column connection detail for steel MRFs (Fig. 2.4a), the beam flanges were welded to the column flanges through complete penetration groove welds, whereas the beam webs were connected to the column by means of bolts.

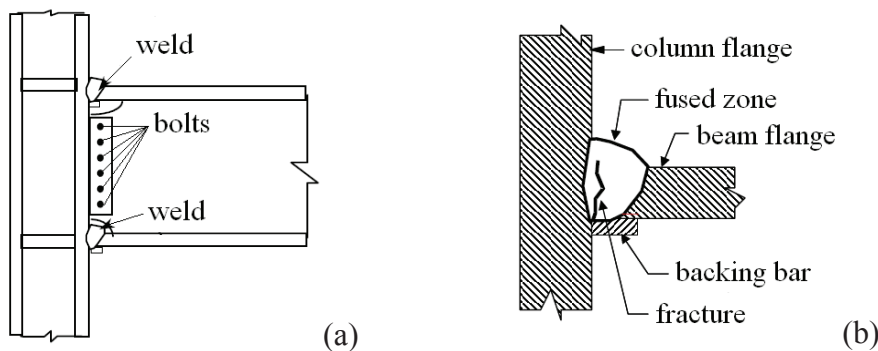


Figure 2.4. (a) Typical pre-Northridge beam-to-column connection for steel MRFs; (b) common zone of fracture initiation (adapted ex FEMA, 2000)

According to the US building code, since its 1988 edition, this kind of constructional detail could be used without supporting calculations or specific testing. Such confidence on the connection performances was based on the results of experimental campaigns carried out during the early 1970's, where the above described constructional detail provided adequate strength and plastic capacity rotation. Although the obtained results were referred to specific beam sizes and load patterns, a significant confidence in that connection detail led to its use in a variety of member sizes, frame dimensions, shear connectors, flange weld processes and lateral force resisting system configurations (Youssef et al., 1995).

The fractures detected after the Northridge earthquake usually initiated in the complete joint penetration weld between the beam bottom flange and the column flange (Fig. 2.4b), leading to different fracture patterns which could involve the fused zone (Fig. 2.5a), the column flange portion behind the weld (Fig. 2.5b), the whole thickness of the column flange (Fig. 2.5c), or the column web (Fig. 2.5d).

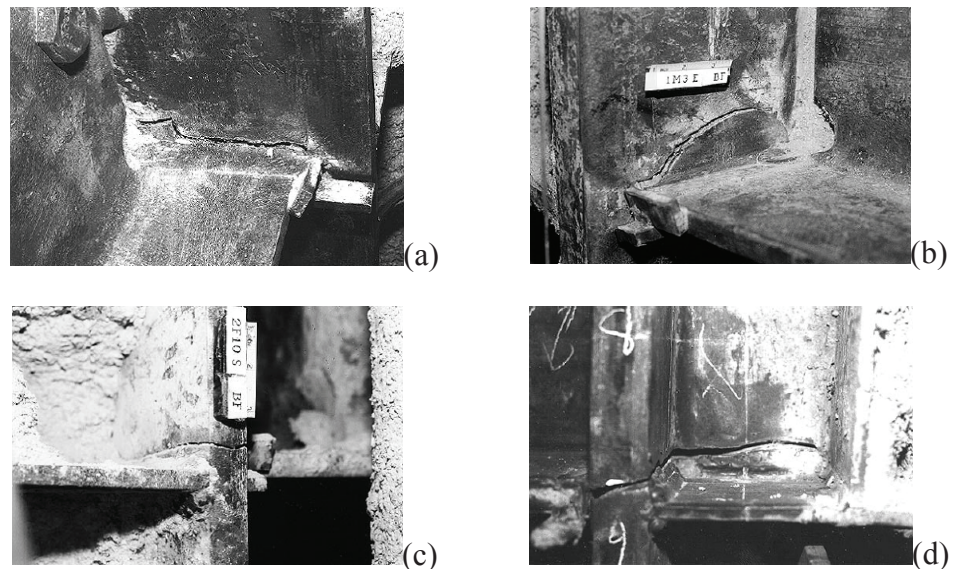


Figure 2.5. Damages occurred in the connections during the 1994 Northridge earthquake: (a) at the fused zone; (b) at the column flange behind the weld; (c) at the column flange; (d) at the column web (FEMA, 2000)

The main causes for the occurrence of the experienced fractures may be summarized as follows (FEMA, 2000; Christopoulos et al., 2002a):

- The cross-section at the beam-to-column interface is the weakest location in the assembly, and it usually undergoes the severest stress peaks;
- The execution of the joint at the beam bottom flange is obstructed by the presence of the beam web and it usually requires multiple passes, resulting in a poor quality welding, with flaws that can potentially be crack initiators;
- The presence of the bottom flange backing bar reduces the possibility of visual inspection of the weld root, with the consequent likely presence of undetected defects;
- The beam flanges carry a non-negligible portion of the shear stresses, which are usually ignored in the design, causing additional stress demands in the weld joints;
- The presence of the weld access holes may induce severe stress concentrations in the beam flanges, with the consequent possibility of low-cycle fatigue problems;
- The large shear deformability of weak panel zones, quite spread in the common practice with this kind of details, leads to high stress and strain demands in the joint between beam flange and column flange;
- The low toughness of the welding consumables used by many building erectors, eventually compromised by excessive deposition rates, can result in large defects which can potentially induce cracks at stresses approximating the yield strength of the beam steel, making the development of ductile behaviour impossible;
- The large depth of the beams, due to the spread use of low redundant structures characterized by a small number of moment resisting connections, increases the strain demand on the beams and, as a consequence, on the welded connections;
- The use of beams characterized by elevated steel grades makes the joint metal under-matched, with consequent increase of its vulnerability;

- The increase of the base material yield stress, due to the loading rate, increases the stress demand in the weld joints;
- The presence of the floor slab, acting together with the beam steel, results in the increase of the tensile strains at the beam bottom flange.

On the basis of the above considerations, the necessity of making several changes to the past practice was strongly felt. At this aim, the FEMA-funded SAC Steel Project was addressed to develop practical and simple models for predicting the stiffness, resistance and ductility of connections for steel MRFs (Roeder, 2000; Kunnath and Malley, 2002).

Several and large efforts were made for studying and modelling structural solutions able to guarantee the ductile behaviour of connections for steel MRFs. Figure 2.6 shows some of the typical systems examined in the experimental research (Roeder, 2000), all aiming at improving the connection performance.

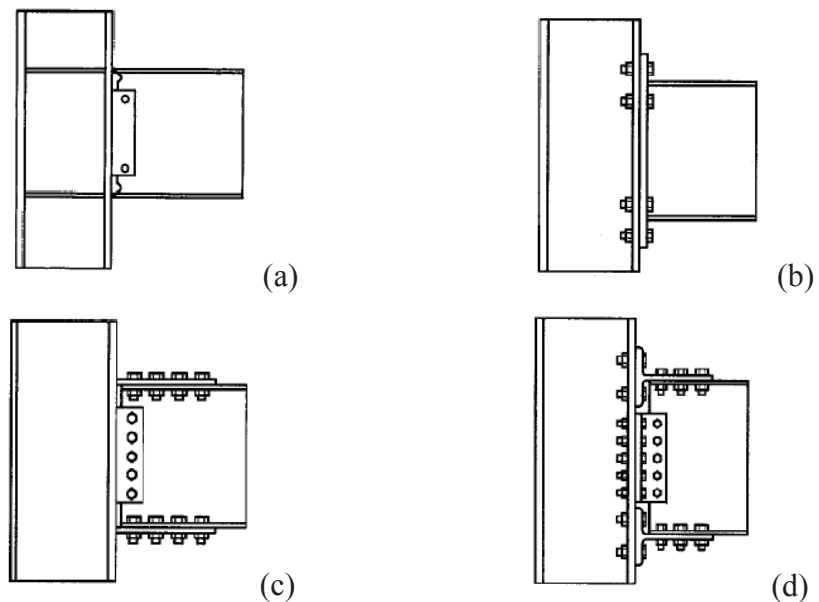


Figure 2.6. Typical connections studied after the Northridge earthquake: (a) welded flange-welded web; (b) extended end plate; (c) bolted flange plate; (d) bolted T-stub (Roeder, 2000)

Figure 2.7 shows the detail of other studied connections, namely the Reduced Beam Section (RBS – Fig. 2.7a) and the welded haunch (Fig. 2.7b), conceived for moving the plastic hinge location at some distance from the beam-to-column interface, preserving the connection from the risk of brittle fractures.

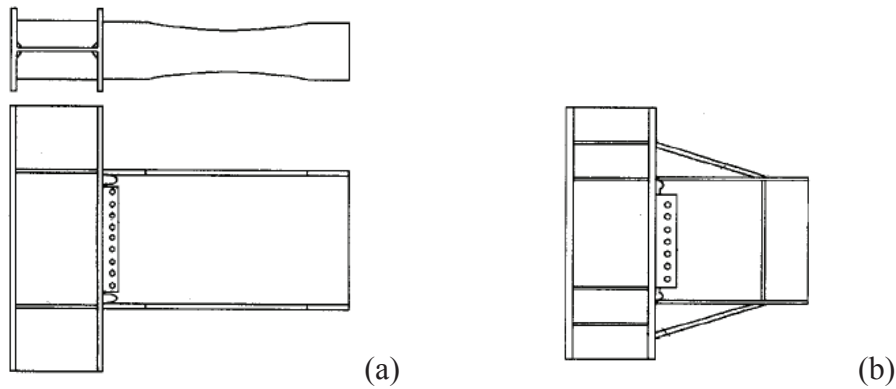


Figure 2.7. Constructional details for moving the plastic hinge location: (a) Reduced Beam Section; (b) welded haunch (Roeder, 2000)

2.2 PTED CONNECTIONS

2.2.1 PTED connections in precast pre-stressed structures

From the historical point of view, the conception of PTED beam-to-column connections, characterized by a flag-shaped cyclic behaviour, was firstly referred to precast pre-stressed reinforced concrete structures. The main motivation was that, despite the clear technological advantages offered by precast reinforced concrete constructions, such as the quality control and the speed of erection, their structural peculiarities are usually neglected in the case of constructions in seismic areas. This is due to the brittle behaviour of high resistant steel strands, whose failure would lead to the brittle collapse of the whole construction.

In general, the most spread beam-to-column node type in precast structures is a sort of emulation of the one typical of ordinary reinforced concrete structures, since the precast structural members are mutually connected by cast-in-place nodal areas. In the case of correctly designed ordinary reinforced concrete structures, such type of connection allows the formation of plastic hinges at the beam ends, whereas this must be avoided in the case of precast structures, due to the brittle behaviour of their beams (Pampanin, 2003). An alternative for endowing precast pre-stressed structures with ductility features is represented by the use of PTED connections, which were extensively studied experimentally at the NIST (National Institute of Standard and Technology) in the USA, and within the PRESS (PREcast Seismic Structural Systems) research programme (Nakani et al., 1999). The principle of such systems is that the beams and columns essentially act as rigid bodies, whereas the deformations of the system are concentrated at the beam-to-column joints (Stanton et al., 1997).

The first step towards this kind of ductile nodes in precast pre-stressed structures was made by Priestley and Tao (1993), who conceived connections with partially de-bonded tendons (Fig. 2.8). In this way, the elongation mainly occurs in the de-bonded part of the tendons, whose length can be tailored so that the strains are always elastic. Such solution leads to connections characterized by a bi-linear elastic cyclic behaviour, which are self-centring but do not dissipate the input energy.

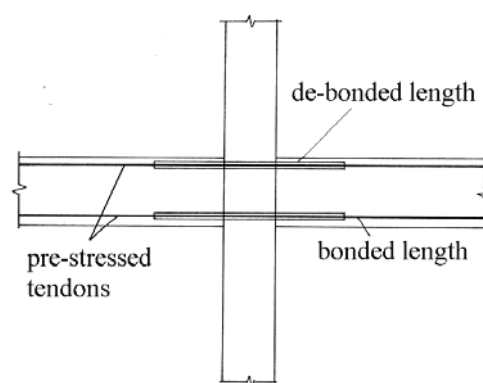


Figure 2.8. Scheme of the self-centring beam-to-column connection with partially de-bonded tendons (Priestley and Tao, 1993)

Afterwards, Stanton et al. (1997) proposed a system with both partially de-bonded tendons, aimed at guaranteeing the self-centring capability, and bonded mild steel bars, located at the top and bottom sides of the beam ends, aimed at dissipating the input energy (Fig. 2.9). Such systems, in which a PT and an ED system are associated, are called “hybrid systems” and result in the desired flag-shaped cyclic behaviour.

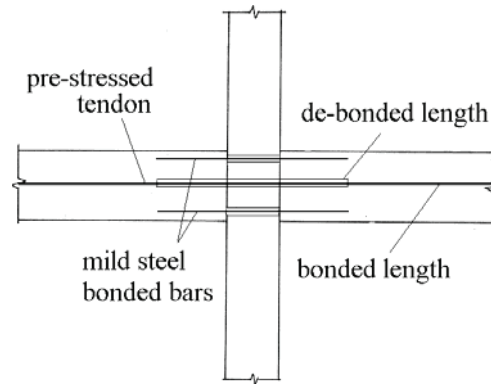


Figure 2.9. Scheme of the self-centring energy dissipating “hybrid” beam-to-column connection with partially de-bonded tendons and bonded bars (Stanton et al., 1997)

2.2.2 Why PTED connections in steel MRFs?

In the field of steel structures, the results of the researches mentioned in section 2.1.3 led to the definition of constructional details able to assure a ductile behaviour, with the full development of plastic hinges in the beams. The expected performances consist in the formation of stable mechanisms either through yielding of the beams, yielding of the panel zones or a combination of both, without any brittle fracture. Unfortunately, these stricter requirements result in the increase of fabrication and erection costs of moment resisting frames (Christopoulos et al., 2002a). In addition, provided that such improved or innovative connections work as desired, they are expected to result in significant yielding and local buckling in the beams under the design earthquake (Ricles et al., 2001; Christopoulos et al., 2002a). In fact, the

structural damage present in a steel moment resisting frame after a severe earthquake is accepted as the price for the energy dissipation capacity, in the perspective of the ductile behaviour guaranteed by the above discussed global collapse mechanism.

The assessment of the state of a structure strongly damaged by a severe earthquake and the prevision of its performances in case of a possible following earthquake are rather difficult. In general, a structure damaged by a major earthquake may be susceptible of partial or total loss if static incipient collapse is reached. In addition, its behaviour in case of following earthquakes may be severely impaired due to the occurred structural damage. Moreover, the distorted configuration of the structure may induce concern in the occupants and may increase the repair costs of non-structural elements (Pampanin et al., 2002). At last, in some cases, the demolition of the structure can be the only viable choice.

Based on the above considerations and taking into account the experience matured in the field of precast pre-stressed reinforced concrete structures, the concept of hybrid systems, characterized by the presence of both a system dedicated to the re-centring of the structure and a system dedicated to the dissipation of the input energy, was applied to steel moment resisting frames.

PTED beam-to-column connections are conceived as a suitable alternative to welded rigid connections for steel MRFs. They are aimed at guaranteeing a ductile and stable behaviour during severe earthquakes, together with both self-centring and energy dissipation capabilities, resulting in a flag-shaped cyclic behaviour.

The main advantages offered by PTED beam-to-column connections are summarized by Ricles et al. (2001), and are reported herein:

- No field welding is required, so the possible occurrence of brittle fractures, as the ones experienced during the 1994 Northridge earthquake, is prevented;
- Conventional materials and skills are sufficient for assembling the connections, differently from the case of typical rigid connections, whose full penetration welds require particular care;
- The initial stiffness of the connection is similar to that of a typical welded connection;

- The connection behaviour is self-centring without residual deformations, so that no residual drifts are expected in a PTED-equipped moment resisting frame, provided that no significant residual deformations occur at the column bases;
- The main structural elements, namely the beams and the columns, remain essentially elastic;
- The damage is confined to ad-hoc sacrificial devices located in the connection, which are devoted to the dissipation of the input energy;
- The sacrificial devices, which are the only elements expected to sustain inelastic deformations, are easily replaceable, so the performances of the structure after a major earthquake are practically the same as the initial ones, provided that the low-cost substitution of the above devices is carried out.

2.2.3 PTED connections mechanical behaviour

PTED beam-to-column connections are expected to provide a flag-shaped cyclic hysteretic behaviour (Fig. 2.10), which is characterized by non-linearity, self-centring capability and energy dissipation capacity.

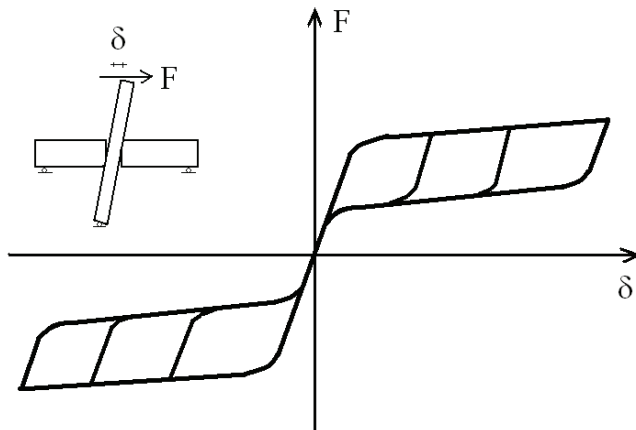


Figure 2.10. Typical flag-shaped hysteretic behaviour in a PTED connection

In steel frames equipped with PTED connections, the transmission of the internal forces between beams and columns is essentially guaranteed by the PT action, which generates an uniform distribution of contact stresses in compression at the beam-to-column interface (Fig. 2.11). Shear force is transmitted by the friction between beam and column, due to the normal contact stresses. Anyway, the presence of redundant shear bearing systems, like bolted top-and-seat angles (Ricles et al., 2001) or ad-hoc slotted shear tabs (Christopoulos et al., 2002a), may be considered.

After the application of the PT force, the beams and columns are in close contact (Fig. 2.11), and the node behaves like a typical rigid one, it being able to transmit both bending moments and shear forces without beam-to-column relative rotations, for small values of bending moments.

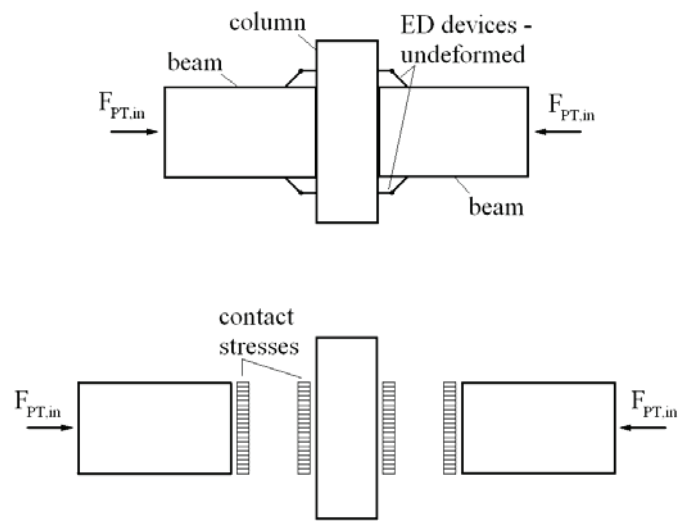


Figure 2.11. PTED beam-to-column connection at the application of the PT force: whole assembly and free body diagrams

The force value in the PT elements is the initial one ($F_{PT,in}$), and the ED devices are undeformed.

As far as the bending moment increases, the contact stresses at the compressed side of the beam-to-column interface rise, whereas the stresses at

the tensile side reduce, up to get equal to zero (Fig. 2.12). The corresponding bending moment is usually referred to as the decompression moment (M_{dec}). At this stage, beams and column are still in full contact, and so the behaviour of the connections is still linear. The force in the PT elements is equal to $F_{PT,in}$, since they do not undergo any elongation, and no deformation in the ED devices occurs.

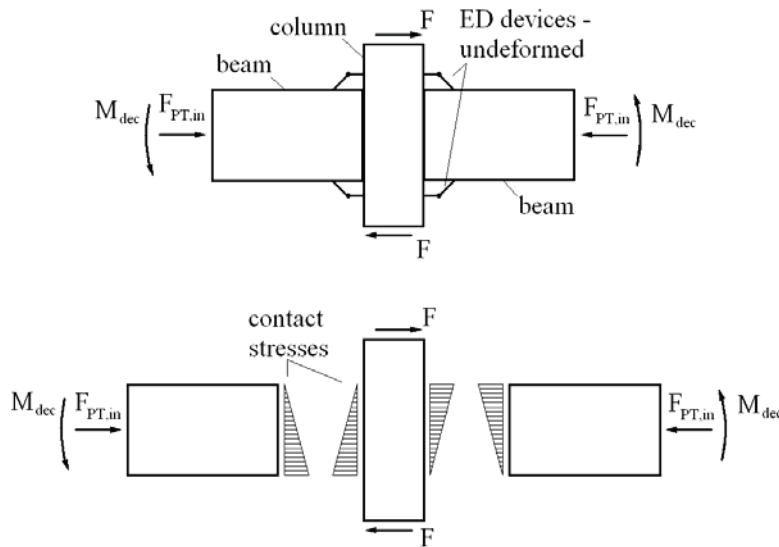


Figure 2.12. PTED beam-to-column connection at the decompression: whole assembly and free body diagrams

For larger values of the bending moment, a gap opens at the beam-to-column interface, with consequent extent reduction of the beam compressed area (Fig. 2.13). The internal forces in the node are transmitted by the contact forces at the beam-to-column interfaces, concentrated in the above mentioned limited contact area, together with the forces and moments occurring in the ED devices.

The gap opening entails the two following phenomena:

- The PT elements elongate in elastic field: the corresponding force (F_{PT}) increases so that the related returning action tends to bring the connection towards the initial configuration, instant by instant;

- The ED devices deform, due to the relative movement between beams and column: the input energy is dissipated in a stable way and the possible damage is confined to the ED elements.

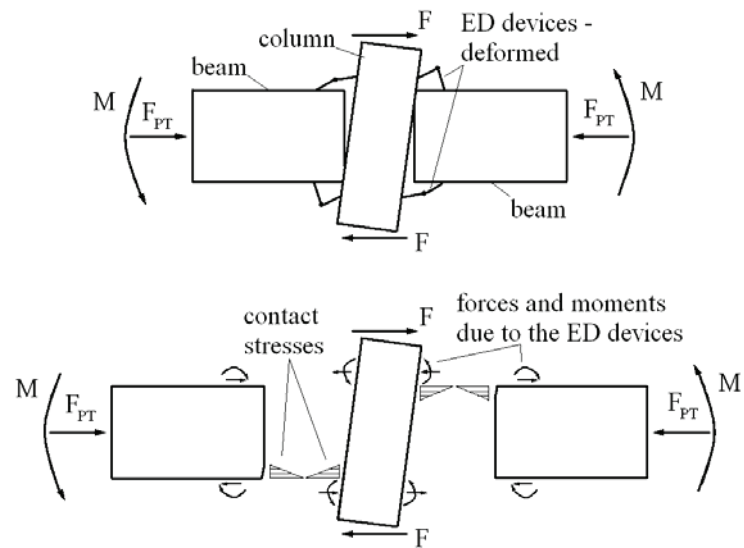


Figure 2.13. PTED beam-to-column connection after the gap opening: whole assembly and free body diagrams

Due to the gap opening, the connection behaviour becomes non-linear. The behaviour of the main structural elements, namely the beams and the columns, is linear elastic, as well as the PT element one, and the main source of non-linearity is the change of the mutual constraint conditions at the beam-to-column interface. The inelastic deformations occurring in the Ed devices are, in addition, another source of non-linearity.

After the opening of the interface gap, the stiffness of the system essentially depends on the elastic stiffness of the PT elements and on the stiffness of the ED devices (pre- or post-elastic one, depending on the displacement demand).

When the earthquake ends, the connection is expected to undergo no residual deformations, except for those occurring in the ED devices, and so well designed PTED-equipped MRFs should sustain no residual drifts.

Obviously, the PT system must be designed to guarantee the full contact at the beam-to-column interface in the serviceability conditions, together with the adequate friction for the shear resistance. Furthermore, it must behave in elastic range in case of severe earthquakes, because the breaking of PT elements would lead to the loss of the self-centring properties of the system and, what is more concerning, to the collapse of the whole structure, due to the lack of shear transmission capability.

2.3 PRIOR RESEARCH ON PTED CONNECTIONS

2.3.1 *Preliminary remarks*

Up to today, several types of beam-to-column connections have been proposed for the actual implementation of the PTED concept in steel moment resisting frames. The main differences among the proposed systems lie in the technological solutions conceived for the PT and ED systems. In particular, the proposed PT systems are based on the use of high resistant steel strands or bars, whereas the proposed ED systems are based on yielding or friction mechanisms.

The validation process of PTED connections is ongoing, based on both experimental and numerical campaigns. The carried out studies have been focused on the cyclic performances of the connections, as well as on the dynamic behaviour of frames equipped with PTED connections.

In the following, a brief overview of the studies on PTED connections performed all over the world is presented. The focused experimental and numerical campaigns are organized on the basis of the selected PT and ED arrangements. Particular attention is paid to the proposed technological solutions, the type of analyses carried out and on the investigated parameters.

2.3.2 *PT steel strands and ED bolted steel top-and-seat angles*

Ricles et al. (2001; 2002b) and Garlock et al. (2005), at the University of Lehigh (USA), have studied a PTED beam-to-column connection system in which the PT system is based on a series of high resistance steel strands,

whereas the ED system is composed by bolted steel top-and-seat angles. The considered connection assemblage is shown in Figure 2.14a, which is referred to an external node.

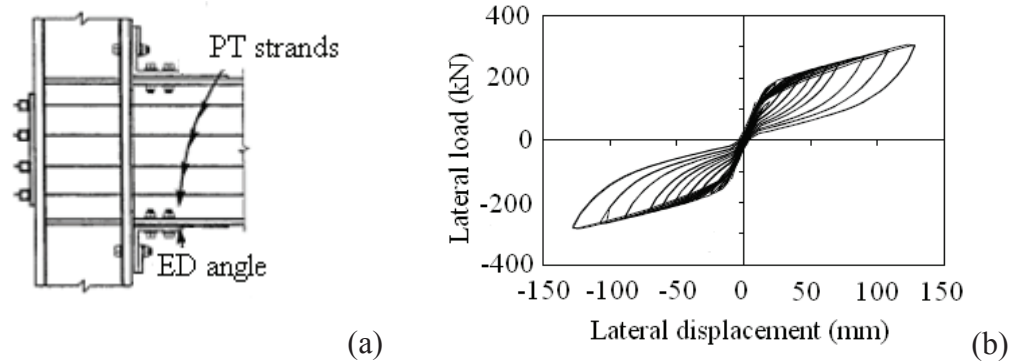


Figure 2.14. PTED connections with PT strands and ED bolted steel top-and-seat angles: (a) typical node; (b) experimental force-displacement curve (Ricles et al., 2001, 2002b)

When the gap at the beam-to-column interface opens, the steel strands elongate in elastic range and the angles deform, undergoing plastic deformations in the stress concentration zones. The dissipative mechanism is based on the formation of three cylindrical plastic hinges at each angle, one next to the column bolt washers and two in the angle fillet.

Besides the dissipation of the input energy, which is their primary scope, the ED angles are useful also during the phases of erection, since they guarantee the capability of bearing the vertical loads before the post-tensioning of the steel strands. In addition, although the PTED connection is conceived for carrying the shear forces only through the friction at the beam-to-column interface, the ED angles may act as a redundant shear bearing system, which could prevent the structural collapse due to vertical loads in the case of unexpected failure of the strands.

The proposed connection has been studied both experimentally and numerically.

Ricles et al. (2002b) have carried out experimental tests on cruciform shaped beam-to-column assemblages, which have proved the effectiveness of

the adopted technical solution, as shown in Figure 2.14b, where a force-displacement flag-shaped hysteretic curve is plotted. In all the tests, the same beam size has been considered, whereas steel wide flange or composite concrete filled steel tubes have been used for the columns. The experimental campaign has focused on the influence, on the PTED connections behaviour, of a series of parameters, namely the presence of shim plates, the presence of beam flange reinforcing plates, the features of the top-and-seat angles, and the presence of the post-tensioning force. The tests have evidenced that the shim and reinforcing plates are necessary to control the inelastic deformation of the beams, that the size and geometry of the angles influence the connection moment capacity and the energy dissipation capacity, and that the strands must be designed to remain elastic in order to assure the self-centring and load carrying capability of the system.

Considering the importance of the ED devices on the connection performances, Garlock et al. (2003) have focused on the behaviour of bolted steel top-and-seat angles, with the aim of determining how the angle size and geometry, together with the presence of washer plates, affect the connection stiffness, strength, energy dissipation capacity and resistance to low cycle fatigue. The performed tests have evidenced the following main results: for all the considered specimens, the initial stiffness has remained constant in subsequent cycles; the yield mechanism has consisted in the formation of three plastic hinges in the angles; the post-yield stiffness has been sensibly smaller than the elastic one, but it has not got equal to zero, so showing significant material and geometrical hardening.

The studies by Garlock et al. (2005) are an expansion of the work by Ricles et al. (2002b), since they have been related to similar PTED connections, focusing on different parameters. In particular, such studies have investigated the effects, on the connection behaviour, of the value of initial post-tensioning force, of the number of strands used in the connection and of the length of the beam flange reinforcing plates. The main results of this experimental campaign can be summarized as follows: larger values of the initial post-tensioning force increase the capability of the connection to achieve larger bending moments, but, at the same time, they can lead to undesirable beam flange buckling phenomena, with consequent reduction of the PT force itself; the buckling phenomena can be avoided by using longer reinforcing plates

and/or by using a smaller initial post-tensioning force; the yielding of strands can be avoided by using a larger number of strands, which allow to achieve also a larger connection moment and greater ductility.

With regard to the numerical analyses, the model set up by Ricles et al. (2001), based on fiber elements, has been developed and implemented aiming at performing both parametric inelastic static analyses of interior beam-to-column connections (Fig. 2.15a) and dynamic time history analyses of a whole steel moment resisting frame (Fig. 2.15b).

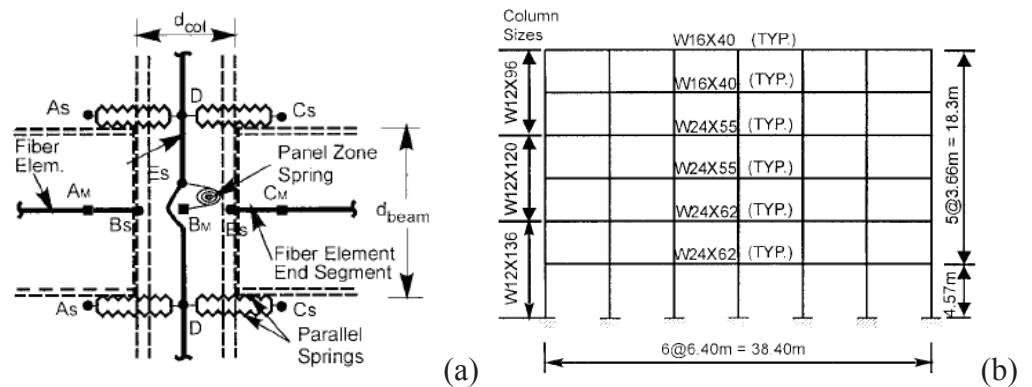


Figure 2.15. Numerical analyses : (a) model of an interior connection; (b) six-bay six-storey frame subjected to dynamic time history analyses (Ricles et al., 2001)

The parametric inelastic static analyses have focused on the effects, on the system behaviour, of connection details such as the level of post-tensioning force, the presence of shim and beam flange reinforcing plates, the geometrical features of the angles. The analytical model has been used also for dynamic time history analyses of a six-storey steel moment resisting frame equipped with PTED connections, which have proved to guarantee self-centring capability and adequate stiffness, strength and ductility. Moreover, the analyzed frames with PTED connections have exceeded the performance of a frame with typical welded connections subject to the same earthquake records.

2.3.3 PT steel bars and ED confined steel bars

Christopoulos et al. (2002a, b), at the University of California in San Diego (USA), have studied a PTED connection in which the PT system is based on a couple of high resistant steel bars, whereas the ED system is made of steel bars threaded in steel couplers and placed into steel confining cylinders (Fig. 2.16a). Both couplers and confining cylinders are welded to the beam flanges and/or to the continuity plates of the column.

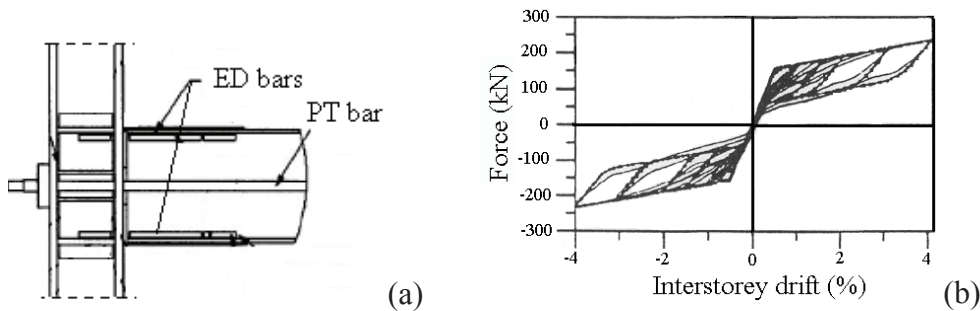


Figure 2.16. PTED connection with PT and ED bars: (a) typical node; (b) experimental force-displacement curve (Christopoulos et al., 2002a, b)

During the seismic action, due to the gap opening, the confined steel ED bars are subjected to cycles of tension and compression, developed in the plastic field, which guarantee the necessary energy dissipation capacity. The confining cylinders prevent the ED bars from buckling in compression, so assuring a stable cyclic behaviour.

For erection purposes, Christopoulos et al. (2002a) have suggested to use slotted shear tabs, welded to the column flange and bolted to the beam web. They are also useful to provide a redundant shear bearing mechanism, which could prevent the structural collapse in case of unexpected failure of the PT bars.

Christopoulos et al. (2002b) have performed experimental analyses on the confined steel ED bars, with the aim of assessing their tension-compression cyclic behaviour, verifying the capability of the coupler welds to withstand the axial capacity of the ED bars, and evaluating the effectiveness of the confining cylinders in limiting the buckling of the ED bars. The obtained results have

shown the adequate stability and the good energy dissipation characteristics of the hysteretic behaviour of the system.

In addition, they have validated experimentally the connection with PT bars and ED bars by performing a test on an external beam-to-column connection. In Figure 2.16b the force-displacement experimental cyclic curve is shown. The main result of the carried out experimental test is that the proposed connection is able to undergo large deformations with energy dissipation characteristics, while keeping the beam and column undamaged and without residual drift.

Finally, they have carried out an experimental study on a half-scale 3 columns-2 beams simple steel frame equipped with PTED internal and external connections. The test on the frame has confirmed the results obtained on the external beam-to-column connection, namely the effectiveness of the system with PT and ED bars in providing both self-centring and energy dissipation capabilities.

With regard to the numerical analyses, Christopoulos et al. (2002a) have modelled their connection by defining adequate equivalent springs and have studied the seismic response of MRFs equipped with them. The analytical models of both internal and external PTED connections used for the numerical analyses are shown in Figure 2.17. Three buildings, of respectively 3, 6 and 10 storeys, have been considered in the analyses. They were first designed as welded moment resisting frames and then the corresponding PTED connections were designed. Also in this case, the results have confirmed the self-centring and energy dissipation capabilities of moment resisting frames endowed with PTED connections.

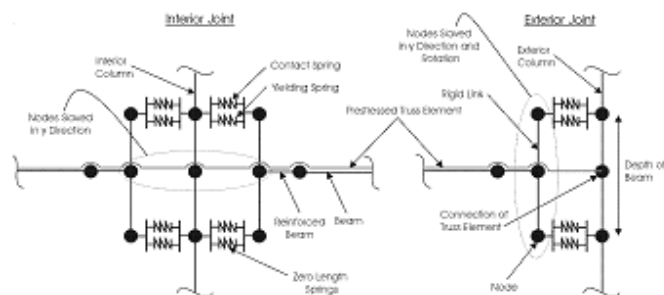


Figure 2.17. Analytical models of internal and external PTED connections with PT and ED bars (Christopoulos et al., 2002a)

2.3.4 PT steel strands and ED friction devices

Several PTED connection systems, based on differently arranged friction devices, have been proposed and studied up to today (Rojas et al., 2005; Wolski et al., 2006; Tsai et al., 2007).

Rojas et al. (2005), at the University of Lehigh (USA), have proposed a PTED connection in which the PT system is made of high resistance steel strands, whereas the ED system is based on friction devices, each of them consisting of a friction plate sandwiched by two brass shim plates (Fig. 2.18a). Friction devices are located at the top and bottom of the beam ends, and they dissipate the input energy during the cyclic gap openings, due to the relative displacements between the beams and the columns.

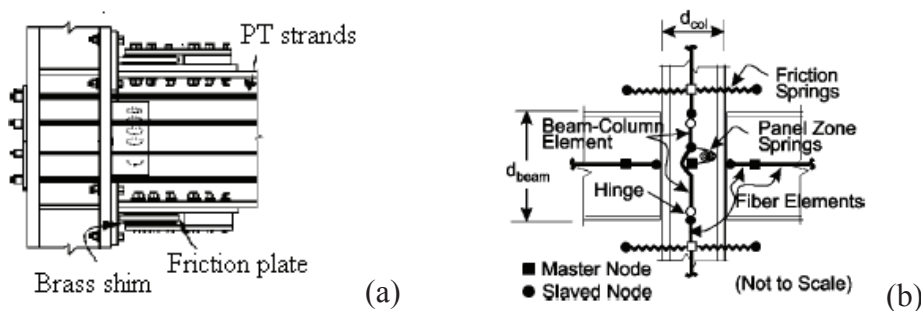


Figure 2.18. PTED connection with PT strands and ED top-and-seat friction devices: (a) typical node; (b) numerical model (Rojas et al., 2005)

The PTED system proposed by Rojas et al. (2005) has been studied by means of an analytical model based on fiber elements (Fig. 2.18b), somehow similar to that developed by Ricles et al. (2001), which has been used for performing inelastic static pushover and dynamic time history analyses. The seismic performance of the frames have proved to be satisfactory in terms of strength, storey drift, local deformation and self-centring capability.

Wolski et al. (2006), at the University of Lehigh (USA), have introduced a PTED connection type once again endowed with high resistant steel strands, as PT arrangement, but characterized by an ED system composed of friction devices placed only below the beam bottom flange (Fig. 2.19a). Such a technological solution has been proposed in order to avoid interferences

between the friction devices and the composite floor slab. The performed experimental studies have shown the excellent energy dissipation provided by the connection, together with the full self-centring properties, as it can be noted on the basis of Figure 2.19b, where the experimental cyclic response of the system, in terms of moment-rotation relationship, is plotted.

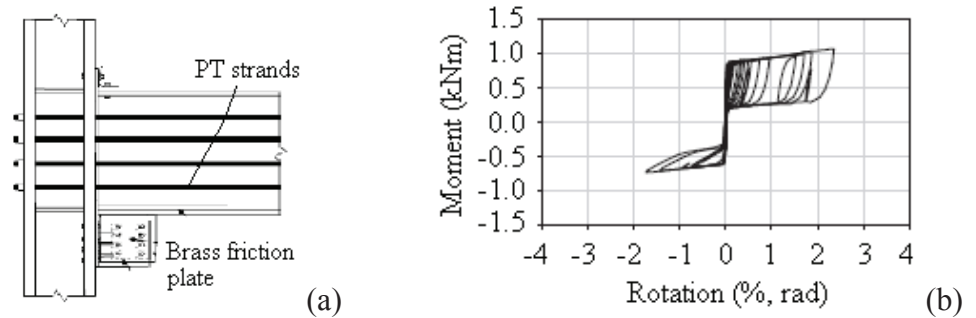


Figure 2.19. PTED connection with PT strands and ED bottom friction devices: (a) typical node; (b) experimental moment-rotation curve (Wolski et al., 2006)

In the connection type conceived by Tsai et al. (2007), at the National Taiwan University (Taiwan), the PT arrangement is composed of high resistant steel strands, whereas bolted web friction devices work as ED system (Fig. 2.20a). An analytical model of the system has been presented. In addition, the results of cyclic uni-axial tests conducted on isolated bolted web friction devices have been shown and discussed. At last, full-scale tests on beam-to-column assemblages equipped with the proposed system have been carried out, in which the investigated parameters included the initial PT force, the washer type and the number and size of high-strength bolts used to connect the beam web and the ED friction device.

The obtained results have confirmed the self-centring properties of the proposed connection, together with a very stable cyclic behaviour, without stiffness and strength degradation (Fig. 2.20b).

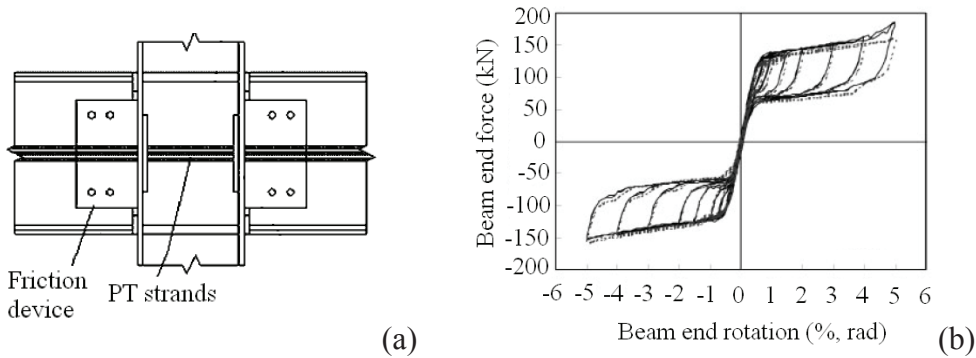


Figure 2.20. PTED connection with PT strands and ED bolted web friction devices: (a) typical node; (b) experimental force-rotation curves (Tsai et al., 2007)

2.3.5 PT steel strands and ED reduced flange steel plates

Chou et al. (2006), at the National Chiao Tung University of Hsinchu (Taiwan), have proposed a PTED beam-to-column connection type characterized by the presence of high resistant steel strands, as PT system, and reduced flange steel plates, as ED system (Fig. 2.21a).

The ED reduced flange steel plates have been welded to the column and bolted to the beam flanges. They have been conceived to work and dissipate the input energy through inelastic cycles in tension and compression. At this aim, in order to guarantee the stability of the cyclic behaviour, they have been confined so that buckling phenomena have been prevented.

A campaign of experimental tests has been carried out, in which concrete filled steel tubes have been used as columns and wide flange profiles have been used as beams. The experimental results have shown the system capability of reaching a 4% inter-storey drift without strength degradation, whereas a reduction of strand force, re-centring capability and moment capacity has been evidenced at a drift equal to 5% (Fig. 2.21b).

In addition, analytical formulations useful for describing the connection behaviour have been provided, and a finite element model of the beam-to-column tested connections has been set up and validated.

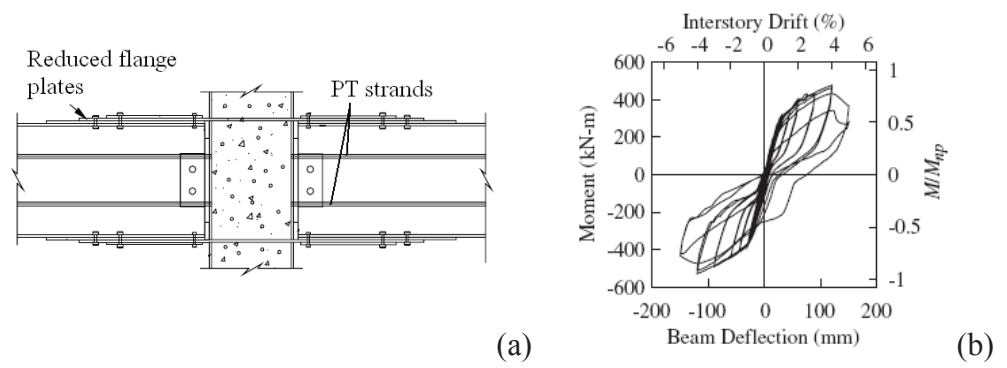


Figure 2.21. PTED connection with PT strands and ED reduced flange plates: (a) typical node; (b) experimental moment-drift curves (Chou et al., 2006)

Chapter 3

FE analyses for the study of PTED connections

3.1 FINITE ELEMENT ANALYSES

3.1.1 *Why FEA for studying PTED connections?*

The behaviour of connections can not be interpreted through the classical St. Venant hypotheses in linear elasticity, due to the stress concentrations that connections are usually subjected to. Suitable models can be obtained on the basis of plastic theory, looking for equilibrated solutions which are consistent with strength criteria. Consequently, the characterization of connections, in terms of stiffness, strength and deformation capability, requires experimental analyses and/or numerical investigations (Ballio and Mazzolani, 1983). This even more applies in the case of PTED connections, whose mechanical behaviour is characterized by several sources of non-linearity, such as material plasticity (in the energy dissipating devices based on yielding mechanisms), large displacements, friction and/or contact interactions.

As briefly described in Chapter 2, the investigation process on PTED beam-to-column connections is ongoing in different parts of the world, and it is just based on both experimental and numerical analyses. In this research, the study is carried out by means of Finite Element Analyses (FEA), which, if performed on adequately calibrated models, can well support the experiments.

In general, Finite Element Analyses are widely used in the product development cycles as a tool complementary to the experimental analyses, since they usually reduce the overall cost of the products and the related development time. In the past, FEA were used in relatively late phases of the product development cycles. On the contrary, in recent years, they are used earlier and earlier in the design cycle, with consequent reduction of costs and development time. In fact, FEA allow for:

- Identifying the forming problems prior to the tooling fabrication;
- Minimizing the tooling rework;
- Reducing the overall prototyping effort while identifying the possible shortcomings in the design;
- Minimizing the amount of material used during the fabrication process.

In addition, FEA often are the only way to get an answer in the case of particular problems, such as, for example, the mechanical behaviour of a system subjected to extreme loading conditions which are impossible to duplicate in an experiment (ABAQUS, 2006).

The numerical results obtained through a Finite Element Analysis further allow to investigate aspects which may be difficult to understand or measure during the experimental tests. So, even if a system has already been studied experimentally, its Finite Element modelling is useful to obtain complementary information. Moreover, the reliable calibration of a FE model against the experimental results allows to perform numerical analyses in which several parameters of interest may be varied, without the necessity of additional expensive experimental campaigns.

On the basis of the above considerations, the results of this research, entirely based on FE numerical analyses, may provide an useful contribution in the development process related to PTED beam-to-column connections for steel Moment Resisting Frames.

3.1.2 Generalities on the Finite Element Method

The Finite Element Method may be considered as a mathematical implementation of the natural process applied by human beings in approaching to complex problems. In fact, as a general rule, human mind

tends to subdivide complex systems into their individual components, or “elements”, whose behaviour is easily understandable, and then it rebuilds the original system for studying its whole behaviour (Zienkiewicz et al., 2004).

In general, a model may be defined as a simplified representation of reality. The degree of simplification depends on the problem peculiarities and on the particular aspects to investigate. In a macroscopic phenomenological perspective, the majority of the surrounding objects and systems appears as continuous. In some cases, it is necessary to consider the systems as continuous, in the sense that the above mentioned conceptual subdivision process is continued indefinitely, and so the problem may be defined in terms of infinitesimal concepts and solved through sets of differential equations. In other cases, a good accuracy of results may be obtained also using a finite number of elements. These problems are usually called “discrete”, and they can be solved by means of computers also in the case of very large number of elements. On the contrary, since the capacity of computers is finite, continuous problems, which are characterized by the presence of infinite elements, can be solved exactly only by mathematical manipulations, which are often possible only in case of oversimplified problems. On the basis of the latter consideration, the wide interest in discrete models is fully understandable, and it is arguable that the approximation of the results is better as far as the number of finite elements increases (Zienkiewicz et al., 2004).

The discretization of a continuous problem may be pursued in different manners. In general, as mentioned before, a continuous problem is defined on a continuous physical domain and is governed by differential equations. The main differences in the discretization approaches depend on which “object” is selected for the discretization. So it is possible to operate either on the differential equations governing the problem, such as in the case of the finite difference methods, or on the physical domain, such as in the case of the finite element method. It is worth noticing that the former approach is the one followed by mathematicians, whereas the latter is peculiar to engineers.

A possible simple definition of the Finite Element Method may be the following (Zienkiewicz et al., 2004): “a method of approximation to continuous problems such that the continuum is divided into a finite number of parts (elements), the behaviour of which is specified by a finite number of

parameters, and that the solution of the complete system as an assembly of its elements follows precisely the same rules as those applicable to standard discrete problems". The standard discrete problems, on the other hand, can be defined as problems in which:

- it is possible to identify a set of discrete parameters contemporarily describing the behaviour of each element and of the whole system;
- for each element, a set of quantities can be computed in terms of the above system parameters;
- the system equations imposed on the system quantities lead to the identification of the unknown system parameters, and so allowing to describe the whole system behaviour.

Besides the solid mathematical basis of the method, it appears quite intuitive and its steps, referred to a general structural problem, may be summarized as follows:

- the continuum domain is subdivided into a finite number of elements, which are separated by imaginary lines and interconnected at the vertices of the elements, namely at the nodes, forming the finite element mesh;
- since the nodal displacements are the basic unknown of the discrete problem, each finite element is preliminarily characterized by defining a set of functions which univocally define the displacements;
- based on the mechanical characterization of each element, the strain and stress states within each element are put in relation with the element displacements, which depend on the nodes ones;
- starting from the equations related to the single finite element, the whole equation system is assembled, leading to the definition of a global matrix governing the problem; the prescribed boundary conditions are eventually imposed;
- the problem equation system is solved, so determining the unknown nodal displacements and, consequently, the strain and stress state in the system.

An example of finite element model is shown in Fig. 3.1.

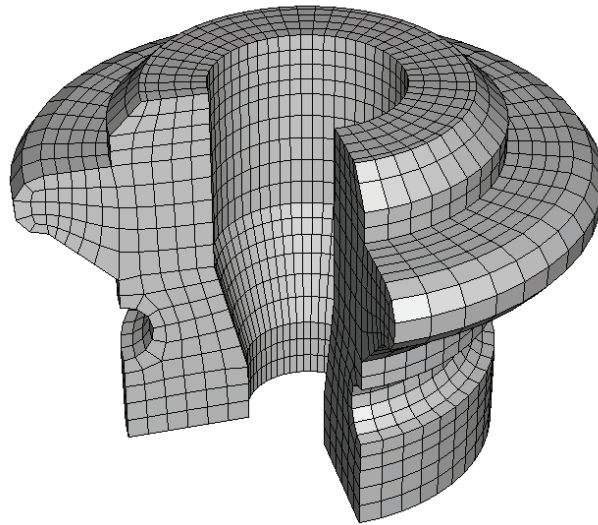


Figure 3.1. Example of finite element model: a tri-dimensional structural body

3.2 FEA BY THE ABAQUS COMPUTER PROGRAM

3.2.1 Preliminary remarks

The numerical analyses developed in this research are entirely carried out by means of the ABAQUS multi-purpose computer program (ABAQUS, 2004), based on the Finite Element Method. This program is chosen on the basis of its capability of reliably facing up complex problems which may be affected by strong non-linearities. Such peculiarity is fundamental in the modelling of PTED connections, whose behaviour is noticeably non-linear due to the contemporary presence of material, geometry and boundary conditions non-linearity sources.

In the following sections, the principal features of the used program and environment are illustrated. Such preliminary presentation is aimed at focusing on the program peculiarities, in order to create a clearly

understandable basis for the choices made in the modelling of the PTED connections presented in the following chapters.

3.2.2 *The ABAQUS complete environment*

In ABAQUS the creation of the model, the development of the analysis and the visualization of the results can be carried out by means of the ABAQUS/CAE, i.e. Complete Abaqus Environment. It deals with a user friendly tool which allows to manage all the phases of the numerical analysis, from the definition of the model geometry to the collection of the outputs.

In particular, an ABAQUS analysis consists in three main steps:

- Pre-processing;
- Simulation;
- Post-processing.

In the Pre-processing phase, the finite element model of the real problem is created. In the Simulation phase, the program solves the numerical problem defined in the model. In the Post-processing phase, the results of the analysis are obtained.

The essential components useful for describing a physical problem to be analysed and the results to be obtained in an ABAQUS analysis are: the discretized geometry, the element section properties, the material data, the loads and boundary conditions, the analysis type, and the output requests.

3.2.3 *Finite Elements in ABAQUS*

In ABAQUS a wide range of finite elements is available, in order to match the different requirements related to the physical problems of interest.

In general, each finite element is characterized by five features, which are listed in the following:

- Family;
- Degrees of freedom;
- Number of nodes;

- Formulation;
- Integration.

The element family is essentially related to the used geometry type. The most commonly used families in stress analyses are shown in Figure 3.2.

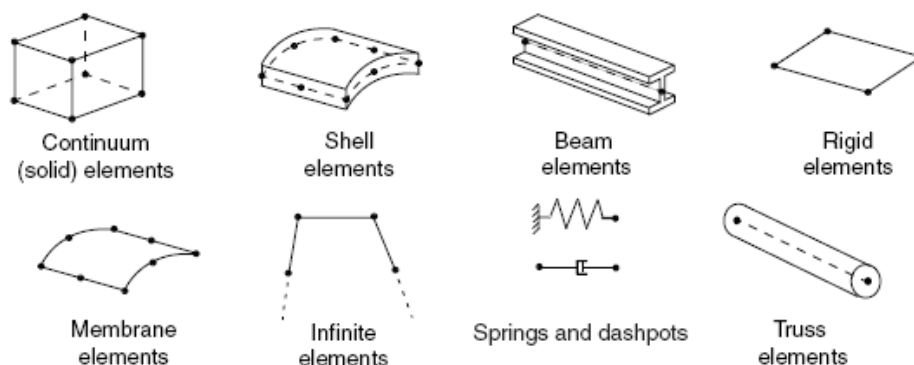


Figure 3.2. Finite element families available in ABAQUS (2004)

The degrees of freedom are the discrete parameters constituting the fundamental unknowns of the problem.

The number of nodes per element defines the order of interpolation used for defining the deformed shape of the element edges. So, a finite element with two nodes per edge (one at each corner of the element) uses a linear interpolation. In other words, the deformed edges are still segments, and consequently such types of elements are usually called first-order or linear elements. On the other hand, elements with mid-side nodes use quadratic interpolation, the deformed edges fitting quadratic curves, and so they are usually called second-order or quadratic elements.

The formulation is referred to the mathematical theory used for defining the element behaviour. Lagrangian or Eulerian formulations may be used, the former being referred to problems in which the material associated to an element remains associated to that element during the whole analysis, and the latter being referred to problems in which the elements are fixed in space and the material flows through them.

The integration indicates the way different quantities are integrated over the volume of each element. Both full and reduced integration options are available, they being referred to the number of points required to integrate the polynomial terms in the stiffness matrix in an element.

In this research the mesh of the models is always composed by continuum tri-dimensional linear elements with reduced integration (C3D8R). They are 8-nodes hexahedral elements with one integration point at the centre, which usually give the best results for the minimum cost. In addition, their features are practically essential in the case of simulations involving both material plasticity and contact interactions, as described in sections 3.2.4 and 3.2.6.

3.2.4 *The definition of the materials*

ABAQUS provides a wide range of material types, which allow to cover problems involving metals, plastics, rubbers, foams and so on. With particular regard to ductile materials, such as steel, plasticity can be reliably caught, also accounting for hardening phenomena, and so the non-linearity due to the material characteristics can be well included in the models.

Usual engineering measures of strain and stress are the so called “nominal strain” (ε_{nom}) and “nominal stress” (σ_{nom}). Nominal strain is defined as the ratio between the total elongation (Δl) of the specimen in tension and its initial length (l_0): $\varepsilon_{nom} = \Delta l / l_0$. Nominal stress is defined as the ratio between the actual force (F) on the specimen and initial value of its cross-section area (A_0): $\sigma_{nom} = F / A_0$.

In order to both adequately consider the occurrence of finite deformations and take into account the nearly incompressible nature of the plastic deformations in ductile metals, ABAQUS requires the material be defined in terms of “true strain” (ε) and “true stress” (σ). True strain is conceptually obtained from nominal strain by considering the limit $\Delta l \rightarrow dl \rightarrow 0$. True stress is obtained by imposing that the actual volume of the part undergoing plastic deformations is the same as the initial one: $A_0 \cdot l_0 = A \cdot l$.

On the basis of the above considerations, the nominal vs. true relationships are the following ones:

$$\varepsilon = \ln(1 + \varepsilon_{nom}) \qquad \sigma = \sigma_{nom} (1 + \varepsilon_{nom}).$$

In addition, the plasticity model in ABAQUS requires the definition of the plastic true strain values (ε_{pl}), which is obtained by subtracting the true elastic strain (σ/E) from the total true strain (ε):

$$\varepsilon_{pl} = \varepsilon - \sigma/E.$$

Some limitations on the selection of the finite elements are present in the case of problems involving metal plasticity, due to the incompressible nature of plastic deformations. In fact, incompressibility involves an additional kinematic constraint on the finite element, consisting in imposing the volume at the integration points to remain constant. In some kinds of elements, this limitation makes the finite element overconstrained, with consequent stiffer behaviour. The phenomenon is usually called “volumetric locking”. For instance, fully integrated second-order solid elements are strongly susceptible to volumetric locking. On the contrary, reduced integration solid elements, characterized by fewer points at which the incompressibility constraints must be satisfied, are not overconstrained and so they can be used for most elastic-plastic simulations.

The latter consideration, together with the reduction of the computational cost of the analysis when compared to the case of fully integrated elements, is at the basis of the selection of reduced integration elements in the presented numerical analyses.

3.2.5 *Non-linear problems*

The analyses presented in this work are carried out by means of the ABAQUS/Standard implicit solver, which uses the Newton-Raphson method to obtain solutions for non-linear problems.

In general, in a non-linear analysis the solution cannot be calculated by solving a single system of equations, as would be done in a linear problem, and so the solution may be found by gradually and incrementally applying the specified loads, proceeding toward the final solution. Therefore, ABAQUS/Standard breaks the simulation into a number of load increments and finds the approximate equilibrium configuration at the end of each increment, by means of an iterative procedure.

An iteration is here defined as an attempt to find an equilibrium solution. If the model is not in equilibrium at the end of the iteration, ABAQUS/Standard tries another iteration. At each iteration, the obtained solution should be closer to equilibrium, and sometimes the program may need many iterations to obtain a solution. For each iteration, ABAQUS/Standard forms the model's stiffness matrix and solves a system of equations. Consequently, in a computational costs perspective, each iteration is equivalent to a complete linear analysis. The latter consideration underlines the large computational expense of a non-linear analysis in ABAQUS/Standard.

The increment is complete when an equilibrium solution is obtained. The sum of all of the incremental responses is the approximate solution for the non-linear analysis. Thus, ABAQUS/Standard combines incremental and iterative procedures for solving non-linear problems.

The size of the load increments used for the solution of non-linear problems is automatically adjusted by ABAQUS/Standard. The user has to suggest the size of the first increment in each step of the simulation, and this can improve the control on the simulation convergence by the user, who can indicate a small or large fraction of the increment size depending on the expected non-linearity at the beginning of the step.

3.2.6 Contact

Contact problems, in which two adjacent surfaces may be either in close contact or not during the simulated physical process, are suitably treated by ABAQUS/Standard.

A contact interaction is essentially defined through the identification of the surfaces in contact and of the related interaction properties, the latter characterizing the behaviour in the normal and tangential direction, referred to the contact surfaces. In the following, a brief description of the most important interaction properties provided by ABAQUS/Standard is given, it being focused only on the interactions worth of notice for the analyses described in this work.

With regard to the normal behaviour, the distance separating two surfaces is called "clearance", and the contact constraint is applied when the clearance between two surfaces becomes equal to zero (Fig. 3.3a). In the contact formulation, there is no limit to the contact pressure magnitude which can be

transmitted between the surfaces. When the contact pressure between the surfaces in contact becomes equal to zero or negative, the surfaces separate and the contact constraint is removed. This behaviour is called “hard” contact.

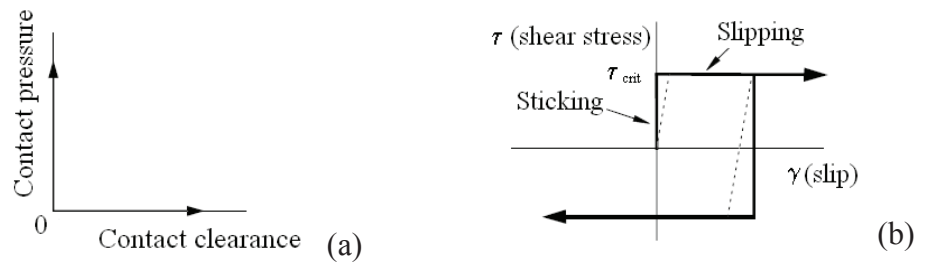


Figure 3.3. Interaction properties in contact interactions: (a) “hard” normal contact interaction; (b) frictional behaviour (ABAQUS, 2004)

With regard to the tangential behaviour, the relative sliding between the contact surfaces and the related friction forces are calculated. Due to the complexity of this kind of calculation, either “finite sliding” or “small sliding” formulations can be adopted, the latter being much less expensive, from a computational point of view.

A common model for describing tangential friction forces is the Coulomb one, in which, as well known, the tangential motion is zero until the shear stress reaches a critical value (τ_{crit}), related to the normal contact pressure (p) according to the following equation:

$$\tau_{crit} = \mu p$$

where μ is the friction coefficient. The behaviour of the Coulomb friction model is summarized in Figure 3.3b, where it is plotted by a thick line.

In ABAQUS/Standard the discontinuity between the sticking and slipping states can result in convergence problems. Consequently, the program is endowed with a penalty friction formulation with an allowable “elastic slip” (dotted line in Fig. 3.3b). The “elastic slip” is a small amount of relative motion between the surfaces that occurs when the surfaces should be sticking, and the penalty stiffness is automatically selected by the program, so that the

“elastic slip” is a very small fraction of the characteristic element length. In case of negligible friction behaviour, a frictionless tangential interaction may be conveniently used, which is much less expensive than the friction one in terms of computational efforts.

In case of contact interactions, particular care is required in the definition of the finite element mesh, both in terms of mesh refinement and element selection. With regard to the mesh refinement, it has to be underlined that ABAQUS/Standard uses a pure master-slave contact algorithm, in which the nodes on the slave surface can not penetrate the segments making up the master surface, whereas no restrictions are placed on the master surface, which can consequently penetrate the slave surface between slave nodes, as shown in Figure 3.4. Consequently, in order to prevent non-physical material interpenetrations, the mesh of the slave surface should be finer than the master surface one.

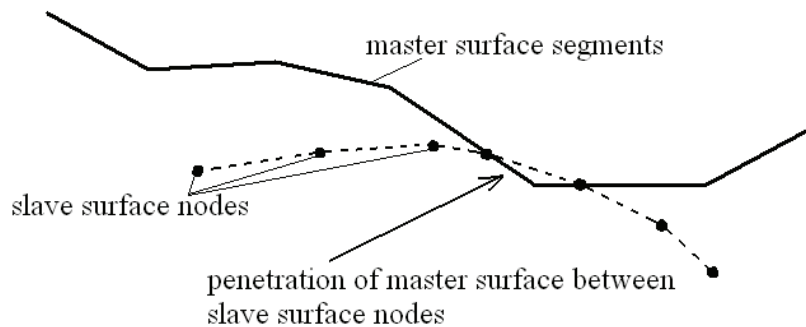


Figure 3.4. Behaviour of master and slave surfaces in contact simulations (ABAQUS, 2004)

With regard to the elements to use in a contact interaction, in general, first-order elements have to be preferred for the slave surfaces, since second-order elements can sometimes cause problems in contact simulations due to the way these elements calculate consistent nodal loads for a constant pressure (ABAQUS, 2004).

At last, Figure 3.5 shows the algorithm followed by ABAQUS/Standard in solving contact problems, whose knowledge is useful for calibrating model parameters which can lead toward a converged solution.

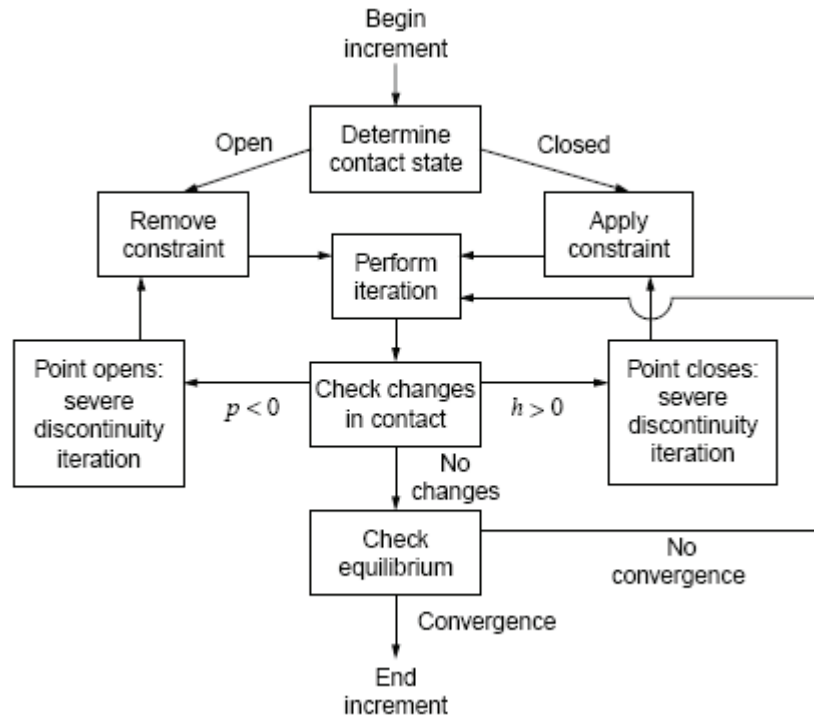


Figure 3.5. Contact algorithm in ABAQUS/Standard (ABAQUS, 2004)

At the beginning of each increment, the program examines the state of all contact interactions, controlling whether slave nodes are open or closed. It consequently applies a constraint for each closed node and removes constraints from any node where the contact state changes from closed to open. Subsequently, an iteration on the configuration updated on the basis of the calculated corrections is carried out. Before checking for equilibrium of forces or moments, ABAQUS/Standard first checks for changes in the contact conditions at the slave nodes. If there is interpenetration ($h > 0$), the point is closed, whereas if there is a negative contact pressure ($p < 0$), the point is

opened. In both cases, it deals with a “severe discontinuity iteration”, where the contact constraints are changed accordingly and no equilibrium check is carried out. Such iterations are repeated until no changes in the contact status occur, and the last of them is the first equilibrium iteration following the severe discontinuity ones. After each equilibrium iteration, equilibrium convergence checks are carried out. If convergence is achieved, the increment is completed; otherwise the iteration process has to restart (ABAQUS, 2004).

Chapter 4

PTED connections with PT and ED bars

4.1 THE REFERENCE EXPERIMENTAL STUDY

This chapter is focused on the FE analysis of the PTED beam-to-column connection for steel MRFs introduced and studied by Christopoulos et al. (2002a, b). The objective is to reproduce the performed experimental test, by means of reliable FE models, and, consequently, to investigate in detail the related system behaviour. This type of connection is shown in Figure 4.1, where the component parts are visible.

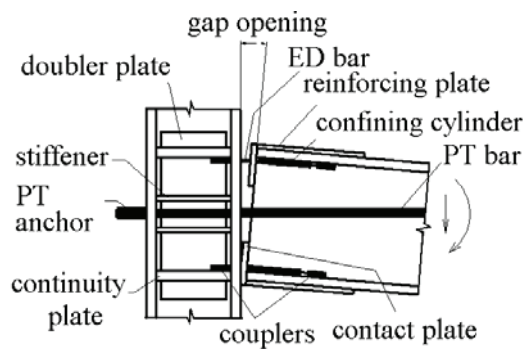


Figure 4.1. Detail of the PTED connection with PT and ED bars, by Christopoulos et al. (2002a, b)

The PT bars, post-tensioned in elastic range for providing both the load carrying capacity and the self-centring capability, are anchored against the external flange of the column. The ED bars are threaded into steel couplers, which are welded to the beam flanges and to the column continuity plates, and are inserted into steel confining cylinders. The latter ones are necessary for preventing the ED bars from buckling in compression, after their yielding in tension due to the gap opening mechanism peculiar of PTED connections. The contact plates represent the actual interface between beam and column, and guarantee a smooth interface between them. The reinforcing plates are intended to prevent the occurrence of inelastic deformations in the beam flanges due to the large compression stresses. The stiffeners help the column in carrying the concentrated forces induced by the anchoring system of PT bars. The doubler plates, welded to the column web, support it against the large shear force demand peculiar of that area.

During an earthquake, the ED bars undergo cycles of axial inelastic deformation in tension and compression, so dissipating the seismic input energy. At the same time, the PT bars, instant by instant, tend to bring the connections towards the initial configuration, thanks to the returning action they are subjected to, which is caused by their elastic elongation due to the gap opening. Consequently, after the seismic shocks, if no plastic deformations take place at the bases of the frame columns, the structure returns to the initial configuration, the main structural elements are undamaged and the ED bars, which are the only damaged component parts, can be easily replaced.

The reference full-scale test specimen, consisting in an external beam-to-column connection, is shown in Figure 4.2. Both the W24x76 beam and the W14x211 column are made of A992 steel, characterized by a nominal yield stress equal to 345 MPa. The PT force is applied by two 46 mm diameter DSI (Dywidag Systems International) bars, with ultimate stress equal to 1030 MPa. The initial value of PT force is equal to 655 kN per bar. The ED bars are made of 22 mm diameter DSI threaded bars, with a nominal yield stress equal to 400 MPa. The characteristics of the connection component parts in terms of thickness of plates, diameter of bars, yielding and ultimate stress of the materials, are given in Table 4.1. Details on the design of the test specimen can be found in (Christopoulos et al., 2002a).

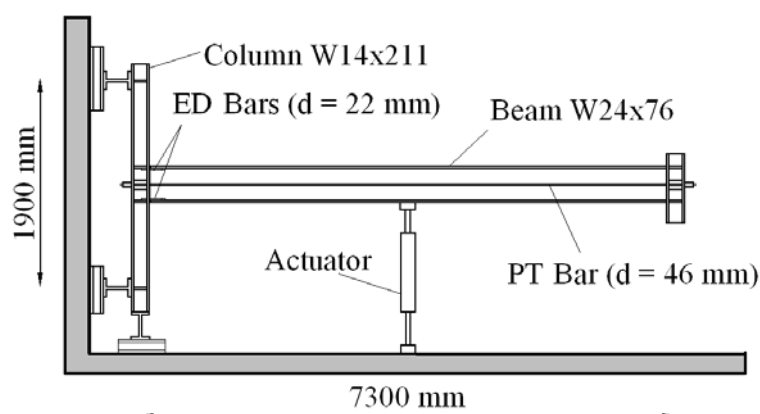


Figure 4.2. PTED beam-to-column external connection test specimen (Christopoulos et al., 2002a)

Table 4.1. Geometrical and mechanical features of the tested connection component parts

Component parts	Thickness (t), Diameter (d) (mm)	Yield stress (f_y), Ultimate stress (f_u) (MPa)
Contact plates	$t = 25$	$f_y = 345$
Continuity plates	$t = 25$	
Doubler plates	$t = 9.5$	
Reinforcing plates	$t = 12$	
Stiffeners	$t = 17$	
PT bars	$d = 46$	$f_u = 1030$
ED bars	$d = 22$	$f_y = 400$

The load history consists in the application of a series of cyclic vertical displacements at the beam mid-span section, by means of an actuator, and it is shown in Figure 4.3, where it is expressed in terms of imposed drift, which is defined as the ratio between the applied vertical displacement and the distance between the beam mid-span and the axis of the column.

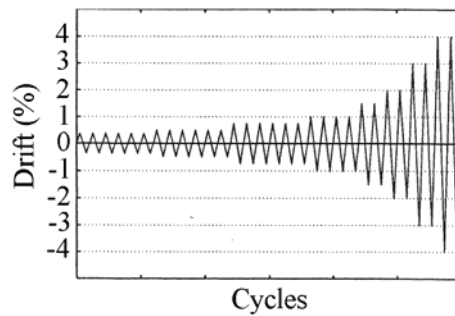


Figure 4.3. Cycles of imposed drifts during the experimental test (Christopoulos et al., 2002a)

The experimental results, expressed in terms of both force-drift and moment-gap opening curves (Fig. 4.4), show the excellent self-centring and energy dissipation capabilities of the tested system. In addition, it is evident that the tested connection behaves as a “rigid” one for small values of the imposed drift. During the test, the maximum measured force is approximately equal to 240 kN, whereas the maximum measured bending moment is equal to 870 kNm.

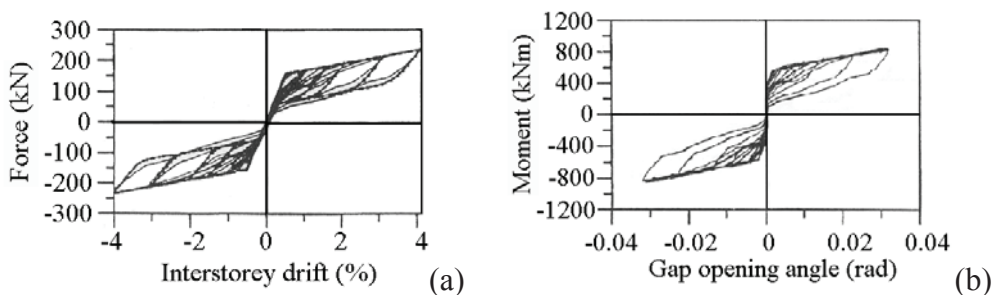


Figure 4.4. Experimental results on the PTED connection with PT and ED bars: (a) force-drift curve; (b) moment-gap opening angle curve (Christopoulos et al., 2002a)

4.2 FINITE ELEMENT MODELS

4.2.1 *The geometry of the models*

Two finite element models are developed for the numerical study of the PTED connection with PT and ED bars. In both cases, the geometrical details of the tested connection are faithfully reproduced (Fig. 4.5).

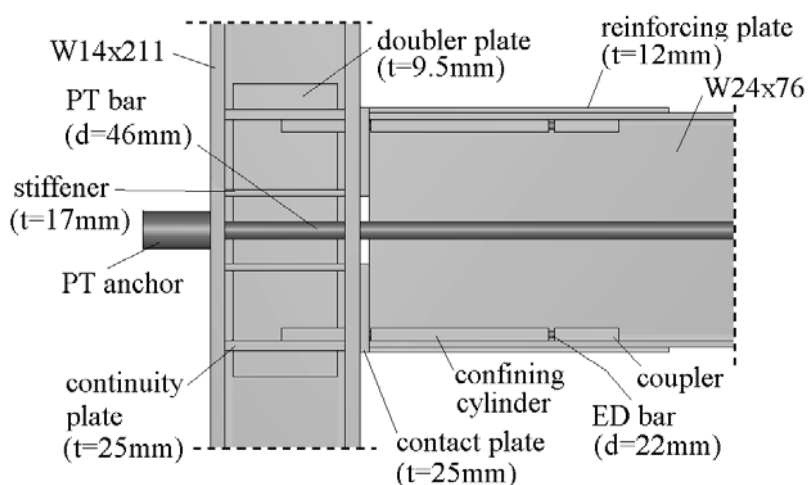


Figure 4.5. Geometrical details of the PTED connection FE models

The first model (Esposito et al., 2006b – Fig 4.6) is based on the simplifying assumption of exploiting the system symmetry with respect to the mid-plane of beam and column webs (Fig. 4.6b). In this model, adequate additional boundary conditions are considered, which are necessary for preventing the occurrence of out-of-plane displacements of points belonging to the symmetry plane. In principle, the imposed symmetry condition does not allow the out-of-plane buckling phenomena to be caught. Anyway, this aspect does not affect the results, since at the author's knowledge no instable phenomena have been evidenced during the experimental tests.

The second model (Esposito et al., 2007) considers the whole beam-to-column assembly, without simplifying assumptions (Fig. 4.6c). Consequently, it is computationally more expensive than the first one, but it allows to investigate in detail the cyclic behaviour of all the connection component parts. In addition, it proves the reliability of the first model, which exploits the symmetry. In fact, also in this case, in which the out-of-plane displacements in the symmetry plane are allowed, the numerical results are exactly the same as those referred to the first model.

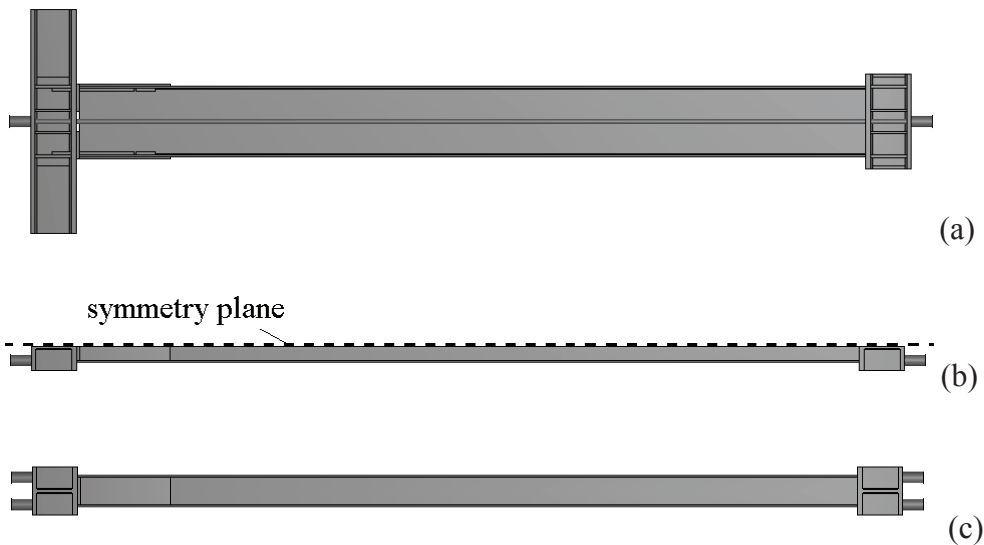


Figure 4.6. Geometry of the numerical models: (a) lateral view; plane views of (b) the symmetry-based simplified model, and (c) of the complete model

Based on the above considerations, it is arguable that the analyses focused on the global behaviour of the connections, as well as those aimed at comparative evaluations, can be carried out on the simplified models, which are computationally cheaper. On the other hand, the analyses aimed at investigating the detailed behaviour of the component parts require the complete models.

The assumptions related to the other modelling issues are the same in the two models, and they are presented in the following sections.

4.2.2 The properties of the materials

Three different materials are considered in the finite element models, and their stress-strain relationships are plotted in Figure 4.7. In particular, an elastic-plastic structural steel (namely SS), a hardening steel (namely HS) and a high resistance steel (namely HRS) are modelled.

The SS material properties are assigned to the column, the beam, the anchors, the continuity plates, the stiffeners, the doubler plates, the contact plates, and the reinforcing plates. The HS material properties are assigned to the ED bars. At last, the HRS material properties are assigned to the PT bars, the couplers, and the confining cylinders.

Information on the above materials, in terms of true stresses and plastic strains, and on the related component parts, is summarized in Table 4.2.

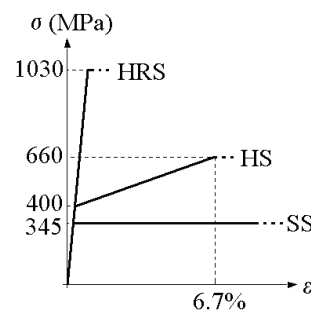


Figure 4.7. Nominal stress-strain relationships of the modelled materials

Table 4.2. Mechanical features of the modelled materials, in terms of true stresses and plastic strains, and associated component parts

Material	Yield stress (MPa)	Ultimate stress (MPa)	Ultimate plastic strain (%)	Component parts
SS	345	345	-	Column, beam, anchors, continuity plates, stiffeners, doubler plates, contact plates, reinforcing plates
HS	400	700	-	ED bars
HRS	1030	1030	-	PT bars, couplers, conf. cylinders

4.2.3 *The interactions between the component parts*

In order to model the interactions between welded component parts, tie constraints are used, so that no relative motion between the surfaces in contact is possible. In particular, tie constraints are considered for modelling the following interactions: beam flange-coupler; beam flange-confining cylinder; beam flange-reinforcing plate; beam end-contact plate; column-continuity plate; column-stiffener; column web-doubler plate; continuity plate-coupler; column flange-PT anchor; reinforcing plate-contact plate. Furthermore, even if PT bars and ED bars are threaded inside anchors and couplers, respectively, the tie constraint is chosen also for modelling those interactions between parts, because the threading is cumbersome to be reproduced and in any case its effects are negligible for the purposes of the study.

Surface-to-surface contacts are used to model the following interactions: column flange-contact plate; column PT hole-PT bar; confining cylinder-ED bar. In general, contacts allow to model the behaviour of parts that can be in contact or not, depending on the system configuration, and they can take into account the friction properties between the surfaces in contact. Therefore, they are useful to catch the beam-to-column gap opening at the column flange-contact plate interface. In addition, they allow to model the interactions between the PT bar and the ED bars with the column PT hole and confining cylinders, respectively, since these parts are not in contact in service conditions, but they could be in contact when seismic loads occur.

In particular, a “penalty friction tangential contact” is used for modelling the interaction between column flange and contact plates, which allows to transmit both shear and normal forces. The considered friction coefficient is equal to 0.33, while the maximum elastic slip is 0.005 times the characteristic slave surface element dimension.

A frictionless tangential behaviour is considered for modelling the PT bar-column PT hole and ED bar-confining cylinder interactions. The first ones come into contact each other for large values of inter-storey drift, while the second ones when the ED bars are in compression and tend to buckle.

Information on the used contact formulations is provided in section 3.2.6.

4.2.4 The load history and the multi-step analysis

The study PTED connection is initially subjected to the post-tensioning of the PT bars and, subsequently, to a series of vertical displacement cycles applied at the mid-span section of the beam (Fig. 4.8). The analysis is subdivided into a number of subsequent static steps, the first one corresponding to the application of the PT action (655 kN per bar) and the other ones corresponding to the application of the imposed drift history.

As respect to the experimental test, the number of cycles in the imposed drift history considered in the model is clearly lower, it consisting in the application of only one cycle for each target drift amplitude. This choice is aimed at reducing the model size, from a computational point of view.

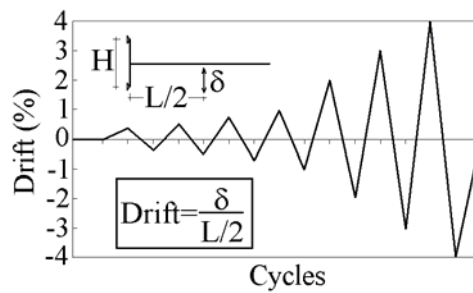


Figure 4.8. Imposed cyclic drift history in the numerical analyses

The sizes of the initial increments in the steps are selected in order to achieve the best convergence speed. A progressive reduction in the initial increment size is chosen, corresponding to the increase of the problem non-linearity. In particular, fractions equal to 0.05 are used for the cycles up to 1% drift, equal to 0.02 for the 2% drift cycle, and equal to 0.01 for the remaining cycles.

4.2.5 The mesh

The finite element mesh (Fig. 4.9) is made by tri-dimensional continuum first-order elements with reduced integration (C3D8R) for all the component parts of the model. In ABAQUS/Standard, this choice matches the

requirements typical of problems involving material plasticity, contact interactions and large size models, as described in section 3.2.

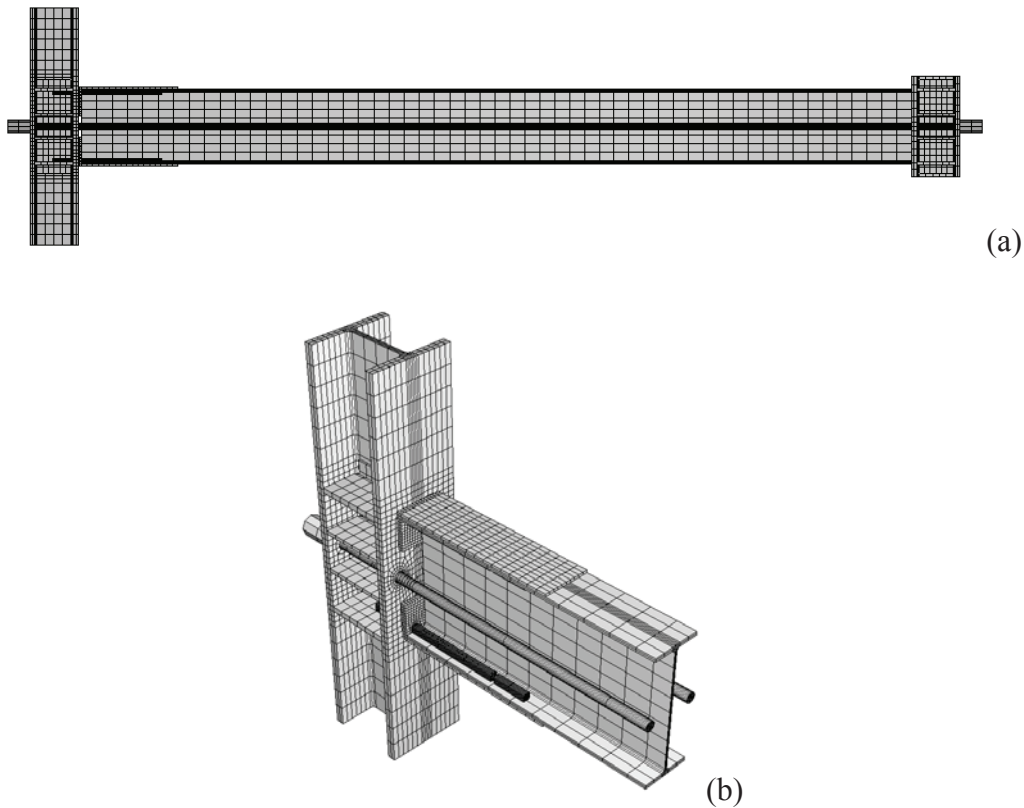


Figure 4.9. Finite element mesh of the complete model: (a) lateral view of the whole model; (b) detail of the nodal area

The mesh refinement of the surfaces involved in contact interactions derives from the rigid master-slave algorithm used in contact by ABAQUS/Standard, described in section 3.2.6, which implies that slave surfaces must be meshed in a finer way than the master ones. In particular, referring to the modelled contact interactions, contact plates have slave surfaces as respect to column flanges, PT bar has slave surface as respect to PT column hole and ED bars have slave surfaces as respect to the confining cylinders.

The mesh of cylindrical parts, such as PT and ED bars, derives from an ad-hoc calibration of the model (Esposito, 2005) based on the results of experimental tests carried out on the ED bars (Christopoulos et al., 2002b). Definitely, a fine mesh in the transversal cross-section of the bars and a coarse mesh in the longitudinal direction are defined, it allowing to achieve a good accuracy of the results.

4.3 NUMERICAL VS. EXPERIMENTAL RESULTS

4.3.1 *Global response curves*

The reliability of the numerical models is evidenced by the comparison of the obtained analytical results with the available experimental ones. In particular, the numerical force-drift and moment-gap opening curves are well superimposed to the experimental ones, as shown in Figures 4.10 and 4.11.

The main characteristics of the connection in terms of global behaviour, namely the initial stiffness, the strength corresponding to the end of linear behaviour, the post-yielding stiffness and the strength corresponding to the target drift (equal to 4%) are successfully caught by the finite element models.

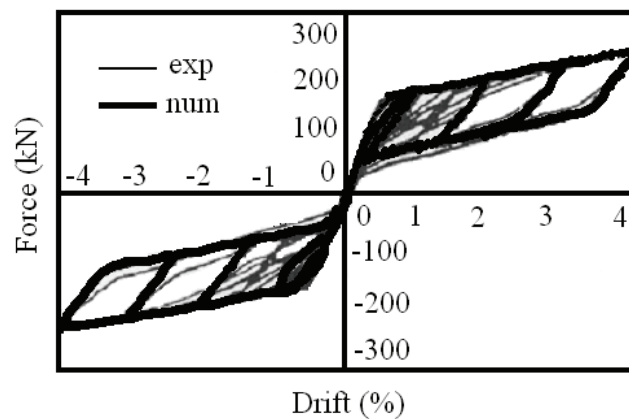


Figure 4.10. Numerical vs. experimental force-drift curves

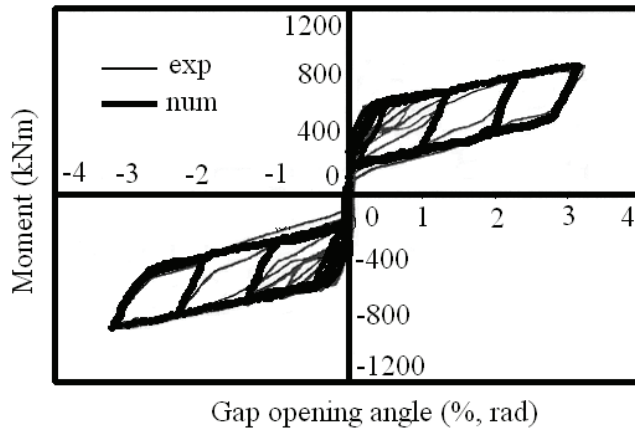


Figure 4.11. Numerical vs. experimental moment-gap opening angle curves

The connection behaviour is linear elastic up to a drift equal to 0.375%, when the gap opens at the beam-to-column interface. The above drift value approximately corresponds to the fully operational level defined in SEAOC Vision 2000 (1995) and so it is possible to argue that the PTED connection behaves like a rigid one in presence of frequent earthquake events.

After the gap opening, the connection stiffness noticeably reduces, as expected on the basis of both the theoretical predictions and the experimental evidence.

At last, both the expected capacity of dissipating the input energy and the capability of returning to the initial configuration at the end of the cyclic history of imposed drifts are adequately caught by the finite element models, as demonstrated by the clearly flag-shaped response curves obtained from the numerical analyses.

4.3.2 Deformed configurations of the node

The numerical results match the experimental ones also considering the deformed configurations of the connection during the different phases of the imposed cyclic drift history.

In Figure 4.12a the lateral view of the whole assembly at the maximum drift reached during the analysis, namely 4%, is shown. Figure 4.12b gives a

plan view of the assembly at the 4% drift, and it confirms that no out-of-plane displacements occur in the considered PTED connection also for large drift values, so justifying the reliability of the results obtained from the symmetry-based simplified model. At last, the detail of the deformed node at the 4% drift is shown in Figure 4.12c, where the gap opening mechanism is clearly visible.

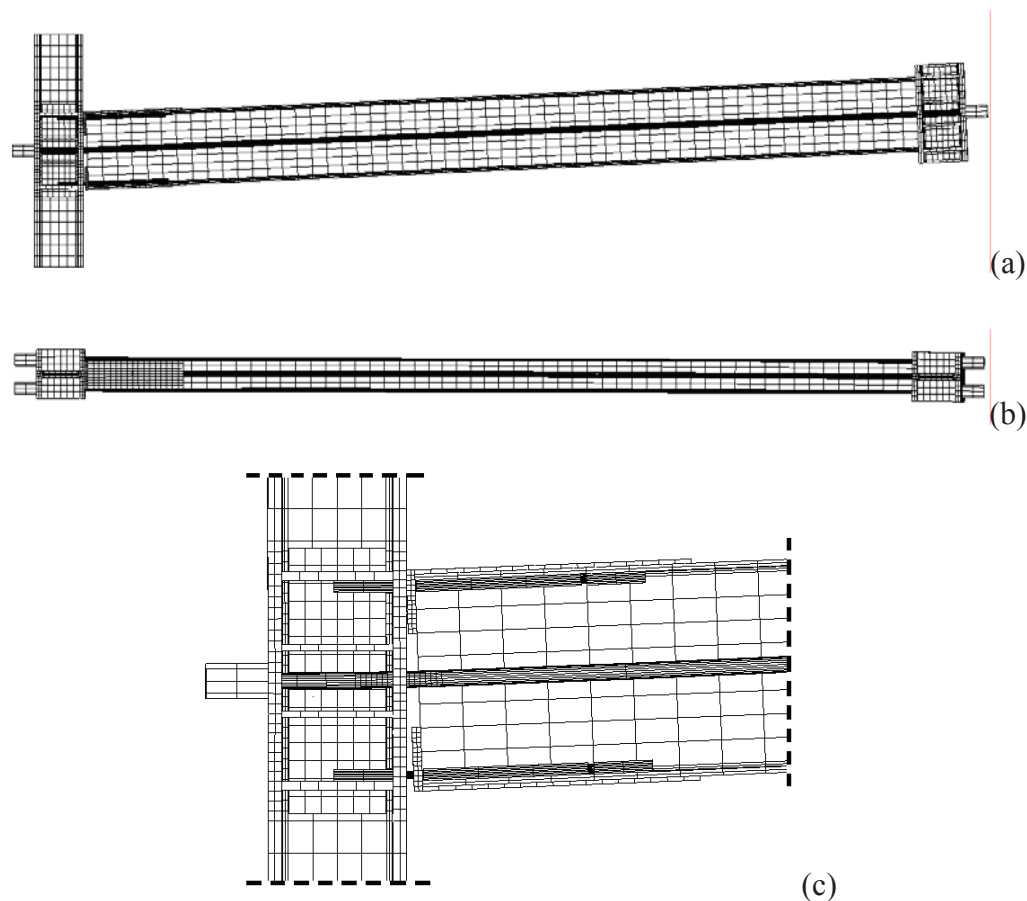


Figure 4.12. Deformed configuration of the study PTED connection: (a) lateral view; (b) plan view; (c) detail of the node

Based on the above results, the calibration of the set up finite element models is very satisfying, and consequently they represent an useful tool for investigating in detail the behaviour of the connection component parts.

4.4 BEHAVIOUR OF THE COMPONENT PARTS

4.4.1 Preliminary remarks

In this section the detailed investigation on the behaviour of the considered PTED beam-to-column connection is carried out (Faggiano et al., 2008). The deformation and stress states of the connection parts are shown, considering four main phases of the cyclic history, namely: after the application of the PT action; at a 0.375% drift, when decompression occurs; at a 4% drift, which is the maximum drift reached in the analysis; at the end of the cycles.

The results are provided by considering, at first, the behaviour of the assembled node, and then, the behaviour of the main component parts of the connection, which are analysed separately.

4.4.2 Assembled node

The deformed configurations of the node, together with the related stress distributions, at the above mentioned relevant drifts, are shown in Figures from 4.13 to 4.16. For each deformed configuration, both a perspective and a lateral view are provided, in order to correctly catch the node behaviour.

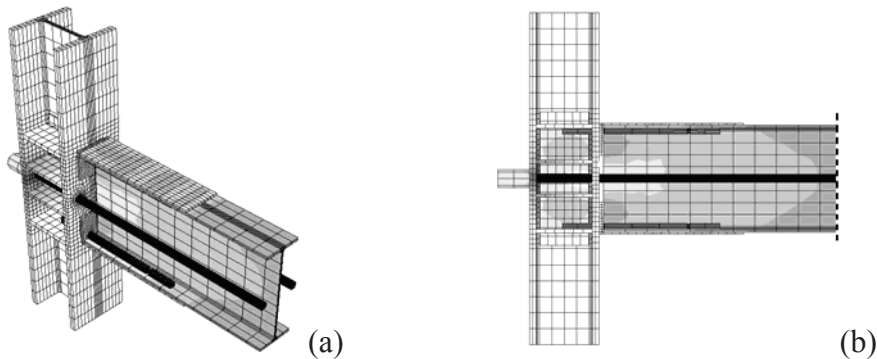


Figure 4.13. Deformation and stress state of the study PTED connection after the post-tensioning: (a) perspective and (b) lateral views

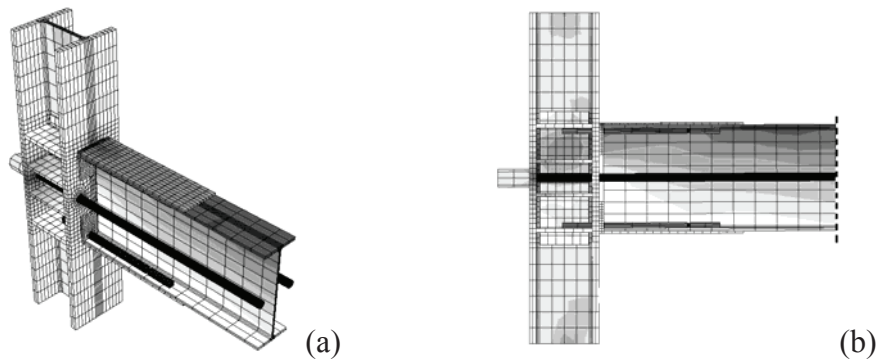


Figure 4.14. Deformation and stress state of the study PTED connection at a 0.375% drift: (a) perspective and (b) lateral views

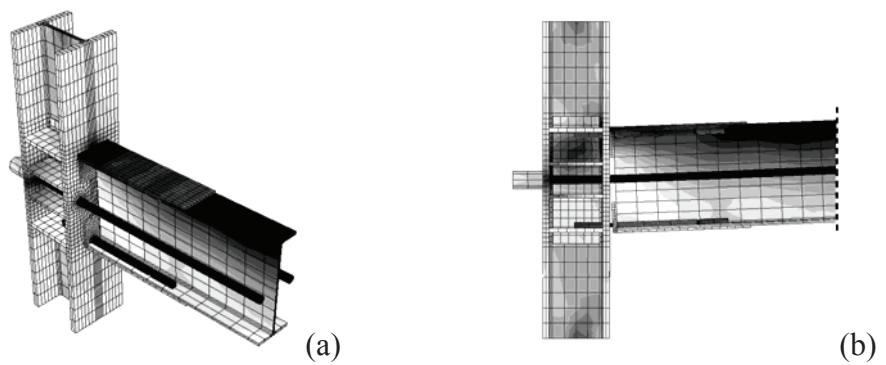


Figure 4.15. Deformation and stress state of the study PTED connection at a 4% drift: (a) perspective and (b) lateral views

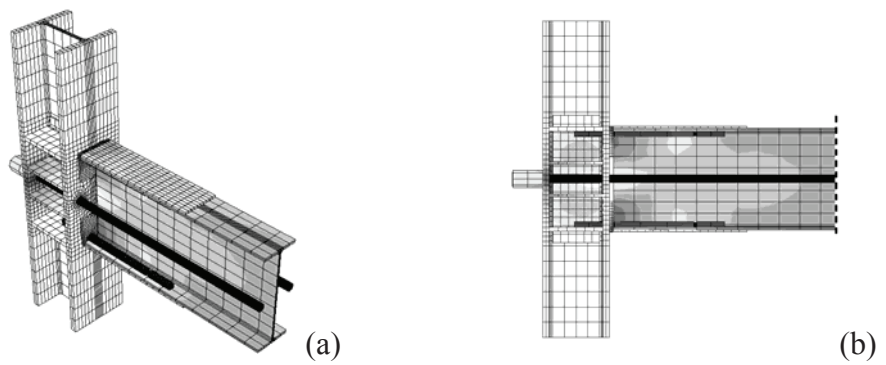


Figure 4.16. Deformation and stress state of the study PTED connection at the end of the cycles: (a) perspective and (b) lateral views

4.4.3 *Beam*

During the cycles of imposed drifts, the beam essentially behaves in elastic range, except for some yielding occurring in very small areas next to the beam-to-column interface and at the end of the reinforcing plates. The deformation and stress states in the beam at the above relevant phases of the analysis are shown in Figure 4.17.

At the end of the post-tensioning (Fig. 4.17a), a stress concentration appears next to the contact plates (located on the left end of the beam), due to the contact pressure.

At a drift equal to 0.375% (Fig. 4.17b), stress concentrations are present in the compressed area (top flange on the left of the beam), whereas no stresses are present in the bottom part of the left end of the beam, due to the loss of contact between beam and column.

At a drift equal to 4% (Fig. 4.17c), the stress distribution evidences the increasing of the stress values in the whole beam and the attainment of the yield stress (plotted in black) in very limited areas of the beam flange, namely at the interface with the column and in the section at the end of the reinforcing plates. The latter is worth of notice, since it is the section, among those taking no advantage of the reinforcing plates effect, which is subjected to the most severe combination of axial force and bending moment. In addition, some residual stresses are visible in the bottom area of the beam left end, which are due to the yielding of the related contact and reinforcing plates occurred during previous cycles.

At the end of the cycles (Fig. 4.17d), the stress distribution is essentially the same as the one after the initial post-tensioning, with the only difference that the stress values in the beam left end, next to the contact plates and to the reinforcing plates end, is slightly larger, due to the occurred yielding of contact plates and beam flanges in very small areas.

The stress history in the most engaged finite element of the flange, at the left end of the beam, during the cycles of imposed drifts is shown in Figure 4.18. The stress in the considered element generally increases with the drift, with the exception of the cycle at 1% drift, when the stress in the beam flange slightly reduces with respect to the previous cycle. This phenomenon is related to the yielding of the contact plates and the consequent redistribution of the stresses between the beam flanges and the reinforcing plates. In fact, for

drifts smaller than 0.75%, when the contact plates show plastic deformations, the stresses in the beam flange and reinforcing plates are practically coincident. Starting from the 0.75% drift, the stresses “migrate” from the beam flange to the reinforcing plates and consequently the stress value in the beam flanges reduces. For larger drifts, the gap between the stresses undergone by reinforcing plates and beam flanges increases, but, at the same time, the stress in the beam flanges increases too.

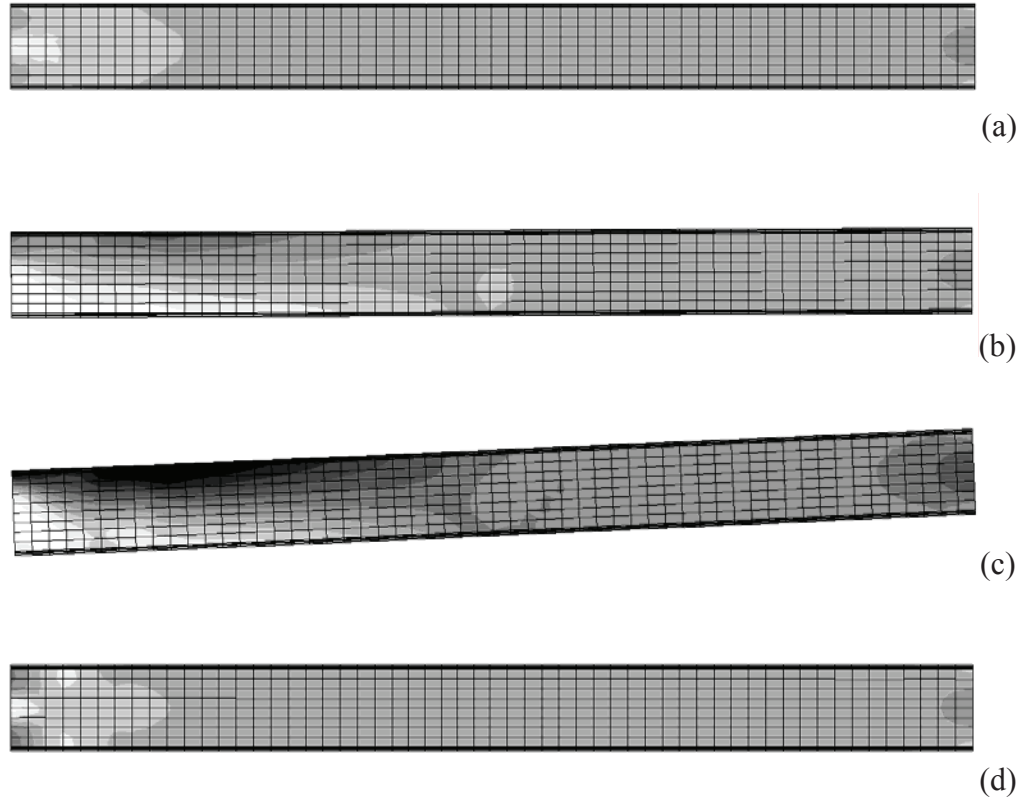


Figure 4.17. Deformation and stress states of the beam in the PTED connection: (a) after the post-tensioning; (b) at a 0.375% drift; (c) at a 4% drift; (d) at the end of the cycles

It is worth noticing that the considered element reaches the yield stress at the maximum drift, namely 4%. At last, some residual stresses are evident after the 2% drift cycle, when the inelastic deformations in the contact plates are worth of notice.

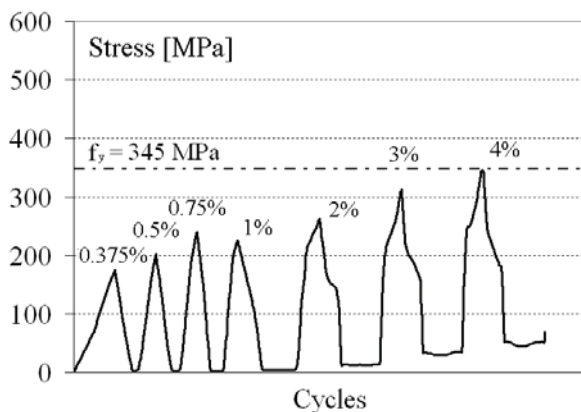


Figure 4.18. Stress history in the most engaged finite element in the beam flange

4.4.4 Column

During the cycles of imposed drifts, the behaviour of the column is always within the elastic range. The deformation and stress states for the relevant drift values are shown in Figure 4.19.

At the end of the post-tensioning (Fig. 4.19a), stress concentrations appear in the contact areas, which are: on the left, next to the location of the PT bars anchors; on the right, next to the location of the beam-to-column contact plates.

At a drift equal to 0.375% (Fig. 4.19b), the stress flow in the column web is clearly visible.

The stress state at 4% drift (Fig. 4.19c) shows the engagement of a large part of the column and, above all, the high stress concentrations in the column web interested by the flow of compression stresses. The latter aspect is worth

of notice, since it evidences the strong demand in terms of shear on the column web.

At the end of the cycles (Fig. 4.19d), the stress distribution is exactly the same as the one due only to the post-tensioning action, provided that no inelastic deformations occur.

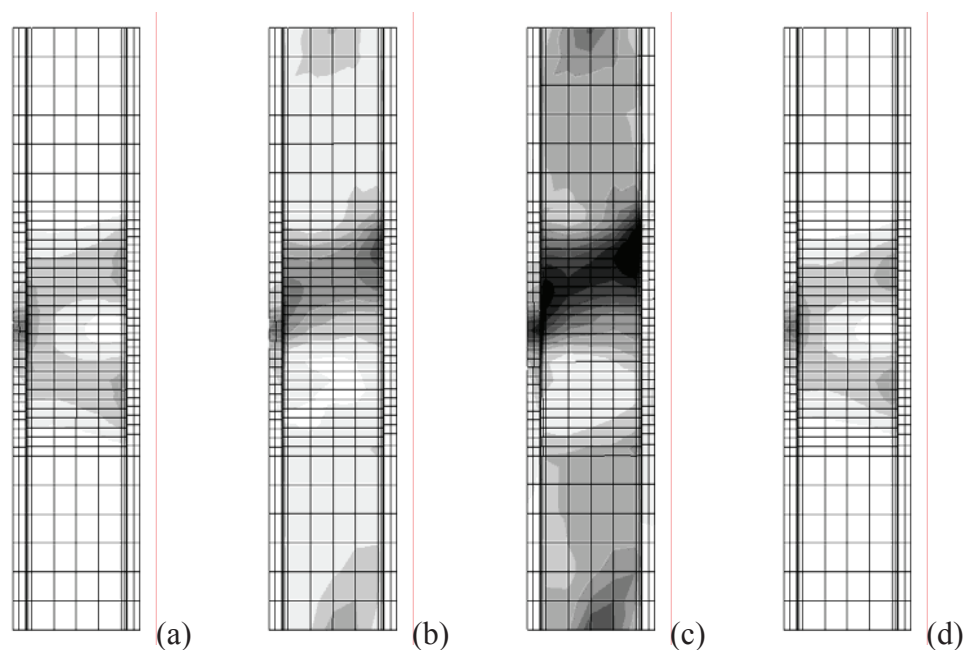


Figure 4.19. Deformation and stress states of the column in the PTED connection: (a) after the post-tensioning; (b) at a 0.375% drift; (c) at a 4% drift; (d) at the end of the cycles

The stress history in the most engaged finite element of the column flange, next to the top beam-to-column contact plate, is shown in Figure 4.20. The stress values increase with the drift, up to reach a level close to the yield stress. The stress distribution present at the end of the cycles is due to the contact pressure caused by the post-tensioning action.

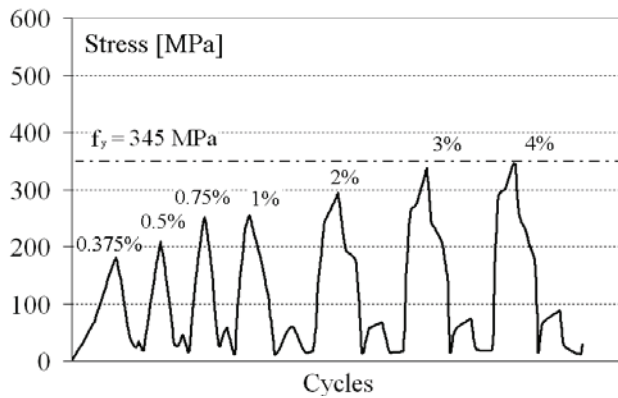


Figure 4.20. Stress history in the most engaged finite element in the column

4.4.5 Contact plates

The contact plates at the beam-to-column interface undergo a large amount of plastic deformations, the yielding starting from small values of imposed inter-storey drifts (0.5%).

The stress distributions in the top contact plate (Fig. 4.21a), for the relevant drift values, are shown in Figure 4.21.

After the application of the post-tensioning force (Fig. 4.21b), the stress concentrations correspond to the area in contact with the beam flange and web.

At a 0.375% drift (Fig. 4.21c), a stress concentration is visible at the top edge. The first yielding occurs at a drift equal to 0.5%, and the yielded zone extends as the drift increases.

The stress distribution referred to the 4% drift is shown in Figure 4.21d, where the large yielded area is evident.

At the end of the cycles, the stresses in the contact plates are larger than those corresponding to the post-tensioning, due to the occurred yielding, which is added to the effect of the post-tensioning action (Fig. 4.21e).

The stress history in the most engaged finite element of the top contact plate, located in the central part of the top edge, is shown in Figure 4.22. It is worth noticing that the first yielding occurs for a drift equal to 0.5%, and that

at the end of the numerical analysis the residual stress in the considered finite element is noticeable, it being equal to about 200 MPa.

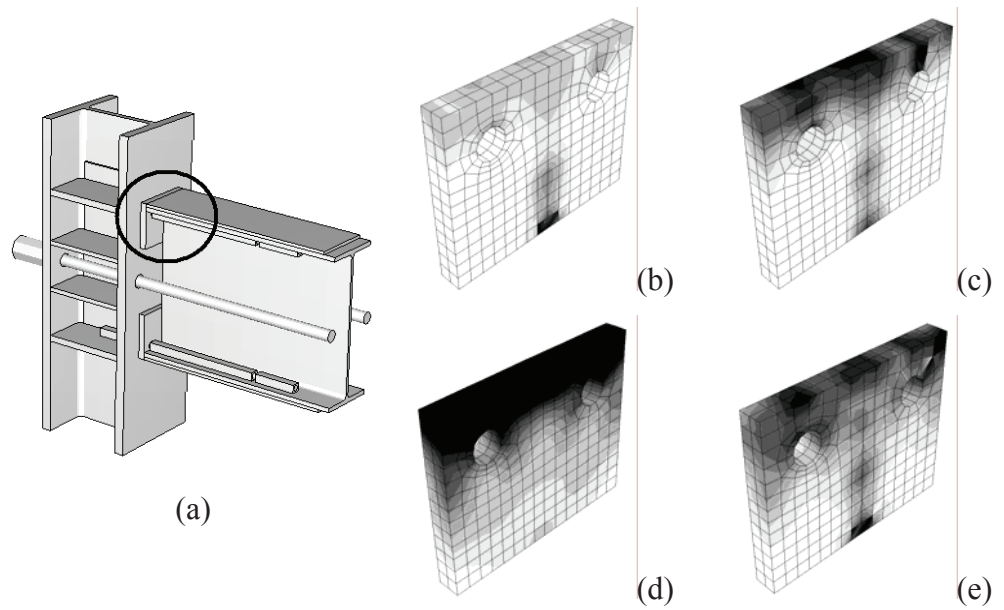


Figure 4.21. Deformation and stress states of the top contact plate (a) in the PTED connection: (b) after the post-tensioning; (c) at a 0.375% drift; (d) at a 4% drift; (e) at the end of the cycles

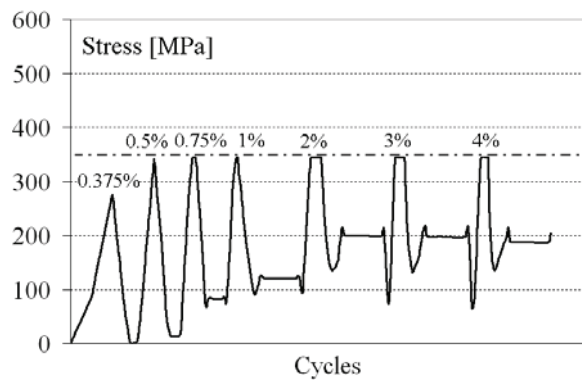


Figure 4.22. Stress history in the most engaged finite element in the top contact plate

4.4.6 Reinforcing plates

The reinforcing plates support the beam flanges in bearing the compression stress concentrations due to the gap opening, according to the mechanical behaviour of the PTED connections. The behaviour of the reinforcing plates during the considered cycles of drifts shows some extent of inelastic deformations.

The stress distributions of the top reinforcing plate (Fig. 4.23a) for the relevant drift values are shown in Figure 4.23.

The stress state after the post-tensioning (Fig. 4.23b) is not uniform and this is probably due to the presence of the couplers inside the beam flanges, since they are slightly loaded when the initial post-tensioning occurs.

At a drift equal to 0.375% (Fig. 4.23c) the overall stress in the reinforcing plate increases and stress concentrations are visible at the plate end, next to the location of the contact plates (left side in figure).

The yielding of the reinforcing plate starts at a 3% drift; at a drift equal to 4% the extension of the yielded area is not negligible, as it appears in Figure 4.23d.

After the end of the cycles, some residual stresses due to the previously occurred yielding are present at the plate end, as shown in Figure 4.23e.

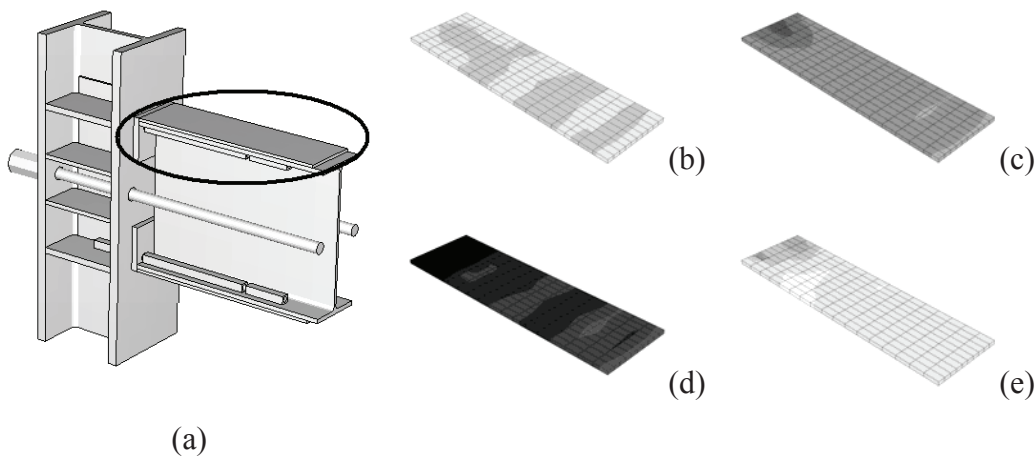


Figure 4.23. Deformation and stress states of the top reinforcing plate (a) in the PTED connection: (b) after the post-tensioning; (c) at a 0.375% drift; (d) at a 4% drift; (e) at the end of the cycles

The described stress history is evident considering the stress history of a finite element at the reinforcing plate end, next to the contact plate (Fig. 4.24).

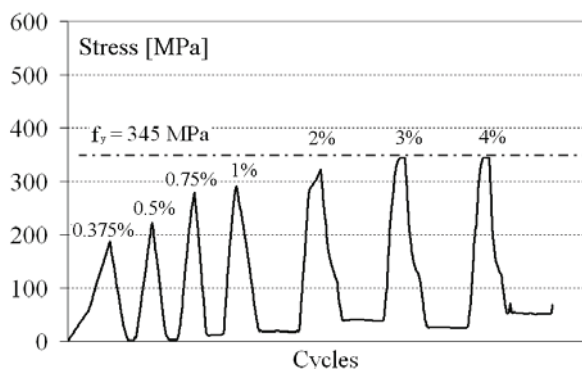


Figure 4.24. Stress history in the most engaged finite element in the top reinforcing plate

4.4.7 Continuity plates

The continuity plates support the column flanges in bearing the stresses coming from the beam flanges, above all when the gap at the beam-to-column interface opens. The behaviour of the continuity plates during the cycles of drift is always in the elastic range. The stress distribution of the top flange continuity plate (Fig. 4.25a) for the relevant drift values is shown in Figure 4.25.

After the initial post-tensioning, the stress level in the continuity plates is very small (Fig. 4.25b), some stresses being visible in the area next to the intersection between the flange and the web of the column, at the beam side.

When the imposed drift increases, the stress in the continuity plates grows in terms of both extension and values (Fig. 4.25c, d).

At the end of the cycles (Fig. 4.25e), the deformation and stress state at the contact plates is exactly the same as the one after the post-tensioning application, since no inelastic deformation occurs in the continuity plates, as also shown in Figure 4.26, in which the stress history in the most engaged finite element in the top continuity plate is plotted.

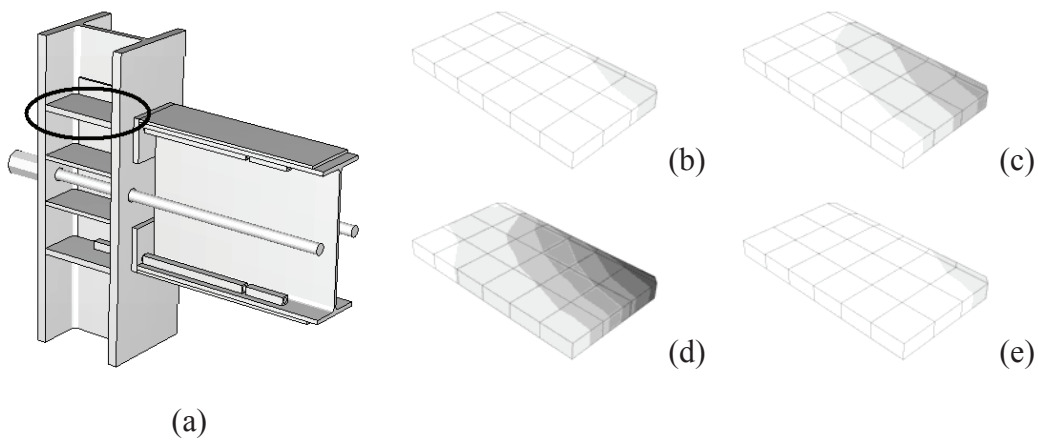


Figure 4.25. Deformation and stress states of the top continuity plate (a) in the PTED connection: (b) after the post-tensioning; (c) at a 0.375% drift; (d) at a 4% drift; (e) at the end of the cycles

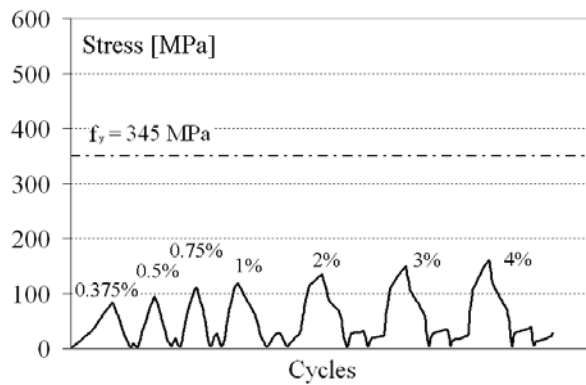


Figure 4.26. Stress history in the most engaged finite element in the top continuity plate

4.4.8 Stiffeners

The stiffeners are used to support the column flanges in bearing the stresses due to the action provided by the PT bars anchors. The behaviour of the

stiffeners during the cycles of drift is always in the elastic range. The stress distribution of the top stiffener (Fig. 4.27a) for the relevant drift values is shown in Figure 4.27.

The most engaged areas in the stiffeners are located next to the PT anchors (left in Fig. 4.27). As it is evident since the application of the post-tensioning action (Fig. 4.27b), the stress engagement of the stiffeners increases as the drift amplitudes do (Fig. 4.27c, d) and returns to the initial values and distribution at the end of the cycles (Fig. 4.27e).

Moreover, after the application of the post-tensioning action, the stress in the stiffeners never falls below 115 MPa, due to their engagement for both positive and negative imposed drifts, they being very close each other. In addition, above all for the smallest drift values, the stress peaks in the top stiffener occur for negative drifts. In fact, due to the local rotations of the PT anchors, the top stiffeners are compressed at negative drifts while the bottom stiffeners at positive drifts.

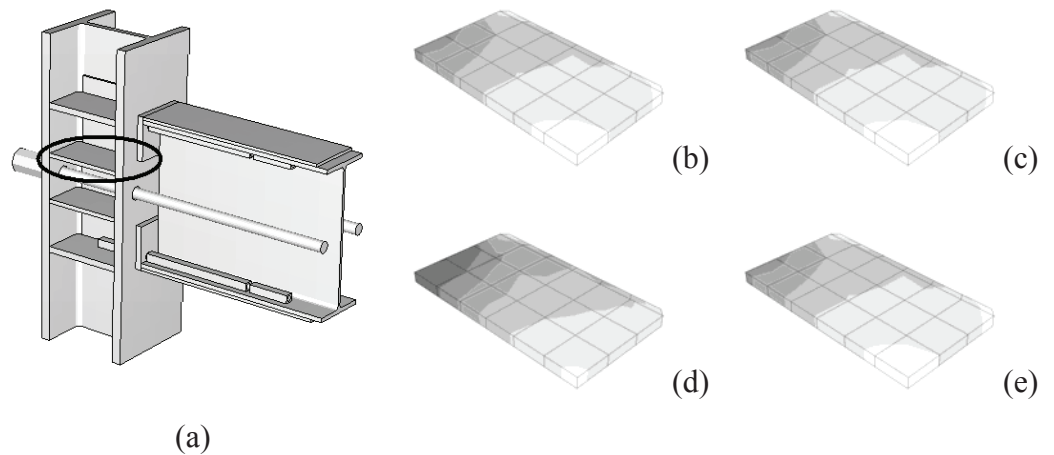


Figure 4.27. Deformation and stress states of the top continuity plate (a) in the PTED connection: (b) after the post-tensioning; (c) at a 0.375% drift; (d) at a 4% drift; (e) at the end of the cycles

No yielding occurs in the stiffeners, as shown in Figure 4.28, where the stress history in the most engaged finite element belonging to the top stiffener is plotted.

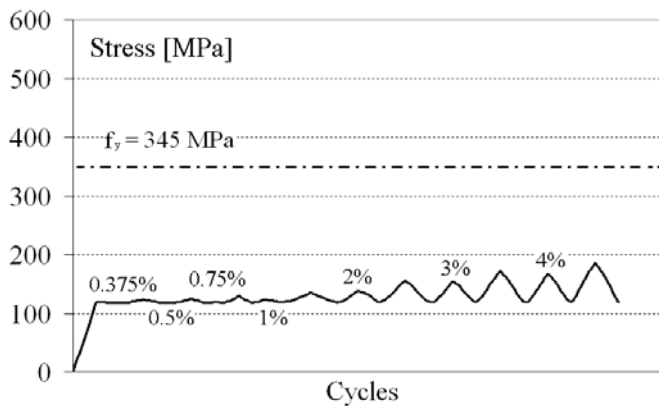


Figure 4.28. Stress history in the most engaged finite element in the top stiffener

4.4.9 Doubler plates

The doubler plates (Fig. 4.29a) are subjected to a strong shear demand, as already evidenced for the column web. The deformation and stress states for the relevant drifts is shown in Figure 4.29.

A symmetrical stress concentration occurs after the application of the post-tensioning action (Fig. 4.29b), with stress peaks in the areas next to the beam-to-column contact plates.

After the gap opening, stress concentrations occur on the side of the compressed beam flange (top part of the doubler plates, for positive drifts), as shown in Figure 4.29c, d, for drifts ranging from 0.375% to 4%.

At the end of the cycles (Fig. 4.29e), the stress state of the doubler plates is the same as at the post-tensioning action application, due to the absence of inelastic deformations.

The latter consideration is confirmed by the curve plotted in Figure 4.30, where the stress history in the most engaged finite element in the doubler plate is shown.

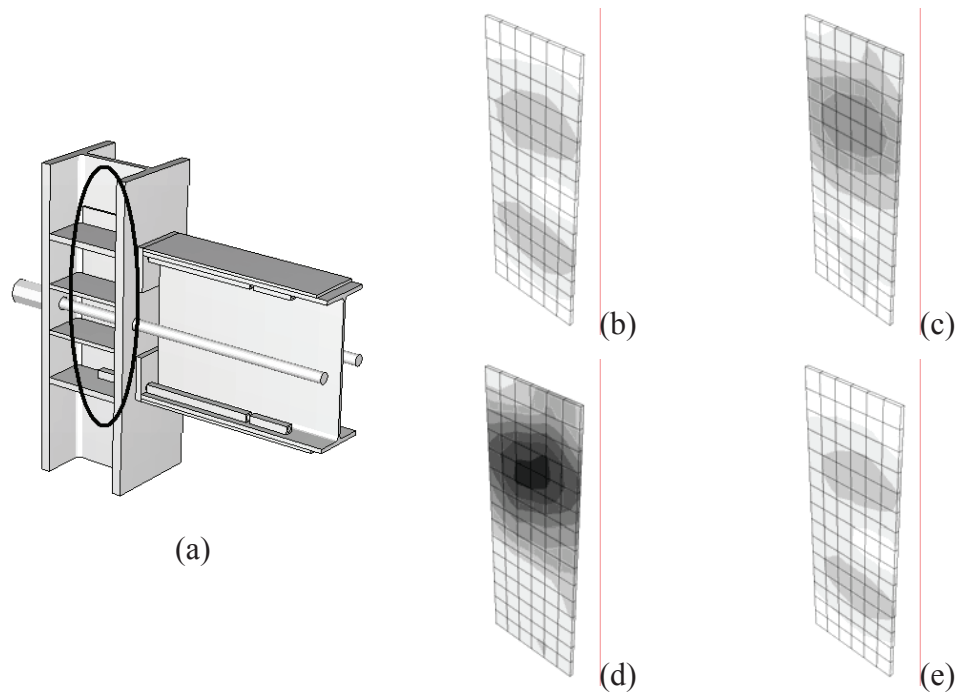


Figure 4.29. Deformation and stress states of a doubler plate (a) in the PTED connection: (b) after the post-tensioning; (c) at a 0.375% drift; (d) at a 4% drift; (e) at the end of the cycles

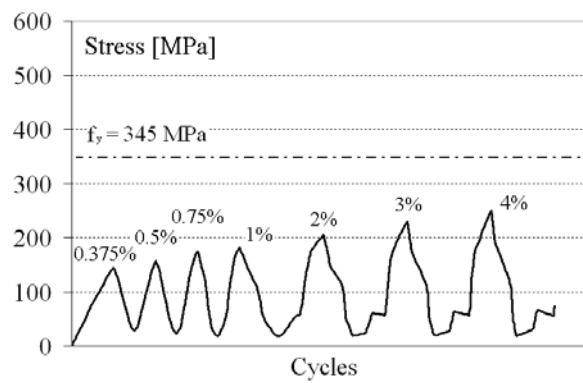


Figure 4.30. Stress history in the most engaged finite element in the doubler plate

4.4.10 *PT bars*

The PT bars, together with the ED bars, are the actual core of the PTED connection system. They have two main functions: 1) compressing the columns to the beams, in order to provide the necessary capacity of transferring the vertical shear and the bending moment in the nodes; 2) re-centring the structure in case of a seismic event. The PT bars behaviour must always be elastic, since their yielding would lead to the loss of the re-centring capability and, what is of more concern, the loss of the capacity of bearing the shears due to vertical loads. Both numerical and experimental results (Christopoulos et al., 2002a, b), show that no yielding occurs for the particular considered system.

Some concern is caused by the possible contact between the PT bars and the perimeter internal surface of the holes in the column flanges where they are located (Fig. 4.31a), since the consequent local rotations of the bars, occurring at large drifts, could create a dangerous bending effect on the PT bars, which would increase the tensile stresses caused by the already present tension state, the latter being due to the initial post-tensioning and to the PT bars elastic elongation. The above condition is confirmed by the curves plotted in Figure 4.31b, where the stress history in three remarkable points is shown. The NLR curve is referred to a cross-section of the PT bars where no relative rotations occur. The initial stress is equal to about 400 MPa and it cyclically increases when the interface gap opens, due to the elastic elongation of the PT bars. It is worth noticing that, in such section, the stress variation is not influenced by the sign of the drift, since the PT bar is located at the mid-depth of the beam and its elongation is the same for both top and bottom gap openings. The stress value at a 4% drift is equal to about 600 MPa, largely lower than the 1030 MPa limit for the considered high resistant steel. The TLR and BLR curves, on the contrary, are referred to top and bottom points of a cross-section of the PT bars where local rotations occur, next to the holes in the column flange. The local rotations cause a dangerous condition in the bars, since the added bending increases the stress up to about 1000 MPa. This evidence confirms the necessity of particular care in the design of the PT system, by adopting adequately large safety factors. At the end of the cycles, the stress value in all the considered elements is equal to the initial one, as it was expected due to the elastic behaviour of the PT bars.

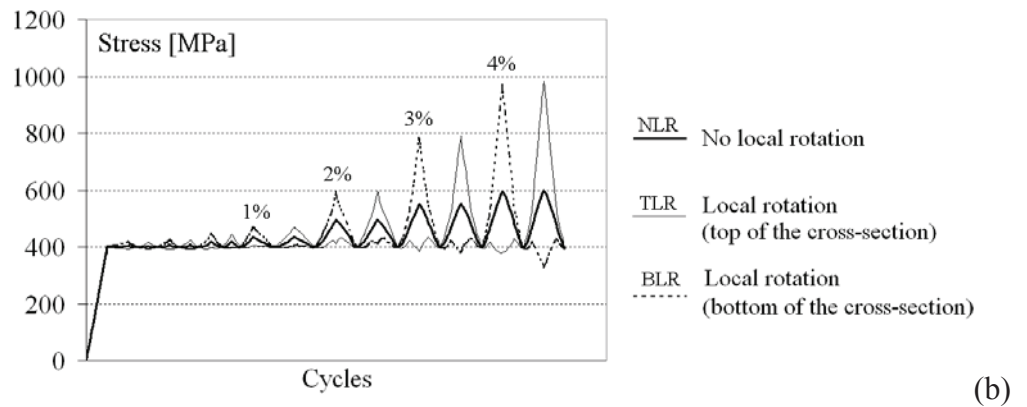
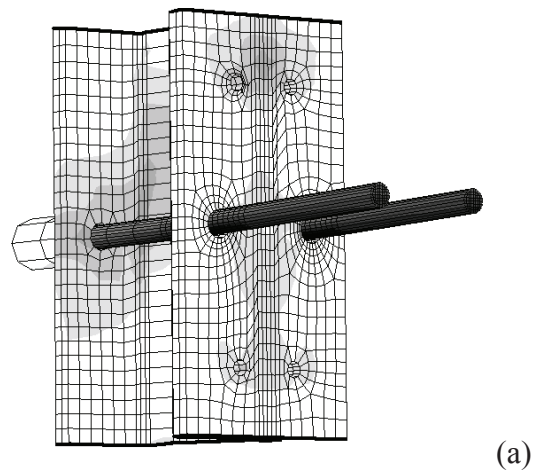


Figure 4.31. Behaviour of PT bars: (a) deformed configuration at 4% drift; (b) stress history

4.4.11 ED bars

The ED bars are the dissipative part of the study PTED beam-to-column connection. Dissipation of the input energy occurs by means of cycles of inelastic axial deformations. Due to the slenderness of such steel bars, they are confined by steel cylinders, which prevent the possible buckling in

compression (Christopoulos et al., 2002a, b). The stability of the cyclic behaviour of the considered ED bars is shown in Figure 4.32, where the numerical relationship between the gap opening and the axial force in the ED bars is plotted.

The deformed shape and the stress distribution of ED bars show inelastic deformations mainly in the middle parts. The presence of transversal displacement components demonstrate the tendency to buckle of the bars in compression after the hardening elongation, which are restrained by the steel confining cylinders.

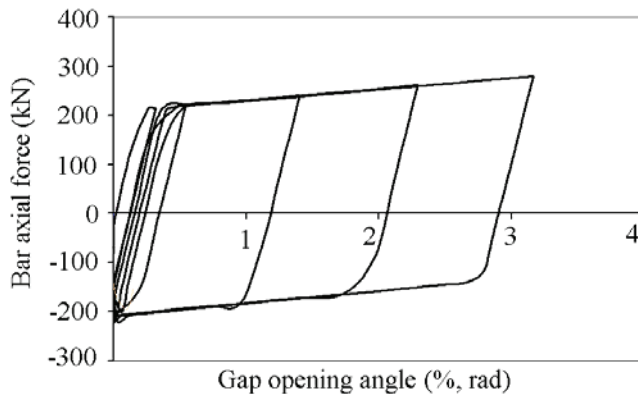


Figure 4.32. Numerical relationship between the bar axial force and the gap opening angle

4.5 SYNTHESIS OF RESULTS

In this chapter the numerical analysis of a PTED beam-to-column connection for steel moment resisting frames, characterized by the presence of PT and ED steel bars, is illustrated and discussed. The finite element models are implemented by the ABAQUS advanced computer program.

Two numerical models are presented, the first one being characterized by a symmetry-based simplifying assumption, and the second one having no simplifications. Both the models are calibrated on the basis of the experimental tests performed by Christopoulos et al. (2002a, b), who have

proposed and tested such a connection system. A very good approximation is achieved by the models and so they are used for studying the behaviour of the connection under cycles of imposed drift.

The experimental evidence is confirmed by the analysis of the stress and strain distribution obtained numerically. The global response of the connection is flag-shaped, with no residual drift and with capacity of dissipating the input energy. The beam essentially behaves in elastic range, with the attainment of the yield stress in very limited areas, namely at the interface with the contact plates and at the end of the reinforcing plates. The column clearly shows a strong shear demand in a limited portion of the web, when the interface gap opens. Stress values close to the yield limit are evidenced in a small area of the column flange, at the interface with the contact plate. However, these are not of concern because the column always behaves in elastic field. Contact and reinforcing plates undergo some inelastic deformations, which can be prevented by using high resistance steel for realizing such component parts. The effective energy dissipation capacity of ED bars is evidenced and the stability of their cyclic behaviour, due to the buckling inhibiting effect of the confining cylinders, is emphasized. The formation of local rotations of PT bars at the column flange PT hole, which induces an increment of the stress state of the PT bar itself, is stressed. The dangerousness of such a condition, due to the lack of ductility in high resistance steel, is underlined, leading to the necessity of limiting the design tension stress in the PT bars.

Chapter 5

PTED connections with PT strands and ED angles

5.1 THE REFERENCE EXPERIMENTAL STUDIES

5.1.1 Preliminary remarks

This chapter is focused on the FE analysis of the PTED beam-to-column connection for steel MRFs conceived and developed by Ricles et al. (2001, 2002b) and by Garlock et al. (2005). The objective is to reproduce the performed test, through reliable FE models, and, consequently, to investigate the system behaviour. The study connection type is shown in Figure 5.1.

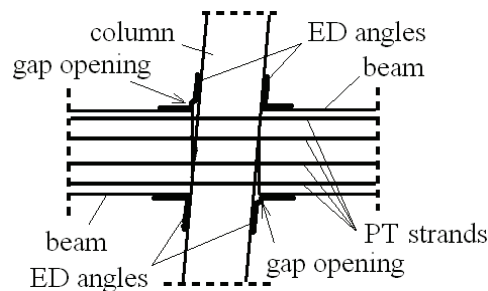


Figure 5.1. Detail of the PTED connection with PT strands and ED bolted angles, by Ricles et al. (2001, 2002b)

Since the behaviour of this type of connections strongly depends also on the inelastic behaviour of the bolted angles, an experimental and numerical campaign, focused on the cyclic response of bolted steel angles, was carried out by Garlock et al. (2003). The obtained results were used in the works on the whole PTED beam-to-column connections by Ricles et al. (2002b) and by Garlock et al. (2005).

In a similar perspective, in this chapter, a preliminary finite element model of a bolted steel angle, tested by Garlock et al. (2003), is developed. Subsequently, the information obtained by that model are implemented in the models of the whole PTED connection, which are referred to a specimen tested by Ricles et al. (2002b).

5.1.2 Experimental test on bolted steel top-and-seat angles

The reference experimental analysis on the cyclic behaviour of bolted steel angles is the one named L8-58-4 in Garlock et al. (2003). The test arrangement is schematically reproduced in Figure 5.2.

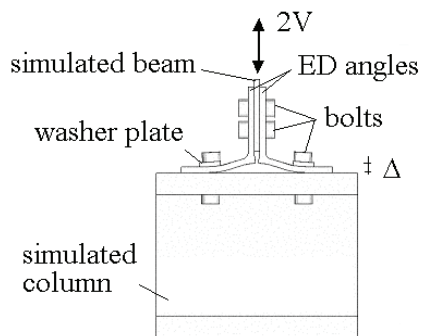


Figure 5.2. Scheme of the reference experimental study on bolted steel angles (Garlock et al., 2003)

The test is arranged so that a steel plate simulates the beam flange in a whole PTED connection, and a W14x176 wide flange profile stub simulates the column. In the test set up, two L203x203x15.9 bolted angles are used, with a measured yield stress equal to 330 MPa and a measured ultimate stress equal to 545 MPa. The column bolts are 25 mm diameter A325 bolts, with a 635

MPa nominal yield stress and 725 MPa nominal ultimate stress. The beam bolts are 32 mm diameter A325 bolts, with a 560 MPa nominal yield stress and a 825 MPa nominal ultimate stress. It is worth noticing that different values of yield and ultimate stress are considered, the former applying to bolts with diameter smaller than 25.4 mm, and the latter applying to bolts with larger diameter. Next to the column bolts, rectangular washer plates are located, with the aim of forcing the development of a cylindrical plastic hinge in the angles.

The test is carried out by imposing cycles of vertical displacements (Δ) to the simulated beam flange, according to the protocol plotted in Figure 5.3a. The corresponding vertical force (V), corresponding to a single angle, is one half of the measured one (according to Fig. 5.2).

The cyclic response of the study specimen is shown in Figure 5.3b, where it is expressed in terms of force (V) vs. displacement (Δ) curves.

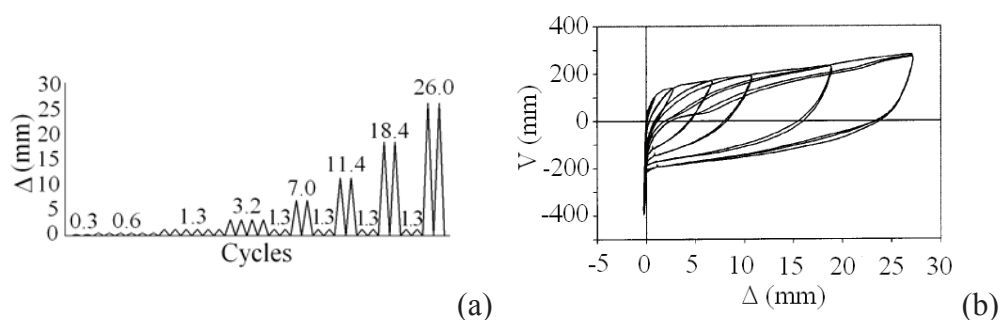


Figure 5.3. Test on bolted angles: (a) imposed displacement history; (b) cyclic response (Garlock et al., 2003)

5.1.3 Experimental test on a whole PTED connection

The reference full-scale test specimen, consisting in a cruciform-shaped internal PTED beam-to-column connection, is the one named PC4 in Ricles et al. (2002b) and it is shown in Figure 5.4. The assemblage is composed by two W24x62 steel beams, with nominal yield stress equal to 248 MPa, and a W14x311 steel column, with nominal yield stress equal to 345 MPa. Four

steel top-and-seat L203x203x15.9 angles are bolted to the beams and the column. The angles are 15.9 mm thick, and their yield and ultimate stresses are 263 MPa and 465 MPa, respectively. 25 mm diameter A325 bolts, with a 635 MPa nominal yield stress and 725 MPa nominal ultimate stress, are used for connecting the angles to both the beams and the column. Shim plates, with size equal to 275x254x9.5 mm and measured yield and ultimate stresses equal to 843 MPa and 895 MPa, respectively, are interposed between the angles and the column flanges. Beam flange reinforcing plates, with size equal to 254x57x12.7 mm and measured yield and ultimate stresses equal to 843 MPa and 895 MPa, respectively, are placed at the internal side of the beam flanges. The PT action is applied by means of height high resistance steel strands, with nominal ultimate stress and Young modulus equal to 1865 MPa and 199 GPa, respectively. The cross-section area of each strand is approximately equal to 140 mm², and they are located on both the sides of the beams, four per each side. The total initial PT force is equal to 710 kN.

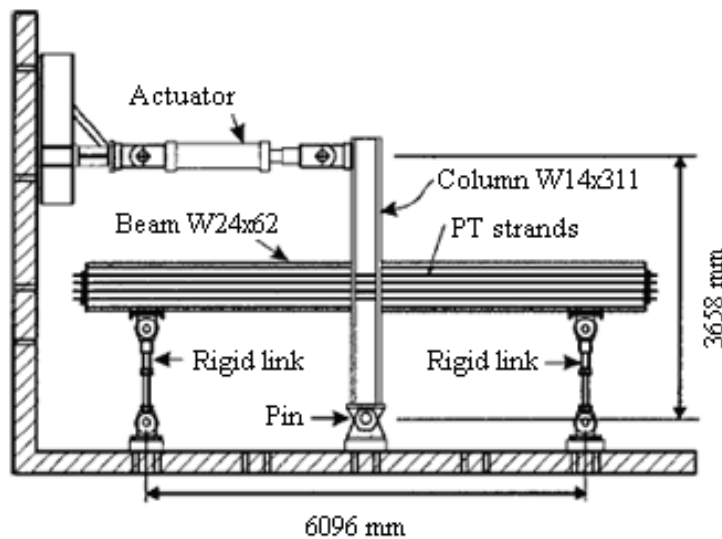


Figure 5.4. PTED beam-to-column internal connection test specimen (Ricles et al., 2002b)

The information related to the component parts of the tested PTED connection is summarized in Table 5.1.

Table 5.1. Geometrical and mechanical features of the tested connection component parts

Component parts	Thickness (t), Diameter (d) (mm)	Yield stress (f_y), Ultimate stress (f_u) (MPa)
Reinforcing plates	$t = 12.7$	$f_y = 843$
Shim plates	$t = 9.5$	$f_y = 843$
PT strands	$d \approx 13.35$	$f_u = 1865$
ED angles	$t = 15.9$	$f_y = 263$

The test consists in the application of cycles of lateral displacements to the top section of the column, characterized by increasing amplitudes. Figure 5.5 shows the displacement protocol, expressed in terms of drift, defined as the ratio between the lateral displacement at the top of the column and the height of the column itself.

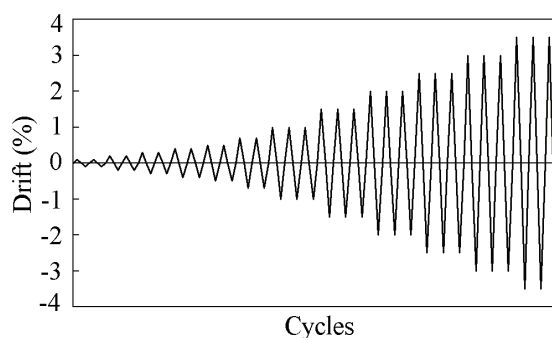


Figure 5.5. Cycles of imposed drift during the experimental test (Ricles et al. 2002b)

The cyclic response of the tested specimen is shown in Figure 5.6, where the lateral force-lateral displacement (Fig. 5.6a) and moment-relative rotation (Fig. 5.6b) experimental curves are plotted. The flag-shaped behaviour of the study PTED connection is evident, characterized by a “rigid” behaviour for small drift values, self-centring capability and energy dissipation capacity.

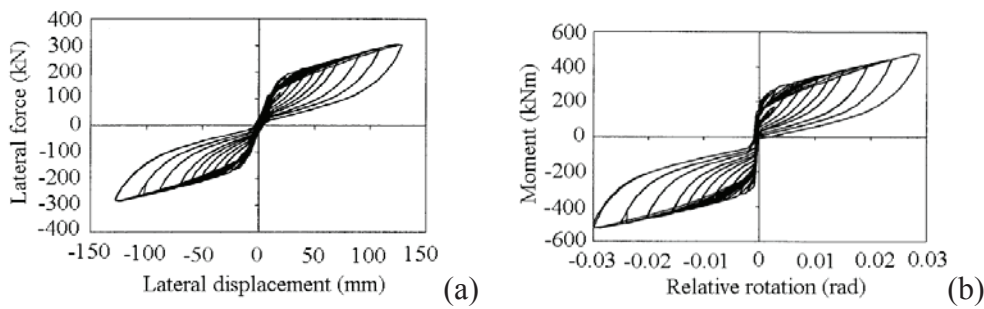


Figure 5.6. Experimental response of the study PTED connection: (a) lateral force-lateral displacement and (b) moment-relative rotation curves (Ricles et al., 2002b)

5.2 PRELIMINARY NUMERICAL STUDY ON ED ANGLES

5.2.1 The finite element model of ED angles

The preliminary numerical study on the ED angles sub-assembly is aimed at calibrating both the finite element mesh and the interaction properties between the connection component parts. The complexity of the ED angles numerical model is much smaller than the whole PTED connection one, with consequent speed advantages in the calibration process. The objective is to match a good approximation of the actual behaviour of the system, together with a reduced computational effort (Esposito et al., 2006a).

The finite element model (Fig. 5.7) faithfully reproduces the above described L8-58-4 specimen (Garlock et al., 2003), with the only difference that, in order to reduce the computational cost, half system is considered, exploiting the symmetry as respect to the column web mid-plane. Accordingly, appropriate boundary conditions are imposed, in order to prevent the out-of-plane displacements and the rotations around in-plane axes. Such modelling assumption does not affect the results, since no out-of-plane

displacements are expected in such simple sub-system. Moreover, a fix joint is modelled at the simulated column base.

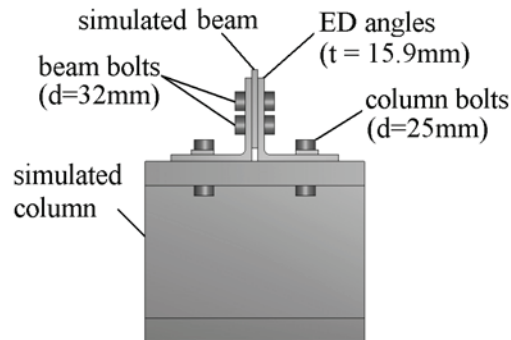


Figure 5.7. Geometrical details of the ED angles sub-assembly FE model

The nominal stress-strain relationships for the materials considered in the model are plotted in Figure 5.8, where reference is made to a structural steel (SSS, for the simulated column, the simulated beam and the washers), a column bolt steel (CBS), a beam bolt steel (BBS), and an angles steel (AS).

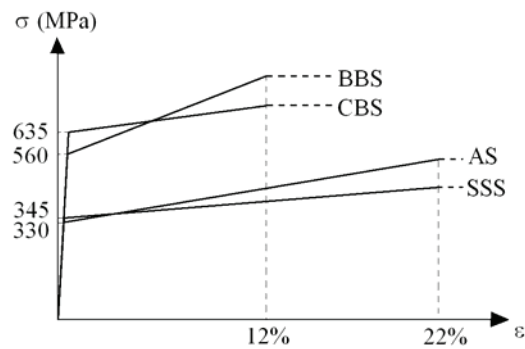


Figure 5.8. Nominal stress-strain relationships of the modelled materials

Information on the above materials, in terms of true stresses and plastic strains, and on the related component parts, is summarized in Table 5.2.

Table 5.2. Mechanical features of the modelled materials in terms of true stresses and plastic strains, and associated component parts

Material	Yield stress (MPa)	Ultimate stress (MPa)	Ultimate strain plastic (%)	Component parts
SSS	345	550	19.6	Simulated beam, simulated column, washer plates
CBS	635	810	10.9	Column bolts
BBS	560	925	10.9	Beam bolts
AS	330	665	19.6	ED angles

With regard to the interactions between component parts, tie constraints, preventing any relative displacements between the adjacent surfaces, are imposed between component parts with negligible relative movement. This is the case, in particular, of the interactions between the simulated beam and the ED angles. Such modelling assumption, which strongly reduces the computational cost of the analysis, is a simplification, since the actual interaction between the mentioned parts is a contact with friction. Anyway, it is justified based on a couple of ad-hoc analyses, in which the system behaviour is studied by considering, for those interactions, once a tie constraint and once a friction contact. As shown in Figure 5.9, the differences are absolutely negligible, and so the former modelling assumption is adopted.

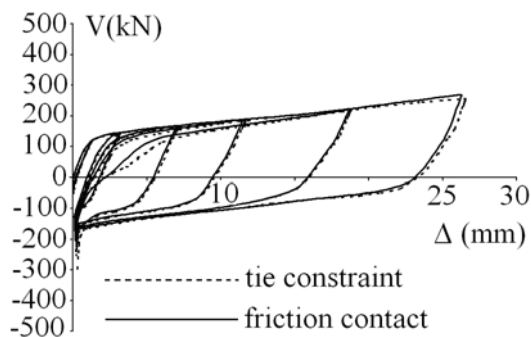


Figure 5.9. Numerical responses in case of tie constraint or friction contact at the interfaces between simulated beam and ED angles

Tie constraints are also used for the bolt nuts-washers and washers-ED angles interactions. On the contrary, penalty friction tangential contacts, with friction coefficient equal to 0.33, are used for the interactions between ED angles and simulated column (Fig. 5.10), whereas frictionless contacts are defined between the bolt shank lateral surfaces and the related holes surfaces.

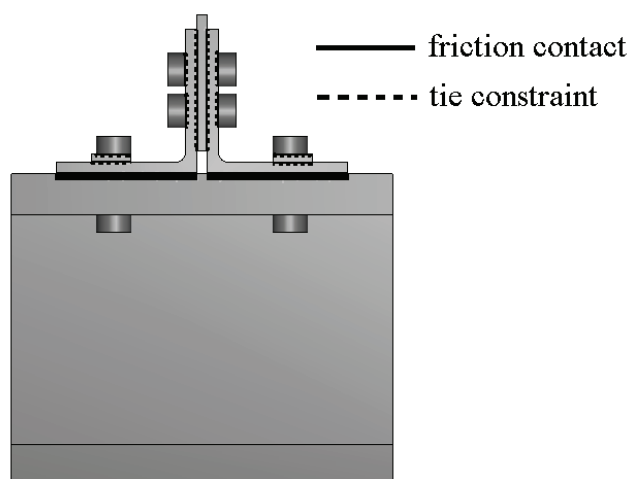


Figure 5.10. Surface-to-surface interactions used in the FE model

The imposed displacement history considered in the model (Fig. 5.11) is similar to the experimental one (Fig. 5.3a), with the differences that the first cycles are neglected and that only one cycle per amplitude is considered, in order to reduce the computational costs. It is worth noticing that the values indicated in Figure 5.11 (Δ_b) are the displacements imposed to the top of the simulated beam flange, which are selected in order to provide the same displacements at the angle bases (Δ , in Fig. 5.2) as the experimental ones.

The size of the initial increments in the steps, each of them corresponding to an imposed displacement, are selected in order to achieve the best convergence speed. For the first cycle, corresponding to the bolts fastening, a fraction equal to 0.05 is considered, whereas, for the remaining steps, fractions equal to 0.02 are used.

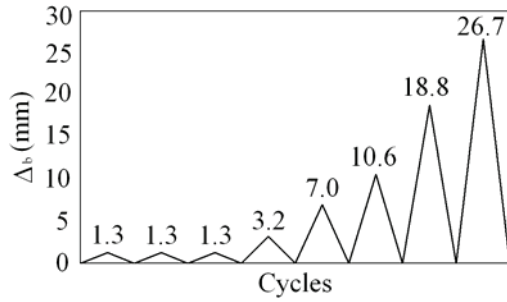


Figure 5.11. Imposed cyclic displacement history in the numerical analysis

The finite element mesh (Fig. 5.12) is made by tri-dimensional continuum first-order elements with reduced integration (C3D8R) for all the component parts of the model. The ED angles are more finely meshed than the simulated column, in order to both adequately catch the behaviour of the angles themselves and match the requirements imposed by the rigid master-slave algorithm used in contact by ABAQUS/Standard, described in section 3.2.6, which implies that slave surfaces must be meshed in a finer way than the master ones.

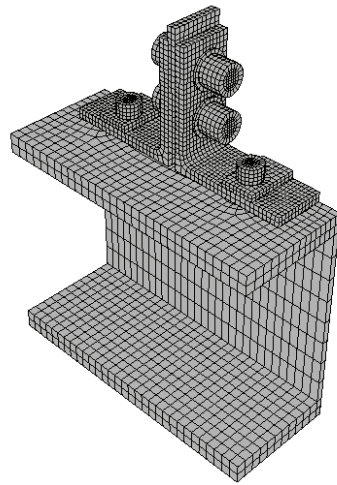


Figure 5.12. Finite element mesh of the ED angles sub-assembly model

5.2.2 Numerical vs. experimental results

The comparison between numerical and experimental results is shown in Figure 5.13, where it is expressed in terms of force-displacements curves. The numerical initial stiffness and yielding force faithfully correspond to the experimental ones, whereas some minor differences are present in terms of ultimate strength, the numerical value being 3% lower than the experimental one, and of amplitude of the last cycle, corresponding to a lower estimation (13%) of the energy dissipation as respect to the experimental evidence.

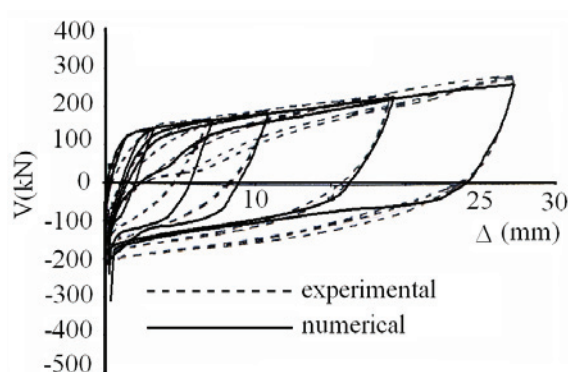


Figure 5.13. Numerical vs. experimental force-displacement curves

Figure 5.14 shows the deformed configurations of the system at the maximum imposed displacement (Fig. 5.14a) and at the end of the cycles (Fig. 5.14b). In the areas plotted in black the yield stress of the angle steel is reached. The dissipative mechanism evidenced experimentally by Garlock et al. (2003), characterized by the formation of three cylindrical plastic hinges, is adequately caught. In particular, the hinges are located next to the washer plates, on the column side, and next to the fillet of each angle leg.

Although some minor discrepancies are present in the numerical results, compared to the experimental ones, the model is sufficiently accurate and suitable. Consequently, the obtained information related to the surface-to-surface interaction properties and to the mesh are useful to be implemented in the finite element model of the whole PTED connection with PT strands and ED angles.

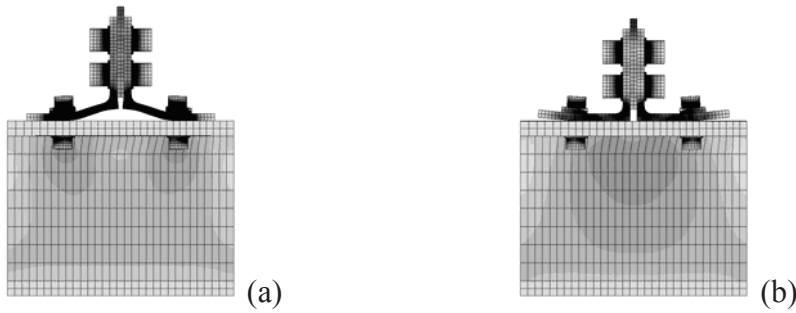


Figure 5.14. Deformed configurations of the ED angles sub-assembly: (a) at the maximum vertical displacement; (b) at the end of the cycles

5.3 FINITE ELEMENT MODELS OF THE PTED CONNECTION

5.3.1 The geometry of the models

In order to carry out the numerical study on PTED beam-to-column connections with PT strands and ED angles, two finite element models are developed, like in the case of the connection with PT and ED bars described in Chapter 4. The geometry of the tested assemblage is faithfully reproduced in both models (Fig. 5.15).

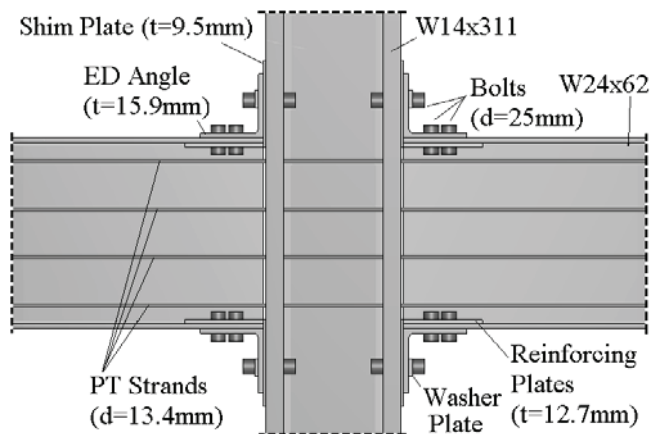


Figure 5.15. Geometrical details of the PTED connections FE models

The first model (Fig. 5.16) exploits the system symmetry with respect to the mid-plane of column and beams webs (Esposito et al., 2006a), as shown in Figure 5.16b. Symmetry boundary conditions are imposed accordingly, so that the out-of-plane displacements of points belonging to the symmetry plane are prevented. As resulting from the experimental results and confirmed by the second model described later on, the symmetry condition does not affect the results.

The second model is not based on symmetry simplifying assumptions, as shown in Figure 5.16c. The increased computational cost of such model is counterbalanced by the possibility of catching out-of-plane phenomena, which could occur considering the ultimate behaviour of the connection, as well as the capability of studying in detail the cyclic behaviour of all the connection component parts.

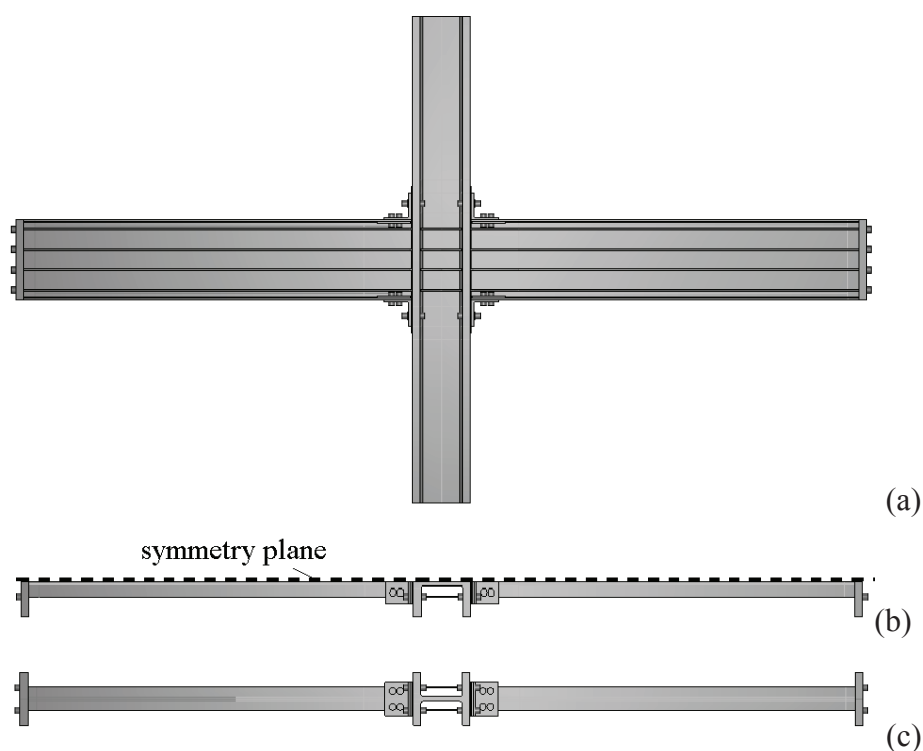


Figure 5.16. Geometry of the numerical models: (a) lateral view; plane views of (b) the symmetry-based simplified model, and (c) of the complete model

The differences in the two models are only referred to the symmetry simplifying assumption, whereas all the other modelling issues are the same and they are described in the following sections.

5.3.2 *The properties of the materials*

The materials considered in the finite element models correspond to the ones used in the reference experimental test. Their mechanical behaviour, expressed in terms of nominal stress-nominal strain curves, is shown in Figure 5.17, according to the information provided in (Ricles et al., 2002b).

The HSS material properties are assigned to the PT strands, the PLS ones to the shim and reinforcing plates, the BOS ones to the bolts, the COS ones to the column, the washers and the anchor plates, the ANS ones to the ED angles, and the BES ones to the beams. With particular reference to the HRS steel, the yield stress is assumed equal to 70% of the ultimate stress, according to the approach followed in (Ricles et al., 2002b).

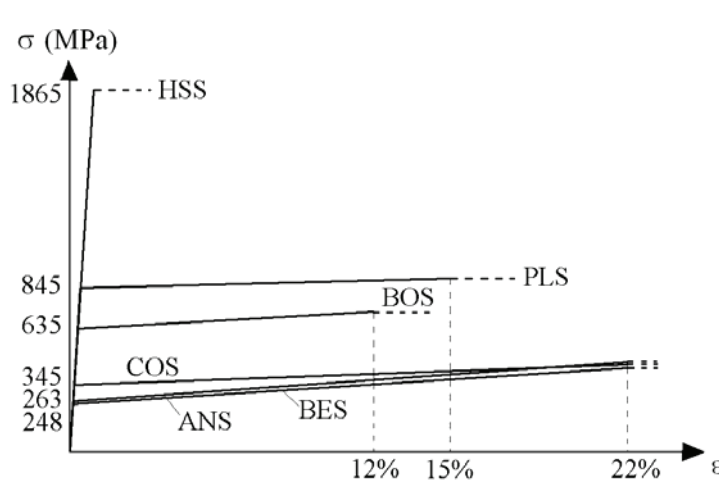


Figure 5.17. Nominal stress-strain relationships for the modelled materials

In Table 5.3 the mechanical features of the above mentioned materials, expressed in terms of true stresses and plastic strains, and the component parts they are assigned to, are summarized.

Table 5.3. Mechanical features of the modelled materials, in terms of true stresses and plastic strains, and associated component parts

Material	Yield stress (MPa)	Ultimate stress (MPa)	Ultimate plastic strain (%)	Component parts
COS	345	550	19.6	Column, washers, anchor plates
BES	248	530	19.6	Beams
PLS	845	1030	13.5	Shim plates, reinforcing plates
BOS	635	810	10.9	Bolts
HSS	1305	1865	-	PT strands
ANS	263	567	19.6	ED angles

5.3.3 The interactions between component parts

In order to model the interactions between welded component parts, tie constraints are used, so that no relative motion between the surfaces in contact is possible. In particular, tie constraints are considered for modelling the following interactions: bolt-washer; washer-ED angle; shim plate-column; reinforcing plate-beam flange; reinforcing plate-bolt; ED angle-beam flange. It is worth noticing that the latter assumption follows on the results of the preliminary analysis carried out on the isolated ED angle sub-assembly, described in section 5.2.

Surface-to-surface contacts are used to model the following interactions: shim plate-beam; shim plate-ED angle; shim plate-reinforcing plate. A “penalty friction tangential contact” is used for modelling the above interactions, so allowing to transmit both shear and normal forces. The considered friction coefficient is equal to 0.33, while the maximum elastic slip is 0.005 times the characteristic slave surface element dimension.

Information on the used contact formulation is provided in section 3.2.6.

5.3.4 The load history and the multi-step analysis

The study PTED connection is initially subjected to the post-tensioning of the PT strands and to the fastening of the bolts and, subsequently, to a series of horizontal displacement cycles applied at the top section of the column

(Fig. 5.18). The analysis is subdivided into a number of subsequent static steps, the first one corresponding to the application of the PT action (87.5 kN per strand) and of the bolt fastening (250 kN per bolt), and the other ones corresponding to the application of the imposed drift history.

As respect to the experimental loading history, only one cycle for each displacement amplitude is considered and the cycles corresponding to drifts of 0.1, 0.3 and 0.5% are neglected, in order to reduce the computational efforts.

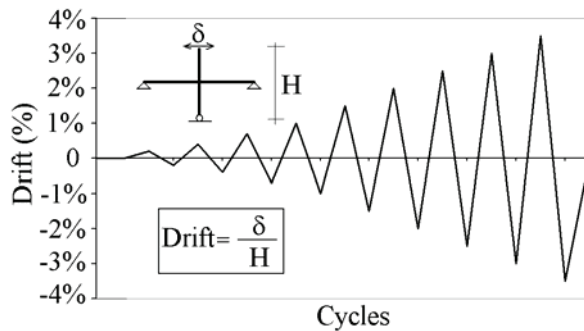


Figure 5.18. Imposed cyclic drift history in the numerical analyses

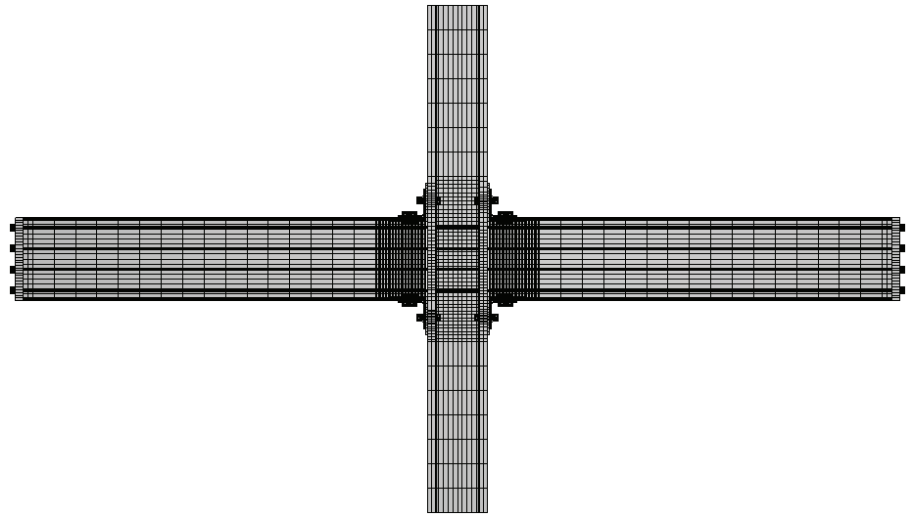
The size of the initial increments in the steps are selected in order to achieve the best convergence speed. A progressive reduction in the initial increment size is chosen, corresponding to the increase of the problem non-linearity. In particular, fractions equal to 0.02 are used for the cycles up to 0.4% drift, equal to 0.01 for cycles up to 1% drift, equal to 0.005 for cycles up to 2%, equal to 0.002 for cycles up to 3%, and 0.001 for the remaining cycles.

5.3.5 The mesh

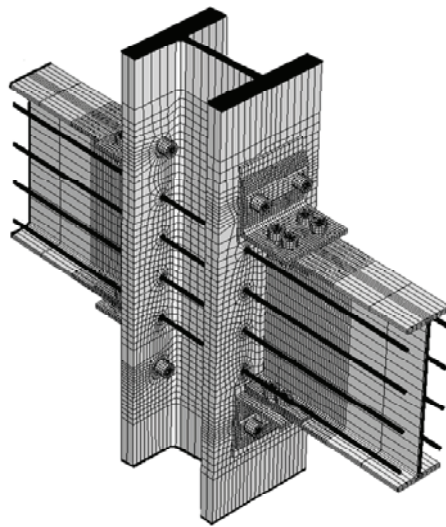
The finite element mesh (Fig. 5.19) is made by tri-dimensional continuum first-order elements with reduced integration (C3D8R) for all the component parts of the model. In ABAQUS/Standard, this choice matches the requirements typical of problems involving material plasticity, contact interactions and large size models, as described in section 3.2.

The mesh refinement of the surfaces involved in contact interactions derives from the rigid master-slave algorithm used in contact by

ABAQUS/Standard, described in section 3.2.6, which implies that slave surfaces must be meshed in a finer way than the master ones. In particular, referring to the modelled contact interactions, the shim plates surfaces involved in contact are master as respect to the ED angles, the beam flanges and to reinforcing plates ones.



(a)



(b)

Figure 5.19. Finite element mesh of the complete model: (a) lateral view of the whole model; (b) detail of the nodal area

5.4 NUMERICAL VS. EXPERIMENTAL RESULTS ON THE PTED CONNECTION

5.4.1 Global response curves

The comparison between the numerical and experimental lateral force-lateral displacement curves is shown in Figure 5.20.

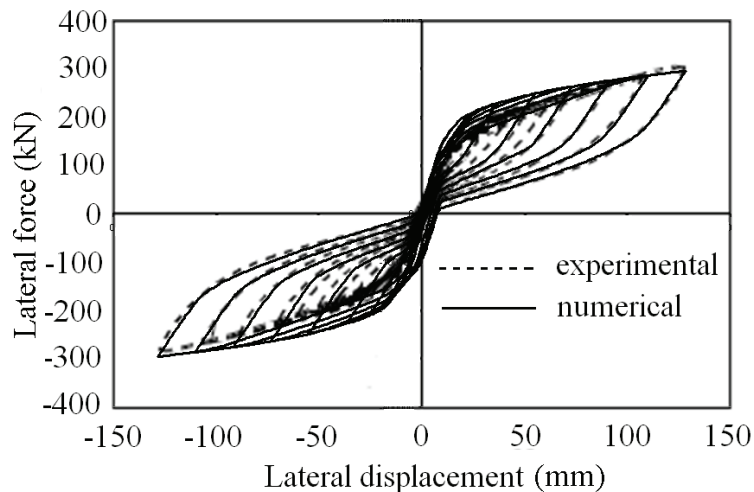


Figure 5.20. Numerical vs. experimental force-displacement curves

Some differences are present in terms of both stiffness and strength for the first five cycles. In fact, the numerical values of stiffness and strength are about 30% and 10% larger than the experimental ones, respectively. The overestimation of the initial stiffness is maybe due to the use of cylindrical solid finite elements for modelling the PT strands, which are actually more deformable, they being the assembling of more than one steel wire. With regard to the scatter of strength in the first cycles, it is maybe due to the fact that the beams of the tested PC4 specimen were left in place after previous tests, where some minor yielding in the beams occurred (Ricles et al., 2002b).

On the other hand, the experimental response of the considered system is successfully reproduced at the last four cycles.

The connection behaviour is linear elastic up to a drift equal to 0.25%, which approximately corresponds to the fully operational level according to the SEAOC Vision 2000 indications (1995). This result confirms that the PTED connection behaves like a traditional welded one under frequent earthquakes.

After the gap opening, the connection stiffness noticeably reduces, as expected on the basis of both the theoretical predictions and the experimental evidence.

At last, both the expected capacity of dissipating the input energy and the capability of returning to the initial configuration at the end of the cyclic history of imposed drifts are adequately caught by the finite element models, as demonstrated by the flag-shaped response curves obtained from the numerical analyses

5.4.2 Deformed configurations of the node

The numerical results match the experimental ones also considering the deformed configurations of the connection during the different phases of the imposed cyclic drift history.

In Figure 5.21a the lateral view of the whole assemblage at the maximum drift reached during the analysis, namely 3.5%, is shown. Figure 5.21b gives a plan view of the assemblage at the 3.5% drift, and it confirms that no out-of-plane displacements occur in the considered PTED connection also for large drift values, so justifying the reliability of the results obtained from the symmetry-based simplified model. At last, the detail of the deformed node at the 3.5% drift is shown in Figure 5.21c, where the gap opening mechanism is clearly visible.

Although some minor imperfections are present in the numerical model calibration, it anyway appears useful for investigating the stress and strain states of the connection during the simulated test.

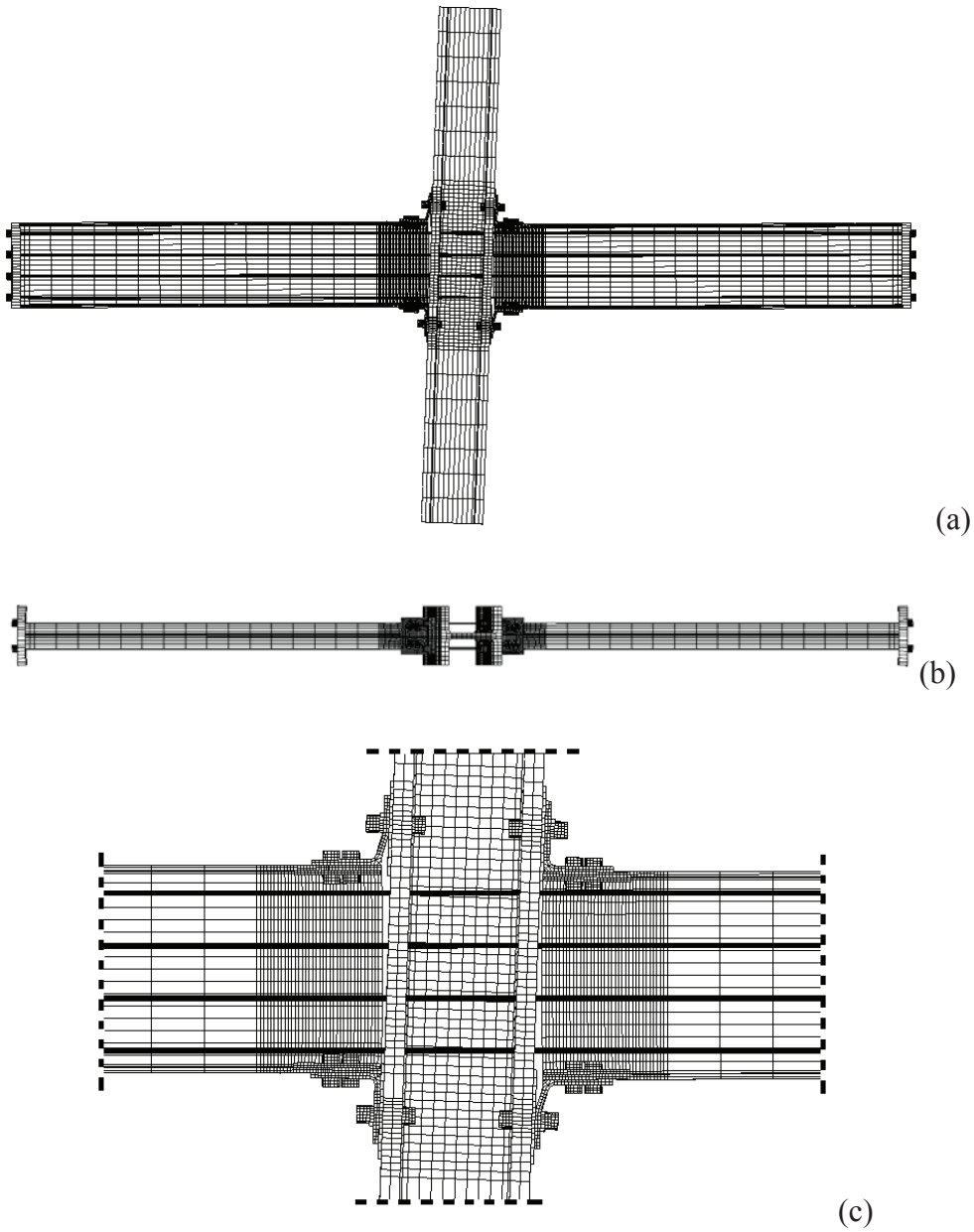


Figure 5.21. Deformed configuration of the study PTED connection: (a) lateral view; (b) plan view; (c) detail of the node

5.5 BEHAVIOUR OF THE COMPONENT PARTS

5.5.1 Preliminary remarks

In this section the detailed investigation on the behaviour of the considered PTED beam-to-column connection is carried out. The deformation and stress states of the connection parts are shown, considering four main phases of the cyclic history, namely: after the application of the PT action; at a 0.4% drift, when decompression occurs; at a 3.5% drift, which is the maximum drift reached in the analysis; at the end of the cycles.

The results are provided by considering, at first, the behaviour of the assembled node, and then, the behaviour of the main component parts of the connection, which are analysed separately.

5.5.2 Assembled node

The deformed configurations of the node, together with the related stress distributions, at the above mentioned relevant drifts, are shown in Figures from 5.22 to 5.25. For each deformed configuration, both a perspective and a lateral view are provided, in order to correctly catch the node behaviour.

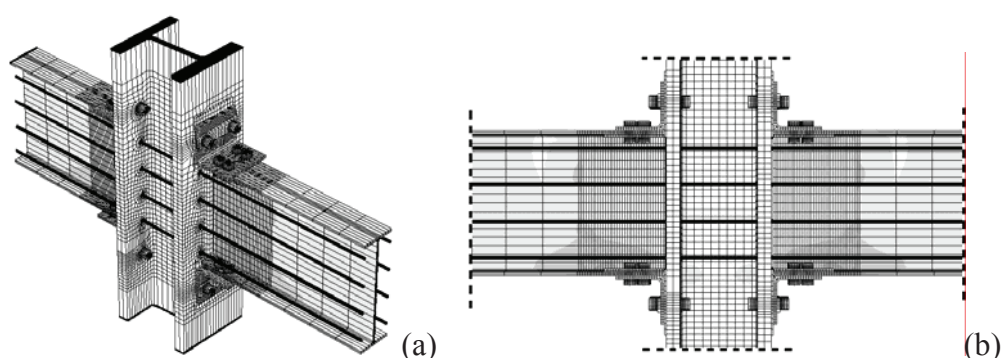


Figure 5.22. Deformation and stress state of the study PTED connection after the post-tensioning: (a) perspective and (b) lateral views

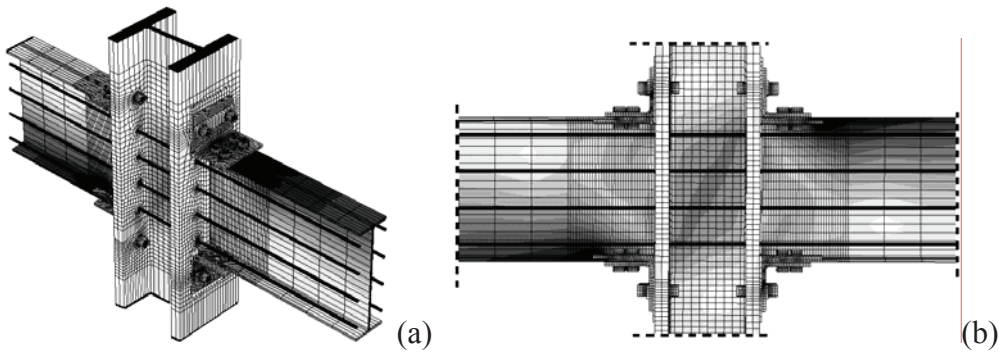


Figure 5.23. Deformation and stress state of the study PTED connection at a 0.4% drift: (a) perspective and (b) lateral views

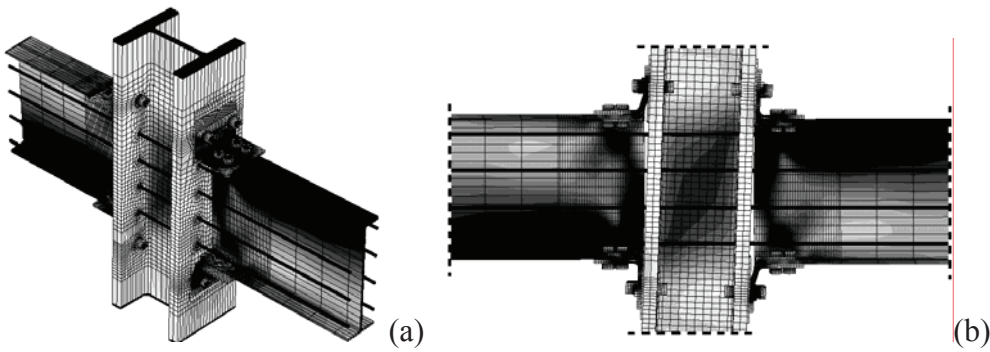


Figure 5.24. Deformation and stress state of the study PTED connection at a 3.5% drift: (a) perspective and (b) lateral views

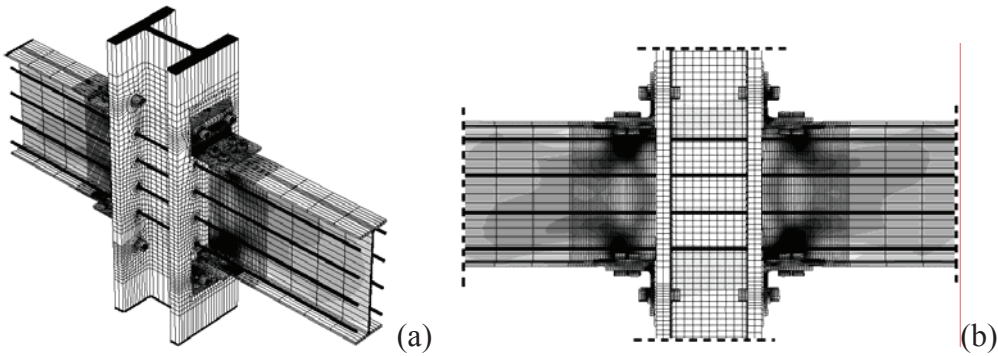


Figure 5.25. Deformation and stress state of the study PTED connection at the end of the cycles: (a) perspective and (b) lateral views

5.5.3 Beams

During the cycles of imposed drifts, the behaviour of the beams is essentially elastic, except for some yielding undergone in a limited area of the beam ends at the beam-to-column interface and at the end of the ED angle legs. Figure 5.26 shows the deformation and stress states in the beam at the end of the post-tensioning, at drifts equal to 0.4%, 3.5%, and at the end of the cycles.

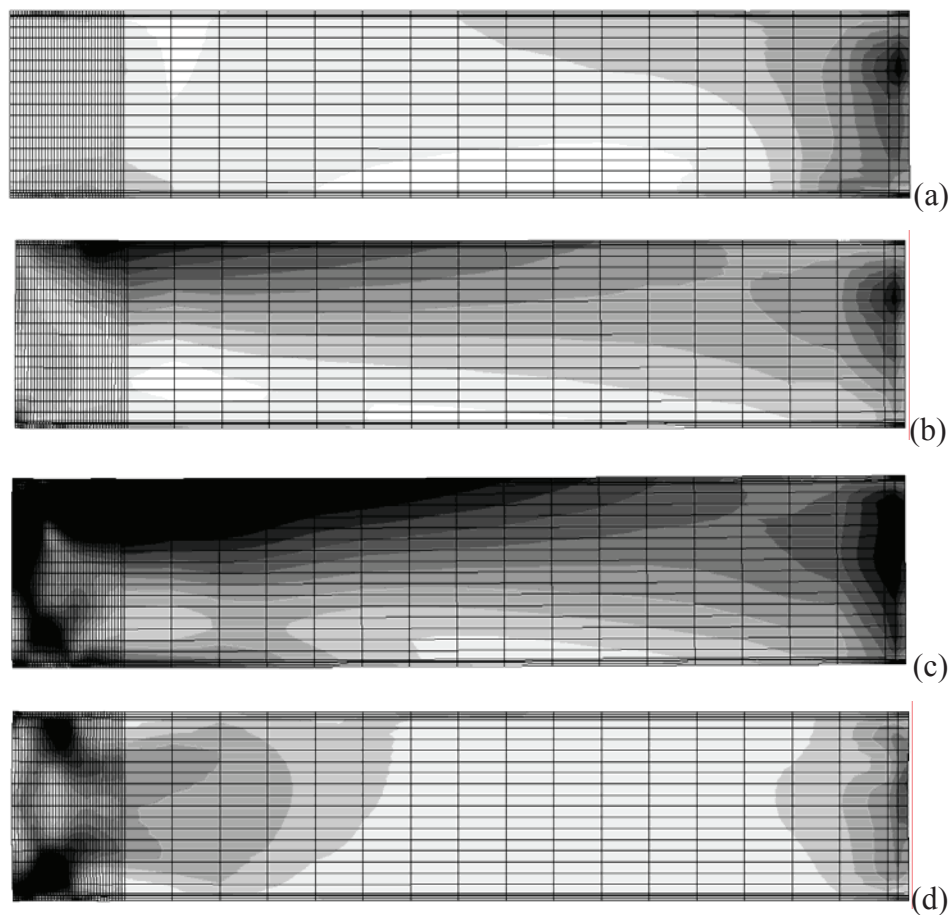


Figure 5.26. Deformation and stress states of the beam in the PTED connection: (a) after the post-tensioning; (b) at a 0.4% drift; (c) at a 3.5% drift; (d) at the end of the cycles

After the post-tensioning (Fig. 5.26a), stress concentrations are visible at the beam ends, due to the contact stresses with the column and with the plates for the anchorage of the PT strands.

At a drift equal to 0.4% (Fig. 5.26b), stress concentrations are present in the compressed area (top flange on the left of the beam), and the largest extent is visible at some distance from the beam left end, after the location of the ED angles and the reinforcing plates. With regard to the bottom flange of the beam end, despite it is not in contact with the column flange, a stress distribution is evident, it being due to the presence of the steel ED angle.

At a drift equal to 3.5% (Fig. 5.26c), the yield stress is reached in a portion of the flange and web.

At the end of the cycles (Fig. 5.26d), the stress distribution shows the small yielded areas, next to the ED angles location.

The stress history in a finite element of the beam flange is plotted in Figure 5.27. It is evident that the stress in the considered element increases with the drift, the peaks being attained when the flange is in compression, and the yield stress is exceeded after the 2% drift. A residual stress, larger than the initial one due to the post-tensioning action, is visible at the end of the cycles, due to the above described small yielding.

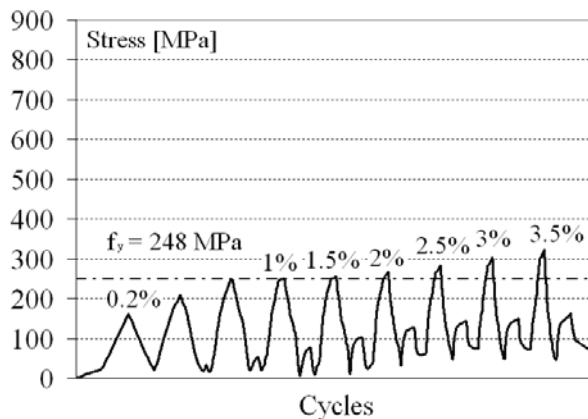


Figure 5.27. Stress history in the most engaged finite element in the beam flange

5.5.4 Column

During the cycles of imposed drift, the behaviour of the column is always within the elastic range. The deformation and stress states for the relevant drift values are shown in Figure 5.28.

At the end of the post-tensioning (Fig. 5.28a), the stress values in the column are very small, due to the large size of the column component parts.

At a 0.4% drift (Fig. 5.28b), the stress flow in the column web is evident, and its intensity increases as far as the drift does (Fig. 5.28c).

At the end of the cycles (Fig. 5.28d) the stress distribution is the same as the one after the post-tensioning, so confirming the elastic behaviour.

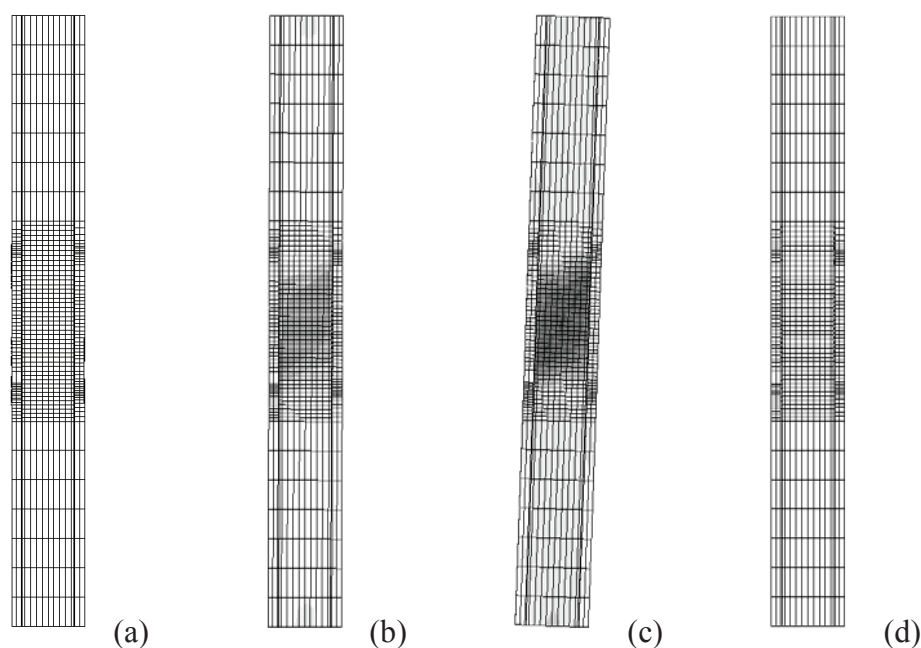


Figure 5.28. Deformation and stress states of the column in the PTED connection: (a) after the post-tensioning; (b) at a 0.4% drift; (c) at a 3.5% drift; (d) at the end of the cycles

The stress history in the most engaged finite element of the column web is plotted in Figure 5.29. The stress increases with the drift, but it is always

largely below the yield limit. It is worth noticing that the stress present at the end of the cycles is due to the post-tensioning action.

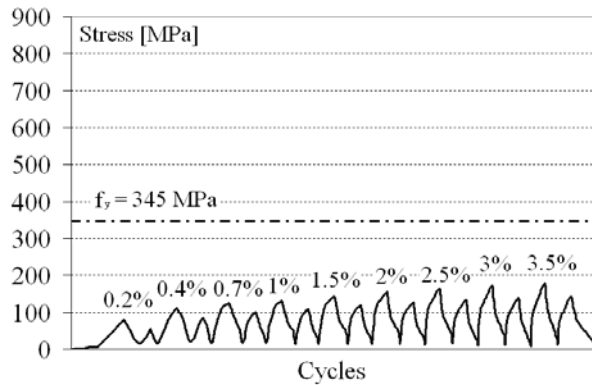


Figure 5.29. Stress history in the most engaged finite element in the column web

5.5.5 Reinforcing plates

The reinforcing plates support the beam flanges in carrying the compression stress concentrations when the gap at the beam-to-column interface opens. In the study connection, the reinforcing plates are located in the inner part of the beam flanges, and so their effectiveness is not complete, the best location being outside the flanges.

The numerical analyses show that the maximum stress concentrations in the reinforcing plates occur just beyond the location of the beam bolts, where the ED angles end, as shown in Figure 5.30, which depicts the stress distribution in one of the top reinforcing plates (Fig. 5.30a) during the cycles of imposed drift.

After the post-tensioning (Fig. 5.30b), stress peaks are visible around the holes, due to the prying action of the bolts.

At a drift equal to 0.4% (Fig. 5.30c) the maximum stresses are visible around the holes and beyond them, with respect to the interface with the

column. Such distribution may be explained considering that, since the plate of the ED angle directly bolted to the beam flange acts as an additional reinforcing plate, it transfers the compression stresses to the beam flange by means of the friction between flange and ED angle.

For larger drift values (Fig. 5.30d), stress concentrations are visible also on the column side, the maximum extent being still after the ED angle location. Based on the above observations, it is clear that the stress distribution in the reinforcing plates does not depend only on the contact force at the interface with the beam, but it is made rather complicated by the presence of the bolts.

Although no inelastic deformations occur in the study reinforcing plates, due to the extremely high value of their yield limit, residual stresses are present at the end of the cycles (Fig. 5.30e), due to the local yielding of the beam flange bolted to them. This condition is confirmed by Figure 5.31, where the yielded areas at the 3.5% drift in the beam, reinforcing plate and ED angle are shown.

In Figure 5.32 the stress history in the most engaged finite element of the top reinforcing plate is plotted.

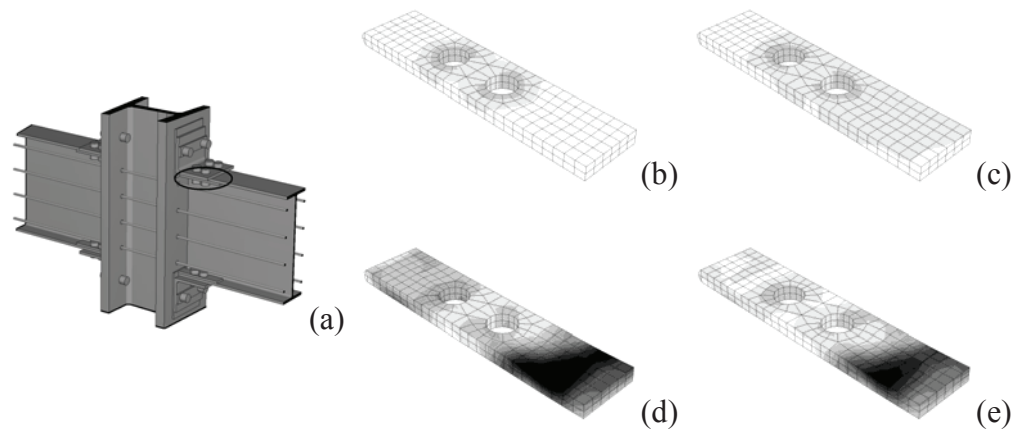


Figure 5.30. Deformation and stress states of the top reinforcing plate (a) of the PTED connection: (b) after post-tensioning; (c) at a 0.4% drift; (d) at a 3.5% drift; (e) at the end of the cycles



Figure 5.31. Detail of the beam, reinforcing plate and ED angle: yielded areas at a drift equal to 3.5%, causing the residual stresses in the reinforcing plates

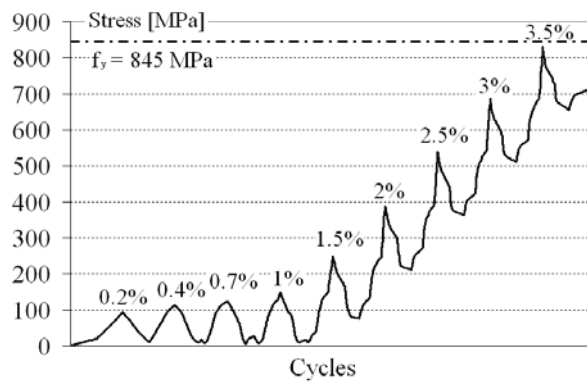


Figure 5.32. Stress history in the most engaged finite element in the top reinforcing plate of the PTED connection

5.5.6 Shim plates

The shim plates guarantee a smooth surface at the beam-to-column interface and provide the tolerance gap necessary for the erection of the frame. Their behaviour during the cycles of imposed drift is elastic.

The stress distribution in a top shim plate (Fig. 5.33a), for the relevant drift values, is shown in Figure 5.33.

After the application of the PT force (Fig. 5.33b), the stress values are extremely small, whereas they increase as the drift does (Figs. 5.33c, d), the maximum stresses being concentrated in the area in contact with the beam flange and with the ED angle, beneath the bolt holes.

After the end of the cycles, the stress distribution is practically the same as the one after the post-tensioning phase (Fig. 5.33e).

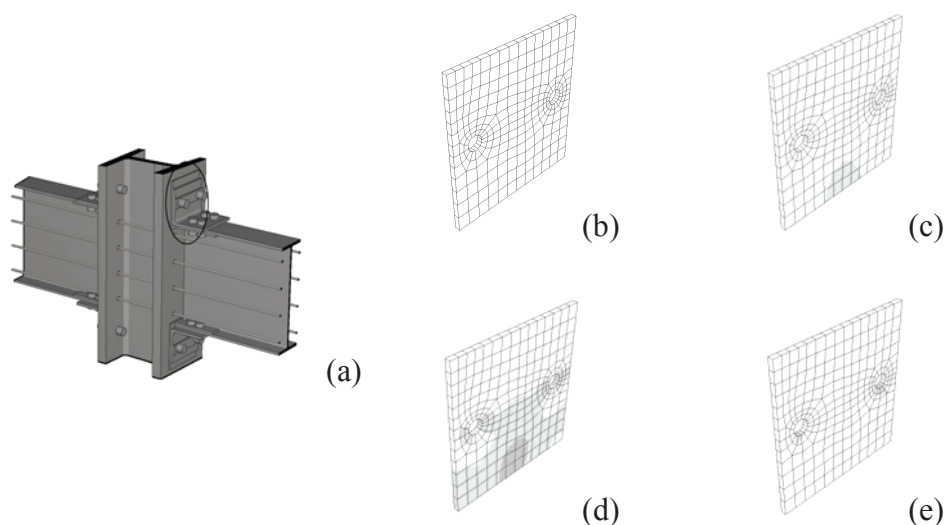


Figure 5.33. Deformation and stress states of the top shim plate (a) of the PTED connection: (b) after post-tensioning; (c) at a 0.4% drift; (d) at a 3.5% drift; (e) at the end of the cycles

Figure 5.34, which shows the stress history in the most engaged finite element of the shim plate, confirms that no yielding occurs during the cycles of imposed drift.

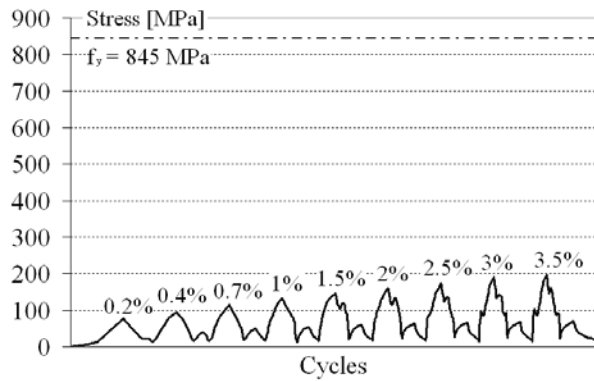


Figure 5.34. Stress history in the most engaged finite element in the top shim plate of the PTED connection

5.5.7 PT strands

The PT strands are, together with the ED devices, the component parts which mainly characterize the PTED systems. Their principal functions are: 1) compressing the columns to the beams, in order to provide the necessary capacity of transferring the vertical shear and the bending moment in the nodes; 2) re-centring the structure. PT strands must always behave elastically, because any yielding would lead to the loss of re-centring capability and, above all and more concerning, to the loss of the shear load carrying capacity.

In this study, differently from the other connection component parts, the modelling of the PT strands is quite approximated. In fact, they are modelled as cylinders, whereas they are actually obtained by assembling several wires. So, in the modelled strands the flexural stiffness is larger than the real strands one, and this could affect the numerical results with regard to the contact phenomena between the strands and the holes in the column flanges. The above contact interaction is consequently neglected in the models, since the corresponding results would be inaccurate. Anyway, the results in terms of axial forces in the strands are suitable and are discussed in the following.

During the cycles of imposed drift, the behaviour of the PT strands is elastic, as shown in Figure 5.35, where the stress history in a top strand is plotted. Stress reductions are visible for large drift values, which are caused

by the minor yielding, with consequent shortening, of the beams. At the author's knowledge, no yielding in the beams occurred during the experimental tests (Ricles et al., 2002b). Anyway, such numerical result highlights the absolute necessity of preventing any yielding in the main structural elements, which could lead to the inefficiency of the PT system and, consequently, of the whole moment resisting frame.

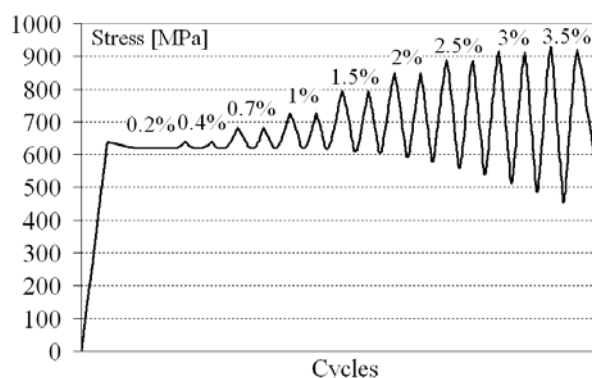


Figure 5.35. Stress history in the PT strands of the PTED connection

For large drift values, the strands can go in contact with the column flange holes. This condition can worsen the stress state in the strands, and, consequently, particular care is required in their design, with the necessity of large safety margins.

5.5.8 ED angles

The ED steel angles are the dissipative part of the study PTED beam-to-column connection. In addition, they provide a redundant contribution to the vertical shear load carrying mechanism.

The dissipation of the input energy takes place through cycles of inelastic deformations within three cylindrical plastic hinges, which form when the beam-to-column gap opens. Such dissipative mechanism was experimentally found by Garlock et al. (2003), and it is confirmed by the numerical results.

The deformation and stress distribution of a top ED angle (Fig. 5.36a), for the relevant drift values, is shown in Figure 5.36.

After the post-tensioning phase (Fig. 5.36b), stress concentrations are evident around the bolt holes, due to the prying action applied to the bolts.

At a drift equal to 0.4% (Fig. 5.36c), stress concentrations appear next to the fillet of each angle leg and near the location of the column bolts. These are the areas interested by the formation of cylindrical plastic hinges, for larger drift values, as shown in Figures 5.36d, referred to the 3.5% drift.

At the end of the cycles (Fig. 5.36e), large residual stresses are present in the angle, as it was expected, due to the occurred inelastic deformations.

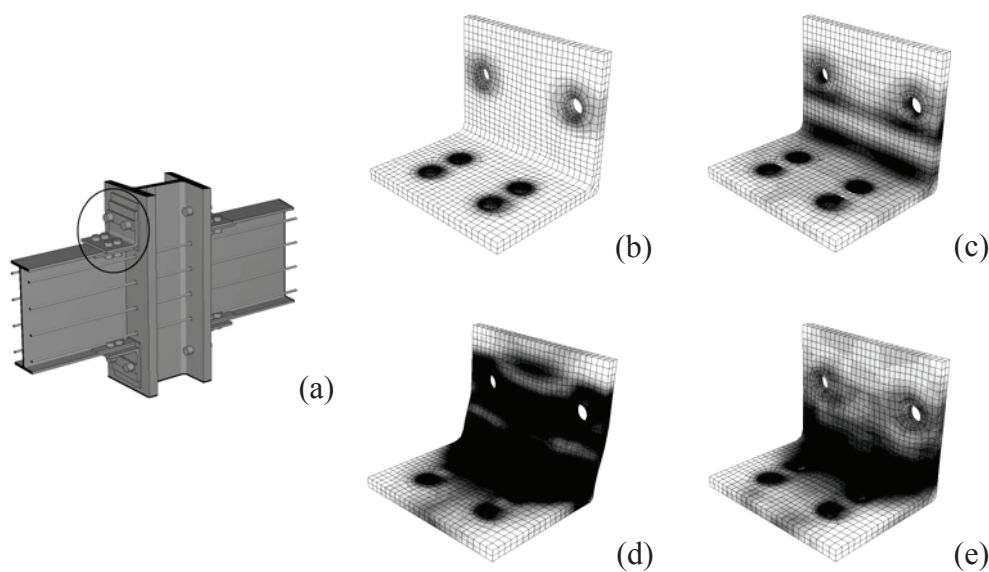


Figure 5.36. Deformation and stress states of the top ED angle (a) of the PTED connection: (b) after post-tensioning; (c) at a 0.4% drift; (d) at a 3.5% drift; (e) at the end of the cycles

The stress history in the most engaged finite element of the angle is shown in Figure 5.37, where it is apparent that the first yielding occurs for relatively small drift values.

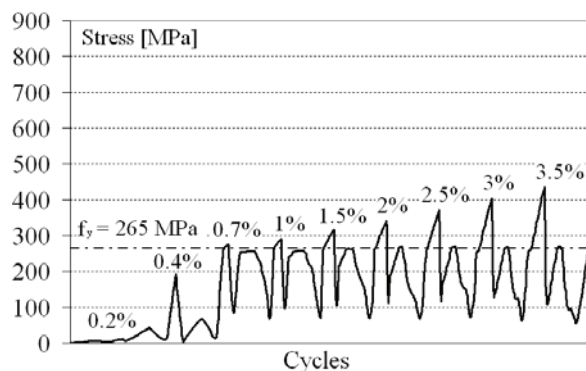


Figure 5.37. Stress history in the most engaged finite element in the top ED angle of the PTED connection

5.6 SYNTHESIS OF RESULTS

In this chapter the numerical analysis on a PTED beam-to-column connection for steel moment resisting frames, characterized by the presence of PT strands and ED angles, is illustrated and discussed.

A preliminary model of the ED sub-assembly is presented, aimed at the modelling optimization with regard to the surface-to-surface interactions and the finite element mesh. The obtained results show that the use of tie constraints for the interaction between the beam flanges and the ED angles leads to good results, without requiring large computational efforts. In addition, the set up calibration of the mesh for the surfaces in contact allows to adequately reproduce the experimental results.

With regard to the whole PTED beam-to-column connection, two numerical models are presented, the first one being characterized by a symmetry-based simplifying assumption, and the second one having no simplifications. Both the models are calibrated on the basis of the experimental tests performed by Ricles et al. (2002b), who have proposed and tested such a connection system. A good approximation is achieved by the models and so they are used for studying the behaviour of the connection under cycles of imposed drift.

The experimental evidence is confirmed by the analysis of the stress and strain distribution obtained numerically. The beams essentially behave in elastic range, with some yielding in limited portions of the flanges and the web. On the other hand, no inelastic deformations occur in the column. The shim and reinforcing plates behave elastically, but the effectiveness of the latter ones appears negatively influenced by their location, at the internal side of the beam flanges. The ED angles provide a good and stable capacity of energy dissipation, showing the yielding mechanism obtained also during the experimental tests. The PT strands are able to guarantee load carrying capacity and self-centring capability, provided that no inelastic deformation, with consequent shortening, occurs in the main structural elements. The possibility of contact between PT strands and column holes implies the necessity of large safety factors in their design.

Chapter 6

Comparison with welded connections

6.1 INTRODUCTORY REMARKS

Since Post-Tensioned Energy Dissipating beam-to-column connections are proposed as an alternative solution for steel moment resisting frames in seismic areas, the comparison of their behaviour with that of welded rigid connections is worth of interest. From the theoretical point of view, a PTED beam-to-column connection is expected to behave like the corresponding rigid one for low drift levels, showing the same initial stiffness. In addition, a PTED connection is expected to behave linearly until the gap at the beam-to-column interface opens, whereas the behaviour of a welded connection is linear up to the yielding in the main structural members. At last, the capacity of dissipating the input energy in a PTED connection is expected to be provided by yielding or friction mechanisms within the ad-hoc ED systems, while, in a welded connection, it is obtained through inelastic deformations in the main structural elements.

For both PTED and welded connections, the above behavioural peculiarities are separately confirmed by the experimental evidence. Anyway, at the author's knowledge, no experimental results are available on the direct performance comparison between PTED and welded connections. Consequently, in order to provide quantitative information on both the differences and the similarities of behaviour peculiar of the two connection types, a direct comparison is carried out and presented in this chapter.

The study is focused on the behaviour of the PTED connections presented in Chapters 4 and 5, and it considers the corresponding welded nodes. In particular, starting from the beams and column assemblages of the study PTED connections, welded rigid assemblages are taken into account.

The comparisons are carried out at both global and local level. The former ones are referred to connection properties like the stiffness, the maximum borne forces and moments, the capacity of dissipating the input energy, and the residual deformations. The latter ones are focused on the detailed behavioural analysis of the deformation and stress states of the assemblages component parts, during all the phases of the imposed drift cyclic history.

The study is based on numerical analyses, performed by the ABAQUS multi-purpose computer program. The models of the PTED connections are the ones presented and discussed in previous chapters, which are calibrated directly against the experimental results. With regard to the welded connections models, no experimental results, referred to the study beam and column sizes, are available. Consequently, the calibration of the welded connection models is carried out by considering the results of an experimental campaign on welded rigid connections (Ricles et al., 2002a) with different beams and column sizes. The modelling assumptions are then extrapolated and extended to beams and column assemblages characterized by the same geometrical features as the ones present in the study PTED connections.

In the following sections, the calibration of the finite element models of the welded connections is firstly presented. Then, the comparative analyses focused on the systems corresponding to the PTED connection with PT and ED bars and to the PTED connection with PT strands and ED angles, respectively, are separately carried out and discussed.

6.2 CALIBRATION OF THE WELDED CONNECTION MODEL

6.2.1 *The reference experimental study*

The calibration of the numerical model of the rigid connection is carried out on the basis of the tests presented by Mao et al. (2000) and by Ricles et al. (2002a) on a beam-to-column welded node. In particular, the test specimen

named T1 is considered, which consists in an exterior beam-to-column connection composed by a 3960 mm long W14x311 column and a 4500 mm long W36x150 beam, both made of A572 Grade 50 steel (nominal yield stress equal to 345 MPa). The detail of the nodal area is shown in Figure 6.1.

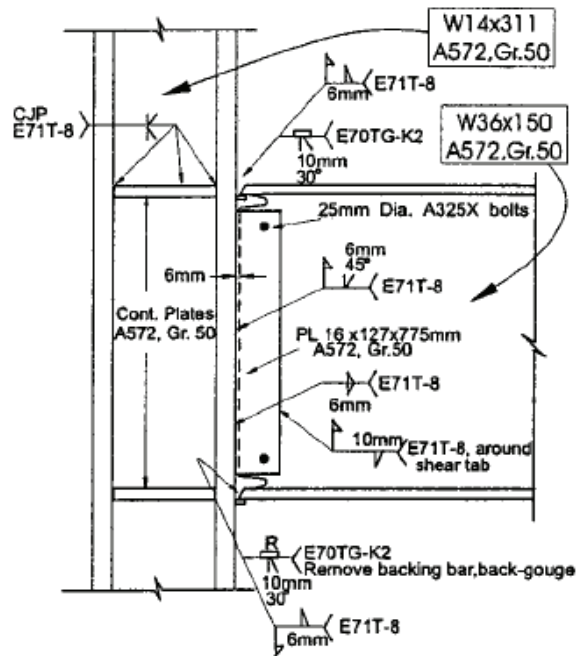


Figure 6.1. Detail of the T1 welded node subjected to experimental analysis (Mao et al., 2000; Ricles et al., 2002a)

The beam flanges are connected to the column flange by means of full penetration groove welds. The beam web too is groove welded directly to the column flange, and a supplementary fillet weld is present around the edges of the 16 mm thick shear tab. No column web doubler plates are present, whereas 25 mm thick continuity plates are used. Both shear tabs and continuity plates are made of A572 Grade 50 steel, with a nominal yield stress equal to 345 MPa.

The measured yield and ultimate stress values for all the connection component parts are summarized in Table 6.1.

Table 6.1. Measured yield and ultimate stresses for the welded connection component parts in the experimental test (Ricles et al., 2002a)

Component part	Yield stress (MPa)	Ultimate stress (MPa)
Beam flange	380	494
Beam web	426	518
Column flange	326	480
Column web	339	483
Continuity plates	263	434
Shear tab	453	592

The load history consists in the application of a series of cyclic horizontal displacements to the column top section, by means of an actuator, and it is shown in Figure 6.2, where it is expressed in terms of imposed drift, which is defined as the ratio between the horizontal displacement and the column height. The maximum reached drift is equal to 5%.

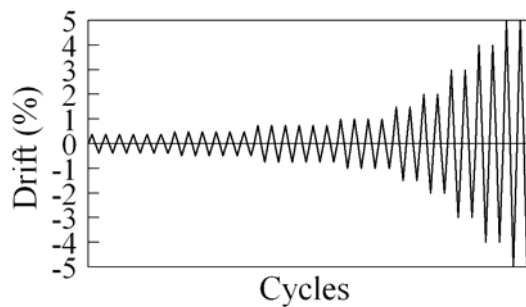


Figure 6.2. Cycles of imposed drifts during the experimental tests (Ricles et al., 2002a)

In Figure 6.3 the experimental response of the welded connection, expressed in terms of lateral force-drift, is plotted.

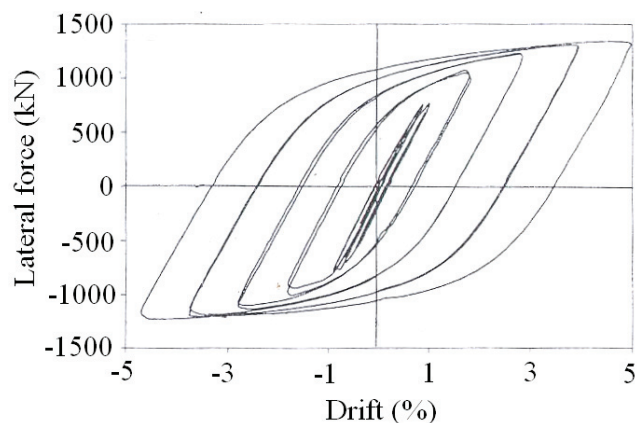


Figure 6.3. Experimental lateral force-drift curve on the tested welded connection (Mao et al., 2000)

6.2.2 Focused aspects for the calibration

The finite element model of the “calibration” node described in this section is aimed at obtaining modelling information as general as possible, in order to extend it to beam-to-column assemblages characterized by different geometrical features.

In this perspective, the attention is particularly focused on the material hardening characteristics, on the finite element mesh, and on the interaction modelling issues at the beam-to-column interface. The following observations can be drawn:

- Differently from the case of PTED systems, in the welded rigid connections large inelastic deformations are expected to occur in the beams. Consequently, the hardening properties of the steel used for the main structural elements play an important role in the cyclic behaviour of the whole rigid connection, whereas they are less important in the modelling of beams and columns in PTED connections if, as expected, they do not undergo inelastic deformations.
- The mesh refinement may influence the possibility of catching instable phenomena, which are typical of traditional rigid nodes under strong

seismic actions, while absent in the PTED connections. In particular, local instability would be missed in case of excessively coarse mesh. Therefore the finite element mesh of the model must derive from a compromise between accuracy and low computational costs.

- The actual interaction between beam and column in a welded node is influenced by the geometrical details of the connection and by the presence of welding residual stresses in the heat affected zone. Three levels of precision could be considered for such modelling: (1) considering both the actual geometrical details and the welding residual stresses; (2) considering the geometrical details and neglecting the welding residual stresses; (3) considering a tie constraint between the beam-to-column contact surfaces, so that no relative movement between them is possible, and assigning the properties of the welding metal to a small part of the beam extremity. In this study, the possibility of using the third simplified modelling is evaluated and justified.

6.2.3 *The “calibration” finite element model*

The actual geometry of the connection is not reproduced in detail, since the consideration of very peculiar geometrical features may lead to not generally valid results. On the contrary, the followed approach consists in adopting a model which is slightly simplified but unaffected by behaviour peculiarities strictly connected to the connection detail (Esposito et al., 2007).

In particular, the detail of the weld access holes, the weld backing bar, the weld fillets and the temporary bolts in the shear tab are not considered in the model. On the contrary, the continuity plates and the shear tab are modelled (Fig. 6.4).

It is worth noticing that the geometrical details at the beam-to-column interface in a welded connection may strongly influence its behaviour with regard to the fracture phenomena. These are neglected in this study, but they are taken into account, as a general problem of traditional welded connections, in the general comparative evaluation.

The materials are modelled according to the experimental test results provided by Ricles et al. (2002a) and summarized in section 6.1.1. In Table 6.2 the mechanical features of the above mentioned materials, expressed in terms of true stresses and plastic strains, and the component parts they are

assigned to, are summarized. The used labels are related to the component parts they are referred to. For all the modelled materials isotropic hardening is considered.

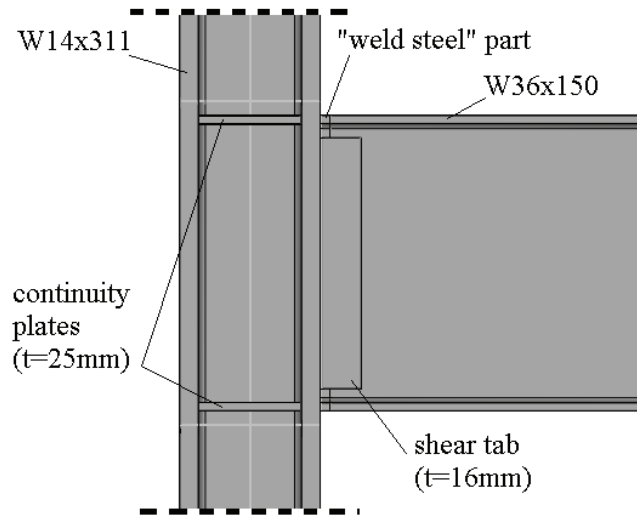


Figure 6.4. Geometrical details of the “calibration” welded connection FE model

Table 6.2. Mechanical features of the modelled materials in terms of true stresses and plastic strains, and associated component parts

Material	Yield stress (MPa)	Ultimate stress (MPa)	Ultimate strain plastic (%)	Component parts
BFS	380	570	13.7	Beam flanges
BWS	425	600	13.7	Beam web
CFS	325	550	13.7	Column flanges
CWS	340	560	13.7	Column web
CPS	265	500	13.7	Continuity plates
STS	455	680	13.7	Shear tab
WS	500	650	4.57	Weld steel

With regard to the interaction between the beam and the column, the actual geometrical details and the thermal residual stresses are neglected. A tie constraint is used at the contact surfaces, and for a short length of the beam (30 mm long) the material properties are those of the welding metal (WS). This modelling choice is consistent with the above explained idea of achieving modelling information which are not strictly dependent on the connection interface details.

Tie constraints are also used for modelling the interactions between welded component parts, namely: column-continuity plates; column-shear tab; beam-shear tab.

The imposed displacement history considered in the model (Fig. 6.5) is similar to the experimental one (Fig. 6.2), with the difference that only one cycle per amplitude is considered, in order to reduce the computational costs.

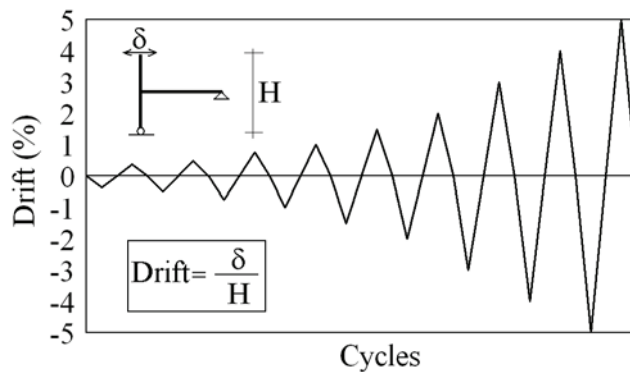


Figure 6.5. Imposed cyclic drift history in the numerical analyses

The size of the increments is selected in order to achieve a good convergence during the analysis, by reducing the initial increment size as far as the non-linearities increase.

The finite element mesh of the “calibration” model is made by tri-dimensional continuum first-order elements with reduced integration (C3D8R) for all the component parts of the model. The nodal area is more finely meshed than the rest of the model (Fig. 6.6) in order to adequately catch the possible instable phenomena which can occur there.

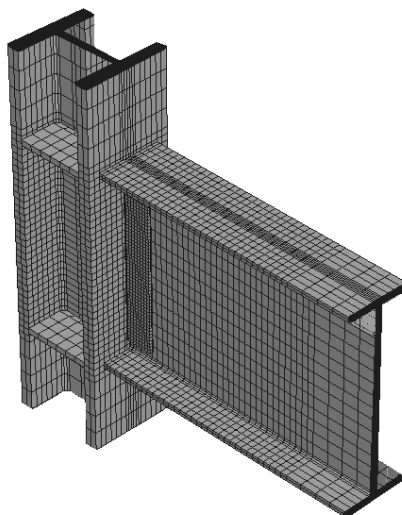


Figure 6.6. Detail of the finite element mesh of the “calibration” model nodal area

6.2.4 Numerical vs. experimental results

The comparison between the numerical and experimental lateral force-drift curves is shown in Figure 6.7.

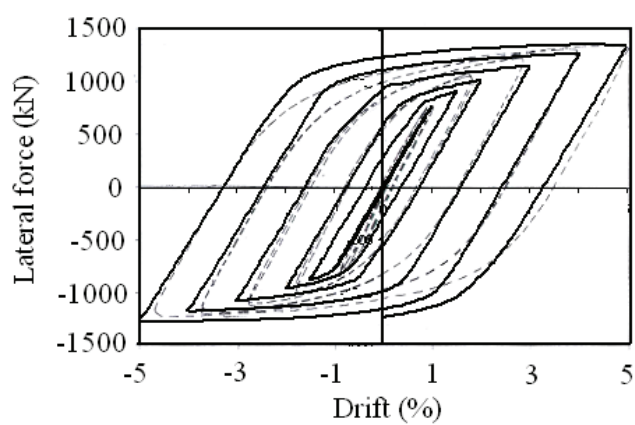


Figure 6.7. Numerical vs. experimental lateral force-drift curve for the “calibration” study

The numerical results appear in good agreement with the experimental ones. In fact, the stiffness and strength are caught with good approximation in all the cycles. However, some differences are evident in terms of dissipated energy, for which the error is of about 3% in the first cycles up to about 6.5% in the last cycles.

The obtained degree of approximation can be ascribed to the above mentioned adopted simplifying assumptions. Considering that a rigid node could be realized using a number of different connection details, which would affect the node behaviour, it seems useless reaching an extreme precision referred to a particular node geometry. On the other hand, a study like this one, although affected by some simplifications for the node detail, appears more interesting and can lead towards general conclusions.

6.3 PT AND ED BARS VS. WELDED CONNECTION

6.3.1 *General*

This section deals with the comparison between the cyclic behaviour of a PTED and a welded rigid beam-to-column connection. The PTED connection is the one endowed with PT high strength steel bars and ED confined steel bars, proposed by Christopoulos et al. (2002b) and modelled by Esposito et al. (2006b, 2007), which is presented in Chapter 4. The welded rigid connection is assembled starting from the same beam and column as the PTED ones.

The description of the finite element model of the PTED connection is carried out in Chapter 4 and consequently it is not reported herein. On the other hand, the model of the welded connection is presented in the following section (Esposito et al., 2007).

6.3.2 *The finite element model of the welded connection*

The finite element model of the welded connection is based on the acquired information related to the above described “calibration” model.

The geometrical assemblage is similar to the one shown in Chapter 4, with the difference that the beam length is one half as respect to the Christopoulos one, the beam ending at the actuator location. This is possible because the

behaviour of the welded rigid connection is not influenced by the presence of the beam part beyond the actuator position. On the contrary, the behaviour of the PTED connection is strongly influenced by the beam length, since the PT system length, and consequently its stiffness, directly depends on length of the beam.

The detail of the node is shown in Figure 6.8. Besides the W24x76 beam and the W14x211 column, a 16 mm thick shear tab, four 25 mm thick continuity plates (two per each side), and two 9.5 mm thick doubler plates (one per each side) are considered.

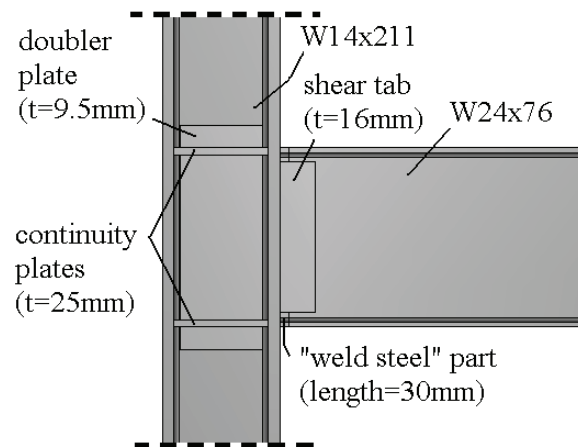


Figure 6.8. Geometrical details of the welded connection FE model

Two different materials are used in the model (Fig. 6.9): a structural steel (SS) and a weld steel (WS). For all the component parts of the connection the structural steel is considered, with the exception of the extreme part of the beam (30 mm long) which is characterized by the WS material (Fig. 6.8).

In Table 6.3 the mechanical features of the above mentioned materials, expressed in terms of true stresses and plastic strains, are summarized.

With regard to the interactions between the connection component parts, the assumptions made for the “calibration” model are considered. So, tie constraints are used for all the interactions between surfaces welded each other, namely: column-continuity plates; column-doubler plates; column-shear

tab; beam-shear tab. In addition, with regard to the interaction between the beam and the column, the actual geometrical details and the thermal residual stresses are neglected. A tie constraint is used at the contact surfaces, and for a short length of the beam (30 mm long) the material properties are those of the welding steel (WS).

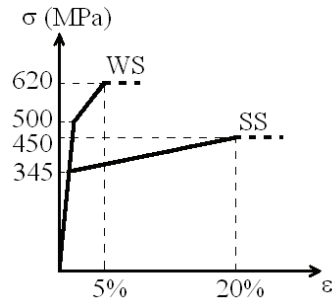


Figure 6.9. Nominal stress-strain relationships for the modelled materials

Table 6.3. Mechanical features of the modelled materials, in terms of true stresses and plastic strains, and associated component parts

Material	Yield stress (MPa)	Ultimate stress (MPa)	Ultimate plastic strain (%)	Component parts
SS	345	540	17.9	Beam, column, continuity plates, doubler plates, shear tab
WS	500	650	4.57	“Weld” part of the beam

The welded connection is subjected to the same imposed drift history as the one used for the model of the PTED connection, which is described in Chapter 4 and shown, for the sake of the reader’s convenience, in Figure 6.10.

The size of the initial increments in the steps are selected in order to achieve the best convergence speed. Fractions equal to 0.05 are used for the cycles up to 1% drift, and equal to 0.01 for the remaining cycles.

The finite element mesh is similar to that of the “calibration” model. It is composed by tri-dimensional continuum first-order elements with reduced integration (C3D8R) for all the component parts of the model. The nodal area is more finely meshed than the rest of the model, as shown in Figure 6.11.

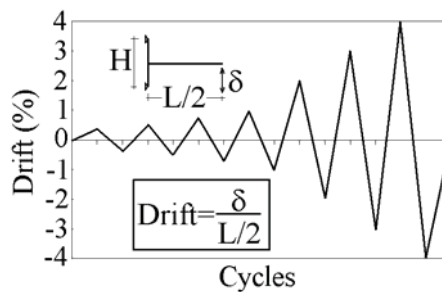


Figure 6.10. Imposed cyclic drift history in the numerical analysis

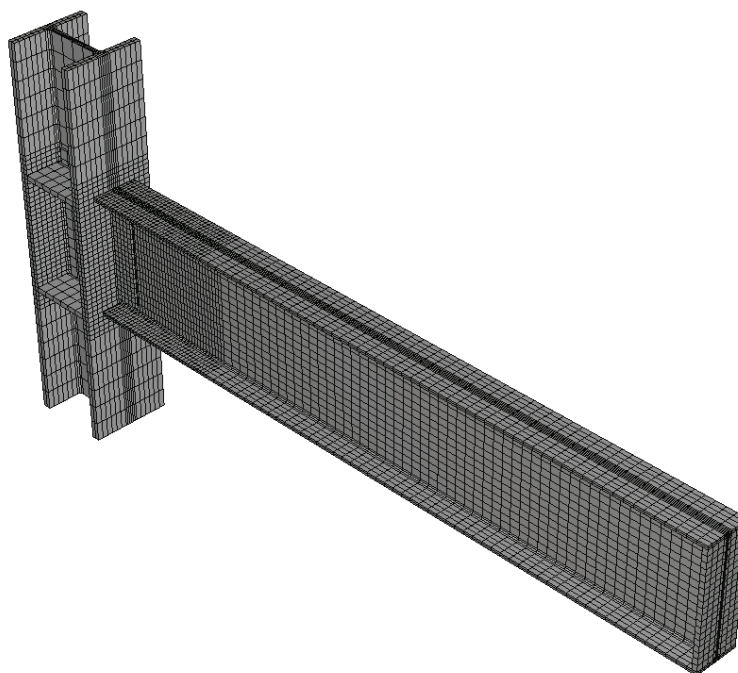


Figure 6.11. Finite element mesh of the welded connection model

6.3.3 Comparison between PTED and welded connection global responses

The force-drift and moment-rotation curves, obtained from the numerical analyses, are shown in Figure 6.12.

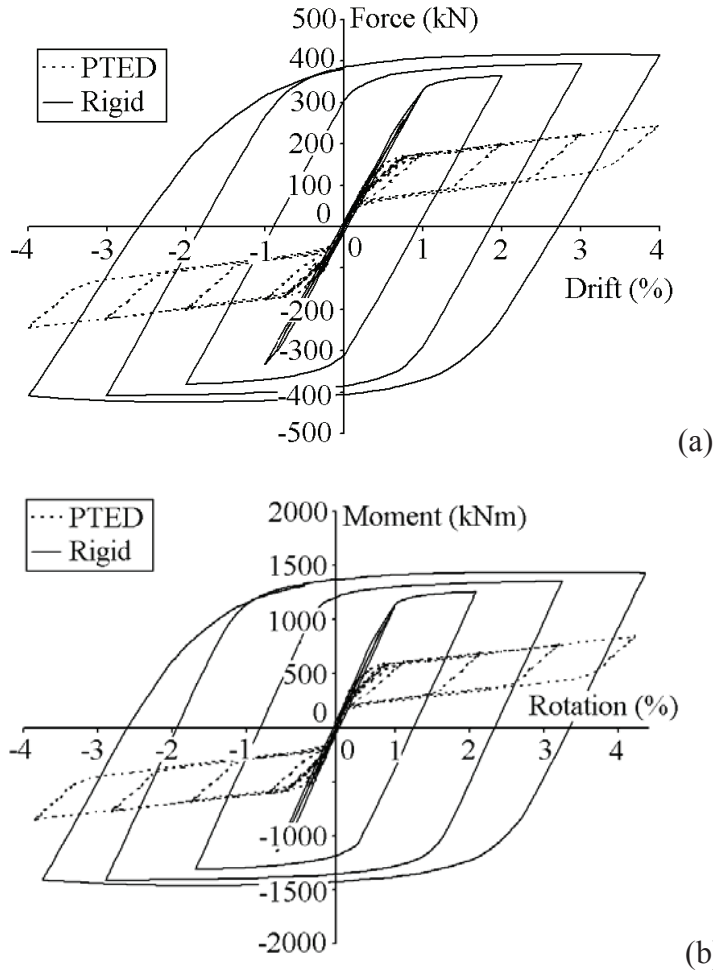


Figure 6.12. Numerical results in the PTED and rigid connections: (a) force-drift, (b) moment-rotation relationships.

The rotation (θ) is measured considering the relative rotation between a section at a distance equal to 1.7 times the beam depth and the interface section, according to Figure 6.13.

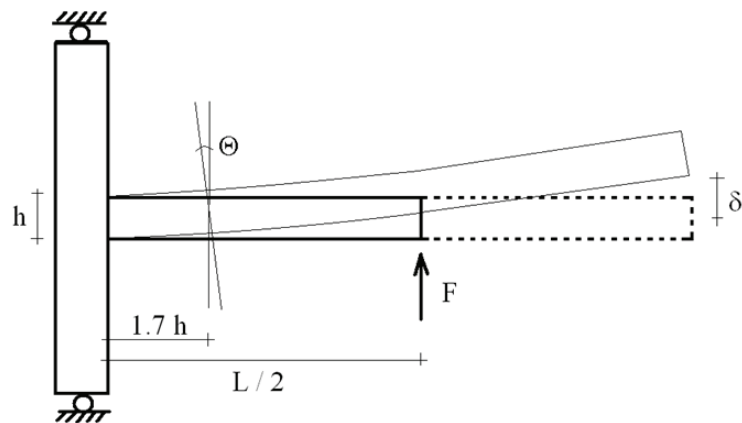


Figure 6.13. Definition of the rotation Θ

The behaviour of the two connections is perfectly the same up to a drift equal to 0.375%, which approximately corresponds to the fully operational level defined in SEAOC Vision 2000 (1995). Consequently, it is possible to observe that the PTED connection behaves like a rigid one in presence of frequent earthquake events.

The behaviour of the PTED connection is linear elastic up to about 0.375% drift, at a 124 kN force, whereas the welded rigid node behaves linearly up to a couple of drift and force more than twice larger than the PTED ones, namely about a 1% drift and a 331 kN force. It is worth underlining that the sources of non-linearity are different in the two cases. In fact, the PTED connection shows a linear elastic behaviour until there is full contact between the beam and column; afterwards, when the gap opens at the interface, the behaviour of the connection becomes non-linear. On the contrary, the welded rigid node response is linear up to reach the yielding in the structural elements, when damage occurs in the beam.

In Table 6.4 the cyclic response of the two connections is compared in terms of maximum force (F_{max}), residual drifts (d_{res}), maximum moment (M_{max}), residual nodal rotation (Θ_{res}) and dissipated energy, the latter being expressed as the ratio between the area of the PTED loop (A_{PTED}) and that of the welded rigid one (A_R).

Table 6.4. Comparison between the responses of the two systems

Drift (%)	F_{\max} (kN)			d_{res} (%)			M_{\max} (kNm)			Θ_{res} (%)			$A_{\text{PTED}}/A_{\text{R}}$
	PTED	Rigid	P/R	PTED	Rigid	P/R	PTED	Rigid	P/R	PTED	Rigid	P/R	
0.375	124	124	1.0	0.0	0.0	-	428	428	1.0	0.0	0.0	-	-
1.0	176	331	0.53	0.0	0.0	-	607	1141	0.53	0.0	0.0	-	-
2.0	200	364	0.55	0.0	0.9	0.0	687	1256	0.55	0.0	1.04	0.0	20.8%
3.0	222	393	0.56	0.0	1.8	0.0	766	1357	0.56	0.0	2.10	0.0	16.1%
4.0	243	414	0.59	0.0	2.7	0.0	839	1430	0.59	0.0	3.20	0.0	15.8%

The ratio between the maximum borne forces in the welded rigid and PTED nodes is about 1.8.

During the loading phases, the ratio between the welded rigid node post-yielding stiffness and the PTED one ranges from 1.4, for the 2% cycle, to 0.12, for the 4% cycle. During the unloading phases, the welded rigid node proves to be twice stiffer than the PTED one.

The ratio between the force-drift loops areas, which are representative of the input dissipated energy, referred to the welded rigid and PTED nodes, increases as the drift grows, ranging from about 4.8 (2% drift cycle) to about 6.3 (4% drift cycle).

At the end of the cycles, no permanent deformation is present in the main structural elements of the PTED connection, whereas large damage and out-of-plane displacements are apparent in the beam of the welded rigid node (residual drift equal to 2.7%, and residual rotation equal to 3.2%).

6.3.4 Behaviour of the component parts

The detailed analysis of the deformation and stress states of the PTED connection component parts is presented in section 4.4.

In the following, the cyclic behaviour of the single component parts of the corresponding welded rigid connection is investigated.

For the sake of comparison, the focused drift values are the same as those considered for the PTED connection, namely 0.375%, 4% and end of cycles. In this case, no post-tensioning phase is obviously present.

The results are firstly presented by considering the assembled node, and then by focusing on every connection component part.

Assembled node

The deformed configurations of the node, together with the related stress distributions, at the above mentioned relevant drifts, are shown in Figures from 6.14 to 6.16. For each deformed configuration, perspective, lateral and plan views are provided, in order to correctly catch the node behaviour. Yielded areas are plotted in black.

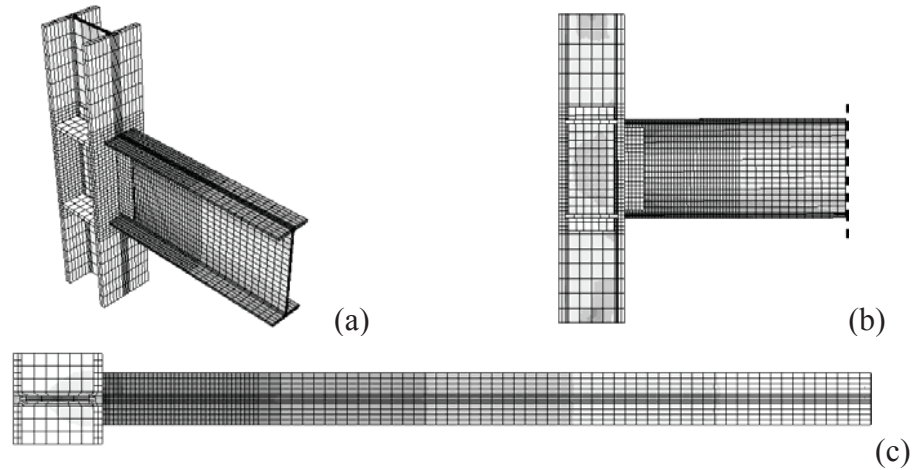


Figure 6.14. Deformation and stress state of the study welded rigid connection at a 0.375% drift: (a) perspective, (b) lateral and (c) plan views

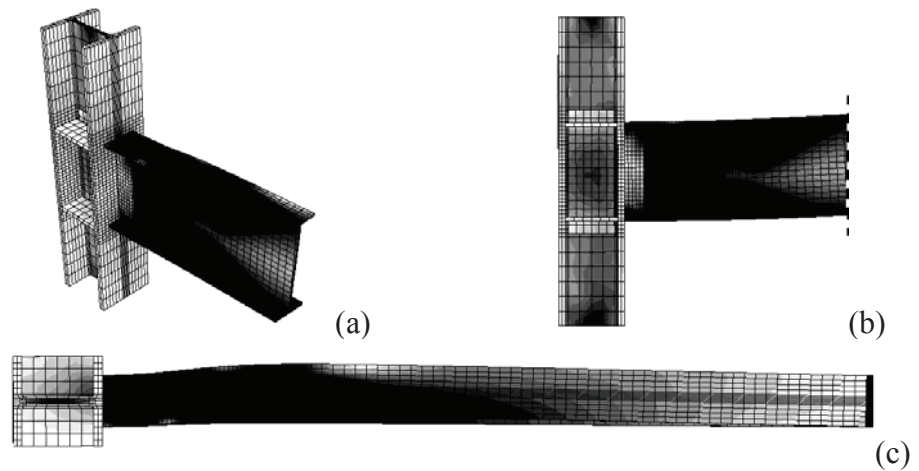


Figure 6.15. Deformation and stress state of the study welded rigid connection at a 4% drift: (a) perspective, (b) lateral and (c) plan views

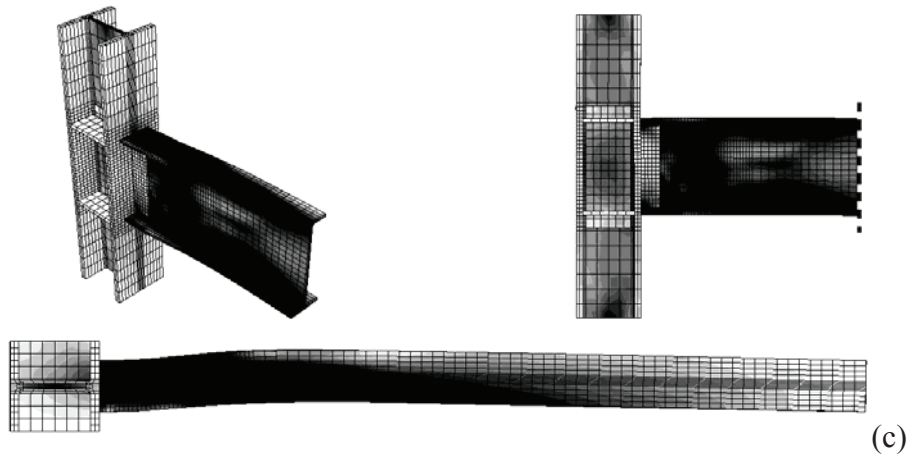


Figure 6.16. Deformation and stress state of the study welded rigid connection at the end of the cycles: (a) perspective, (b) lateral and (c) plan views

Beam

The cyclic behaviour of the beam in the welded rigid connection is completely different from that of the beam assembled in the PTED node. In fact, in the case of rigid connections, the beams are expected to undergo large inelastic deformations, they being devoted to dissipate the input seismic energy through cycles of inelastic deformations in bending.

This situation is confirmed by the obtained numerical results, as shown in Figure 6.17, where the deformation and stress states of the beam at drifts equal to 0.375%, 4% and at the end of the cycles are depicted.

At a drift equal to 0.375% (Fig. 6.17a) the beam is in elastic range and stress concentrations are visible in the flanges and in the web.

Out-of-plane displacements due to buckling phenomena occur starting from the cycle at 3% drift.

At a drift equal to 4% (Fig. 6.17b) the yielded area is extremely large, it covering a length about twice the beam depth.

At the end of the cycles (Fig. 6.17c), large areas of the beam flanges and web are affected by residual stresses due to the inelastic deformations undergone during the analysis. In addition, large residual out-of-plane displacements are present.

At the beam left end there is an area with reduced stresses, corresponding to the location of the tab supporting the beam in bearing the vertical shear.

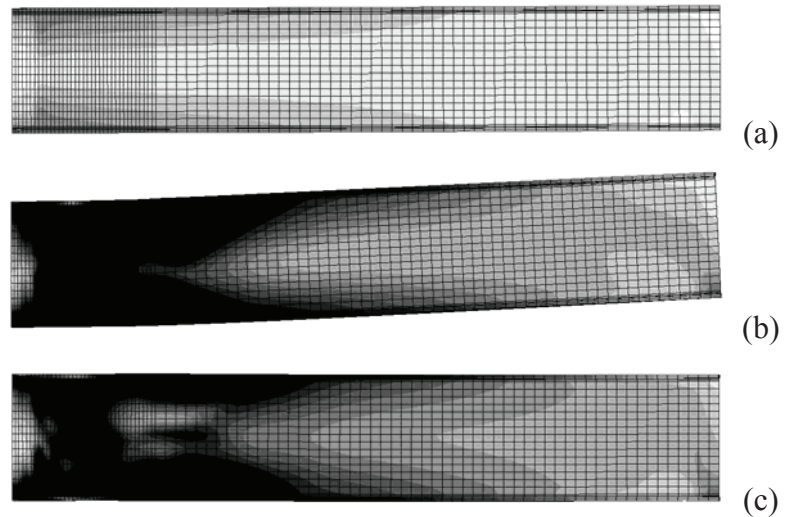


Figure 6.17. Deformation and stress states of the beam in the welded rigid connection: (a) at a 0.375% drift; (b) at a 4% drift; (c) at the end of the cycles

In Figure 6.18 the stress history in a finite element in the top flange of the beam is shown. The stress in the element is lower than the yield stress up to a drift equal to 1%, confirming that the loss of the linear behaviour is caused by the yielding in the beam, as it was expected. Starting from the cycle at 2% drift, the stress in the considered element increases due to the hardening properties of the steel.

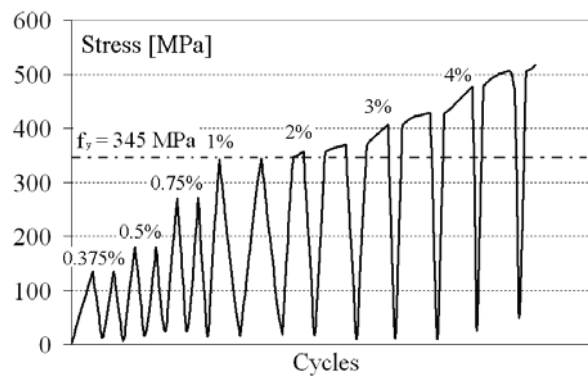


Figure 6.18. Stress history in the most engaged element in the beam flange

Column

The column in the welded rigid node is subjected, during the cycles of imposed drifts, to large stresses, in both the flanges and the web. The column deformation and stress states at the above indicated drift values are shown in Figure 6.19. No inelastic deformation in the column is evidenced by the numerical analysis, as shown also in Figure 6.20, where the stress history in the most engaged element of the column flange is plotted.

At a drift equal to 0.375% (Fig. 6.19a) small stresses are visible in the web of the column and their extension corresponds to the beam depth.

Large stress concentrations are visible at a drift equal to 4% (Fig. 6.19b) in the column web, which reduce at the end of the cycles (Fig. 6.19c), without getting zero, due to the inelastic deformations occurred in the beam.

With regard to the stress history in the column flange (Fig. 6.20), it can be noted that for drifts larger than 1% the stress curve is not linear, probably due to the inelastic deformations occurring in the beam.

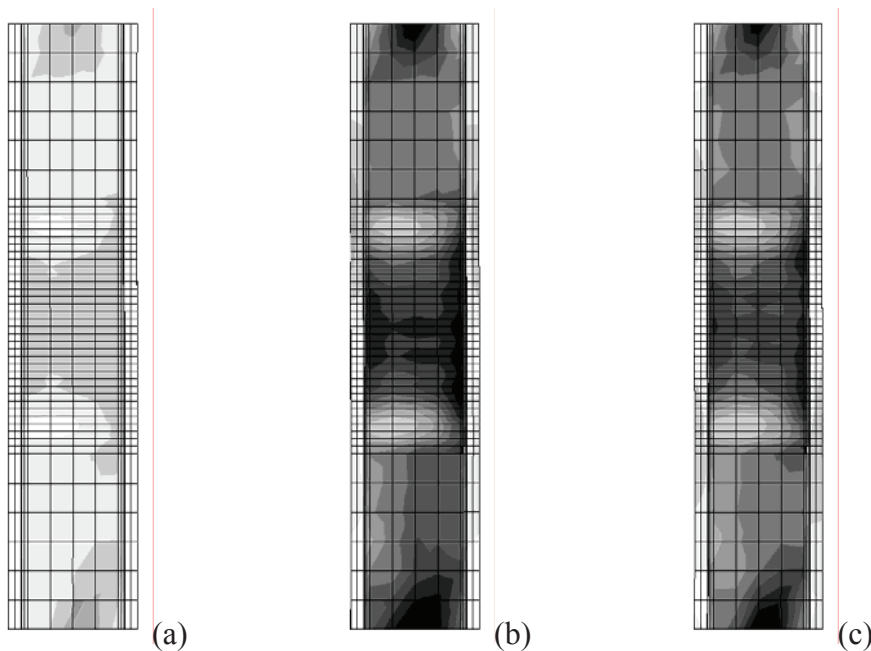


Figure 6.19. Deformation and stress states of the column in the welded rigid connection: (a) at a 0.375% drift; (b) at a 4% drift; (c) at the end of the cycles

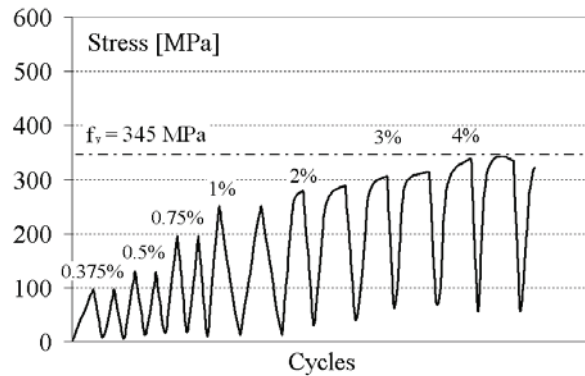


Figure 6.20. Stress history in the most engaged element in the column flange

Continuity plates

The continuity plates in the welded rigid connection show an elastic behaviour during all the cycles of imposed drifts. With regard to the stress distribution at remarkable drift values (Fig. 6.21), no substantial differences as respect to the continuity plates used in the PTED connection can be remarked, up a drift equal 2% (Fig. 6.21b).

For larger drift values, the stress distribution slightly changes. In particular, at a drift equal to 4% (Fig. 6.21c) the edge opposite to the column web shows no stresses. At the same time, the stress values are reduced with respect to the value at 2% drift, due to the buckling of the beam.

At the end of the cycles (Fig. 6.21d), the stress distribution in the considered continuity plate is practically the same as the one at 4% drift.

The stress history of the most engaged element in the continuity plates (Fig. 6.22) shows two interesting phenomena which differentiate their behaviour from that of the continuity plates assembled in the PTED connection (Fig. 4.26). The first main difference is that a continuity plate used in the welded rigid connection is essentially equally stressed under both positive and negative imposed drifts, whereas a continuity plate used in a PTED connection undergoes stress peaks only for drifts of a given sign, corresponding to the compression on the side where the plate is located. The other main difference is that the stress values in the PTED connection continuity plate monotonically increase with the drift, whereas in the

considered welded rigid connection, after the drift equal to 2%, the stress values are essentially constant and they reduce at the 4% drift. This phenomenon can be explained considering the yielding and buckling occurring in the beam for such drift values.

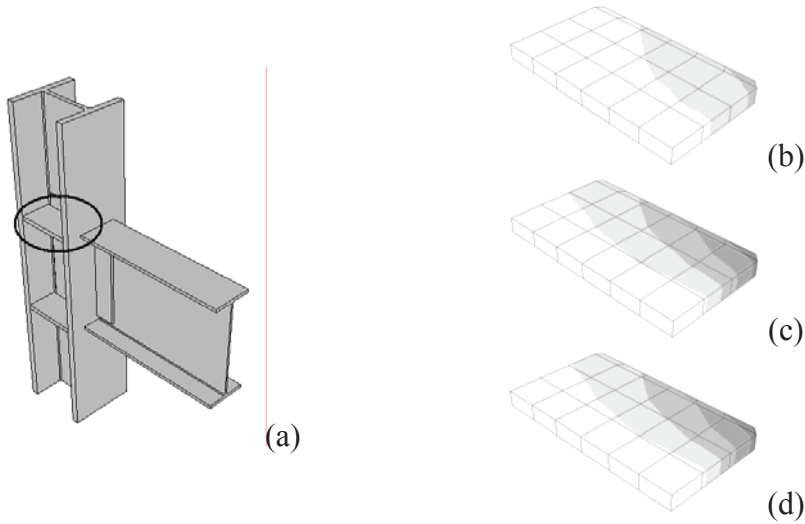


Figure 6.21. Deformation and stress states of the top continuity plate (a) in the welded rigid connection: (b) at a 0.375% drift; (c) at a 4% drift; (d) at the end of the cycles

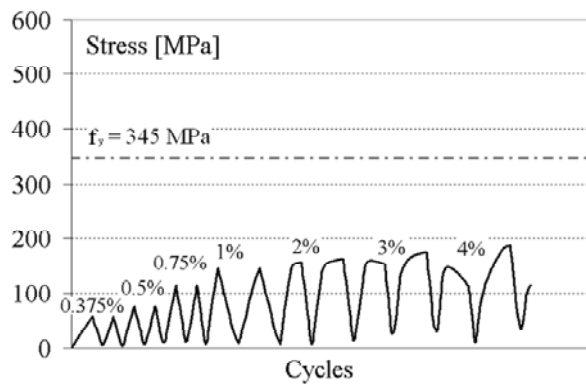


Figure 6.22. Stress history in the most engaged element in the top continuity plate

Doubler plates

The cyclic behaviour of the doubler plates assembled in the welded rigid connection is characterized by some differences from that referred to the PTED connection.

The first difference is related to the extent of the doubler plate area stressed during the cyclic action. In fact, the stress concentrations in the PTED connection doubler plates alternately take place in the top and bottom part of the plates, due to the sign of the drift and the consequent location of the stress flow in the column (Figs. 4.19 and 4.29). On the contrary, the stress concentrations in the rigid connection doubler plates are extended to their whole size, as shown in Figure 6.23. The values of the stresses increase as far as the drifts do (Fig. 6.23b, c) and they are not negligible at the end of the cycles (Fig. 6.23d). Anyway, no yielding occurs in the doubler plates.

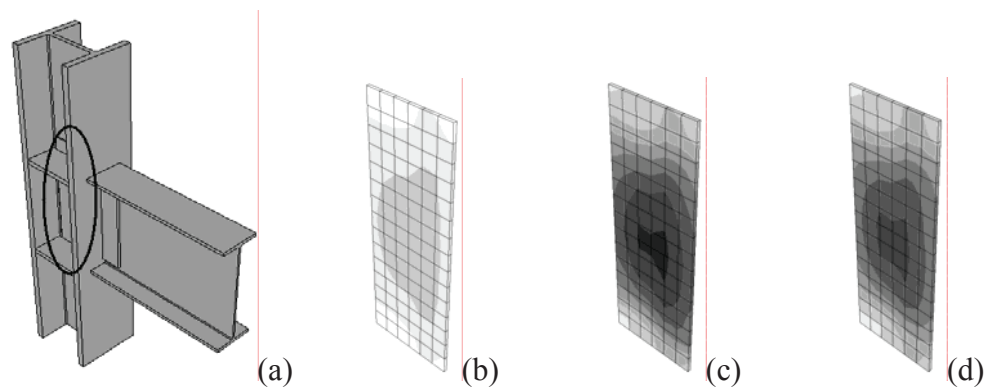


Figure 6.23. Deformation and stress states of the doubler plate (a) in the welded rigid connection: (b) at a 0.375% drift; (c) at a 4% drift; (d) at the end of the cycles

The second difference is evident if Figures 4.30 and 6.24 are compared, the latter being the stress history in the most engaged finite element in the rigid connection doubler plate. As in the case of the continuity plates, the stress values in the PTED connection doubler plates monotonically increase with the drift, whereas in the considered rigid connection, after the drift equal to 2%, the stress values are essentially constant. Also in this case, the phenomenon can be explained considering the yielding and buckling occurring in the beam for such drift values.

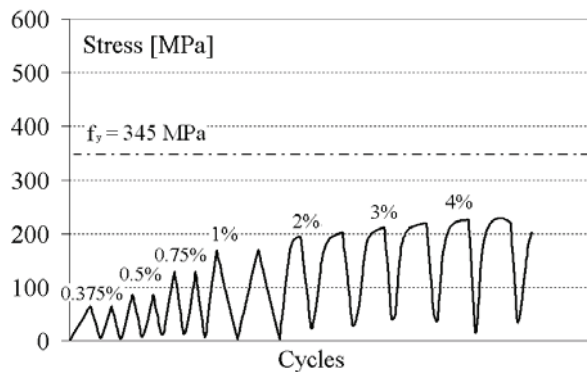


Figure 6.24. Stress history in the most engaged element in the doubler plate

6.4 PT STRANDS AND ED ANGLES VS. WELDED CONNECTION

6.4.1 General

Similarly to the previous one, this section deals with the comparison between the cyclic behaviour of a PTED and a welded rigid beam-to-column connection. The PTED connection is the one endowed with PT high strength steel strands and ED bolted steel top-and-seat angles, proposed by Ricles et al. (2002b) and modelled by Esposito et al. (2006a) and by Faggiano et al. (2007), which is presented in Chapter 5. The welded rigid connection is assembled starting from the same beam and column as the PTED ones.

The description of the finite element model of the PTED connection is carried out in Chapter 5 and consequently it is not reported herein. The model of the welded connection is presented in the following section (Faggiano et al., 2007).

6.4.2 The finite element model of the welded connection

The finite element model of the welded connection is based on the acquired information related to the “calibration” model shown in section 6.2.

The geometrical assemblage is similar to the one presented in Chapter 5. The detail of the nodal area is shown in Figure 6.25. Besides the two W24x62 beams and the W14x311 column, two 16 mm thick shear tabs (one per each beam), and four 15 mm thick continuity plates (two per each side) are modelled.

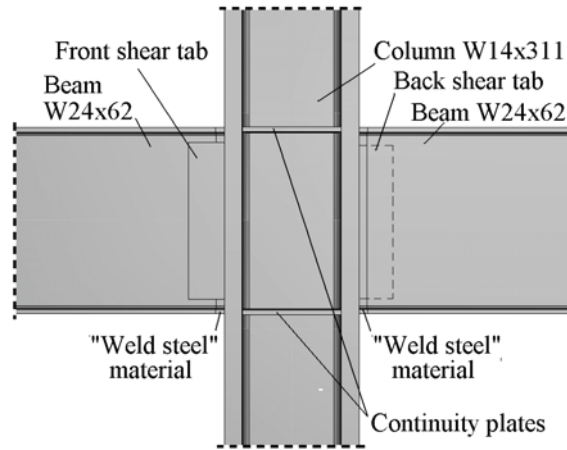


Figure 6.25. Geometrical details of the welded connection FE model

Three different materials are used in the model (Fig. 6.26), according to the reference experimental specimen, namely BS, for the beams, the shear tabs and the beam stiffeners; CS, for the column and the continuity plates; moreover, the WS material is used for the end parts of the beams near the column (30 mm large), which are affected by the welds. For all the materials, isotropic hardening behaviour is considered.

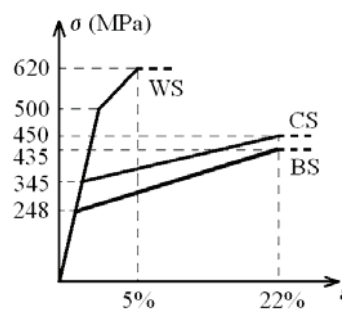


Figure 6.26. Nominal stress-strain relationships for the modelled materials

The mechanical features of the above materials, expressed in terms of true stresses and plastic strains, are summarized in Table 6.5.

Table 6.5. Mechanical features of the modelled materials, in terms of true stresses and plastic strains, and associated component parts

Material	Yield stress (MPa)	Ultimate stress (MPa)	Ultimate plastic strain (%)	Component parts
BS	248	530	19.6	Beams, shear tabs
CS	345	550	19.6	Column, continuity plates
WS	500	650	4.57	“Weld” part of the beams

With regard to the interactions between the connection component parts, the assumptions made for the “calibration” model are considered. So, tie constraints are used for all the interactions between surfaces welded each other, namely: column-continuity plates; column-shear tabs; beams-shear tabs. In addition, with regard to the interaction between the beam and the column, the actual geometrical details and the thermal residual stresses are neglected. A tie constraint is used at the contact surfaces, and for a short length of the beam (30 mm long) the material properties are those of the welding steel (WS).

The same imposed drift history as the one referred to the PTED connection, shown in Chapter 5, is considered for the model of the welded rigid connection. For the sake of the reader’s convenience, it is shown in Figure 6.27.

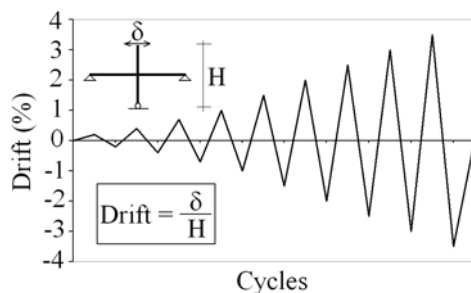


Figure 6.27. Imposed cyclic drift history in the numerical analysis

The size of the initial increments in the steps are selected in order to achieve the best convergence speed. Fractions equal to 0.05 are used for the cycles up to 1% drift, and equal to 0.01 for the remaining cycles.

The finite element mesh is similar to that of the “calibration” model. It is composed by tri-dimensional continuum first-order elements with reduced integration (C3D8R) for all the component parts of the model. The nodal area is more finely meshed than the rest of the model, as shown in Figure 6.28.

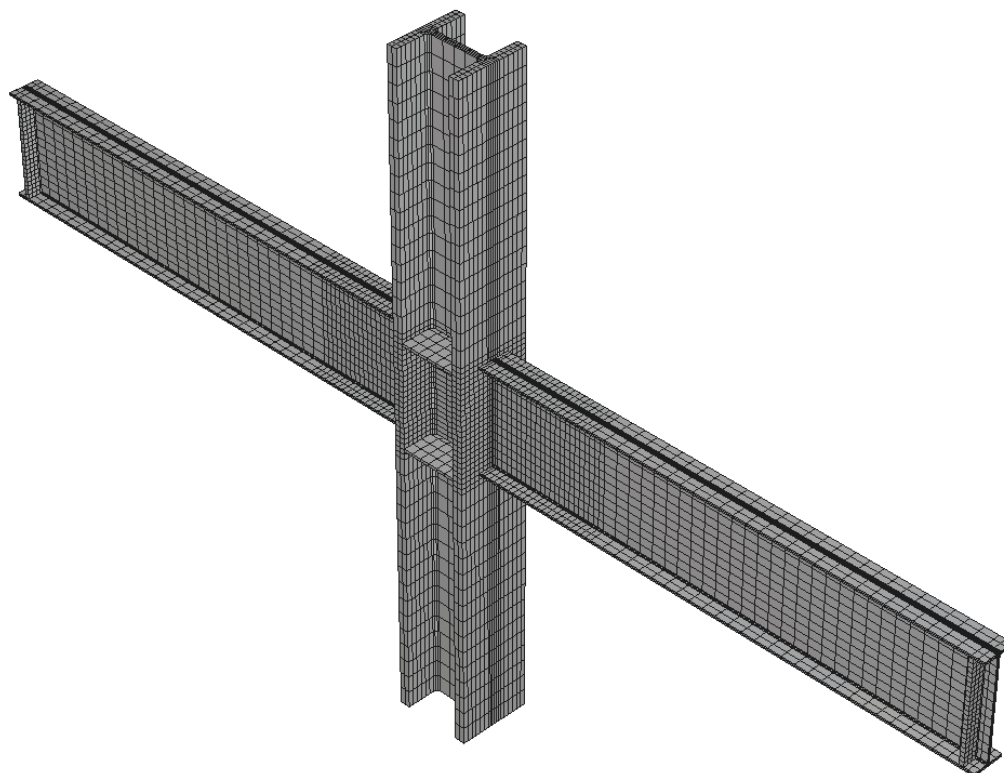


Figure 6.28. Finite element model of the welded connection model

6.4.3 Comparison between *PTED* and welded connection global responses

The force-drift and moment-rotation numerical curves are shown in Figure 6.29.

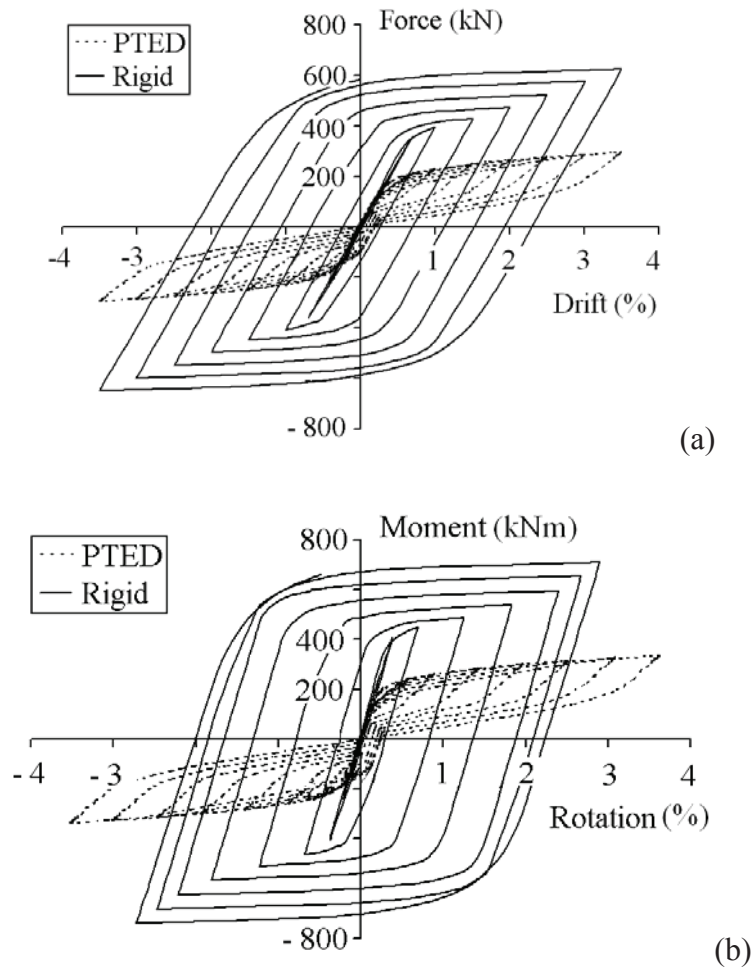


Figure 6.29. Numerical results in the PTED and welded connections: (a) force-drift, (b) moment-rotation relationships

The rotation (θ) is measured considering the relative rotation between a section at a distance twice larger than the beam depth and the interface section, according to Figure 6.30. It is worth noticing that the relative rotations in the rigid node are smaller than the ones in the PTED node, due to the deformation of the web panel of the column, which is considerable in the rigid connection but is negligible in the PTED one.

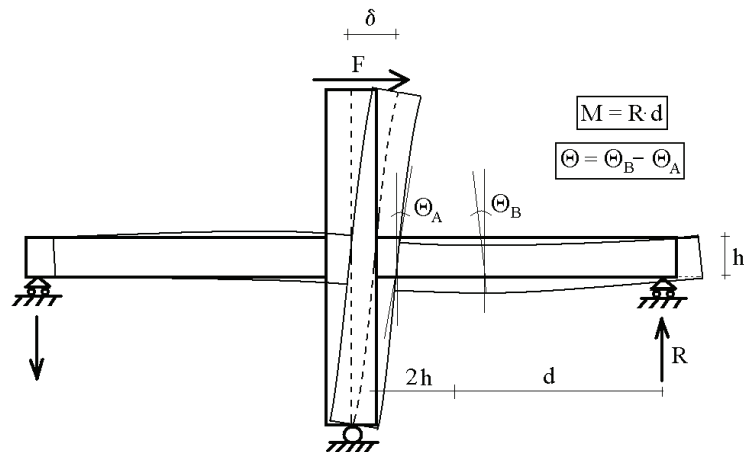


Figure 6.30. Definition of the rotation Θ

The behaviour of the two connections is perfectly the same up to a drift equal to about 0.25%, which approximately corresponds to the fully operational level according to the SEAOC Vision 2000 indications (1995). This result confirms that the PTED connection behaves like a traditional welded one under frequent earthquakes.

The PTED connection behaviour is linear elastic up to a drift equal to about 0.25%, corresponding to a force equal to 137 kN, whereas the rigid connection behaves linearly up to a drift equal to 0.70% at a force equal to 359 kN. The loss of the linear behaviour is due to the gap opening for the PTED system and to the yielding in the beams for the welded rigid node.

The cyclic response of the PTED and welded rigid connections is quantitatively described and compared in Table 6.6, in terms of maximum forces (F_{max}), residual drifts (d_{res}), maximum moments (M_{max}), residual relative rotation (Θ_{res}) and dissipated energy, the latter expressed as the ratio between the area of the PTED loop (A_{PTED}) and the rigid loop (A_R).

The ratio between the maximum borne forces in the welded rigid and PTED connections ranges from 1.2 to 2.1, for the 0.4% and 3.5% drift values, respectively.

During the loading phases, the ratio between the welded rigid node post-yielding stiffness and the PTED one ranges from 0.78, for the 1.5% cycle, to 0.22, for the 3.5% cycle, due to the formation of the plastic hinge in the rigid node, which reduces its stiffness. During the unloading phases, the welded rigid node is approximately 2.3 times stiffer than the PTED one.

Finally, the ratio between the force-drift loops areas, which are representative of the dissipated input energy, referred to the welded rigid and PTED nodes, is equal to 3 for the 1% cycle, and it gets constantly equal to 5 from the 2% cycle.

At the end of the cycles, negligible permanent deformations are present in the PTED connection (residual drift equal to 0.20%, residual relative rotation equal to 0.25%), whereas large plastic deformations are evident in the welded rigid node, with a 2.29% residual drift and a 2.24% residual relative rotation.

Table 6.6. Comparison between the responses of the two systems

Drift (%)	F_{\max} (kN)			d_{res} (%)			M_{\max} (kNm)			Θ_{res} (%)			$A_{\text{PTED}}/A_{\text{R}}$
	PTED	Rigid	P/R	PTED	Rigid	P/R	PTED	Rigid	P/R	PTED	Rigid	P/R	
0.2	110	110	1.00	0.00	0.00	-	127	127	1.00	0.00	0.00	-	-
0.4	176	212	0.83	0.00	0.00	-	201	242	0.83	0.00	0.00	-	-
0.7	210	359	0.58	0.00	0.00	-	240	410	0.58	0.00	0.00	-	-
1.0	227	397	0.57	0.00	0.25	0.00	259	453	0.57	0.02	0.29	0.07	33%
1.5	247	428	0.57	0.03	0.70	0.04	282	488	0.57	0.07	0.82	0.08	23%
2.0	263	472	0.56	0.09	1.10	0.08	299	538	0.56	0.13	1.36	0.09	20%
2.5	275	522	0.53	0.17	1.52	0.11	312	595	0.53	0.19	1.87	0.10	20%
3.0	285	575	0.49	0.19	1.92	0.10	324	655	0.49	0.22	2.09	0.11	20%
3.5	294	624	0.47	0.20	2.29	0.09	335	710	0.47	0.25	2.24	0.11	20%

6.4.4 Behaviour of the component parts

The detailed analysis of the deformation and stress states of the PTED connection component parts is presented in section 5.5.

In the following, the cyclic behaviour of the single component parts of the corresponding welded rigid connection is investigated.

For the sake of comparison, the focused drift values are the same as those considered for the PTED connection, namely 0.4%, 3.5% and end of cycles. In this case, no post-tensioning phase is obviously present.

The results are firstly presented by considering the assembled node, and then by focusing on every connection component part.

Assembled node

The deformed configurations of the node, together with the related stress distributions, at the above mentioned relevant drifts, are shown in Figures from 6.31 to 6.33. For each deformed configuration, perspective, lateral and plan views are provided, in order to correctly catch the node behaviour. The areas where the yield stress of the beam steel is attained are plotted in black.

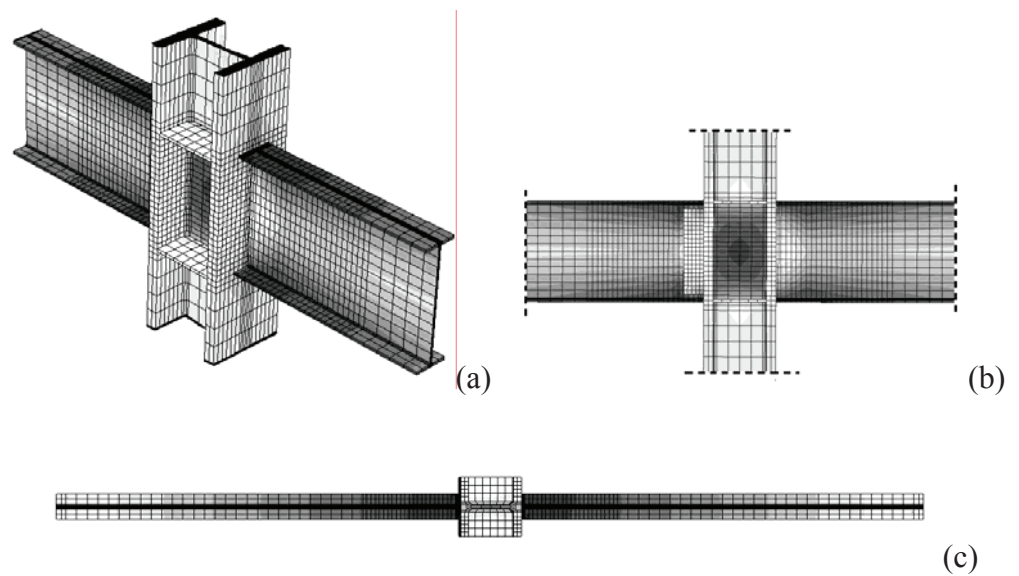


Figure 6.31. Deformation and stress state of the study welded rigid connection at a 0.4% drift: (a) perspective, (b) lateral and (c) plan views

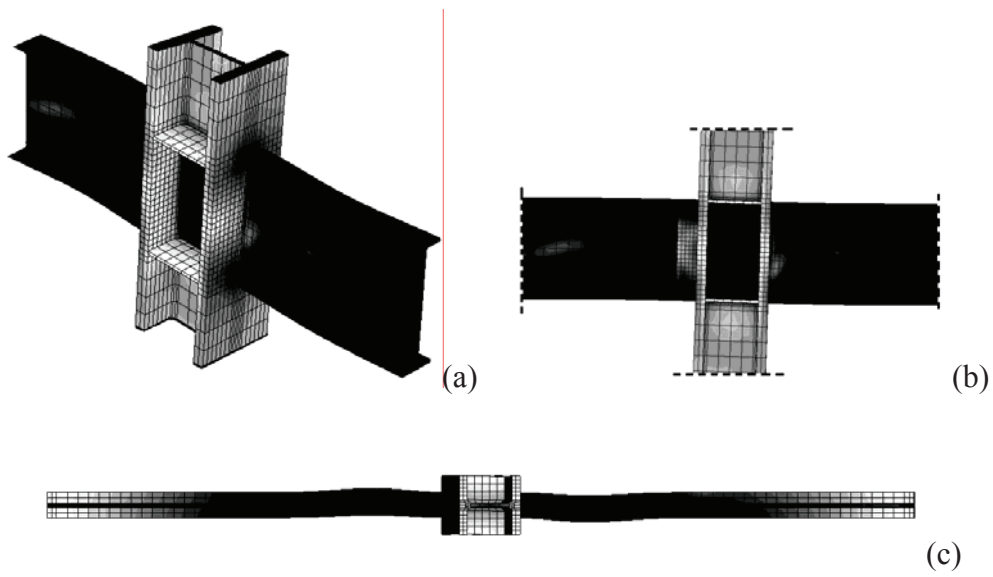


Figure 6.32. Deformation and stress state of the study welded rigid connection at a 3.5% drift: (a) perspective, (b) lateral and (c) plan views

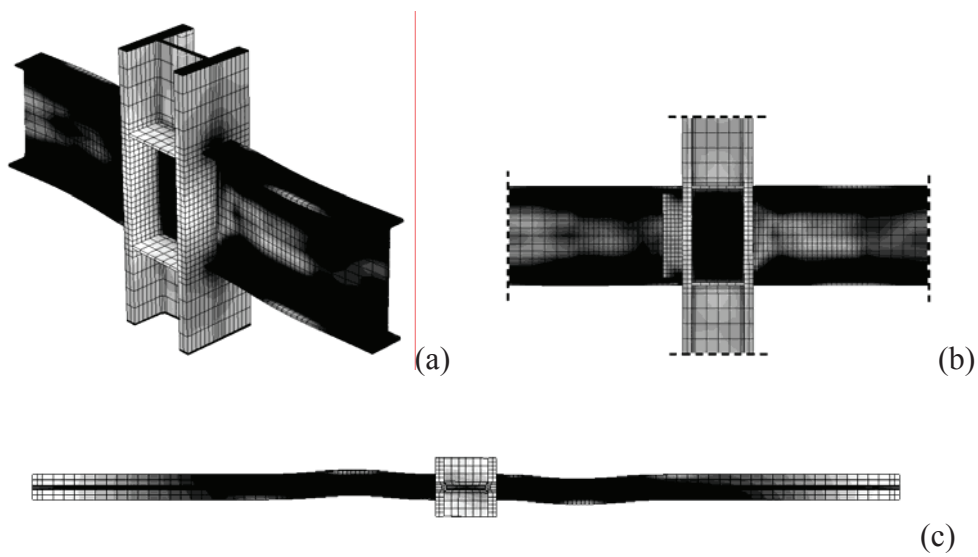


Figure 6.33. Deformation and stress state of the study welded rigid connection at the end of the cycles: (a) perspective, (b) lateral and (c) plan views

Beams

The cyclic behaviour of the beams in the welded rigid connection is completely different from that of the ones assembled in the PTED connection. In fact, in a rigid connection, the beams are expected to undergo large extents of inelastic deformations, since they are the structural elements devoted to the dissipation of the input energy through cycles of bending in the plastic field. The obtained numerical results confirm such situation, as it is shown in Figure 6.34, which illustrates the deformation and stress states of the beam at the above relevant drifts.

At a drift equal to 0.4% (Fig. 6.34a) the beam behaviour is elastic. The areas interested by the largest stress demand, namely the beam flanges next to the column interface, are clearly visible.

At a drift equal to 3.5% (Fig. 6.34b), large portions of the flanges and of the web are in the plastic field.

Residual stresses are present in the beams at the end of the cycles (Fig. 6.34c).

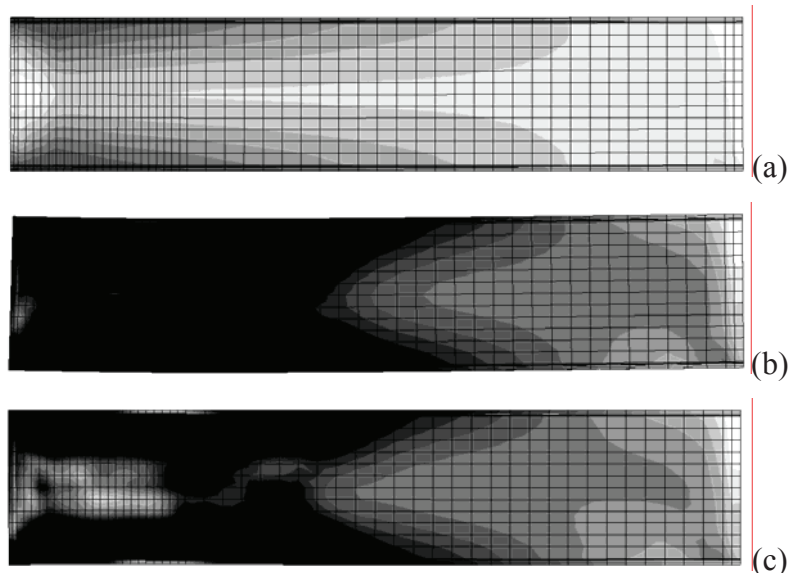


Figure 6.34. Deformation and stress states of the beam in the welded rigid connection: (a) at a 0.4% drift; (b) at a 3.5% drift; (c) at the end of the cycles

The stress history in the most engaged finite element of the beam is plotted in Figure 6.35, which confirms the large excursion in the plastic field starting from the 0.7% drift.

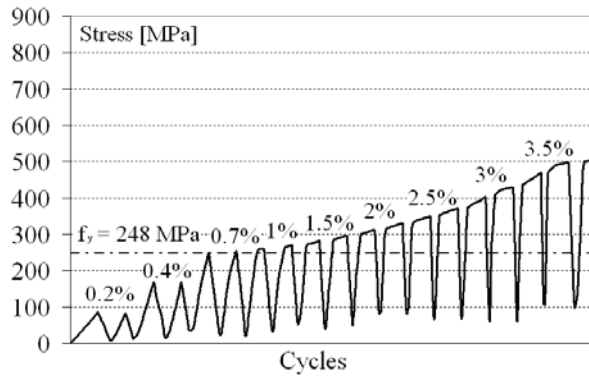


Figure 6.35. Stress history in the most engaged element in the beam flange

Column

During the cycles of imposed drifts, the column of the rigid connection undergoes inelastic deformations (Fig. 6.36).

At a drift equal to 0.4% (Fig. 6.36a), a large stress demand is evident in the node web panel.

At a drift equal to 3.5% (Fig. 6.36b), large yielded areas in the node web panel are visible, with the consequent presence of a residual stress distribution at the end of the cycles (Fig. 6.36c).

The above considerations are confirmed by the curve in Figure 6.37, where the stress history in the most engaged finite element of the column web is plotted.

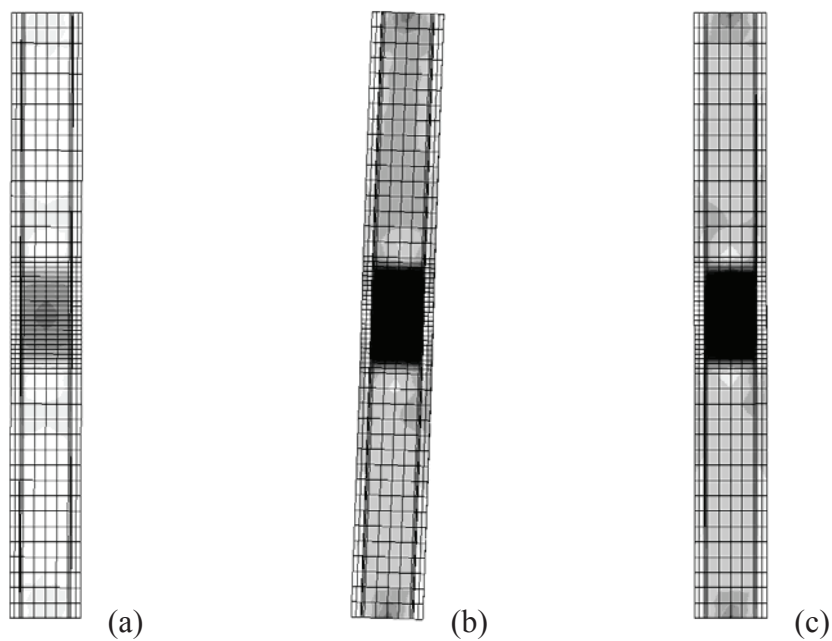


Figure 6.36. Deformation and stress states of the column in the welded rigid connection: (a) at a 0.4% drift; (b) at a 3.5% drift; (c) at the end of the cycles

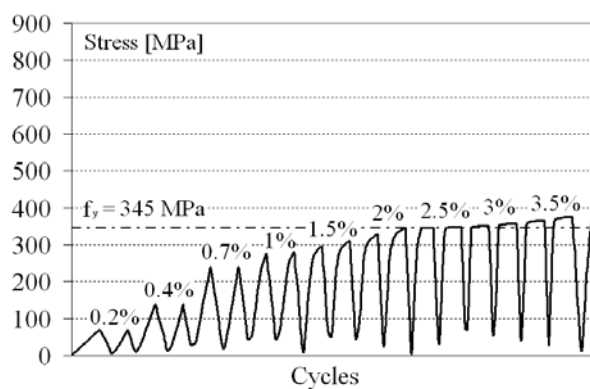


Figure 6.37. Stress history in the most engaged element of the column web

Continuity plates

The continuity plates support the column flanges in bearing the stresses coming from the beam flanges. During the cycles of imposed drift, their behaviour, in the study rigid connection, is always in the elastic field.

The stress distribution in a top continuity plate (Fig. 6.38a) for the above relevant drifts is shown in Figure 6.38.

At a drift equal to 0.4% (Fig. 6.38b), the extent and values of the stresses are quite small.

At larger drifts (Fig. 6.38c) they increase in the area in contact with the column web.

Although the behaviour of the continuity plates is always elastic, residual stresses are present at the end of the cycles (Fig. 6.38d), due to the plastic deformations occurred in the column and beams.

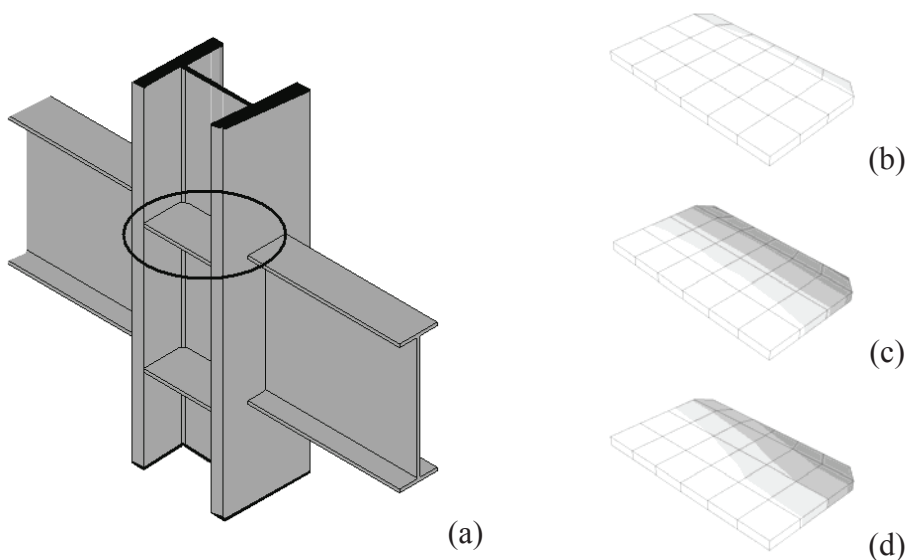


Figure 6.38. Deformation and stress states of the top continuity plate (a) in the welded rigid connection: (b) at a 0.4% drift; (c) at a 3.5% drift; (d) at the end of the cycles

Figure 6.39 shows the stress history in the most engaged finite element of the top continuity plate.

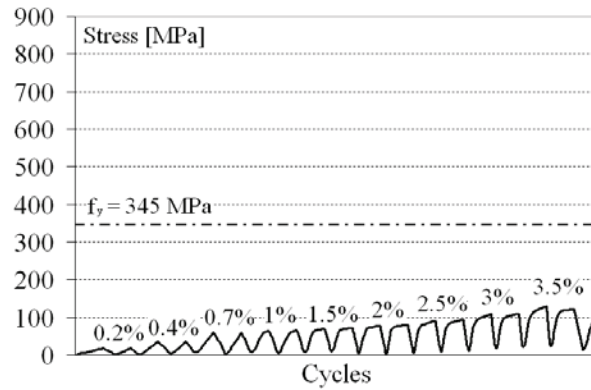


Figure 6.39. Stress history in the most engaged finite element of the top continuity plate

6.5 SYNTHESIS OF RESULTS

This chapter deals with the cyclic behaviour of PTED beam-to-column connections and compares it with the behaviour of welded rigid nodes characterized by the same column and beam assemblage. The reliability of the numerical results is based on the good calibration, referred to the available experimental results, obtained for the used finite element models.

The numerical models are used for investigating and comparing the performances of PTED and rigid connections, in terms of both global and local behaviour. The global comparison is referred to the whole beam-to-column assemblage and is carried out in terms of stiffness, maximum borne forces, dissipated input energy and residual deformations. The local comparison is referred to the cyclic behaviour, in terms of deformation and stress states, of each component part present in the connections.

Two couples of PTED vs. welded rigid connections are studied, the first corresponding to the system with PT and ED bars, by Christopoulos et al. (2002b), and the second corresponding to the system with PT strands and ED angles, by Ricles et al. (2002b). The results are here summarized by considering the two comparative investigations separately.

PT and ED bars vs. welded connection

With regard to the global performances of the PTED and rigid connections, the main results of the performed analyses evidence the following aspects.

The initial stiffness of the PTED connection is the same as the rigid one, up to a drift equal to 0.375%. This means that the PTED connection behaves like a rigid one in case of frequent earthquakes, according to the criteria given in SEAOC Vision 2000. The PTED connection behaviour is linear up to a 0.375% drift, whereas the rigid connection behaves linearly up to a 1% drift.

The forces borne by the rigid connection are about 1.8 times the ones borne by the PTED one.

The dissipation capacity of the PTED connection is smaller than the rigid connection one, ranging from about 20% to about 15% of the latter one.

No residual drifts are present in the PTED connection at the end of the cycles, whereas large yielded areas and out-of-plane displacements are visible in the rigid node, which shows a residual drift equal to 2.7%.

With regard to the local behaviour, the main results of the performed analyses evidence the following aspects.

The beam in PTED connection essentially behaves in elastic range for all the drift values imposed during the analysis, with the attainment of the yield stress in very limited areas, namely at the interface with the contact plates and at the end of the reinforcing plates. The beam in the rigid connection undergoes inelastic deformations in large areas of both the flanges and the web, starting from the cycle at 1% drift. For large drifts, out-of-plane displacements due to buckling phenomena occur.

The column in the PTED connection behaves in elastic field, clearly showing a strong shear demand in a limited portion of the web, when the interface gap opens. Stress values slightly lower than the yield limit are evidenced in a small area of the column flange, at the interface with the contact plate. The stress distribution in the column of the rigid connection is characterized by larger extent, involving the whole length of the column.

The stress demand on the continuity plates in both the PTED and rigid connections is not of concern. The main behavioural difference in the two cases is that in the case of PTED connection the stress engagement in a continuity plate is large only when the corresponding beam flange is

compressed, whereas in the case of rigid connection the contact plate is stressed for both tension and compression of the corresponding beam flange.

With regard to the doubler plates, in both cases the behaviour is elastic. As in the case of continuity plates, the doubler plates stress engagement involves the whole plate of the rigid connection independently from the drift sign, differently from the case of PTED connection, whose doubler plates are stressed in different areas depending on the drift sign.

PT strands and ED angles vs. welded connections

The PTED connection has the same initial stiffness as the rigid connection, thus the same performance in case of low intensity earthquakes. However, the PTED node shows a linear behaviour up to a drift equal to 0.25%, when a gap at the beam-to-column interface opens, whereas the rigid node behaviour is linear elastic up to a 0.70% drift, when the first yield in the beams appears. In terms of bearing capacity, the rigid node can reach a maximum force and moment which are approximately twice the ones attained in the PTED connection. Moreover, in terms of energy dissipation capability, the rigid node is able to dissipate an energy amount 5 times larger than the PTED system, although at the cost of large plasticization and out-of-plane displacements in the beams, due to instability phenomena in the plastic field, against negligible yielding in the PTED connection.

The beams in the PTED connection essentially behave in elastic range, with some yielding in limited portions of the flanges and the web, whereas the beams in the rigid connection undergo large plasticization and out-of-plane displacements. No inelastic deformations occur in the column of the PTED connection, whereas the node web panel of the rigid connection is interested by large yielding.

Based on the above summarized results, it is possible to make the following observations.

The rigid-type behaviour of PTED connections for small drift values is confirmed. Consequently, their behaviour under both service loads and low-intensity earthquakes does not differ from that of welded nodes steel moment resisting frames.

The borne forces and moments, as well as the capability of dissipating energy, of PTED connections are smaller than those of the corresponding welded nodes. Nevertheless, when subjected to severe earthquakes, they are essentially undamaged and capable to return to the initial configuration, whereas welded connections undergo large damage and geometric distortions.

At last, fracture phenomena, which are neglected in this study, are cause of big concern in the case of welded rigid connections, whereas they are not expected in the case of Post-Tensioned Energy Dissipating ones.

Chapter 7

Comparative analysis of PTED connections

7.1 THE STUDY PTED CONNECTIONS

7.1.1 *General*

In this chapter a comparative evaluation of PTED beam-to-column connections characterized by different arrangements for the PT and ED systems is carried out (Esposito et al., 2008).

The comparison is focused on the systems by Ricles et al. (2002b), endowed with PT high strength steel strands and ED bolted steel top-and-seat angles, and by Christopoulos et al. (2002b), endowed with PT high strength steel bars and ED confined steel bars.

The study beam-to-column connection corresponds to the PC4 specimen described by Ricles et al. (2002b), namely a cruciform-shaped internal node made by a W14x311 column and two W24x62 beams (Fig. 7.1).

The detail of the connection endowed with PT high strength steel strands and ED bolted steel top-and-seat angles, herein indicated as the “A” connection, is shown in Figure 7.2a. Its features are described in Chapter 5.

The detail of the connection endowed with PT high strength steel bars and ED confined steel bars, herein indicated as the “B” connection, is shown in Figure 7.2b. For the sake of comparison, it is adapted for meeting the design requisite of the “A” PTED system.

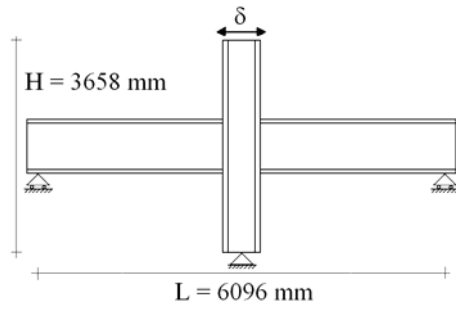


Figure 7.1. Geometry of the PTED assemblages for the comparative analysis

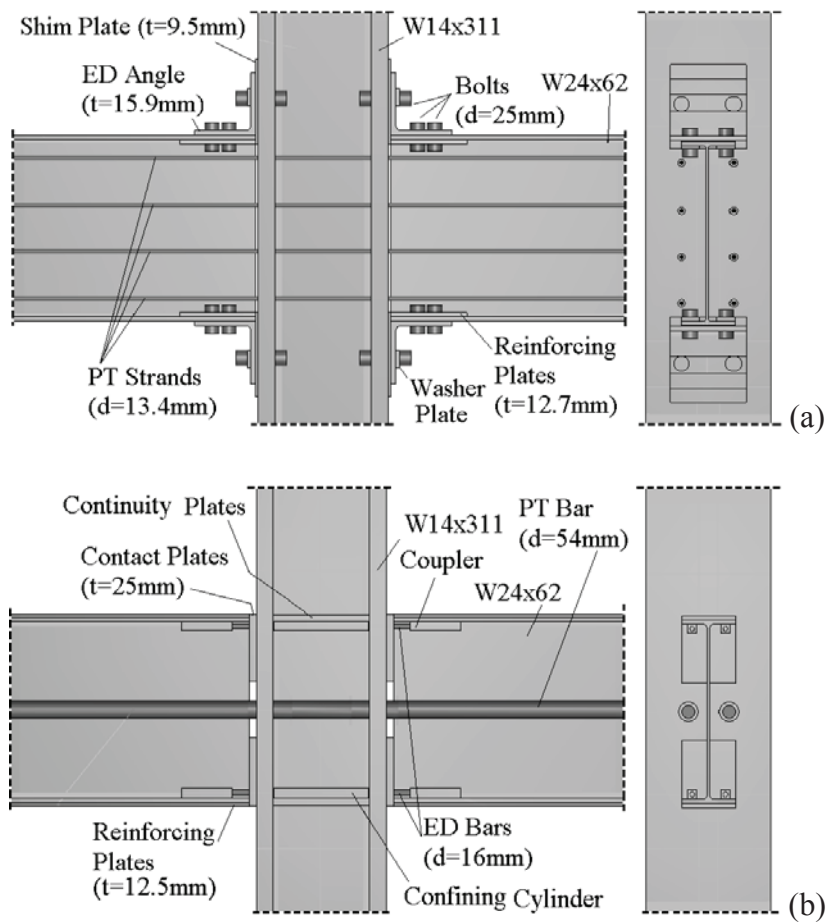


Figure 7.2. Geometrical features of the (a) "A" and (b) "B" connections

7.1.2 Design of the connection with PT and ED bars

The main parameters for the design of the B PTED connection are listed in the following:

- the target beam-to-column gap opening (θ);
- the initial post-tensioning force ($F_{PT,in}$);
- the cross-section area of the PT bars (A_{PT});
- the area of the ED confined bars (A_{ED});
- the unbounded length of the ED bars (L_{ED}).

They are shown in Figure 7.3 and their selection is carried out as described in the following. The materials considered for the PT and ED systems are the same used by Christopoulos et al. (2002b), which are shown in Chapter 4.

The target gap opening θ is equal to 0.028 rad. Such value corresponds to the gap opening reached during the experimental test performed by Ricles et al. (2002b), at an imposed drift equal to 3.5%.

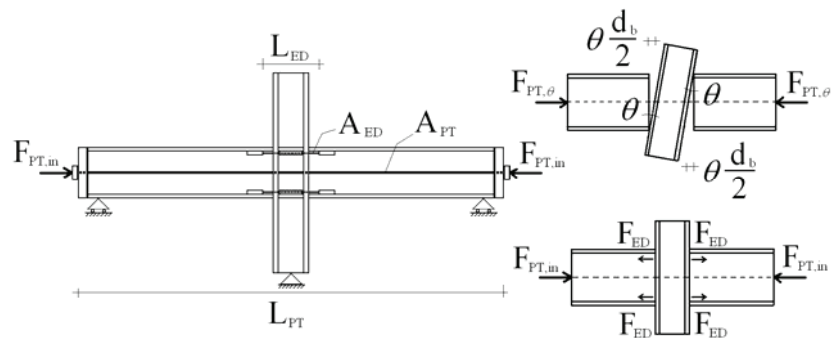


Figure 7.3. Main parameters for the design of the PTED connection with PT and ED bars

The initial post-tensioning force $F_{PT,in}$ is the same as in the A connection, namely 710 kN. Consequently, each PT bar is initially post-tensioned by a 355 kN force. This value corresponds to the 24% of the beam axial yield force,

and so it matches the suggestions provided by Christopoulos and Filiatrault (2002).

The remaining parameters of the B PTED connection are determined according to the suggestions given by Christopoulos and Filiatrault (2002), indicated in the following.

The cross-section area of the PT bars is obtained based on relationship (7.1), which guarantees that, at the target gap opening, the stress in the PT bars is limited to the 70% of the ultimate stress:

$$\sigma_{PT,\theta} = \sigma_{PT,in} + \Delta\sigma = \frac{F_{PT,in}}{A_{PT}} + n\theta \frac{d_b/2}{L_{PT}} E_{PT} < 0.7 f_{PT,u} \rightarrow$$

$$\rightarrow A_{PT} > \frac{F_{PT,in}}{0.7 f_{PT,u} - n\theta \frac{d_b/2}{L_{PT}} E_{PT}} \quad (7.1)$$

In relationship (7.1) $f_{PT,u}$ is the ultimate stress of PT bars steel, n is the total number of gap openings in the connection, d_b is the depth of the beam, L_{PT} is the whole length of the PT bars, and E_{PT} is the Young module of the PT bar steel (Fig. 7.3). Considering that $f_{PT,u}$ is equal to 1030 MPa, n is equal to 2, d_b is equal to 603 mm, L_{PT} is equal to 6295 mm, and E_{PT} is equal to 206000 MPa, the minimum required area for the couple of PT bars is equal to 4213 mm². Consequently, two 54 mm diameter PT bars are selected.

The area of a couple of ED bars (A_{ED}) is chosen on the basis of relationship (7.2), which guarantees that the connection is able to self-centre also after the yielding of the ED bars, during the load cycles:

$$2F_{ED} < F_{PT,in} \quad (7.2)$$

In relationship (7.2) $F_{ED}=A_{ED}\sigma_{ED}(\theta)$ is the total force developed by a couple of ED bars (Fig. 7.3) at the target gap opening θ , and the stress $\sigma(\theta)$ accounts also for the hardening phenomena in the ED bar steel. Considering that, based on the material properties used for the ED bars, the stress at the target gap opening is equal to 530 MPa, A_{ED} must be smaller than 335 mm². Consequently, the diameter of the ED bars is chosen equal to 16 mm.

The ED bars unbounded length (L_{ED}) is equal to 600 mm, which is approximately equal to the beam depth (d_b), according to the suggestions by Christopoulos and Filiatrault (2002).

Beam flange 25 mm thick continuity plates are considered, even though they are not present in the A connection, they being not required thanks to the large thickness of the column parts. Anyway, they are necessary for locating the steel cylinders necessary for confining the ED bars.

The beam-to-column contact plates are 25 mm thick, whereas the beam flange reinforcing plates are 12.5 mm thick, as in the test described in (Christopoulos et al., 2002b). The length of reinforcing plates is selected in order to prevent any yielding in the beams, due to the combined action of PT force and bending moment, according to the results evidenced by the stress distribution in the beam presented in section 4.4.

It is worth noticing that the arrangement considered for the comparative analyses is only one among the possible solutions, since in a PTED connection the design requirements can be, in general, fulfilled by adopting different combinations of the connection component parts.

7.2 THE NUMERICAL MODELS

7.2.1 *The geometry of the models*

The finite element model of the A PTED connection is one of those presented in Chapter 5, which exploits the symmetry of the system with respect to the beams and column web mid-plane.

The finite element model of the B PTED connection has the same beam and column assemblages as the A ones, and the PT and ED component parts described in section 7.1.2. Also the B PTED connection model exploits the symmetry condition.

The choice of the “symmetric” models is based on the fact that they are less expensive from a computational point of view. As shown in Chapters 4 and 5, this modelling assumption does not affect the response of the systems, at least up to the imposed drift values considered in the analyses, and so it is very effective in the perspective of a comparative study.

The geometry of the models corresponds to the details shown in Figure 7.2, with the exception of the symmetry assumption.

7.2.2 *The properties of the materials*

In model A, the features of the materials are those described in Chapter 5. With regard the B PTED connection model, the materials of beams and column are the same as the A ones, whereas the materials of the remaining component parts are those presented in Chapter 4. For the sake of the reader's convenience, the mechanical features of the modelled materials, expressed in terms of true stresses and plastic strains, are summarized in Table 7.1.

Table 7.1. Mechanical features of the modelled materials, in terms of true stresses and plastic strains

Component parts		Yield stress (MPa)	Ultimate stress (MPa)	Ultimate plastic strain (%)
Column		345	550	19.6
Beams		248	530	19.6
A	Washer plates	345	550	19.6
	Shim and reinforcing plates	845	1030	13.5
	Bolts	635	810	10.9
	PT strands	1305	1865	-
	ED angles	263	567	19.6
B	Continuity, contact and reinforcing plates	345	550	19.6
	PT bars, couplers and confining cylinders	1030	1030	-
	ED bars	400	700	-

7.2.3 *The interactions between the component parts*

With regard to the modelling of the interactions between adjacent component parts, the same assumptions made in previous chapters are made. In particular, tie constraints are used for modelling the interaction between

welded surfaces, which can not have relative displacements, and contact interactions are used between surfaces which can be or not in contact during the analysis. The detailed list of the tied surfaces for the A PTED connection is presented in Chapter 5, whereas for the B PTED connection the assumptions are in all similar to those illustrated in Chapter 4.

With regard to the contact interactions, it is possible to preliminarily estimate and compare the related computational costs of the two models. The location of the beam-to-column contact interactions for both the A and B models are shown in Figure 7.4. In the A model, friction contacts are used at the following adjacent surfaces: shim plate-ED angle; shim plate-beam end; shim plate-reinforcing plate. Since there are two reinforcing plates for each beam flange, they being located at the internal side of the flanges, the number of friction contact interactions is equal to 16 for the A model. In the B model, friction contacts are used at the interfaces between column and contact plates, for a total number equal to 4. Considering that the analysis cost in ABAQUS/Standard strongly depends on the contact interactions, it is evident that, besides other aspects, the A model is more computationally expensive than the B one.

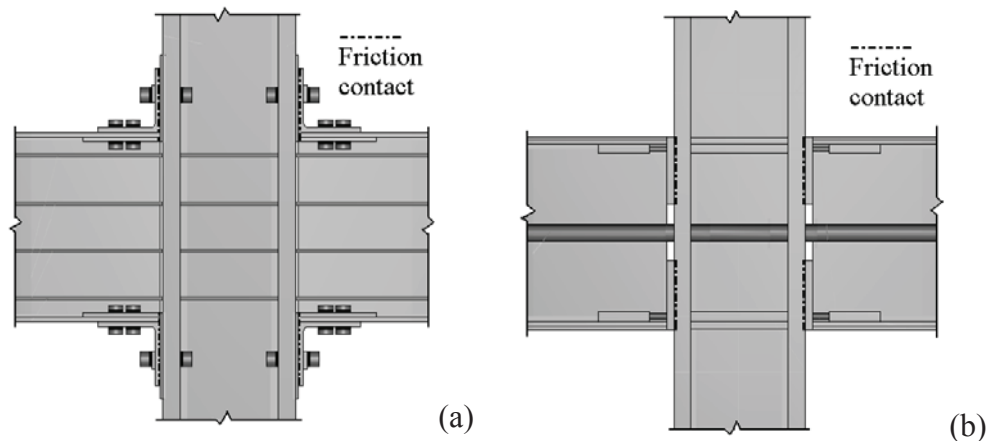


Figure 7.4. Location of the friction contact interactions for (a) the A PTED connection model and (b) the B PTED connection model

7.2.4 The load history

During the first step of the analyses, the pre-loading of bolts, of PT strands (A connection) and of PT bars (B connection) is applied. Each bolt is pre-loaded by a 250 kN force, corresponding to about 80% of the related yielding force. Each PT strand is post-tensioned by a 87.5 kN force, whereas each PT bar is post-tensioned by a 355 kN force, giving raise, in both cases, to the 710 kN total $F_{PT,in}$. In the subsequent steps, the cyclic history of lateral displacements at the top of the column already presented in Chapter 5, and plotted in Figure 7.5 for the sake of the reader's convenience, is applied.

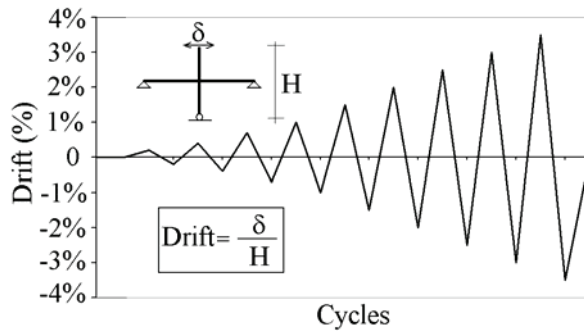


Figure 7.5. Imposed cyclic drift history in the numerical analyses

7.2.5 The mesh

Linear hexahedral solid finite elements are used in the models (Fig. 7.6), they being appropriate for complex non-linear analyses involving contact, plasticity and large deformations. Reduced integration is also used for limiting the computational efforts.

The calibration of the A model is carried out directly against the experimental results, as shown in Chapter 5.

The calibration of the B model is carried out based on the information and assumptions presented in Chapter 4.

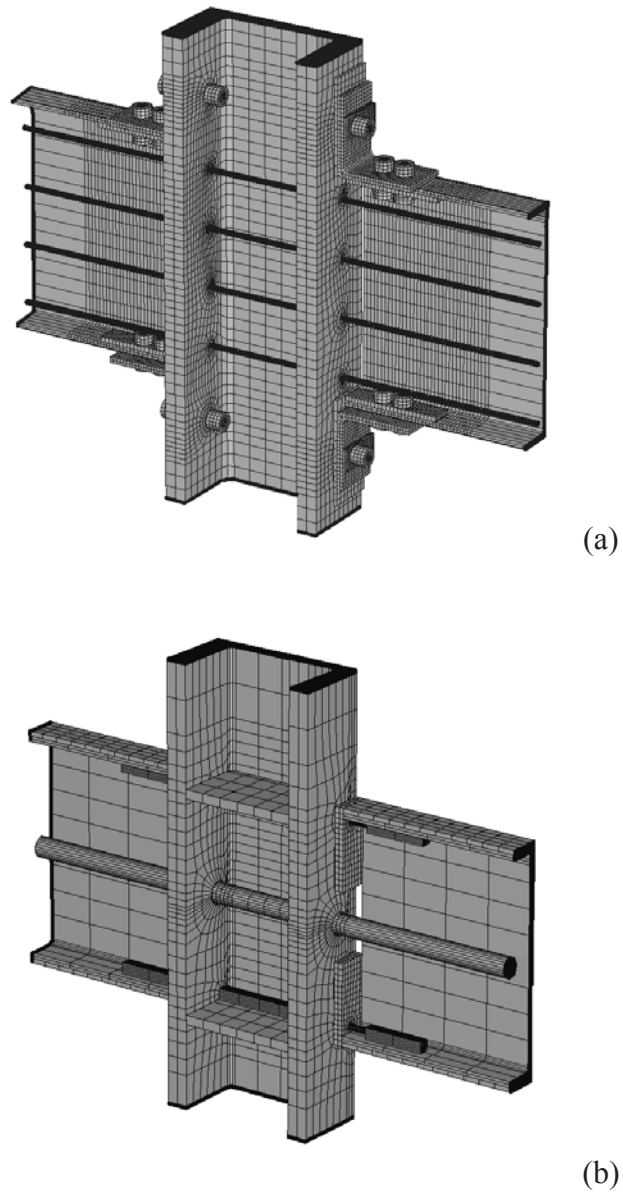


Figure 7.6. Nodal detail of the finite element mesh of (a) the A PTED connection model and (b) the B PTED connection model

7.3 COMPARATIVE EVALUATION

7.3.1 Global response curves

The numerical force-drift cyclic responses of the two considered PTED connections is shown in Figure 7.7. It is useful for carrying out the comparative evaluation of the A and B PTED connections, in terms of stiffness, maximum borne forces, residual drifts and input dissipated energy.

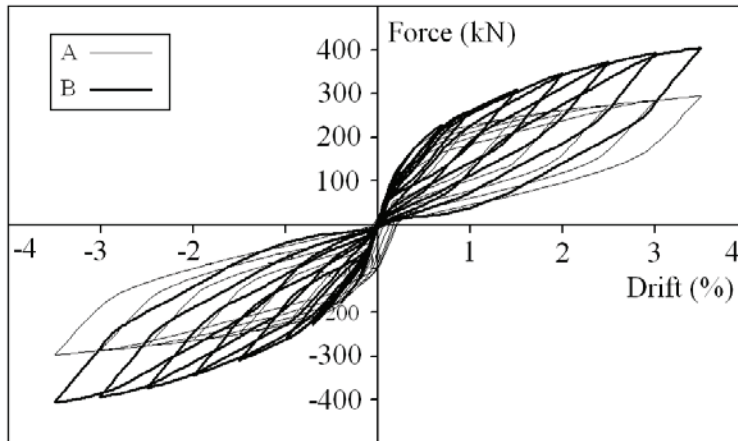


Figure 7.7. Numerical force-drift cyclic curves for the A and B PTED compared connections

For imposed drift values up to 0.25%, the behaviour of the two PTED connections is linear elastic. This behaviour matches the corresponding welded connection's one, as visible in Figure 7.8, where a zoom on the curves up to a drift equal to 1% is shown. In that figure the dotted line represents the response of the welded connection. Such evidence confirms that both the considered PTED connections behave like a traditional rigid node in presence of frequent earthquakes, such as for seismic events with high probability of occurrence, achieving the fully operational performance level.

After the gap opening at the beam-to-column interfaces, the PTED connections behaviour is non-linear. For a drift equal to 0.4%, the lateral force for the A and B PTED connections is the same, namely 175 kN. Beyond the

0.4% drift, the behaviour of the two PTED connections starts to diverge each other. In particular, the B PTED connection shows to be stiffer than the A connection, the ratio between the stiffnesses ranging from 2.0 to 2.3 for the different cycles. This behaviour can be understood considering that the post-gap opening stiffness in a PTED connection essentially depends on the stiffness of the PT system (besides the post-yielding stiffness of the ED system) and that the PT bars are stiffer than the PT strands

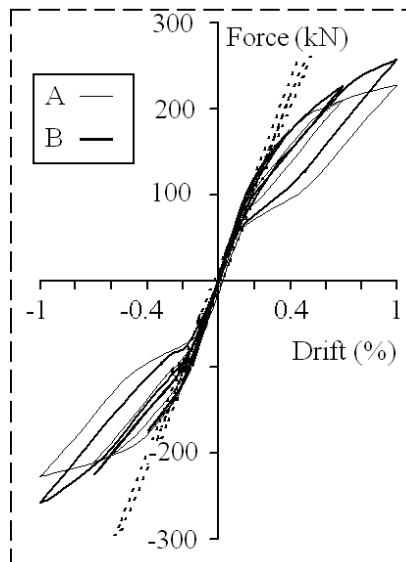


Figure 7.8. Zoom for small drift values in the numerical force-drift cyclic curves

The cyclic response of the A and B PTED beam-to-column connections is quantitatively described and compared in Table 7.2, in terms of maximum forces (F_{max}), residual drifts (d_{res}), and dissipated energy, the latter expressed as the ratio between the area of the loops of A (A_A) and B (A_B) systems.

At the maximum drift considered in the numerical analyses (3.5%), the force in the A connection (294 kN) is 30% smaller than the B one (400 kN).

The cyclic behaviour of both the PTED connections is clearly flag-shaped. In particular, negligible residual drifts occur in the A connection, with a maximum of 0.20% after the 3.5% drift, whereas no residual drifts occur in the B connection.

Table 7.2. Comparison between the responses of the two systems

Drift (%)	F_{\max} (kN)		d_{res} (%)		A_A/A_B
	A	B	A	B	
0.2	110	110	0.00	0.00	-
0.4	175	175	0.00	0.00	-
0.7	210	226	0.00	0.00	-
1.0	227	258	0.00	0.00	1.75
1.5	247	306	0.03	0.00	1.54
2.0	263	340	0.09	0.00	1.25
2.5	275	366	0.17	0.00	1.33
3.0	285	388	0.19	0.00	1.33
3.5	294	400	0.20	0.00	1.33

With regard to the energy dissipation capacity, the study A PTED connection dissipates a larger amount of energy than the B one. In fact, the ratio between the energy dissipated by the A and B connections, which is measured on the basis of the areas of the force-drift loops, ranges from 1.75 to 1.33, among the different cycles.

7.3.2 Deformation and stress states of the connections

The comparison of the deformation and stress states of the two PTED connections during the phases of the imposed drift history allows to obtain useful information on their behavioural peculiarities. In this section the deformed nodes, and the corresponding stress distributions, after the post-tensioning, at drifts equal to 0.4%, 2.0% and 3.5%, and at the end of the cycles, are described. The attainment of the beam steel yield stress (248 MPa) is plotted in black.

The A and B PTED connections, after the post-tensioning phase, are shown in Figure 7.9. In both cases the stress distribution is symmetric with respect to the beams horizontal mid-plane. In the A connection (Fig. 7.9a), the interface between the beams and the column is actually represented by the shim plates, whose location is selected to prevent any contact stresses in the beam web. Consequently, at the beams ends, the flow of compression stresses starts from the beam flanges and slightly affects the beam webs. Corresponding

compression flows are visible in the column web. In the B connection (Fig. 7.9b), the actual interface between beams and column is represented by the contact plates, whose location entails the presence of compression stress flows in both the beams flanges and webs. The column web is conveniently supported by the presence of the continuity plates.

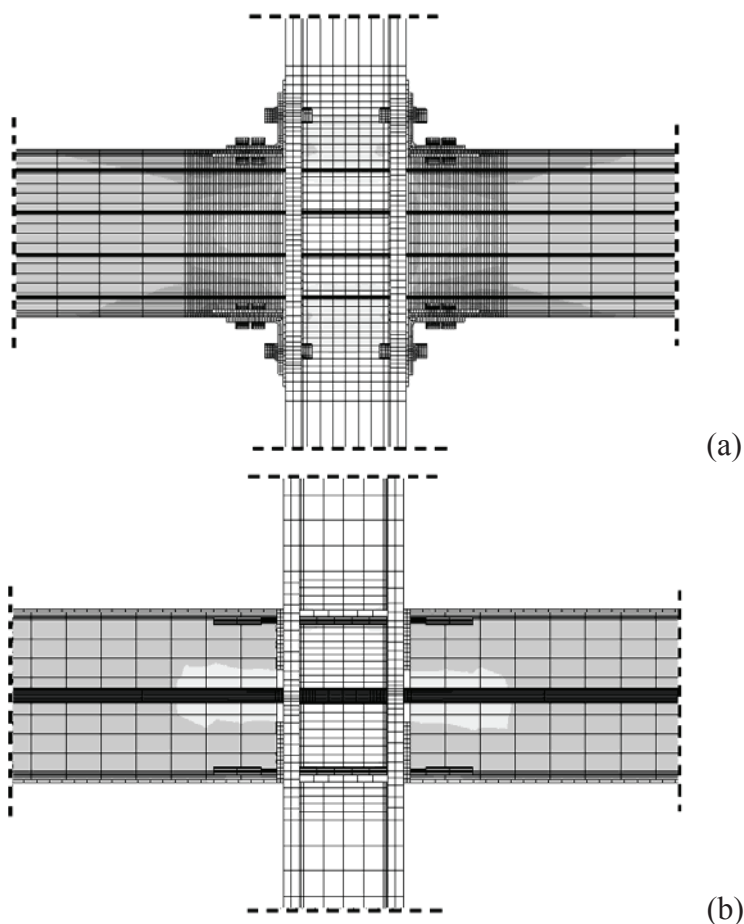


Figure 7.9. Deformation and stress states after the post-tensioning in (a) the A PTED connection and (b) in the B PTED connection

At a drift equal to 0.4% (Fig. 7.10) the interface gap is open in both the connections, although invisible in figure. The stress flow in the column web shows the load carrying mechanism, with stresses going from a compressed

beam flange to the other one. In the beams of the A connection (Fig. 7.10a), besides the stresses in the compressed flanges, some stresses are also present at the tension side, due to the presence of the ED angles. On the contrary, in the B connection (Fig. 7.10b), the stress distribution in the beams affects only the compressed side.

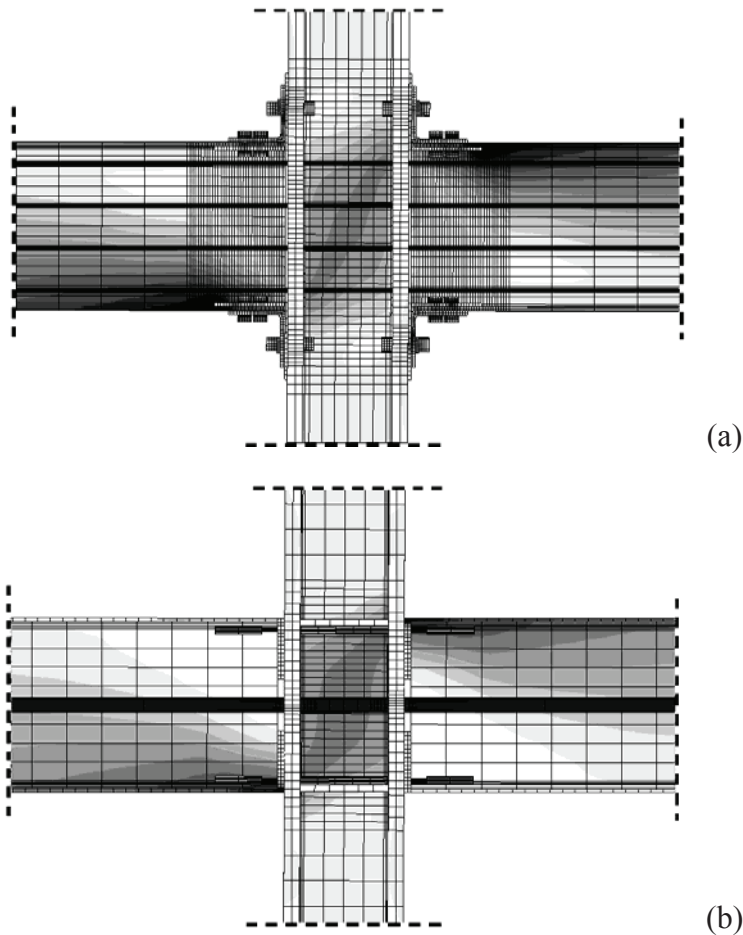


Figure 7.10. Deformation and stress states at a drift equal to 0.4% in (a) the A PTED connection and (b) in the B PTED connection

At a drift equal to 2.0% (Fig. 7.11), the gap opening is clearly visible in both the connections. In the A connection (Fig. 7.11a), large stress

concentrations, up to reaching the yield limit, are present in the compressed flanges of the beams, and the stresses induced in the tension side of the beams by the ED angles are larger. In the B connection (Fig. 7.11b), the compression stress flow is clearly evident. Some stresses are present at the tension side, which are induced by the forces in the elongating ED bars.

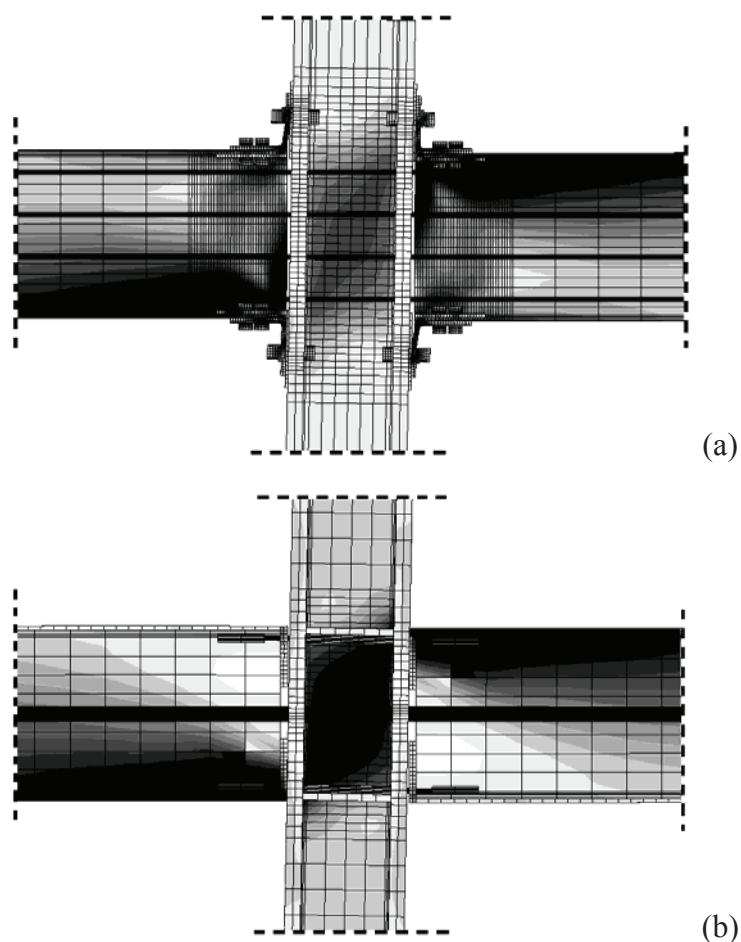


Figure 7.11. Deformation and stress states at a drift equal to 2.0% in (a) the A PTED connection and (b) in the B PTED connection

At the maximum drift reached during the analysis, namely 3.5% (Fig. 7.12), the stress distribution is more marked. In the A connection (Fig. 7.12a),

stress peaks, with some yielding in limited areas, are visible in both the beam flanges and webs. At the end of the ED angles, the stress values are larger since the “reinforcing” action provided by the angle legs is not effective (as noticed in section 5.5). Stress concentrations are also present in the column web. In the B connection (Fig. 7.12b), some yielding occurs in the beam flanges and webs. It is worth noticing that, although the column web in the B connection is plotted in black, no yielding occurs, its yield stress being equal to 345 MPa (whereas the black areas indicate the attainment of 248 MPa stress, namely the yield limit in the beams).

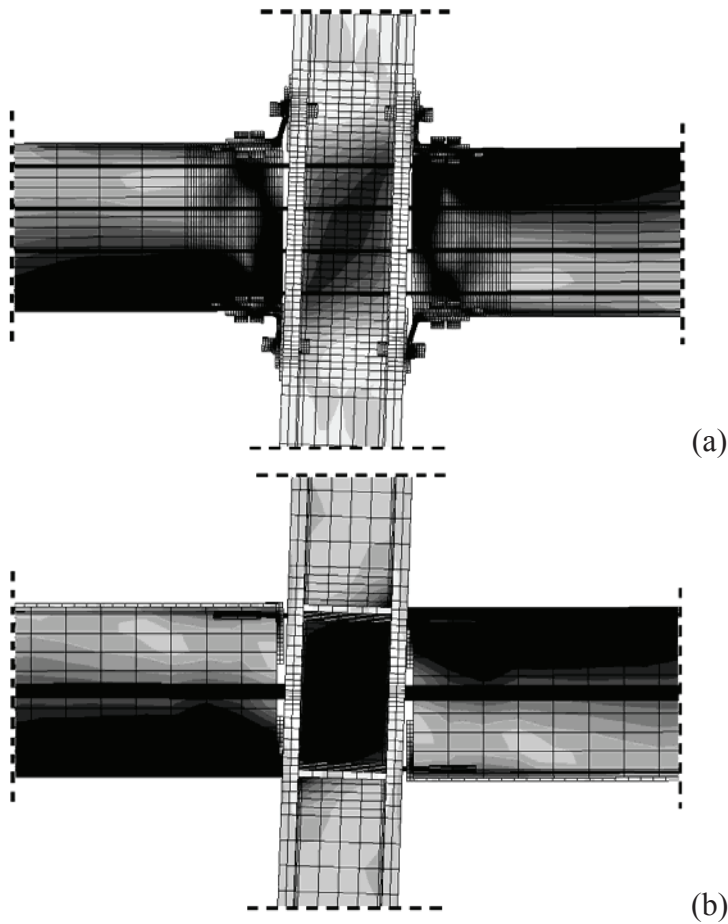


Figure 7.12. Deformation and stress states at a drift equal to 3.5% in (a) the A PTED connection and (b) in the B PTED connection

At the end of the cycles (Fig. 7.13), the stress distribution in both the connections is symmetric. Neither in the A connection (Fig. 7.13a) nor in the B one (Fig. 7.13b) the stress distribution is perfectly the same as that present after the application of the post-tensioning force. In the case of the A connection, small residual stresses are due to some minor yielding in the beams and to the marked yielding in the top-and-seat angles. In the case of the B connection, small residual stresses are essentially due to the minor yielding in the beams.

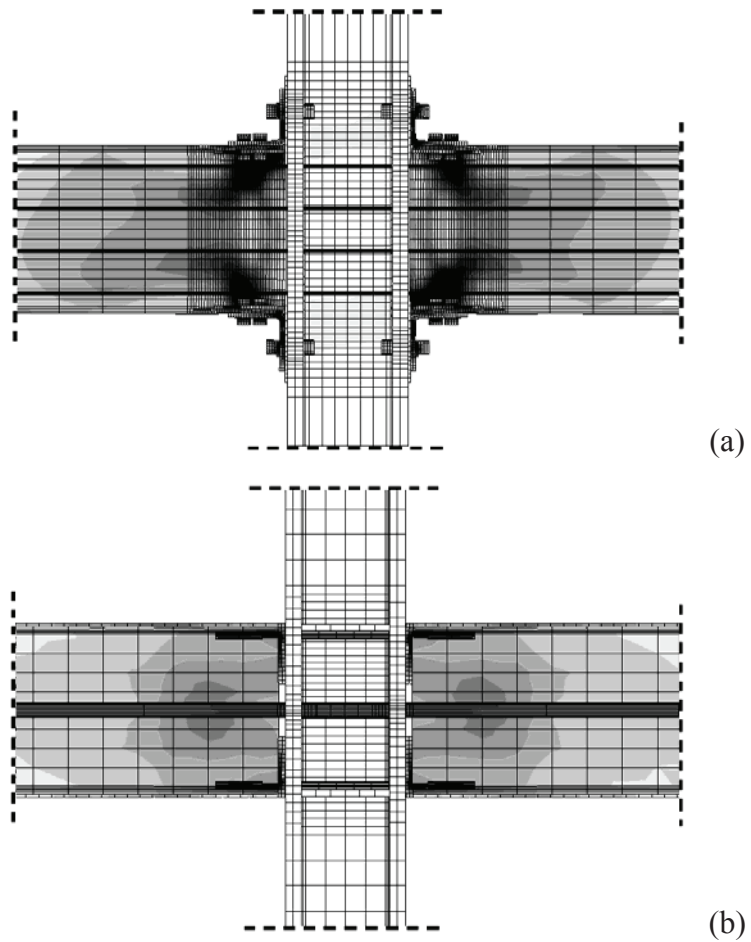


Figure 7.13. Deformation and stress states at the end of the cycles in (a) the A PTED connection and (b) in the B PTED connection

7.4 SYNTHESIS OF RESULTS

Based on the described numerical analyses, aimed at a comparative evaluation of two PTED beam-to-column connections for steel moment resisting frames, the following interesting behavioural aspects can be pointed out.

Before the gap opening, corresponding to small values of the imposed lateral drifts, both the study PTED connections behave like a traditional rigid one, such as a linear force-drift relationship is depicted. This result confirms that the overall behaviour of PTED connections before decompression is not influenced by the PT and ED arrangements. Local differences in the stress and strain states are present, depending on the connection details.

After the gap opening at the beam-to-column interfaces, the connection with PT strands and ED angles shows a less stiff behaviour than the connection with PT and ED bars (with a ratio equal to about 0.45), achieving a 30% smaller maximum force at the maximum drift considered in the analysis. This behaviour is explained considering that the post-gap opening stiffness in a PTED connection mainly depends on the elastic stiffness of the PT elements and on the post-yielding stiffness of the ED elements. Consequently, as it could be expected, a PTED connection with PT strands and ED angles is more deformable, after the gap opening, than a similar connection with PT and ED bars, due to the larger deformability of the PT strands with respect to the PT bars and of the ED angles, subjected to bending, with respect to the ED bars, subjected to tension. This results is important in the perspective of the global response of a frame equipped with PTED connections, whose performances are strongly affected by the stiffness of the beam-to-column connections. So, the best frame response could be obtained by tailoring the post-gap stiffness of the connections.

The flag-shaped behaviour is achieved in both cases, with a very small extent of residual drift (about 0.20%) only in the connection with PT strands and ED angles. Some inelastic deformations occur at the beam ends and close to the dissipation devices, too.

The energy dissipation in the considered PT strands and ED angles connection is larger than the one in the PT and ED bars connection, the ratio among the force-drift loops ranging from 1.75 to 1.33.

The deformation and stress distributions within the two connections during the cyclic imposed drift history show that the behaviour of the system with PT and ED bars is easier to be interpreted, due to the evidenced clear flows of the compression stresses. As a consequence, this type of connection may be modelled in easier way, and simpler rules could be set up for design purposes.

On the other hand, the connection with PT strands and ED angles, the extent of high stress areas is more limited than in the case of PT and ED bars, due to the stress “distortion” caused by the deformation of the ED angles. In addition, the presence of the ED angles entails the advantageous presence of a redundant shear resisting system.

It is worth noticing that the arrangements considered for the comparative analyses correspond to only one among the possible solutions, since in a PTED connection the design requirements can be, in general, fulfilled by adopting different combinations of the connection component parts. In particular, the geometrical and mechanical features of the parts used for both the PT and the ED systems could be selected in diverse ways, leading to connections characterized by different performances. In this sense, further studies are needed, in which parametric analyses can be carried out with the aim of defining the most performing technological solution and obtaining the mechanical characterization of the system. Anyway, the performed analyses represent a first step in this direction, by providing both qualitative and quantitative information on this topic.

Chapter 8

Monotonic response

8.1 INTRODUCTORY REMARKS

In previous chapters the attention is focused on the cyclic behaviour of PTED connections. In particular, the analysis of the stress and strain states of particular connections subjected to experimental cyclic imposed displacement histories is carried out. Furthermore, the cyclic behaviour of PTED connections is compared to that of welded rigid ones, and a comparative evaluation of PTED connections characterized by different PT and ED arrangements is conducted.

Besides the cyclic behaviour of the connections, the determination of their ultimate response is worth of notice. In fact, the complete mechanical characterization of a connection requires the strength and deformation capacity to be defined. Consequently, the investigation of the system behaviour under monotonic increasing imposed displacements is a necessary step for their complete identification.

Based on the above considerations, this chapter deals with the analysis of the monotonic response of the PTED connection with PT and ED bars considered in Chapter 4. The main purpose of this study is to characterize the system response up to its failure and, at the same time, to determine the contribution to the whole response provided by each component part of the connection.

8.2 THE NUMERICAL MODEL

The geometrical features of the finite element model of the PTED connection with PT and ED bars are exactly the same presented in Chapter 4, shown in Figure 4.5, which faithfully reproduces the tested specimen (Christopoulos et al., 2002a, b). In order to adequately catch the possible out-of-plane displacements associated to buckling phenomena, which can occur at large displacements, no symmetry-based simplifications are adopted.

The modelling of the materials is based on the information reported by Christopoulos et al. (2002a). The bi-linear simplified models adopted in previous models are replaced by multi-linear models which better match the typical response curves of the materials used in the tests, also accounting for degradation characteristics. It is worth noticing that the simpler models used in previous chapters are calibrated directly against the experimental evidence, and they are reliable for the analysis of the considered connections within the deformation ranges considered there. The numerical response of the improved model used in this section well matches the one of the simpler models for the above deformation ranges, in terms of both force-displacement curves and deformation and stress states, and so their reliability is confirmed.

Figures 8.1 and 8.2 show the typical stress-strain curves of the A992 steel and the DSI (Dywidag Systems International) high strength steel used in the tests for the main structural elements and the PT bars, respectively.

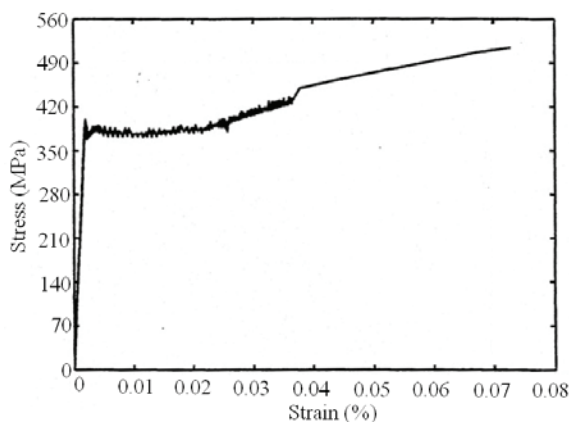


Figure 8.1. Typical response curve for A992 structural steel used in the tests (Christopoulos et al., 2002a)

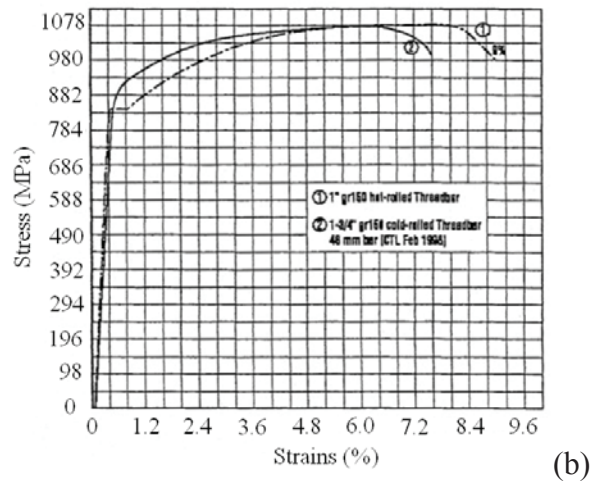


Figure 8.2. Typical response curve DSI high strength steel used in the tests (Christopoulos et al., 2002a)

With regard to the modelled materials, the same labels used in Chapter 4 are used herein. The corresponding nominal stress-strain relationships are shown in Figure 8.3. The ultimate deformation value of the HRS steel is based on Figure 8.2, whereas the ultimate deformation values of both SS and HS steel are assumed by the author.

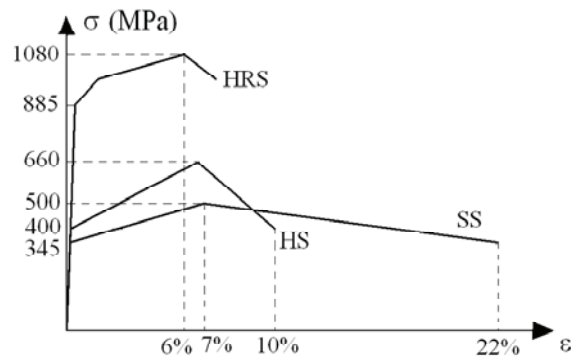


Figure 8.3. Nominal stress-strain relationships of the modelled materials

It is worth noticing that the author is not in possession of the digital data on the above experimental curves. Consequently, these models, although closer to the actual ones, still represent a simplification, they being multi-linear schematizations.

Information on the above materials, in terms of true stresses and plastic strains, and on the related component parts, is summarized in Table 8.1.

Table 8.1. Mechanical features of the modelled materials, in terms of true stresses and plastic strains, and associated component parts

Material	Yield stress (MPa)	Ultimate stress (MPa)	Ultimate plastic strain (%)	Component parts
SS	345	535	19.8	Column, beam, anchors, continuity plates, stiffeners, doubler plates, contact plates, reinforcing plates
HS	400	700	9.3	ED bars
HRS	885	1145	6.8	PT bars, couplers, conf. cylinders

In this study, the collapse of the connection component parts is not directly modelled, and so it is assumed to occur when the ultimate strains of the related materials are attained. Consequently, the SS steel breaks at a 19.8% true plastic strain, the HS steel at a 9.3% true plastic strain, and the HRS steel at a 6.8% true plastic strain.

Improvements of this model would be represented by the use of the actual stress-strain curves for the considered materials and by the capability of catching numerically the failure of the component parts.

The interactions between adjacent surfaces are modelled according to the information reported in Chapter 4.

A two step analysis is carried out. During the first step, the post-tensioning of the PT bars is applied, whereas the second step is devoted to the application of a 730 mm vertical displacement to the mid-span section of the beam, corresponding to a 20% drift.

In order to model the lateral bracings, constraints against the transversal displacements are imposed in the column, at both its ends, and in the beam, at the actuator location and at the end opposite to the column.

The finite element mesh is essentially based on the assumptions made in Chapter 4, with the exception that a relevant refinement is adopted in the part of the beam between the actuator location and the interface with the column (Fig. 8.4). This choice is intended to catch the possible out-of-plane displacements linked to instable phenomena in the beam, which could not be captured in case of excessively coarse mesh.

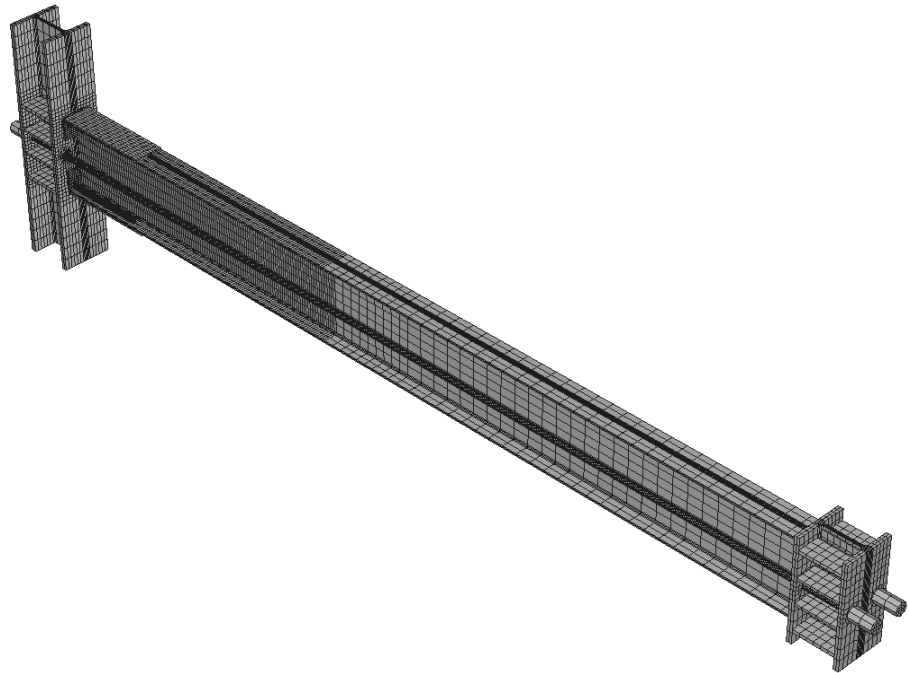


Figure 8.4. Finite element mesh of the model used for the study of the monotonic response of the PTED connection with PT and ED bars

8.3 THE RESPONSE CURVES

The obtained numerical response of the system, in terms of force-drift curve, is plotted in Figure 8.5. In the same figure, the cyclic response of the connection is shown.

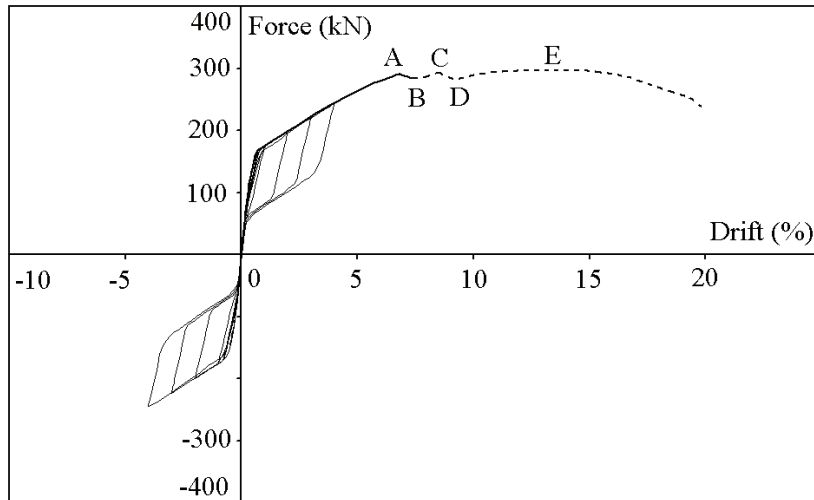


Figure 8.5. Monotonic and cyclic force-drift response of the PTED connection with PT and ED bars

Up to a drift equal to 4%, the obtained monotonic curve is perfectly superimposed to the envelope of the cyclic curve, and this confirms that the models used in previous chapters, which are less refined than the one adopted in this part of the work, are reliable for describing the system behaviour up to the drift values considered in the experimental campaign.

For drifts larger than 4%, the force in the connection increases up to a drift equal to 6.8% (point A), corresponding to the peak stress in the ED bars, attained at a true plastic strain equal to 6.1%. Then, the force reduces, due to the softening behaviour of the ED bars, until the 7.4% drift is reached (point B), corresponding to a 9.3% true plastic strain in the ED bars. This point is assumed as the breaking point for the ED bars. This condition does not correspond to the collapse of the connection, since the PT bars are still able to guarantee a moment capacity. Nevertheless, the remaining part of the curve, plotted with a dotted line, is not real, since it still accounts for the presence of the ED bars, where a constant stress equal to the failure one is present. Anyway, it provides some indications useful for understanding the influence of the different component parts on the connection behaviour and for catching the possible global crisis modes.

A better comprehension of the system behaviour may be achieved if Figure 8.6 is considered, in which the correlation between the connection response (thick line) and the stress states in bottom finite elements of both PT and ED bars is evidenced.

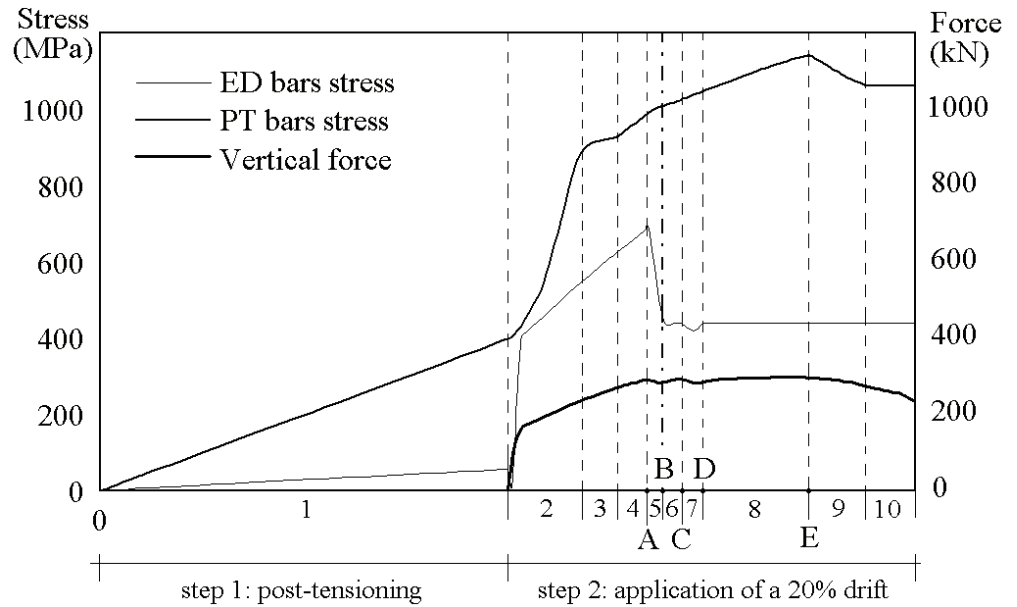


Figure 8.6. Correlation between the system vertical force and the stress states in both the PT and ED bars

Region 1 refers to the post-tensioning phase: the PT bars undergo the initial stress, whereas some small stresses, due to compression, are present in the ED bars. No vertical force is present in the system at this stage.

In region 2, the decompression and gap opening take place. In the first part, the ED bars behaviour is linear elastic. Then, after yielding, its stiffness reduces. As a consequence, the stress in the PT bars increases more than linearly.

Between regions 2 and 3 the 885 MPa stress in the PT bars is reached, with consequent reduction of the curve slope. Then, due to the contact between PT bars and column holes, local rotations occur in the PT bars, with increasing of the slope.

As already observed, point A corresponds to the stress peak in the ED bars. After that point the system response reduces. In this phase, the effects of PT and ED bars are conflicting, in the sense that the contribution by the PT bars is increasing-type, whereas the contribution of the ED bars is decreasing-type. Considering that the overall response reduces, it can be observed that, in this phase, the influence of ED bars on the connection behaviour is larger than the PT bars one. This can be explained considering that the distance between the ED bars and the contact point at the beam-to-column interface is larger than the one of PT bars.

After point B, ED bars collapse. This corresponds to a sudden reduction of the force in the system, which is not caught by the numerical model. In any case, the following considerations may be drawn, they providing qualitative information on the system ultimate behaviour.

In region 6, the total force increases due to the further elongation in the PT bars, until buckling phenomena start (point C). This condition causes a force reduction, due to the shortening of the bottom ED bars (region 7). Afterwards, the buckling phenomena get larger and larger, up to reach the maximum force (point E) and then the collapse of the PT bars, in region 10.

The above results may be summarized as follows. The ED bars are the first elements to collapse. Their contribution in the whole system response is not negligible, due to their large distance from the contact point at the beam-to-column interface. The failure of ED bars does not coincide with the connection collapse, but it worsens the stress state in the PT bars, besides reducing the system response. Possible crisis modes are both the buckling in the beam and the failure of the PT bars steel.

8.4 DEFORMATION AND STRESS STATES

In this section, the deformation and stress states of the connection at the most relevant drifts, based on the previously described response curves, are analysed.

Figure 8.7 shows the system configuration at a drift equal to 5.3%. The stress peaks in the beam, at the end of reinforcing plates, and in the column web, evidenced also in Chapter 4, are visible.

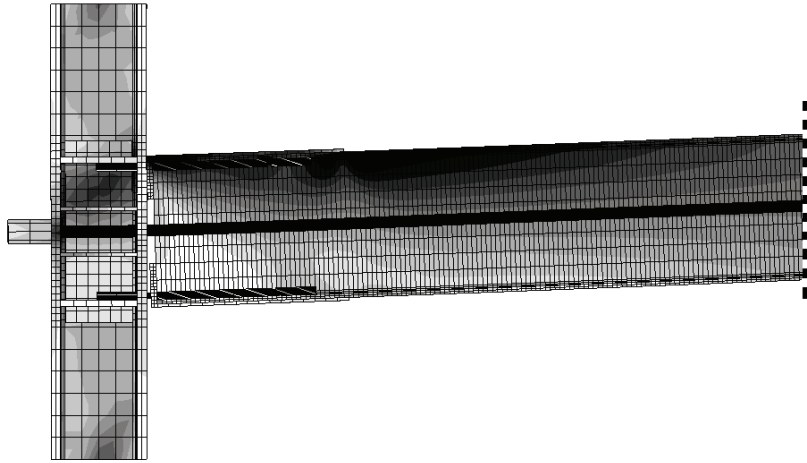


Figure 8.7. Deformation and stress state of the connection at a 5.3% drift

The deformation and stress state of the connection at a drift equal to 6.8%, when the collapse of the bottom ED bars occurs, is shown in Figure 8.8. Strong shear stresses in the column and large yielded areas in the beam are visible.

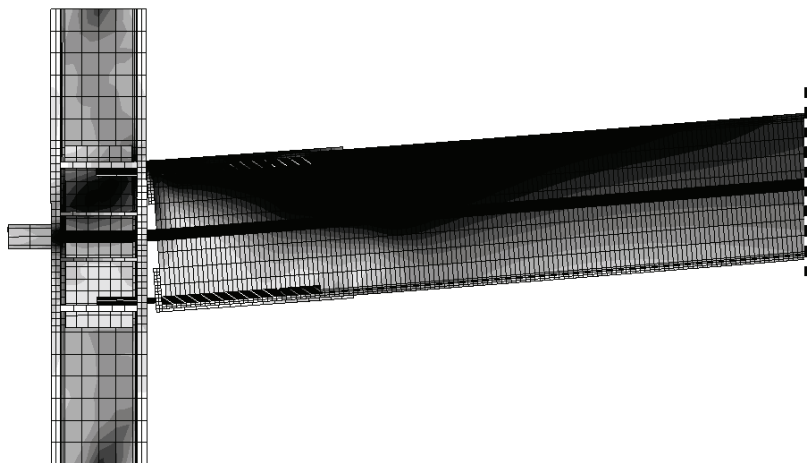


Figure 8.8. Deformation and stress state of the connection at a 6.8% drift, when the failure of the bottom ED bars occurs

At last, Figure 8.9 shows a possible instable collapse mode of the connection, whose plan view is provided. Large yielded areas in the beam flange are visible. It is worth noticing that this condition, even supposing that it is compatible with the deformation capacity of both the ED bars and the PT bars, may lead to the contact between the beam web, which undergoes out-of-plane displacements, and the PT bars, with consequent worsening of stress state.

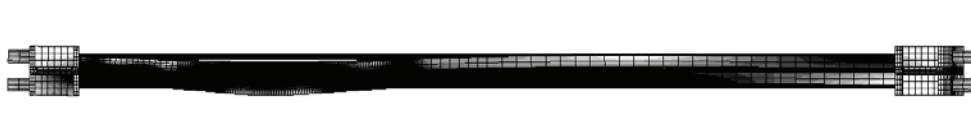


Figure 8.9. Plan view of the connection affected by buckling phenomena at large drifts

8.5 SYNTHESIS OF RESULTS

The study presented in this chapter provides interesting information on the monotonic response of a PTED connection with PT and ED bars, useful for its mechanical characterization. The used finite element model is very refined, and so the main peculiarities of the system response are well caught. Anyway, some improvements, essentially related to the definition of the mechanical properties of the materials and on their failure, are required.

The performed analyses allow to identify the contributions of the different system component parts to the load carrying capacity of the connection, by underlying the mutual effects of the ED and PT bars.

Based on the monotonic response of the considered connection, drift values up to about 7% are achieved without any degradation. Although yielded areas are present in the beam at such drift value, which impair the self-centring response, the connection load carrying capacity is still guaranteed.

The yielding in the ED bars, for small drift values, causes a worsening in the stress state of the PT bars, which are obliged to compensate for the stiffness reduction in the ED bars.

The softening behaviour of the ED bars reduces the overall response of the system, notwithstanding the increasing forces in the PT bars, due to their elongation. This evidence underlines the non-negligible contribution of the ED bars to the load carrying capacity of the connection.

The first collapsed component parts are the ED bars, whose failure is due to excessive tensile deformation. As a consequence, the stress state of the PT bars is even more worsened, according to the above considerations.

The collapse of the connection could be due to breaking of the PT bars or buckling in the beam, the latter being preferable due to its more ductile features. The performed analysis does not allow to predict such condition, due to the presence, in the model, of the ED bars also after their assumed breaking, so confirming the usefulness of improving the finite element model by accounting for the failure of the bars.

A final remark has to be made with regard to the friction resistance at the beam-to-column interface: despite the large imposed drifts, and the corresponding large vertical shear values, no sliding occurs, so giving a confirmation on the system capability of bearing vertical shear by means of friction. This subject is dealt with in detail also in the following chapter, where the behaviour of a frame sub-assembly equipped with PTED connections is analysed under both vertical and horizontal loads.

*Chapter 9***Behaviour under vertical and horizontal loads****9.1 INTRODUCTORY REMARKS**

This chapter deals with the preliminary numerical analysis of the cyclic behaviour of a simple two columns-one beam frame assemblage equipped with PTED beam-to-column connections. The PT system is based on high strength steel bars and the ED system is made by confined steel bars, according to the system proposed by Christopoulos et al. (2002a, b).

For this type of PTED connections, the behaviour under both vertical and horizontal loads is a very important topic. In fact, differently from the connection with PT strands and ED angles, in which the ED devices also provide a redundant shear mechanism, in this case the capability of transmitting the beam shear is provided solely by the friction at the beam-to-column interface. Redundant slotted tabs could be used, but, in any case, the behaviour of the system alone is worth of interest and so it is analysed herein.

9.2 THE NUMERICAL MODEL

The detail of the nodal area in the considered assemblage is shown in Figure 9.1. It is composed by a W24x62 beam and two W14x311 columns. The span length is equal to 6100 mm, whereas the column height is equal to

3658 mm. The other component parts of the system are: 54 mm diameter PT bars; 16 mm diameter ED bars, 600 mm long; 25 mm thick contact plates; 12.5 mm thick reinforcing plates; 25 mm thick continuity plates; 20 mm thick stiffeners. It is worth noticing that this geometry corresponds to the one presented in Chapter 7. Since external connections are present in this case, appropriate steel stiffeners, necessary for supporting the column flanges in bearing the forces due to the PT anchors, are considered.

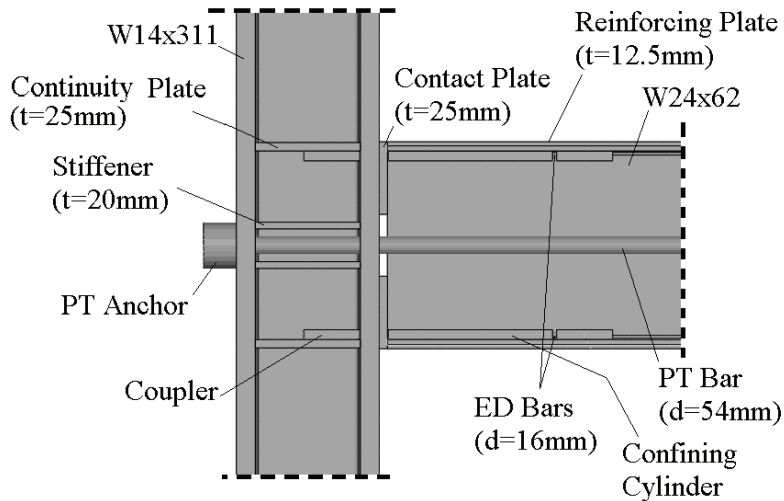


Figure 9.1. Detail of the nodal area in the frame assemblage

The symmetry-based assumption is made in this case (Fig. 9.2), and the modelling of the materials is similar to the one presented in Chapter 7. These simplifying choices, which strongly reduce the calculation time, are suitable since the cyclic behaviour of the system is investigated at small drift values, as observed in previous chapter. The model without the symmetry-based simplification should be used in future research, since it could be necessary for catching unsymmetrical phenomena, like the buckling ones, which could take place at large drifts.

The interactions between adjacent surfaces are modelled according to the choices described in Chapter 7: tie constraints are used for the interaction

between welded surfaces, friction contacts are considered for the interactions between columns and contact plates, and frictionless contacts are used for the interactions between PT bars and column holes and between ED bars and confining cylinders.

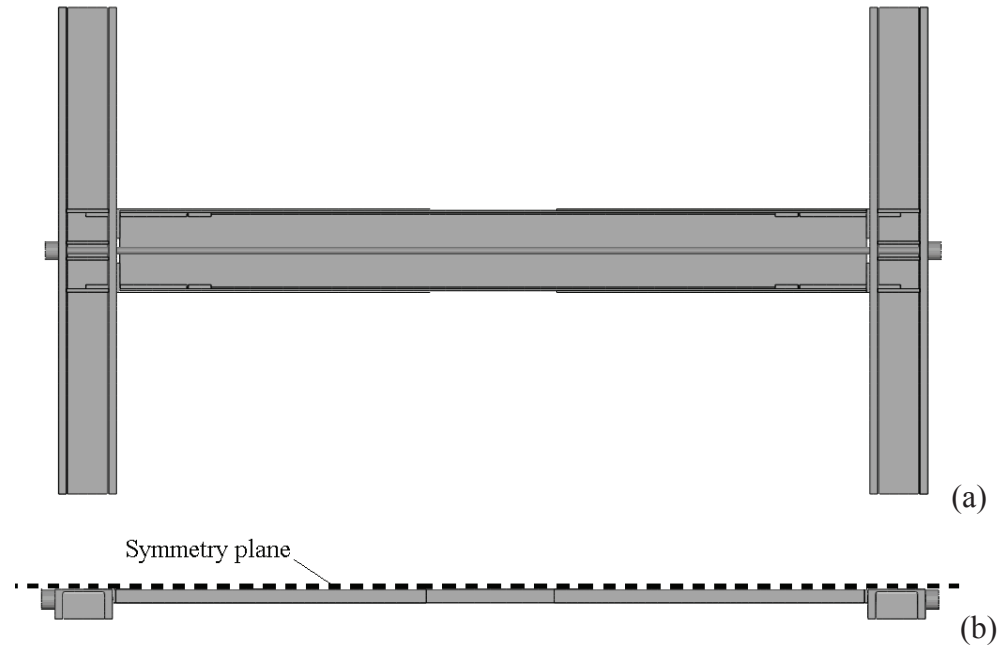


Figure 9.2. Geometrical features of the two columns-one beam assemblage: (a) lateral and (b) plane views

The initial post-tensioning force ($F_{PT,in}$) is equal to 710 kN. The vertical load is calculated starting from a dead load equal to 4.0 kN/m² and a live load equal to 2.0 kN/m². Considering an inter-axis equal to 5 m and the system as extracted from a perimeter frame, the distributed vertical load is equal to 15 kN/m. This value is consistent with the friction resistance of the considered PTED connections. In fact, according to the indications by Christopoulos and Filiatrault (2002), in order to achieve the self-centring behaviour, the design shear (V_D) must meet the requirement expressed by relationship (9.1):

$$V_D \leq \mu(F_{PT,in} - 2F_{ED}) \quad (9.1)$$

where F_{ED} is the total force developed by a couple of ED bars at the target gap opening. Relationship (9.1) guarantees that, after a seismic event, which causes the F_{ED} force in the ED bars, the vertical shear at the beam-to-column interface is lower than the shear resistance. The latter, indicated at the second member of the relationship, is obtained by multiplying the friction coefficient ($\mu = 0.33$) by the normal force present after the seismic event, equal to the difference between the residual post-tensioning force ($F_{PT,in}$, if neither yielding in the PT bars nor shortening of the beams occurs) and the force developed by the ED bars.

A multi-step analysis is considered. In the first step, the post-tensioning of the PT bars is carried out. In the second step, the vertical distributed load is applied to the beam. In the subsequent steps, the application of a series of cyclic horizontal displacements to the top sections of the columns is conducted.

The finite element mesh of the model (Fig. 9.3) is made by linear hexahedral solid finite elements with reduced integration (C3D8R).

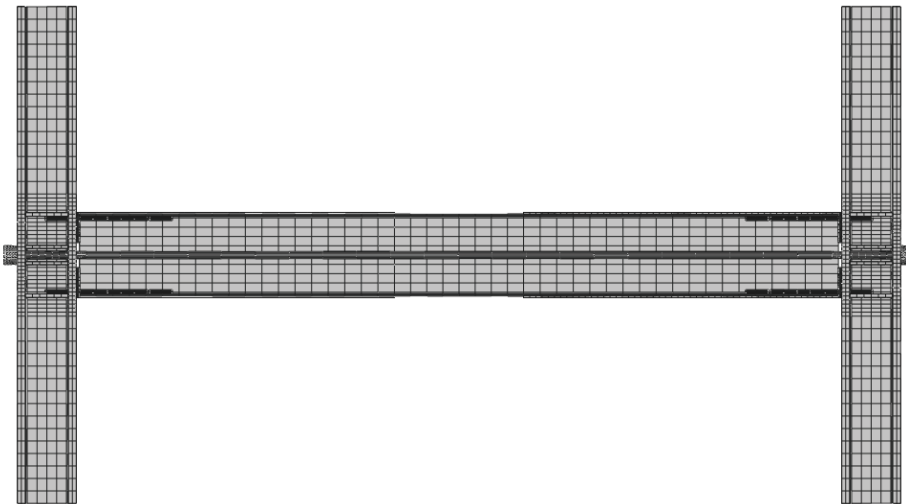


Figure 9.3. Finite element mesh of the model

9.3 THE SYSTEM RESPONSE

The cyclic response of the considered two columns-one beam frame assemblage, equipped with PTED connections, is shown in Figure 9.4, where it is expressed in terms of lateral force-drift relationship.

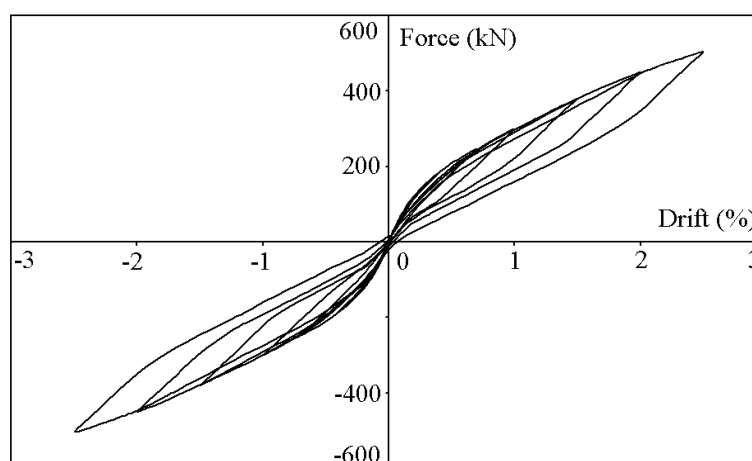


Figure 9.4. Cyclic response of the frame sub-assemblage up to a 2.5% drift

The cyclic behaviour of the system is flag-shaped, with self-centring capability and energy dissipation capacity.

Besides the presented analysis of the system subjected to vertical loads, an additional ad-hoc analysis without considering the vertical loads has been carried out. The force-drift response curves, with or without vertical loads, are perfectly superimposed, and so, at least for the drift values considered in the analyses, the system global response is not influenced by the presence of vertical loads.

Decompression, with consequent loss of the linear behaviour and reduction of the overall stiffness, occurs for small drifts, starting from 0.2%. It is worth noticing that, in presence of vertical loads, the decompression is not contemporary in the two PTED connections of the frame sub-assemblage (Fig. 9.5). In fact, the bending moment due to vertical loads reduces the contact

stresses in the top part of the beam ends, and increases them in the bottom part. Consequently, the decompression firstly occurs in the PTED connection where the moment induced at the beam ends by the lateral load is consistent with the pre-existing one, due to vertical loads.

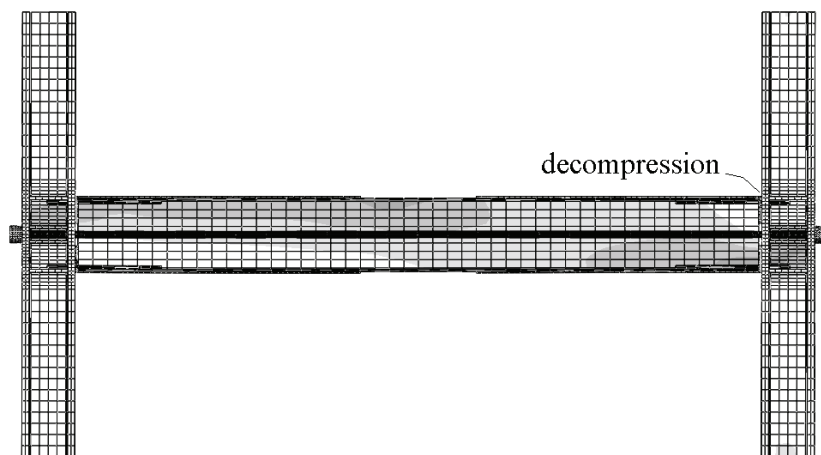


Figure 9.5. Deformation and stress state at a 0.2% drift

In Figure 9.6 the deformation and stress state of the system at a drift equal to 2.5%, either in absence or in presence of the vertical loads, is compared.

In absence of vertical loads (Fig. 9.6a), the stress flow in the system is clear and simple. Starting from the left PT anchor, the stresses flow across the column web, and then in the contact area of the beam end. In the beam, a diagonal stress distribution is present, from one contact area to the other one. The contact stresses flow across the left column web, up to the left PT anchor.

The presence of vertical loads slightly changes the distribution of stresses in the system. In fact, as visible in Figure 9.6b, the central symmetry of stresses, characteristic of the previously described condition, is distorted by the stresses due to the vertical loads.

With regard to the capability of transmitting the shear forces present in the beam, in the performed analysis no slip occurs at the beam-to-column interface. This is evidently due to the sufficient shear resistance provided, at the interface, by the friction between the parts in contact.

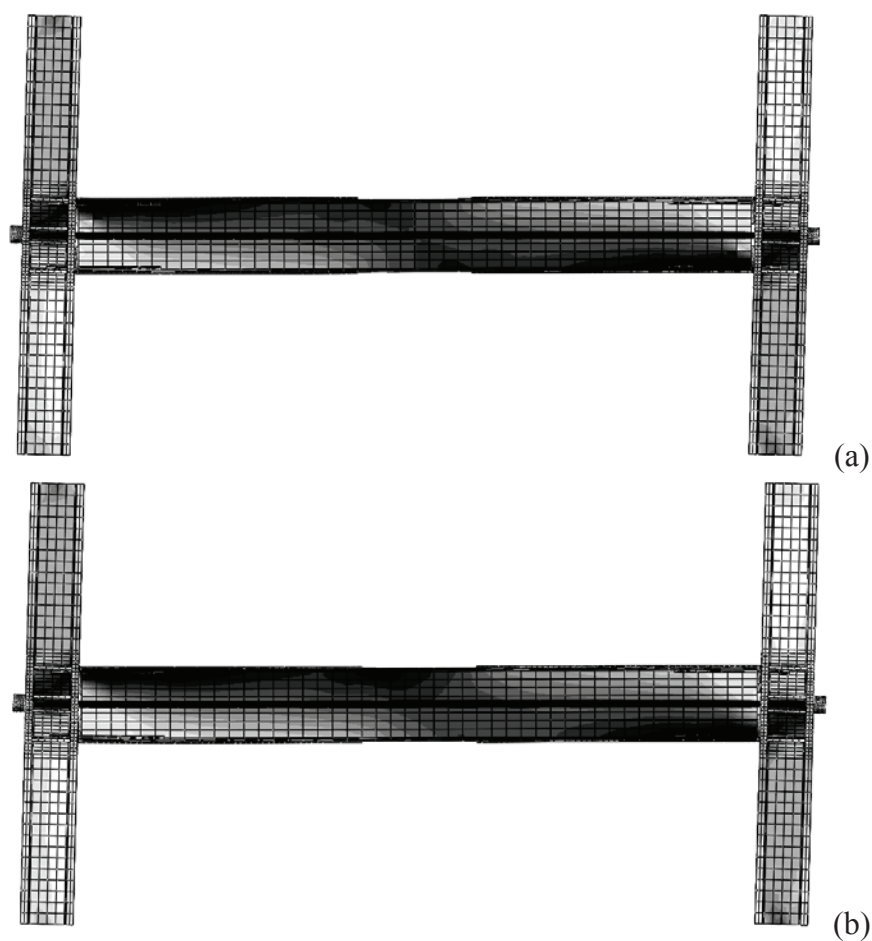


Figure 9.6. Deformation and stress state of the system at a 2.5% drift: (a) with vertical loads; (b) without vertical loads

9.4 SYNTHESIS OF RESULTS

The part of the research presented in this chapter is in phase of development. Accordingly, the analyses shown are affected by some simplifications. At first, the symmetry-based simplified model is used, which is not able to catch possible asymmetric phenomena, like the buckling ones. In

addition, the drift values are smaller than those usually considered in previous chapters. Consequently, the analyses require to be improved by removing the symmetry hypothesis and by considering larger drift values. Anyway, the obtained results are presented since they provide useful indications on the investigated topics.

Based on the performed analyses, the following main aspects are worth of notice.

Up to the considered drift values, the system behaviour is self-centring, either or not under vertical loads in the beam.

Decompression occurs for small drift values, and it is not contemporary in the two PTED connections, due to the pre-existing bending moments at the beam-to-column interfaces, which add up with the ones induced by horizontal loads.

The stress flow in the beam, due to horizontal loads, is distorted by the vertical loads, which increase the compression state in the top flange with consequent risk of buckling phenomena.

The friction at the beam-to-column interface is able to guarantee the necessary resistance against the vertical shear coming from the beam, at least for the considered drift ranges.

Conclusive remarks and further developments

This work is the result of a three years research focused on the structural identification of the innovative Post-Tensioned Energy Dissipating (PTED) beam-to-column connections for earthquake resistant steel moment frames.

Due to the novelty of such type of connections, a large amount of studies is required, which are necessary for the development and the subsequent actual implementation of PTED connections in the practice. Consequently, both experimental and numerical studies are ongoing in several parts of the world. The attention is focused on the investigation of both the local behaviour of PTED connections and the seismic performances of steel frames equipped with them.

This study is framed within the investigations on the local behaviour of PTED connections based on numerical analyses. As well known, the numerical approach is a suitable and profitable tool complementary to the experimental one. The use of well calibrated numerical models allows to investigate aspects difficult to catch during the experimental tests. In addition, the economic costs of numerical campaigns are usually lower than those related to an experimental one, especially if parametric analyses are considered.

The analyses are carried out by the ABAQUS multi-purpose finite element computer program. Such analytical tool allows to model in detail PTED connections by catching their main peculiarities, related to the material non-linearity, the large displacements regimes, and the contact interactions.

The presented research provides both qualitative and quantitative information on the behaviour of PTED beam-to-column connections useful for their development, the ultimate goal being the set up of design rules specific for steel moment resisting frames equipped with PTED connections.

The general conceptual layout useful for reaching the above results may be summarized as follows:

- Achieving a deep comprehension of all the behavioural peculiarities of PTED connections subjected to cyclic loads, in order to provide information on the possible weaknesses of the system and to suggest suitable improving solutions.
- Comparing the cyclic behaviour of PTED connections with that of the traditional welded nodes, in order to point out the main performance differences and to underline, on a quantitative basis, the advantages offered by PTED connections.
- Comparing the cyclic behaviour of PTED connections characterized by different PT and ED arrangements, in order to stress the related differences and analogies, with the purpose of determining the optimal structural solution and providing useful design recommendations.
- Determining the ultimate behaviour of the connections, focusing on the roles played by the different component parts, in order to achieve the mechanical characterization of the nodes, which is necessary in phase of design of MRFs equipped with them.
- Investigating the behaviour of frames equipped with PTED connections, in order to evaluate effects of these innovative systems on the frame global behaviour and to assess their capability to bear the combination of vertical and horizontal loads.
- Defining appropriate guidelines for the design of steel frames with PTED connections, in order to allow the diffusion of such systems in the construction practice.

This study has been articulated according to the above conceptual layout. The investigations are principally focused on two particular PTED connection types, characterized by different arrangements for the PT and ED systems. In one case, the PT system is based on high strength steel bars and the ED

system is made by confined steel bars. In the other case, the PT system is composed of high strength steel strands and the ED system is made by bolted steel top-and seat-angles.

The research is still in phase of development, but important results have been achieved, which are summarized herein.

The first preliminary step in this research has been the set up and calibration of refined numerical models of the study PTED connections. The issue requiring the largest care has been the modelling of the interactions between surfaces which can be or not in contact during the cyclic displacement history. This behaviour is peculiar of PTED connections, which are characterized by a “rocking” mechanism at the beam-to-column interface. In addition, other contact interactions have been taken into account, such as those related to the bars or the strands, which may go in contact with the column. The numerical results have matched the experimental ones in a very satisfying way. The peculiar kinematics of the PTED connections has been adequately caught, well reproducing the deformation states of all the connection component parts evidenced during the tests. In addition, the flag-shaped hysteretic response has been obtained.

The reliability of the set up numerical models has allowed for the detailed analysis of the connections behaviour during the experimental tests. The stress distribution within all the connection component parts during the simulated imposed displacement history has been depicted. Useful information on the local behaviour has been so obtained.

With regard to the behaviour of the beams, which are expected to remain elastic during the seismic action, for both the considered PTED connection types, stress concentrations have been evidenced in two specific areas, namely at the interface with the column and at the end of the beam flange reinforcing elements. In the former area, corresponding to the cross-section where the maximum bending moment occurs, large compression stresses are present. In fact, the compression force, due to the combined presence of the PT force, increased after the elongation, and of the bending moment, is borne by a small contact area, whose extent is limited due to the gap opening. In the cross-section corresponding to the end of reinforcing plates, on the other hand, the bending moment is smaller than the one at the beam-to-column interface.

Anyway, the cross-section of the beam is no more supported by the reinforcing plates in bearing the combination of axial force and bending moment. Based on the above considerations, the mentioned cross-sections are critical in the design of PTED connections, and key parameters are represented by the resistance and length of the beam flange reinforcing plates, aimed at supporting the beam in carrying the compression forces due to the contact.

With regard to the behaviour of the columns, in both the analysed cases no yielding has occurred. The analysis of the stress distribution during the imposed displacement history has evidenced strong stress concentrations in the column web, corresponding to a noticeable shear demand. This evidence is mainly concerning in the case of external connections, in which the distance between the internal forces provoking the moment in the column is smaller than the case of internal connections. Based on the above considerations, the use of column web doubler plates is recommended.

Steel plates at the interface between the beams and the column provide an adequate smooth surface for the parts in contact. Their location along the depth of the beams strongly influences the stress distribution in the beams. In the case of the PTED connection with PT and ED bars, the contact plates are the unique interface elements, and they are loaded by the whole compressive forces coming from the beam flanges. Due to the extremely reduced extent of the compressed area, these contact plates have undergone plastic deformations, also for small imposed drift values. This behaviour, which can be prevented by using high strength steel for the contact plates as demonstrated by ad-hoc numerical analyses, has induced large stresses in the beam end, up to reach the yield limit. In the case of the PTED connection with PT strands and ED angles, the contact plates have behaved in the elastic field, thanks to the larger extent of the compressed area, due to the location of the plates and to the presence of the top-and-seat angles. Based on the above considerations, the adoption of high strength steel contact plates is suggested.

Reinforcing plates support the beam flanges for carrying the compression forces due to contact. In the case of PTED connection with PT and ED bars, inelastic deformations have been detected for the largest drift values, with consequent increase of the stress demand in the beam flanges. The use of high strength steel for reinforcing plates would prevent such situation, as confirmed

by an ad-hoc numerical analysis. In the case of PTED connection with PT strands and ED angles, the reinforcing plates were located at the internal side of the beam flanges, with consequent reduction of their effectiveness. Based on the above considerations, the use of externally located beam flange reinforcing plates is recommended.

The behaviour of continuity plates, column web doubler plates, and stiffeners, the latter ones being necessary in the case of external connections for supporting the concentrated forces due to the anchoring of the PT system elements, have been always within the elastic range. Their presence has well supported the column in bearing the forces coming from the beams, so contributing to the preservation of the columns from damage.

The analysis of the behaviour of the component parts of PT and ED systems maybe represents one of the most interesting results of the part of the research focused on the investigation of the system behaviour during the simulated tests.

In both cases, for the largest imposed displacement values, the component parts of the PT system have gone in contact with the holes in the column they were located into. This condition, which may be very dangerous since it can increase the stress state in the PT elements, has proven to be concerning above all in the case of PT system made by high resistant steel bars, whose own flexural stiffness has caused large stresses in the cross-sections undergoing local rotations due to the contact with the column holes. In the case of PT system made by steel strands, this condition, which is not caught by the set up numerical models, maybe appears less concerning, due to the deformability of such type of tendons. Anyway, based on the numerical observations, adequate safety factors are required in the design of the PT system component parts, whose behaviour must always be elastic.

With regard to the ED systems, in both the considered cases the used devices have provided adequate capacity of energy dissipation. The effectiveness of the steel confining cylinders in preventing the steel ED bars from buckling in compression has been confirmed, with consequent stable hysteretic cycles of the bars. In the case of the angles, the analyses have confirmed the dissipative mechanism consisting in the formation of three cylindrical plastic hinges. In addition, the observation of the stress state in the

areas of the beams next to the angles location shows that they somehow support the beam flanges in carrying the compression forces.

Since PTED connections are proposed as an alternative to the welded rigid ones, the comparison of their behaviour with that of welded nodes is worth of interest. The attention has been focused on both the above mentioned PTED connection systems, whose cyclic behaviour has been compared with that of the corresponding welded connections, obtained by considering the same beams and column assemblages present in the tested PTED systems.

The performed analyses have confirmed that the PTED connections behave like the welded rigid ones in presence of service loads or frequent low-intensity seismic actions. In fact, for drift values corresponding to the fully operational performance level defined by SEAOC Vision 2000, the response curves of PTED and welded connections are superimposed. The initial stiffness is the same, and so their behaviour, under low-intensity earthquakes as well as under vertical loads only, shows no difference with respect to the rigid ones.

The loss of linear behaviour has been due to the beam-to-column interface gap opening, in the case of PTED connections, and to the attainment of the yield stress in the beams, in the case of the welded connections. The maximum borne forces and moments in the PTED connections have been lower than the maximum forces in the welded ones. The post-gap stiffness reduction in the PTED connection has to be adequately taken into account when global analyses of steel moment resisting frames incorporating them are carried out.

The capacity of dissipating the input energy in the PTED connections has been quite smaller than that of welded connections, as expected. In fact, the only elements devoted to the dissipation of input energy in the considered PTED connections were the steel cylinders or the top-and-seat angles. On the contrary, in the case of welded connections, large portions of the main structural elements have contributed to the dissipation of energy, by means of cycles of inelastic deformations.

The cost, in a structural perspective only, of the larger capacity of energy dissipation in the welded connections has been represented by the presence of large amounts of residual deformations, together with out-of-plane

displacements, and by the possibility of undergoing fracture phenomena, which can prevent the formation of ductile energy dissipation mechanisms.

After the mechanical comparison with welded rigid connections, the attention has been focused on the performance comparison between PTED connections characterized by the same beams and columns assemblages but different PT and ED systems. The aim of this part of the research has consisted in comparing the response of PTED connections with PT and ED bars, on one side, and with PT strands and ED angles, on the other side. Both qualitative and quantitative information has been obtained.

The initial stiffness of the compared connections has been the same, so confirming the rigid-type behaviour for small values of imposed drifts. This result confirms that the overall behaviour of PTED connections before decompression is not influenced by the PT and ED arrangements. As it was arguable, local differences in the stress and strain states have been evidenced, due to the different connection details.

After the gap opening at the beam-to-column interface, the behaviour of the connection with PT bars has been stiffer than that of the connection with PT strands. This behaviour may be explained considering that the post-gap opening stiffness in a PTED connection essentially depends on the elastic stiffness of the PT elements and on the post-yielding stiffness of the ED elements. Consequently, as it could be expected, a PTED connection with PT strands and ED angles is more deformable, after the gap opening, than a similar connection with PT and ED bars, due to the larger deformability of the PT strands with respect to the PT bars and of the ED angles, subjected to bending, with respect to the ED bars, subjected to tension. In the perspective of the global response of a frame equipped with PTED connections, whose performances are strongly affected by the stiffness of the beam-to-column connections, this result is worth of interest. In fact, the best frame response could be obtained by tailoring the post-gap stiffness of the connections.

Both the connections considered in the comparative analysis have shown the expected flag-shaped cyclic behaviour. Some inelastic deformations have occurred at the end of the beams and next to the dissipation devices.

The connection with ED angles has shown a larger capacity of dissipating energy than the one with ED bars. This condition is not general, since the

capacity of dissipating the input energy mainly depends on the geometrical and mechanical features of the selected ED devices. It is worth noticing that the post-elastic resistance of the ED elements can not be selected as large as one wants, since it may compromise the flag-shaped behaviour of the connection.

The observation of the deformation and stress distributions in the two considered connections during the cycles of imposed displacements shows that the behaviour of the connection endowed with PT and ED bars maybe can be interpreted in an easier way than that of the connection with PT strands and ED angles. This is essentially due to the clear stress flows evidenced in the former case. As a consequence, the response of the former type of connection is probably easier to be interpreted and predicted, and so its modelling could be easier and the related design rules simpler.

On the other hand, the stress peaks in the connection with PT strands and ED angles have interested a smaller length along the beam axis, due to the deformation effects caused by the presence of the top-and-seat angles. It is worth noticing that in this type of PTED connection the presence of the angles provides a redundant shear resisting system, which would resist to the vertical loads also in the case of loss of the PT system, with consequent loss of the friction resistance at the beam-to-column interfaces.

The arrangements considered for the comparative analyses correspond to only one among the possible solutions, since in a PTED connection the design requirements can be, in general, fulfilled by adopting different combinations of the connection component parts. Anyway, the performed analyses have given a first interesting quantitative contribution for the comparative performance evaluation of PTED beam-to-column connections.

In order to achieve useful information for the mechanical characterization of PTED connections, a first study aimed at determining the response of the connection with PT and ED bars under monotonically increasing imposed displacements has been investigated.

The definition of a more refined numerical model has been necessary, in order to better characterize the response of both the materials and the whole assemblage at deformation levels noticeably larger than those considered in the cyclic analyses. It is worth noticing that the previously adopted models,

calibrated against the experimental results, well reproduce the system behaviour for the deformation levels considered in the tests taken as reference.

The improved model is sufficiently accurate, and so the main peculiarities of the investigated problem have been adequately caught. A limitation has been represented by the fact that the failure of the component parts has not been directly modelled, and so their collapse has been assumed when the ultimate strain of materials was achieved.

The performed analysis has allowed to evidence the contributions of the different connection component parts to the load carrying capacity of the system.

The crisis of the ED bars in tension has been found to firstly occur. Anyway, the corresponding drift values have been larger than those usually considered in the seismic design. Such condition does not coincide with the connection collapse, due to the presence of the PT bars, but it provokes a sudden reduction of the connection response.

Possible collapse modes have been identified, they consisting in the breaking of the PT bars or the buckling of the beam, the latter condition being preferable due to its ductility peculiarities.

The slipping at the beam-to-column interface has proven to be a non-concerning topic, since the friction resistance has been adequate to resist the vertical shear corresponding to the large imposed vertical displacements in the beam.

The last part of the research has been focused on the investigation of the behaviour of a frame assemblage equipped with the PT and ED bars connection, with the main purpose of assessing the system capability to both dissipate the input energy and return to the initial configuration under the combination of vertical and horizontal loads.

The study on this topic is in progress, and so a simplified model based on the symmetry simplification has been adopted. Nevertheless, some preliminary information has been obtained.

The flag-shaped response has been guaranteed by the system. The analysis of the deformation and stress states in the system has evidenced the non-symmetric stress demand in the beam, with respect to the horizontal symmetry plane, due to the presence of the vertical loads.

The capability of the system to resist vertical loads thanks to the friction at the beam-to-column interfaces has been evidenced in the considered case.

The attractiveness of PTED beam-to-column connection systems for steel moment resisting frames in seismic areas has been largely confirmed by the performed numerical analyses.

This study is a part of the ongoing general research focused on PTED connections. It has provided both reliable investigation tools and interesting information on the focused topics, so creating a wide and solid basis for the future research.

Investigations similar to those carried out with reference to the two PTED connection types presented in this work should be carried out also considering the other PT and ED system arrangements proposed in recent years.

In order to achieve an adequate optimization of the constructive details for PTED beam-to-column connections, the influence of a series of geometrical and mechanical parameters on the systems behaviour must be appropriately evaluated. This aim could be pursued by means of both experimental and numerical studies. However, considering that an experimental campaign can be much more expensive, in terms of economic costs, than a series of numerical analyses, the use of well calibrated numerical models represents a powerful and relatively cheap tool of investigation. Consequently, campaigns of parametric analyses should be performed on the modelled PTED beam-to-column connections.

The investigation of the monotonic response of the connection with PT and ED bars should be refined, by means of numerical models able to account for failure in the component parts. A similar study should be carried out for the other PTED connection types, the ultimate goal of this part of the research being represented by the mechanical characterization of PTED connections.

The behaviour under both vertical and horizontal loads of earthquake resisting steel moment frames incorporating PTED connections has to be deepened. The presence of the vertical loads, in fact, essentially induces two types of problems: one related to the capacity of transmitting the shear forces at the beam-to-column interface due to the vertical loads, and one related to the additional compression in the beams induced by the vertical loads-induced bending moment. With regard to the former problem, it has to be noticed that,

besides the possible presence of redundant systems like the angles or ad-hoc slotted shear tabs, in the case of PTED connections the transmission of the vertical shear from the beams to the columns is assigned solely to the friction at the beam-to-column interface. So, it is clear that the effectiveness of this kind of connections subjected to the shear coming from both the vertical and horizontal actions is worth of interest. With regard to the latter problem, it is clear that for this kind of connections the local stability of the beams seems to be a more concerning problem than in the case of traditional connections. In fact, the compression stresses in the beams induced by the bending moment, due to the presence of vertical and/or seismic loads, is coupled with the initial compression state which the beams are subjected to, caused by the action of the post-tensioned elements. As a consequence, the risk of local instability phenomena strongly increases.

Besides the effects of vertical loads on the beams, some attention should also be focused on the behaviour of the columns, which, in presence of both vertical and horizontal loads, are subjected to both the compression vertical stresses and to the stress concentrations due to the gap opening mechanism.

Post-Tensioned Energy Dissipating beam-to-column connections require the definition of specific design criteria, to be developed for taking advantage of their peculiar characteristics.

At this aim, the mechanical characterization of PTED connections is necessary, since their stiffness, strength and deformation capability features influence the overall response of frames equipped with them.

In addition, the set up of appropriate design rules for PTED connections is necessary for their actual implementation in the construction practice.

In this perspective, the results of the numerical analyses on the PTED connections, both already carried out and to be developed in future, together with the parallel experimental work, may represent the basis for a proposal of codification for the design of steel MRFs equipped with such type of innovative connections.

References

- ABAQUS, Inc. (2004). ABAQUS Analysis User's Manual, v. 6.5.
- ABAQUS, Inc. (2006). "ABAQUS Seminar: Obtaining a converged solution with ABAQUS", 17th Italian ABAQUS Regional Users' Meeting, Pisa, Italy.
- Ballio, G. and Mazzolani, F.M. (1983). "Theory and design of steel structures", Chapman and Hall Ltd, London, ISBN 0-412-23660-5.
- Chou, C.-C., Chen, J.-H., Chen, Y.-C. and Tsai, K.-C. (2006). "Evaluating performance of post-tensioned steel connections with strands and reduced flange plates", Earthquake Engineering and Structural Dynamics, Vol. 35, p. 1167-1185.
- Christopoulos, C. and Filiatrault, A. (2002). "Seismic response of post-tensioned energy dissipating moment resisting steel frames", Proceedings of the 12th European Conference on Earthquake Engineering, London, UK, paper No. 61.
- Christopoulos, C. and Filiatrault, A. (2003). "Seismic demands on post-tensioned energy dissipating moment-resisting steel frames", Proceedings of the 4th International Conference on the Behaviour of Steel Structures in Seismic Areas (STESSA 2003), Naples, Italy, p. 511-517.
- Christopoulos, C., Filiatrault, A. and Uang, C.M. (2002a). "Self-centering post-tensioned energy dissipating (PTED) steel frames for seismic regions", University of California, Report No. SSRP-2002/06.
- Christopoulos, C., Filiatrault, A., Uang, C.M. and Folz, B. (2002b). "Posttensioned energy dissipating connections for moment-resisting steel frames", ASCE Journal of Structural Engineering, Vol. 128, No. 9, p. 1111-1120.

- Esposito, M. (2005). "Numerical analysis of PTED beam-to-column connection systems for steel MRFs", Graduation thesis (in Italian). Tutors: prof. F.M. Mazzolani, dr. B. Faggiano. University of Naples "Federico II", Naples, Italy.
- Esposito, M. (2007). "FEM modeling of PTED beam-to-column connections for earthquake resisting steel frames", *Pollack Periodica, Akadémiai Kiadó*, Vol. 2, No. 1, p. 101-112.
- Esposito, M., Faggiano, B. and Mazzolani, F.M. (2006a). "Numerical vs. experimental results on a PTED beam-to-column connection for seismic resistant steel frames", *Proceedings of the 5th International Conference on the Behaviour of Steel Structures in Seismic Areas (STESSA 2006)*, Yokohama, Japan, p. 299-304.
- Esposito, M., Faggiano, B. and Mazzolani, F.M. (2006b). "Numerical modelling of PTED connections for steel moment resisting frames", *Proceedings of the 8th International Conference on Computational Structures Technology (CST 2006)*, Las Palmas de Gran Canaria, Spain, paper No.117.
- Esposito, M., Faggiano, B. and Mazzolani, F.M. (2007). "Numerical study for the evaluation of PTED beam-to-column connections for steel MRFs", *Proceedings of the 3rd International Conference on Structural Engineering, Mechanics and Computation (SEMC 2007)*, Cape Town, South Africa, p. 1075-1080.
- Esposito, M., Faggiano, B. and Mazzolani, F.M. (2008). "Comparison between PTED beam-to-column connections based on numerical analyses", *Proceedings of the 5th European Conference on Steel and Composite Structures (EUROSTEEL 2008)*, Graz, Austria, p. 639-644.
- Faggiano, B., Esposito, M. and Mazzolani, F.M. (2007). "Numerical evaluation of PTED beam-to-column connections for steel MRFs: PT strands – ED angles versus traditional rigid connections", *Proceedings of the 5th International Conference on Advances in Steel Structures (ICASS 2007)*, Singapore, p. 571-576.

- Faggiano, B., Esposito, M. and Mazzolani, F.M. (2008). "Behavioural investigation on a PTED beam-to-column connection based on numerical analyses", Proceedings of the 14th World Conference on Earthquake Engineering (14WCEE), Beijing, paper No. 05-06-0152.
- FEMA – Federal Emergency Management Agency (2000). "FEMA 350 – Recommended seismic design criteria for new steel moment-frame buildings".
- Garlock, M.M., Ricles, J.M. and Sause, R. (2003). "Cyclic load tests and analysis of bolted top-and-seat angle connections", ASCE Journal of Structural Engineering, Vol. 129, No. 12, p. 1615-1625.
- Garlock, M.M., Ricles, J.M. and Sause, R. (2005). "Experimental studies of full-scale posttensioned steel connections", ASCE Journal of Structural Engineering, Vol. 131, No. 3, p. 438-448.
- Kunnath, S.K. and Malley, J.O. (2002). "Advances in seismic design and evaluation of steel moment frames: recent findings from FEAM/CAS phase II project", ASCE Journal of Structural Engineering, Vol. 128, No. 4, p. 415-419.
- Mao, C., Ricles, J.M., Lu, L.W. and Fisher, J.W. (2000). "Seismic testing of welded beam-to-column moment connections". Proceedings of the 3rd International Conference on the Behaviour of Steel Structures in Seismic Areas (STESSA 2000), Montreal, Canada, p. 719-726.
- Nakaki S.D., Stanton J.F. and Sritharan S. (1999). "An overview of the PRESSS five-story precast test building", PCI Journal, Vol. 44, No. 2, p. 26-39.
- Pampanin S. (2003). "Alternative design philosophies and seismic response of precast concrete buildings" (Ph. D thesis' synthesis), Fib-news, December 2003.
- Pampanin, S., Christopoulos, C. and Priestley, M.J.N. (2002). "Residual deformations in the performance-based seismic assessment of frame structures", European School for Advanced Studies in Reduction of Seismic Risk, Research Report ROSE – 2002/02.

- Peng, S.W. (2001). "Seismic resistant connections for concrete filled tube column-to-WF beam moment resisting frames", PhD dissertation, Lehigh University, Bethlehem, Pennsylvania, USA.
- Priestley, M.J.N. and Tao, J.R. (1993). "Seismic response of precast prestressed concrete frames with partially debonded tendons", *PCI Journal*, Vol. 38, No. 1, p. 58-69.
- Ricles, J.M., Sause, R., Garlock, M.M. and Zhao, C. (2001). "Posttensioned seismic-resistant connections for steel frames", *ASCE Journal of Structural Engineering*, Vol. 127, No. 2, p. 113-121.
- Ricles, J.M., Mao, C., Lu, L.W. and Fisher, J.W. (2002a). "Inelastic cyclic testing of welded unreinforced moment connections", *ASCE Journal of Structural Engineering*, Vol. 128, No. 4, p. 429-440.
- Ricles, J.M., Sause, R., Peng, S.W. and Lu, L.W. (2002b). "Experimental evaluation of earthquake resistant posttensioned steel connections", *ASCE Journal of Structural Engineering*, Vol. 128, No. 7, p. 850-859.
- Ricles, J.M., Sause, R., Wolski, M., Seo, C.Y. and Iyama, J. (2006). "Post-tensioned moment connections with a bottom flange friction device for seismic resistant self-centering steel MRFs", *Proceedings of the 4th International Conference on Earthquake Engineering*, Taipei, Taiwan, paper No. 108.
- Roeder, C.W. (2000). "SAC program to assure ductile connection performance", *Proceedings of the 3rd International Conference on the Behaviour of Steel Structures in Seismic Areas (STESSA 2000)*, Montreal, Canada, p. 659-666.
- Rojas, P., Ricles, J.M. and Sause, R. (2005). "Seismic performance of post-tensioned steel moment resisting frames with friction devices", *ASCE Journal of Structural Engineering*, Vol. 131, No. 4, p. 529-540.
- SEAOC – Structural Engineers Association of California (1995). "Vision 2000, Performance Based Seismic Engineering of Buildings".
- Stanton, J., Stone, W.C. and Cheok, G.S. (1997). "A hybrid reinforced precast frame for seismic regions", *PCI Journal*, Vol. 42, No. 2, p. 20-32.

- Tsai, K.-C., Chou, C.-C., Lin, C.-L., Chen, P.-C. and Jhang, S.-J. (2007). "Seismic self-centering steel beam-to-column moment connections using bolted friction devices", *Earthquake Engineering and Structural Dynamics*, doi: 10.1002/eqe.779.
- Youssef, N.F.G., Bonowitz, D. and Gross, J.L. (1995). "A survey on steel moment-resisting frame buildings affected by the 1994 Northridge earthquake", Building and Fire Research Laboratory, National Institute of Standards and Technology, Gaithersburg, MD.
- Wolski, M., Ricles, J.M. and Sause, R. (2006). "Seismic resistant self-centering steel moment resisting frames with bottom flange friction devices", *Proceedings of the 5th International Conference on the Behaviour of Steel Structures in Seismic Areas (STESSA 2006)*, Yokohama, Japan, p. 481-487.
- Zienkiewicz, O.C., Taylor, R.L. and Zhu, J.Z. (2004). "The Finite Element Method: its basis and fundamentals" (sixth edition).

